UAB

Universitat Autònoma de Barcelona

Contribuciones metodológicas para una mejor comprensión del cambio global en la Península Ibérica. Aplicación al estudio de las tendencias de las series climáticas y de la expansión forestal

Mario Padial Iglesias

Tesis doctoral en Geografía — 2022
Universitat Autònoma de Barcelona

U B

Universitat Autònoma de Barcelona

Tesis doctoral

Programa de Doctorado en Geografía

_____

Contribuciones metodológicas para una mejor comprensión del cambio global en la Península Ibérica. Aplicación al estudio de las tendencias de las series climáticas y de la expansión forestal

Methodological contributions for a better understanding of global change in the Iberian Peninsula. Application to the study of climate series trends and the forest expansion

_____

Mario Padial Iglesias

Junio de 2022

Directores:

Xavier Pons Fernández

Miquel Ninyerola Casals

Pere Serra Ruiz

Departament de Geografia

Facultat de Filosofia i Lletres

Universitat Autònoma de Barcelona

AGRADECIMIENTOS

AGRADECIMIENTOS

En primer lugar, agradecer a todas las personas que han prestado su apoyo y contribuido de alguna forma en esta tesis, un proceso que ha implicado varios años de experiencias, trabajo dedicado, alguna que otra incidencia, y unas horas de programación.

Agradecimientos a GRUMETS, por ofrecerme la oportunidad de trabajar en un grupo de referencia en el desarrollo de técnicas y aplicaciones basadas en SIG y teledetección. Agradecer la confianza inicial por parte de Xavier Pons, Miquel Ninyerola y Pere Serra a la hora de otorgar la beca FPI que ha sustentado mi pervivencia en estos cinco años de tesis y por el trabajo dedicado en el conformado de las investigaciones realizadas.

Agradecer al Ministerio de Ciencia, Innovación y Universidades (MCIU) por financiar esta tesis a través de la beca FPI BES-2016-078262 dentro del contexto del proyecto ACAPI ("Análisis del cambio global en la Península Ibérica: un laboratorio integrado del clima y las cubiertas del suelo 1950-2030") y del proyecto NEWFORLAND ("Los nuevos bosques ibéricos bajo el cambio global: Un enfoque multiescala").

Al Departament de Geografia de la Universitat Autònoma de Barcelona, por prestar los espacios necesarios para llevar a cabo los distintos trabajos realizados y las numerosas reuniones acometidas. Gracias Maria Antònia Casellas por tu apoyo, interés y buena gestión. Igualmente, a mis compañeros/as de doctorado por los buenos momentos compartidos, por las conversaciones e ideas recibidas.

A mis compañeras/os de despachos, Òscar González, Guillem Closa, Núria Cartes, Alaitz Zabala, Cristina Cea y Catalina Roca, tan importantes a la hora de debatir, comentar, reflexionar y buscar soluciones a las incidencias y problemáticas surgidas, contribuyendo significativamente en distintos momentos del desarrollo de esta tesis.

También a mis compañeros de casa, por estos años de intensa y muy enriquecedora convivencia, especialmente por la diversidad que siempre ha existido alrededor de la misma mesa y bajo el mismo techo.

Finalmente, agradecer a mi familia por aportarme toda una base experiencial y humana desde tempranas edades. La conexión con el medio natural, los ciclos naturales, plantación, recolección, el suelo y su estructura, …el trabajo dedicado y exigente desde aquel tiempo…todo ello ha servido para comprender procesos detectados remotamente mediante tecnologías de teledetección. Es en este punto donde el conocimiento experto y en parte vivencial, ha acompañado el desarrollo de esta tesis, tratando de aportar un poco de consistencia, la mejora de la certidumbre asociada a los datos elaborados en base a conocimientos tradicionales y experiencias vitales. A vosotros, en la distancia y tan cerca, desde siempre.

Gracias también a la vida, por aportar luz en momentos de menor *lucidez*.

ÍNDICE

ÍNDICE

RESUMEN / RESUM / SUMMARY

RESUMEN

Actualmente, los estudios sobre las dinámicas del clima y de los cambios de usos y cubiertas del suelo son fundamentales para identificar tanto la magnitud y la velocidad de lo que se ha dado en llamar cambio global, como las principales fuerzas impulsoras de dichos cambios. Dichas fuerzas no son homogéneas en el tiempo ni en el espacio, por lo que es importante conocer con detalle sus patrones espaciotemporales y los efectos que presentan sobre, entre otros, los ecosistemas naturales y agrarios. Asimismo, deben contemplarse no solamente aspectos de geografía física sino también factores socioeconómicos. Para realizar estos estudios en grandes territorios, pero con un nivel de detalle que no conlleve el riesgo de visiones superficiales, se requiere trabajar con conjuntos extensos de información (*Big Data*) que deben ser procesados adecuadamente (no toda aproximación es igual de válida). Por este motivo, es importante establecer soluciones metodológicas que corrijan problemas y maximicen la calidad de la información, previamente a ser ésta utilizada en análisis del cambio global.

La presente tesis tiene como objetivo principal contribuir al análisis de las dinámicas de cambio global en la Península Ibérica (PI) a través del estudio de las series temporales climáticas de las estaciones meteorológicas y de la expansión forestal a partir de información obtenida mediante teledetección. Para abordar este objetivo principal, previamente será necesario implementar estrategias para la mejora de la calidad de la información producida a partir de los sensores ya que esta será la que nos permitirá analizar las tendencias y generar las métricas para cuantificar los cambios y sus impactos.

En primer lugar, se evalúa el rendimiento y la influencia de diferentes métodos de relleno de datos faltantes a partir de las tendencias climáticas de la temperatura y la precipitación, identificando los patrones espaciotemporales a nivel peninsular, así como la aplicabilidad de los métodos a la hora de reducir las inconsistencias espaciotemporales en las superficies climáticas derivadas. Los distintos métodos de relleno muestran resultados similares cuando comparamos las tendencias temporales de cambio, pero, como indicaremos más abajo, con diferencias a nivel espacial, lo cual no es una aportación menor. Se observa también que el relleno conlleva una reducción de la variabilidad de las series climáticas, aunque se consigue operar con unos datos más homogéneos y comparables.

En segundo lugar, se desarrollan un conjunto de reglas de filtrado para poder ser aplicadas a áreas de verdad-terreno como paso previo a ejecutar procesos de clasificación de cubiertas del suelo a partir de datos de teledetección. Esta acción es necesaria cuando exista la posibilidad que dicha "verdad" contenga inconsistencias no menores, ni que sean semánticas con respecto a nuestros objetivos. Y ello es especialmente frecuente cuando dicha verdad-terreno se haya derivado de bases de datos auxiliares. El objetivo último en este caso es obtener una cartografía de cubiertas del suelo multitemporal de la máxima calidad y coherencia espaciotemporal. La aplicación de los filtros propuestos sobre áreas de verdad-terreno ha resuelto los errores más habituales asociados a las categorías naturales y agrícolas, mostrando un incremento substancial en la exactitud global de la cartografía obtenida.

Estas mejoras metodológicas permiten abordar con mayores garantías un análisis del cambio para importantes zonas de la PI. Así pues, se observa que las tendencias climáticas indican un incremento general de 1.45 °C en la temperatura media para toda la PI, pero un

patrón espacial más complejo para el caso de la precipitación. En cuanto a la expansión forestal, se analizan las dinámicas a lo largo de un gradiente latitudinal de gran amplitud (~185 km), representativo de la PI (desde el Pirineo a Sierra Nevada), aplicando también mejoras metodológicas para la extracción y filtrado de las ocurrencias de cambio, el muestreo y el análisis estadístico (*Boosted Regression Trees*), lo cual también permite reducir posibles sesgos en la interpretación de los resultados.

De la diversidad de resultados obtenidos, el principal factor determinante de la expansión forestal se ha relacionado con la distancia a áreas forestales preexistentes, indicando un proceso de densificación inicial y expansión forestal posterior. La expansión de las formaciones de especies caducifolias ha venido además condicionada por la disponibilidad hídrica y concretamente con la distancia a la red hidrográfica. En cambio, los bosques de frondosas perennifolias se han relacionado con factores topoclimáticos (precipitación, temperatura y radiación solar) en contextos de menor disponibilidad hídrica, al igual que los bosques de coníferas, favorecidos además por una mayor distancia a las capitales de provincia. Los factores mostraron variabilidad a lo largo de las regiones bioclimáticas y a nivel temporal, especialmente para caso de los pastizales. Las dinámicas de abandono agrícola fueron las principales causas de aparición de bosques en las regiones mediterráneas, mientras que los nuevos bosques asociados a la sucesión natural lo hicieron fundamentalmente en áreas de montaña mediterránea y eurosiberiana. Los factores inductores de expansión forestal han evidenciado una distribución espacial irregular, acorde a los requerimientos hídricos de los tipos fisionómicos forestales, además de una falta de estacionariedad en los factores determinantes, lo que indica que las fuerzas impulsoras operan de forma distinta a nivel espacial y temporal.

En conclusión, esta tesis aporta información novedosa sobre el cambio global y sus fuerzas inductoras derivada a partir de estrategias metodológicas robustas, también propuestas como novedades, muestra que el trabajo a escala detallada y la atención espacial y temporal son posibles y permiten análisis territoriales más ricos y rigurosos, y deja abiertas nuevas cuestiones y posibilidades de estudio para la ciencia, la planificación y la gestión de la PI.

RESUM

Actualment, els estudis sobre les dinàmiques del clima i dels canvis d'usos i cobertes del sòl són fonamentals per identificar tant la magnitud i la velocitat del que s'ha anomenat canvi global, com les principals forces impulsores dels canvis esmentats. Aquestes forces no són homogènies en el temps ni en l'espai, per això és important conèixer amb detall els seus patrons espaciotemporals i els efectes que presenten sobre, entre d'altres, els ecosistemes naturals i agraris. Així mateix, cal contemplar no només aspectes biogeogràfics sinó també factors socioeconòmics. Per realitzar aquests estudis en territoris amplis, però amb un nivell de detall que no comporti el risc de visions superficials, cal treballar amb conjunts extensos d'informació (Big Data) que han de ser processats adequadament (no tota aproximació és igual de vàlida). Per aquest motiu, és important establir solucions metodològiques que correqeixin problemes i maximitzin la qualitat de la informació, prèviament a ser utilitzada en l'anàlisi del canvi global.

Aquesta tesi té com a objectiu principal contribuir a l'anàlisi de les dinàmiques de canvi global a la península Ibèrica (PI) mitjançant l'estudi de les sèries temporals climàtiques de les estacions meteorològiques i de l'expansió forestal a partir d'informació obtinguda mitjançant teledetecció. Per abordar aquest objectiu principal, prèviament caldrà implementar estratègies per a la millora de la qualitat de la informació produïda a partir dels sensors, ja que aquesta serà la que ens permetrà analitzar les tendències i generar les mètriques per quantificar els canvis i els seus impactes.

En primer lloc, s'avalua el rendiment i la influència de diferents mètodes d'emplenament de dades que falten a partir de les tendències climàtiques de la temperatura i la precipitació, identificant els patrons espaciotemporals a nivell peninsular, així com l'aplicabilitat dels mètodes a l'hora de reduir les inconsistències espaciotemporals en les superfícies climàtiques derivades. Els diferents mètodes de rebliment mostren resultats similars quan comparem les tendències temporals de canvi però, com indicarem més avall, amb diferències a nivell espacial, cosa que no és una aportació menor. S'observa també que el farciment comporta una reducció de la variabilitat de les sèries climàtiques, encara que s'aconsegueix operar amb unes dades més homogènies i comparables.

En segon lloc, es desenvolupen un conjunt de regles de filtratge per poder ser aplicades a àrees de veritat-terreny com a pas previ a executar processos de classificació de cobertes del sòl a partir de dades de teledetecció. Aquesta acció és necessària quan hi hagi la possibilitat que aquesta "veritat" contingui inconsistències no menors, ni que siguin semàntiques respecte als nostres objectius. I això és especialment freqüent quan aquesta veritat-terreny s'hagi derivat de bases de dades auxiliars. L'objectiu últim en aquest cas és obtenir una cartografia de cobertes del sòl multitemporal de la màxima qualitat i coherència espaciotemporal. L'aplicació dels filtres proposats sobre àrees de veritat-terreny ha resolt els errors més habituals associats a les categories naturals i agrícoles, mostrant un increment substancial en l'exactitud global de la cartografia obtinguda.

Aquestes millores metodològiques permeten abordar amb més garanties una anàlisi del canvi per a importants zones de la PI. Així, doncs, s'observa que les tendències climàtiques indiquen un increment general de 1.45 °C en la temperatura mitjana per a tota la PI, però un patró espacial més complex per al cas de la precipitació. Quant a l'expansió forestal, s'analitzen les dinàmiques al llarg d'un gradient latitudinal de gran amplitud (~185 km),

representatiu de la PI (des del Pirineu a Sierra Nevada), aplicant també millores metodològiques per a l'extracció i el filtratge de les ocurrències de canvi, el mostreig i l'anàlisi estadística (*Boosted Regression Trees*), la qual cosa també permet reduir possibles biaixos en la interpretació dels resultats.

De la diversitat dels resultats obtinguts, el factor determinant principal de l'expansió forestal s'ha relacionat amb la distància a àrees forestals preexistents, indicant un procés de densificació inicial i d'expansió forestal posterior. L'expansió de les formacions d'espècies caducifòlies ha estat condicionada a més per la disponibilitat hídrica i concretament per la distància a la xarxa hidrogràfica. En canvi, els boscos de frondoses perennifòlies s'han relacionat amb factors topoclimàtics (precipitació, temperatura i radiació solar) en contextos de menor disponibilitat hídrica, igual que els boscos de coníferes, afavorits a més per una distància més elevada a les capitals de província. Els factors van mostrar variabilitat al llarg de les regions bioclimàtiques i temporalment, especialment per al cas de les pastures. Les dinàmiques d'abandonament agrícola van ser les causes principals d'aparició de boscos a les regions mediterrànies, mentre que els nous boscos associats a la successió natural ho van ser fonamentalment en àrees de muntanya mediterrània i eurosiberiana. Els factors inductors d'expansió forestal han evidenciat una distribució espacial irregular, d'acord amb els requeriments hídrics dels tipus fisionòmics forestals, a més d'una manca d'estacionarietat en els factors determinants, cosa que indica que les forces impulsores operen de manera diferent a nivell espacial i temporal.

En conclusió, aquesta tesi aporta informació nova sobre el canvi global i les seves forces inductores derivada a partir d'estratègies metodològiques robustes, també proposades com a novetats, mostrant que el treball a escala detallada i l'atenció espacial i temporal són possibles. També permeten anàlisis territorials més riques i rigoroses, i deixa obertes noves qüestions i possibilitats d'estudi per a la ciència, la planificació i la gestió de la PI.

SUMMARY

Currently, studies on climate dynamics and land use and land cover changes are essential to identify the magnitude and speed of what has been called global change and the main driving forces of these changes. These forces are not homogeneous in time or space, so it is important to know their spatiotemporal patterns and the effects they have on, among others, natural and agricultural ecosystems. Evenly, aspects of physical geography and socioeconomic factors must be considered. To carry out these studies in large territories, but with a level of detail that does not entail the risk of superficial visions, it is necessary to work with extensive datasets of information (Big Data) that must be appropriately processed (not every approach is equally valid). For this reason, it is important to establish methodological solutions that correct problems and maximize the quality of the information before it is used in the analysis of global change.

The main objective of this thesis is to contribute to the analysis of the dynamics of global change in the Iberian Peninsula (IP) through the study of the climatic time series of meteorological stations and the forest expansion dynamics based on information obtained through remote sensing. To address this objective, it will previously be necessary to implement strategies to improve the quality of the information produced from sensors since this information will allow us to analyze the trends and generate the metrics to quantify the changes and their impacts.

Initially, the performance and influence of different gap-filling methods are evaluated from the climatic trends of temperature and precipitation, identifying spatiotemporal patterns at the IP scale, and the applicability of methods to reduce spatiotemporal inconsistencies in derived climatic surfaces. The different gap-filling methods show similar results when we compare the temporal trends of change, but, as we will indicate below, with differences at the spatial level, which is not a minor contribution. It is also observed that the gap-filling entails a reduction in the variability of the climatic series, although, in return, it is possible to operate with more homogeneous and comparable data.

Secondly, filtering rules are developed to be applied to ground truth areas as a previous step to perform land cover classification processes from remote sensing data. This task is necessary when there is a possibility that this "truth" contains inconsistencies that are not minor, nor that they are semantic concerning our objectives. Moreover, this is especially frequent when this ground truth has been derived from auxiliary databases. The ultimate goal, in this case, is to obtain a multitemporal land cover mapping of the highest quality and spatiotemporal coherence. Applying the proposed filters to ground truth areas resolves the most common errors associated with natural and agricultural categories, showing a substantial increase in the overall accuracy of the cartography obtained.

These methodological improvements make it possible to address with greater guarantee analysis of change for important areas of IP. Thus, it is observed that climate trends indicate an overall increase of 1.45 °C in the mean temperature for all IP, but a more complex spatial pattern for precipitation. Regarding forest expansion, the dynamics along a latitudinal gradient of large amplitude (~185 km) and representative of the IP (from the Pyrenees to the Sierra Nevada mountain range) are analyzed, also applying methodological improvements for the extraction and filtering of the occurrence locations of change, the

sampling and statistical analysis (*Boosted Regression Trees*), which also allows reducing possible biases in the interpretation of the results.

From the diversity of results obtained, the main factor of the forest expansion has been related to the distance to previous forests, indicating a process of initial densification and subsequent forest expansion. The expansion of broadleaf deciduous forest formations has also been conditioned by water availability and specifically by the distance to the hydrographic network. On the other hand, broadleaf evergreen forests have been related to topoclimatic factors (precipitation, temperature, and solar radiation) in contexts of lower water availability, as well as coniferous forests, also favored by a greater distance from the provincial capitals. The factors showed variability across bioclimatic regions and at the temporal level, especially in the case of grasslands. The abandonment of agricultural activities was the leading cause of new forests' appearance in the Mediterranean regions, while the new forests related to natural succession dynamics occurred mainly in Mediterranean and Eurosiberian mountain areas. The driving factors of forest expansion have shown an irregular spatial distribution, according to the water requirements of the forest physiognomic types, in addition to a lack of stationarity in the inducing factors, which indicates that the driving forces operate differently at the spatial and temporal level.

In conclusion, this thesis provides novel information on global change and its driving forces derived from robust methodological strategies, also proposed as novelties, shows that working on a detailed scale and spatial and temporal attention is possible, allowing richer and more rigorous territorial analyses and leaving open new questions and possibilities of study for science, planning and management of the IP.

INTRODUCCIÓN

1. INTRODUCCIÓN

1.1. Análisis del cambio global en la Península Ibérica

Los cambios producidos en las cubiertas del suelo y sus implicaciones en el cambio global son un desafío importante para las ciencias humanas y medioambientales (Turner et al., 2007). De hecho, las dinámicas de las cubiertas del suelo son consideradas como uno de los procesos clave implicados en problemas ambientales como la eutrofización, la acidificación de suelos y masas de agua, la desertificación, la pérdida de suelo, la pérdida de biodiversidad, el efecto invernadero o el cambio climático en si mismo (Briassoulis, 2020). De ahí la relevancia de su estudio.

Los ecosistemas terrestres mediterráneos son considerados laboratorios de referencia para llevar a cabo investigaciones sobre los procesos de cambio global en el territorio (Doblas-Miranda et al., 2015, 2017) debido a su clima transicional, la gran variabilidad espacial y temporal de sus condicionantes medioambientales, su extensa y única biodiversidad, así como su amplio rango de condiciones socioeconómicas. En este contexto, las principales formaciones vegetales (*e.g.*, pastizales, matorrales y bosques) han mostrado sensibilidad a diversas fuerzas inductoras de cambio, y especialmente a sus interacciones (Sala et al., 2000). En efecto, estos ecosistemas son especialmente sensibles a cambios atmosféricos globales debido a la naturaleza transicional entre regiones áridas y templadas, a una mayor aridez climática, a la mayor frecuencia, extensión e intensidad de incendios forestales o la degradación de los suelos y la escasez hídrica, entre otros impactos (Doblas-Miranda et al., 2017). Como resultado de esta heterogeneidad a distintas escalas en el territorio, así como el efecto de las perturbaciones y la gran variabilidad inter e intra-anual medioambiental, ha derivado en una biota singular y diversa, especialmente vulnerable al efecto del cambio climático (Malcolm et al., 2006).

La Península Ibérica (PI) es un área representativa dentro del contexto mediterráneo, de gran diversidad, valor ecológico y vulnerabilidad de sus ecosistemas terrestres. Su complejo relieve (con una elevación media alrededor de 635 m s.n.m. y más de 17 380 km² por encima de 1 500 m s.n.m.) crea un mosaico climático heterogéneo, que se combina con gradientes topoclimáticos en las cadenas montañosas (Ninyerola et al., 2000). Este contexto es una zona de especial interés para estudios de cambios de usos y cubiertas del suelo, como por ejemplo el análisis del incremento forestal (del Barrio et al., 2010; Hill et al., 2008) asociado a procesos de abandono de las tierras de cultivo, especialmente en áreas de montaña (MacDonald et al., 2000; Bielsa et al., 2005; Serra et al., 2008; Lasanta et al., 2017; Vilà-Cabrera et al., 2017). Al igual que ha sucedido en otras regiones de Europa, la PI se ha visto afectada por el fenómeno del abandono rural, generando dinámicas poblacionales hacia grandes ciudades que han dejado atrás territorios rurales, especialmente aquellas con escaso valor para la agricultura (Loidi, 2017). De otro lado, a pesar de que los datos indican un incremento progresivo de la cubierta forestal durante el siglo pasado, los datos oficiales no proporcionan suficiente información sólida para determinar el patrón espaciotemporal de este incremento, la interacción con otros procesos, además de sus posibles factores impulsores. Las aproximaciones que abarcan grandes áreas geográficas de la PI son aún limitadas (Palmero-Iniesta et al., 2021; Vidal-Macua et al., 2018). Por tanto, existe la necesidad de generar estudios que cubran áreas de territorio extensas para conocer los factores implicados en la expansión forestal desde una perspectiva espacial y temporal más

amplia, como es la que esta Tesis aborda, aportando nuevos datos especialmente de interés para la definición de estrategias de gestión y planificación del paisaje a medio y largo plazo. En este contexto la teledetección satelital proporciona información espaciotemporal crucial que permite cartografiar las transformaciones históricas de los usos y cubiertas del suelo, a una resolución espacial y temática elevada (Zhu and Woodcock, 2014; Sishodia et al., 2020; Calderón-Loor et al., 2021). No obstante, esta información no siempre está disponible, o no con la calidad y coherencia necesarias (Mantovani and Setzer, 1997).

1.2. Relevancia y necesidad de la generación de información de detalle

Históricamente el progreso de los cambios de usos y cubiertas del suelo fue coordinado, entre 1994 y 2005, a través del proyecto "*Land Use and Land Cover Change* (LUCC)", conjuntamente con otros programas internacionales, sirviendo como punto de partida de otras iniciativas globales y regionales, como el "*GlobCover*" de la Agencia Europea del Espacio, ESA, a 300 m de resolución (Arino et al., 2008), o el "*LCLUC Program*" de la NASA (Justice et al., 2015). Desde el año 2006, el "*Global Land Project*" dio continuidad al proyecto LUCC, con el objetivo de sintetizar conocimientos y metodologías de investigación, a la vez que identificar prioridades científicas (Verburg et al., 2015). Entre los principales desafíos que afrontó dicho proyecto, destacamos (i) mejorar la comprensión de la interacción compleja entre los componentes sociales y ambientales del sistema integrado de las cubiertas del suelo, y (ii) ampliar la comprensión de procesos a nivel local y regional para alcanzar la comprensión a nivel global (Rounsevell et al., 2012). En consecuencia, se fue gestando un nuevo campo de investigación denominado *Land Change Science* (LCS), que buscaba mejorar la comprensión de los patrones y dinámicas de cambios de usos y cubiertas del suelo que afectan la estructura y función del sistema Tierra (Gutman et al., 2004). Esta perspectiva requería de la integración de los aspectos sociales o humanos con los subsistemas naturales o biofísicos, así como con la Ciencia de la Información Geográfica. Por otro lado, las interacciones existentes entre los subsistemas biofísicos y humanos, implicaban involucrar a científicos de distintas ramas de las ciencias naturales, sociales y espaciales, para desarrollar trabajos de investigación y solventar, entre otros, problemas metodológicos relacionados con la fusión de diferentes tradiciones analíticas (Rindfuss et al., 2004). Este carácter multidisciplinar ha sido motivado por el creciente interés en identificar los factores impulsores y sus impactos, las interacciones socioambientales, así como la conexión entre distintas regiones del planeta, o a escala más local, entre las ciudades y su entorno rural más próximo. Además, esta perspectiva socioecológica ha derivado en una mayor consciencia sobre las interacciones humanas con el medio natural, a través, por ejemplo, de la gestión del territorio y de la provisión de servicios ecosistémicos (Alcaraz-Segura et al., 2013; Grêt-Regamey and Weibel, 2020). Hoy en día, la LCS se considera un campo consolidado que ha producido una riqueza de innovaciones metodológicas, centrándose en el monitoreo y la descripción de patrones de cambios de usos y cubiertas del suelo, identificando sus impulsores y entendiendo sus relaciones (Rindfuss et al., 2008; Magliocca et al., 2015).

La continuidad de estos estudios, iniciados en la década de 1990 del siglo pasado, requiere de la generación de mapas de usos y cubiertas del suelo, base de estudios de las dinámicas del territorio a mayor nivel de detalle. En este sentido, la Ciencia de la Información Geográfica, incluyendo disciplinas como la teledetección desde satélite y el análisis espacial, ha demostrado ser eficaz en la generación de cartografía temática histórica para caracterizar

el estado de las cubiertas a mayor resolución espacial, temporal y temática que antaño, además de su efectividad a la hora de realizar análisis de cambios entre momentos temporales. Estos estudios, además, requieren de un conjunto de variables predictoras (socioeconómicas o biofísicas), así como de metodologías de modelización estadística que relacionen las dinámicas con un conjunto de predictores. Todo ello en un contexto que requiere la gestión de cada vez mayores volúmenes de datos debido al interés en el análisis de áreas de estudio más amplias con un nivel de resolución espacial suficientemente elevado como para poder capturar los cambios de forma consistente.

1.3. Generación de variables en la era *Big Data*

La revolución digital se ha expandido de forma imparable entre distintas disciplinas y aspectos de nuestra vida. Actualmente, la cantidad de información que se genera dobla su volumen de año en año (Helbing et al., 2019; Efthymiou–Egleton et al., 2020), lo que además ha venido acompañado de un incremento en la capacidad de procesamiento computacional (*e.g.*, paralelización de procesos), permitiendo que algoritmos de inteligencia artificial y aprendizaje automático sean capaces de procesar de forma eficiente enormes volúmenes de información. Dentro del contexto de la Ciencia de la Información Geográfica (*Geographic Information Science, GIScience*), el incremento de la información geográfica disponible ha contribuido en gran medida a una mayor capacidad de análisis de, entre otros, los procesos naturales, así como el abordaje de su relación con las dinámicas antrópicas. Para ello, instituciones públicas y organizaciones privadas han contribuido en gran medida a una mayor democratización de la información, favoreciendo su acceso libre. Además, el desarrollo e instalación de nuevos sensores *in-situ* y *ex-situ* han propiciado la generación de cada vez más extensas y sólidas bases de datos.

En las últimas décadas, la puesta en órbita de un mayor número de sensores a bordo de plataformas satelitales ha propiciado mejoras en la resolución espacial, temporal, espectral y radiométrica de las imágenes. Además, el compromiso de dar continuidad temporal a proyectos consolidados de teledetección espacial ha permitido la generación de extensas bases de datos históricas, como la del programa Landsat. Este programa se basa en una constelación operada por la Administración Nacional de Aeronáutica y el Espacio (NASA), cuya producción y comercialización de imágenes es gestionada por el Servicio Geológico de los Estados Unidos (USGS), que provee de forma gratuita desde 2008 su repositorio de imágenes (Woodcock et al., 2008). A ello se suma la reciente puesta en órbita del nuevo satélite Landsat 9 en septiembre del 2021. Esta larga trayectoria constituye una de las misiones más longevas (desde 1972 hasta la actualidad) de imágenes captadas sobre la superficie terrestre—un repositorio integrado por más de diez millones de imágenes, de hasta 11 bandas espectrales distintas y con una resolución máxima de 15 m. Otras iniciativas, como las llevadas a cabo por la Comisión Europea (CE) junto con la Agencia Europea del Espacio (ESA), complementan la constelación Landsat a través de instrumentos Sentinel del programa Copernicus, particularmente los Sentinel 2. Además, la ESA ha proporcionado una nueva colección de imágenes del Landsat *Multispectral Scanner System* (MSS), para Europa y norte de África, lo que amplía el repositorio de imágenes disponibles particularmente para los primeros años de la misión Landsat (Northrop et al., 2017).

A nivel de sensores *in-situ*, otras iniciativas de colaboración internacional han creado y mantienen extensas bases de datos climáticas internacionales de libre acceso, como es el caso del *Global Historical Climatology Network* (GHCN) gestionada por la NOAA (*National*

Oceanic and Atmospheric Administration). En 2022 esta base de datos contiene más de 119 000 estaciones distribuidas por más de 218 países y territorios, aportando datos diarios de las variables de precipitación y temperatura, convirtiéndose en un recurso de interés para el desarrollo de investigaciones en distintas disciplinas (Jaffrés, 2019). Además, otras organizaciones a escala estatal o regional son proveedoras de series temporales de datos climáticos como son la Agencia Estatal de Meteorología, (AEMET) de España, el Sistema Nacional de Informação de Recursos Hídricos, (SNIRH) de Portugal o el Servei Meteorològic Nacional de Andorra (SMN). Para el caso de la AEMET, la agencia proporciona una extensa red de estaciones meteorológicas, compuesta por más de tres mil estaciones con registros históricos de temperatura y algo más de seis mil de precipitación. A éstas se añaden, para el contexto ibérico, las de Andorra y Portugal, ampliando en algo más de cien las estaciones disponibles con datos de temperatura y de setecientas de precipitación.

Por otro lado, en cuanto a la información socioeconómica, a escala europea, cada diez años se realiza el Censo de Población y Viviendas y el Censo Agrario, recopilando información sobre las principales características (geográficas, demográficas, sociales, económicas y agrarias) de un país, que abarca desde las divisiones geográficas más locales (*e.g.*, secciones censales) hasta los niveles nacional e internacional. Los censos se basan en la legislación estadística europea que establece qué estadísticas clave, datos y metadatos deben producir los países de la Unión Europea. En este sentido *Eurostat*, la oficina estadística de la CE, es la responsable de definir el marco legislativo para los censos en el contexto europeo, armonizando las estadísticas para hacerlas comparables. El Instituto Nacional de Estadística (INE) de España provee de los Censos de Población y Viviendas para los años de referencia 1991, 2001 y 2011, estando los datos de 2021 pendientes de finalización a fecha de esta Tesis. Además, se dispone de los Censos Agrarios de España para los años 1982, 1989, 1999, 2009 y 2020, este último recientemente publicado en mayo de 2022.

Toda esta extensa cantidad de información disponible (imágenes de satélite, series climáticas, información socioeconómica), exige un compromiso claro por parte del investigador de hacer un uso adecuado de los datos, desde su adquisición, pasando por el tratamiento ordenado de los mismos empleando un marco metodológico consistente, hasta su posterior utilización en modelos estadísticos, todo ello para la obtención de resultados lo más fiables y robustos posible.

1.3.1. Usos y cubiertas del suelo

Tal como se ha introducido, el análisis de los cambios sobre el territorio precisa de la caracterización del estado de las cubiertas en distintos momentos temporales. Para ello, la teledetección permite derivar esta información como fase previa a cualquier análisis multitemporal de las dinámicas de los usos y cubiertas del suelo. Es importante tener en cuenta que la fiabilidad temática de la cartografía obtenida influenciará decisivamente en la calidad de los resultados obtenidos en los modelos estadísticos, lo que repercutirá finalmente en el análisis y en la toma de decisiones (Fuller et al., 2003).

Así pues, la producción cartográfica requiere de áreas de verdad-terreno fiables, consistentes espacial y temporalmente para abordar cartografías de grandes áreas de territorio (Amani et al., 2019). A diferencia de lo que ocurría hace años no en raras ocasiones, cuando se aceptaba acríticamente la veracidad de tales áreas, actualmente existe un mayor conocimiento sobre la incidencia de los errores en las áreas de entrenamiento, y

particularmente sobre los algoritmos de aprendizaje automático (Elmes et al., 2020). A fin de reducir su afectación y mejorar la calidad temática de los mapas se requieren estrategias de control de calidad aplicables sobre las áreas de verdad-terreno, más aún cuando se derivan a partir de bases de datos preexistentes, como pueden ser el Sistema de Información sobre Ocupación del Suelo de España (SIOSE), o la base de datos *CORINE Land Cover*, entre otros. Habiendo constatado tales errores y sus efectos en nuestros trabajos, una parte del empeño de esta Tesis se puso en el diseño de filtros basados en el índice de Vegetación de la Diferencia Normalizada (*Normalized difference vegetation index*, NDVI), de las propias imágenes, los cuales se mostraron particularmente eficaces a la hora de reducir errores típicos asociados a la escala, errores de asignación, o diferencias interanuales e intraanuales entre las imágenes y la base de datos auxiliar utilizada. La elección del NDVI no es fruto de la casualidad ni de un deseo de simplificación, sino del hecho incontestable que, con la excepción de sensores simplemente en color natural, es el más potente del denominador espectral común de los sensores disponibles en teledetección. Para ello se diseñó un banco de pruebas sobre distintos contextos geográficos y momentos temporales, derivando áreas de verdad-terreno de la base de datos SIOSE y empleando el clasificador *k-nearest neighbor* (*kNN*) para evaluar la funcionalidad de las reglas.

Detalles sobre las estrategias de filtrado, se abordan de forma extensa en el artículo 2 de la Tesis. Estas estrategias se han empleado en el artículo 3 en la generación de mapas de cubiertas y de sus capas de incertidumbre asociadas. Además, parte de las clasificaciones generadas en esta Tesis, pueden consultarse a través del servidor web del 'e-Laboratorio del cambio global de la Península Ibérica', accesible desde https://www.ogc3.grumets.cat/acapi/wms/USOS.

1.3.2. Variables climáticas

Las variables climáticas son de interés a la hora de evaluar las dinámicas de las cubiertas vegetales, ya que determinan la producción biológica, los patrones de distribución de especies o las dinámicas entre cubiertas, jugando un papel relevante en un contexto de cambio climático. Para su generación, se requiere una red suficientemente densa (bastante en un territorio como la PI) de estaciones meteorológicas que recopilen información histórica, así como estrategias de interpolación espacial (como la regresión múltiple con corrección de residuos, s*plines,* inverso de la distancia ponderada o *kriging*) para derivar superficies espacialmente continuas (Ninyerola et al., 2007). Estas superficies permiten determinar el estado de la variable en cada momento temporal. No obstante, la existencia de series temporales incompletas genera discontinuidades en las superficies derivadas, generando inconsistencias espaciotemporales más evidentes cuando se comparan distintas fechas (*e.g.*, tasa de cambio) o cuando se requieren métricas (*e.g.*, velocidad del clima) en distintos momentos temporales (Loarie et al., 2009; Dobrowski et al., 2013; Brito-Morales et al., 2018). A modo de ejemplo, solo el 30 % de la estructura de la base de datos de temperatura media mensual corresponde a observaciones reales (periodo 1950–2019), porcentaje que se eleva hasta el 35 % para el caso de la precipitación acumulada mensual en la PI. Debido a esta problemática, se han analizado distintas estrategias de relleno de datos faltantes con el objetivo de (i) evidenciar el efecto del relleno de series sobre las tendencias climáticas, y con ello (ii) estudiar la identificación de los patrones espaciotemporales existentes, además de (iii) reducir las discontinuidades espaciotemporales de las superficies derivadas para mejorar la definición de las variables

climáticas en la modelización estadística. Estas mejoras benefician la generación de variables de estado y variables dinámicas climáticas, en estudios de dinámicas de las cubiertas u otros relacionados. Estos aspectos de detallan ampliamente en el artículo 1 de la Tesis.

1.3.3. Variables socioeconómicas

La influencia de la actividad antrópica sobre las dinámicas de cubiertas, así como su interacción con otras variables (Müller et al., 2013; Doblas-Miranda et al., 2017; Vidal-Macua et al., 2017), se estableció a partir de un conjunto de predictores derivados de los censos históricos de Población y Viviendas y de los Censos Agrarios, disponibles a nivel municipal y conformadas en bases de datos espaciales.

Se consideraron relevantes las variables de los Censos de Población, tales como el número total de habitantes, la densidad de población, así como la estructura de edad de la población (porcentaje de población menor de 16 años, entre 16-64 años, o mayor de 65 años), el índice de envejecimiento (porcentaje que representa la población mayor de 65 años sobre la población menor de 16 años) y la estructura de la población ocupada por sectores. A partir de los Censos Agrarios se incluyeron variables tales como el número unidades de trabajo año, el número de explotaciones agrarias, el número de unidades ganaderas y la superficie agraria útil. Es posible acceder a parte de las variables socioeconómicas recopiladas a través del servidor web del 'e-Laboratorio del cambio global de la Península Ibérica', accesible desde https://www.ogc3.grumets.cat/acapi/wms/SOCIO/.

1.3.4. Otras variables explicativas

De forma sintética, se describen a continuación otros factores potencialmente explicativos de las dinámicas de las cubiertas analizadas.

- Variables topoclimáticas: la pendiente, la curvatura del terreno y la radiación solar se derivaron de un modelo digital de elevaciones (MDE) a 10 m de resolución obtenido a partir de datos LiDAR que proporciona el Plan Nacional de Ortofotografía Aérea (PNOA). Además, se establecieron otras variables de estado climáticas (temperatura media y precipitación acumulada, número de episodios de sequía, y número de episodios húmedos) generadas específicamente para cada periodo temporal de análisis.
- Distancias y accesibilidad: constituidas por la distancia euclidiana a las áreas forestales preexistentes, la distancia a la red hidrográfica y la distancia a las áreas protegidas (Parques nacionales y parques naturales, declarados para cada periodo de análisis). Además, se incluyeron las variables de coste de distancia a las áreas urbanas, a las capitales de provincia, y a las carreteras principales y carreteras secundarias, consideradas estáticas al no existir una influencia temporal en la evolución de las redes de transporte consideradas.
- Geología: permite caracterizar el substrato litológico, en función de su acidez, alcalinidad y neutralidad en base a los principales grupos litológicos. Además, de forma novedosa se ha incluido como variable de estado la "erosión potencial (laminar y en regueros)" que proporciona el Inventario Nacional de Erosion de Suelos (INES).

Adicionalmente se elaboró una base de datos histórica de perímetros de incendios forestales ocurridos en la PI, a través de la recolección y homogenización de la información

facilitada por las administraciones locales de cada Comunidad Autónoma, así como de Portugal. Esta información se ha utilizado para enmascarar las posiciones que han sufrido incendios y, por tanto, siendo de gran utilidad para el análisis de la expansión forestal. Detalles adicionales de las variables descritas y las fuentes utilizadas se describen en los materiales suplementarios del artículo 3.

1.4. Objetivos e Hipótesis

El objetivo general de la Tesis es contribuir al análisis de las dinámicas de cambio global en la PI a través del estudio de las series temporales climáticas de las estaciones meteorológicas y de la expansión forestal a partir de información obtenida mediante teledetección. Para abordar este objetivo principal, previamente será necesario implementar estrategias para la mejora de la calidad de la información producida a partir de los sensores ya que esta será la que nos permitirá analizar las tendencias y generar las métricas para cuantificar los cambios y sus impactos. Las estrategias metodológicas se centran, por un lado, en la mejora de la calidad de la información generada (variables predictoras y mapas de usos y cubiertas del suelo) y, por otro lado, en la propuesta de mejoras previas a la modelización estadística de las dinámicas de las cubiertas, aplicadas concretamente en el análisis de la expansión forestal.

Del objetivo general se vertebran los siguientes objetivos específicos:

1. Conocer y aplicar métodos avanzados para la generación de variables, su recopilación para el sistema de la PI en el período 1987-2017 (dinámicas de cubiertas) y 1950-2019 (dinámicas climáticas).

> 1.1. Completar la espacialización de los datos climáticos.
> 1.2. Generar mapas de cubiertas del suelo mediante teledetección espacial.
> 1.3. Generar una base de datos socioeconómica y su cartografía asociada.

2. Investigar las dinámicas de cambio global en lo que se refiere a series climáticas y a expansión forestal.

> 2.1. Investigar la repercusión de distintos métodos de relleno de series climáticas en las tendencias del clima, así como los principales patrones climáticos observados con dichos métodos.
> 2.2. Investigar las principales fuerzas inductoras de la expansión forestal en relación con la actividad antrópica, la dinámica del clima y otros factores físicos y socioeconómicos.

Se plantean a continuación las siguientes hipótesis de trabajo subyacentes a los objetivos anteriores:

- (H_0) Existen estrategias metodológicas que permiten mejorar: (i) la generación de variables predictoras, especialmente las climáticas, afectadas por la existencia las series temporales incompletas; (ii) la fiabilidad de las áreas de verdad-terreno utilizadas en la producción cartográfica (básicamente rechazando las que no parecen fiables en base a criterios objetivables); (iii) la representatividad de las muestras utilizadas en el análisis de las dinámicas territoriales, y en particular de la expansión forestal.

Se parte de la base experimental en la que se identificaron distintas problemáticas en las fases exploratorias: inconsistencias espaciotemporales en las superficies climáticas, errores

recurrentes en la definición de las áreas de verdad-terreno derivadas de bases de datos auxiliares, e incertidumbre en la calidad, el tamaño y la representatividad espacial de las muestras de las trayectorias de cambio evaluadas.

De la hipótesis general, se derivan otras específicas.

- (H$_1$) La diferencia en la estructura espaciotemporal de las variables de temperatura y precipitación genera que los métodos de relleno de datos faltantes respondan de forma diferente en cuanto a la configuración de parametrizaciones y las tendencias a largo plazo observadas.

Se parte de la hipótesis de que estructuras de bases de datos claramente diferentes (temperatura y precipitación) presenten respuestas también diferentes en cuanto a parametrizaciones y las tendencias, por lo que se analizarán separadamente.

- (H$_2$) Es posible diseñar estrategias de aplicabilidad general que permitan mejorar la selección de áreas de verdad-terreno de calidad para ser utilizadas en la producción cartográfica. Existe relación entre la tipología de error y la categoría temática implicada.

Se parte de la necesidad de reducir la afectación de errores recurrentes en las áreas de verdad-terreno candidatas extraídas de bases de datos auxiliares. Se considera que cada categoría se ve afectada por tipologías concretas de error o por inconsistencias.

- (H$_3$) Un gradiente latitudinal suficientemente ancho a lo largo de toda la PI (transecto) permitiría revelar los diferentes patrones espaciotemporales en cuanto al origen de los principales factores implicados en la expansión forestal de la PI, especialmente a partir del abandono agrícola. Se considera que este gradiente, si no explica todos los procesos peninsulares, sí que al menos debiera arrojar luz sobre gran parte de ellos debido al detalle espacial y la variabilidad de situaciones que cubre.

Se parte de la hipótesis de que la expansión forestal se ha producido de forma ubicua (espacialmente) en a lo largo de todo el transecto, operado inicialmente por procesos de abandono agrícola en áreas rurales aisladas (primer periodo), y un proceso de expansión forestal relacionado con dinámicas de sucesión ecológica (segundo periodo). Los factores determinantes de la expansión forestal presentan una distribución desigual en el transecto.

1.5. Estructura de la Tesis

La estructura de la Tesis se compone de tres artículos científicos orientados a (i) la mejora en la definición de las variables de estado climáticas y las consecuencias informacionales de abordar dicha mejora a través de diferentes aproximaciones, (ii) la obtención de mapas de usos y cubiertas de alta calidad temática, y (iii) el análisis de las dinámicas de la expansión forestal a lo largo de un amplio transecto Norte-Sur en la PI. Por tanto, la coherencia temática de la Tesis queda establecida de acuerdo con el siguiente orden de los artículos desarrollados:

(i) *Does the gap-filling method influence long term (1950–2019) temperature and precipitation trend analyses?* Como principal objetivo, se trata de evaluar el rendimiento y la influencia que presentan diferentes métodos de relleno de datos faltantes sobre las tendencias climáticas a largo plazo, así como sobre los patrones espaciotemporales. Por tanto, también se realiza un primer análisis de las tendencias climáticas de la

temperatura y la precipitación en el contexto peninsular bajo el paradigma de una visión basada en un gran número de estaciones con series completadas. Para ello se analizan diversas metodologías de mejora centradas en la minimización de la afectación de los datos faltantes en la generación de superficies continuas de las variables climáticas.

(ii) *A Framework of Filtering Rules over Ground Truth Samples to Achieve Higher Accuracy in Land Cover Maps*. Este trabajo se centra en el desarrollo y aplicación de un conjunto de estrategias de filtrado para la mejor selección de áreas verdad-terreno derivadas de bases de datos auxiliares, evitando el uso de datos erróneos y consiguiendo con ello mapas de cubiertas de mayor calidad. El estudio identifica las principales fuentes de error vinculadas al uso de imágenes de teledetección con bases de datos auxiliares proveedoras de áreas verdad-terreno.

(iii) *Driving forces of forest expansion dynamics across the Iberian Peninsula (1987–2017): A spatio-temporal transect*. Este estudio identifica las principales trayectorias de expansión forestal a lo largo de las distintas regiones bioclimáticas definidas en un transecto Norte-Sur de anchura Landsat (185 km) en la PI. Asimismo, también identifica los principales factores implicados y sus patrones espaciotemporales. Con ello el artículo aúna los esfuerzos de generación/recopilación de un amplio tipo de variables, la obtención de mapas de usos y cubiertas del suelo espacial y temporalmente coherentes, y contribuye metodológicamente al análisis ordenado y consistente de las dinámicas, empleando métodos estadísticos robustos (*Boosted Regression Trees*) que, por primera vez son previamente sometidos a un filtrado basado en parámetros como la incertidumbre por píxel obtenida en la fase de clasificación digital de las imágenes y otros estrategias. Dicho filtrado permite realizar una aproximación más robusta que en otros trabajos en que no se presta tanta atención al filtrado de los datos.

1.6. Metodología

La metodología de trabajo ha implicado una primera fase de generación y recopilación de variables de estado, incluyendo nuevos datos climáticos para la región de Portugal que dan continuidad espaciotemporal a la base de datos ya disponibles; además, la recopilación de información socioeconómica a nivel municipal a partir de los Censos de Población (1981, 1991, 2001 y 2011) y los Censos Agrarios (1982, 1989, 1999 y 2009) del Instituto Nacional de Estadística (INE), y generación de la cartografía asociada. Se realizó la adaptación de bases cartográficas aportadas por el Registro Central de Cartografía del Instituto Geográfico Nacional, a las fechas de referencia de cada Censo Agrario, a fin de reducir el error de asignación, en tiempos pretéritos, de datos del INE a unidades administrativas no existentes (o geográficamente diferentes) hoy en día.

En cuanto a las variables climáticas se refiere, se consideraron series de temperatura media y precipitación acumulada mensual comprendidas entre 1950–2019 y caracterizadas por una alta variabilidad en el número de observaciones y de fechas de inicio y fin entre las que se recopilaron. Esta irregular distribución espaciotemporal de observatorios y observaciones ha generado un mosaico irregular de datos faltantes en la estructura de la base de datos climática. A ello se suma, además, la pérdida de datos puntuales debido a otros motivos, como son la aplicación de filtros para la exclusión de valores anómalos. Así, se exploraron cuatro métodos de relleno de datos faltantes implementados en el módulo *Emmental* incluido en la versión 9.1 de MiraMon (Pons, 2004), que incluye un método univariado

(autocoherente), y tres métodos multivariados en los que el valor faltante se aproxima en base a las observaciones de las estaciones vecinas próximas (métodos espaciales). Los métodos utilizan distintas aproximaciones a la hora de imputar el valor faltante: la media o moda local (MONTH); la asignación del valor faltante a partir de la identificación de la estación próxima con mayor similitud estadística respecto a la serie problema (menor "error cuadrático medio" (RMSE) o mayor "coeficiente de determinación", R^2) (SIMILAR); el uso de modelos de regresión múltiple empleando un conjunto de regresores (REGR); y, finalmente, el promediado de los valores más próximos ponderados por el inverso de la distancia (IDW). Las tendencias climáticas fueron evaluadas a partir de métricas no paramétricas para la estimación de la magnitud de la tendencia (Sen, 1968; Theil, 1992) y su significación (Kendall, 1975; Mann, 1945). *Scripts* basados en los lenguajes de programación de Matlab, del software R y de MiraMon 9.1 se emplearon para llevar a cabo este análisis. Detalles de las metodologías empleadas se describen ampliamente en el artículo 1.

La fase de producción cartográfica tuvo un peso importante en la Tesis debido a la extensa dedicación temporal dedicada a la obtención de cartografía histórica de elevada exactitud temática, espacial y temporalmente coherente. Ello implicó la descarga y procesamiento de las imágenes, su corrección radiométrica, la generación de índices espectrales (*Normalized Difference Vegetation Index*, NDVI, y *Normalized Difference Water Index*, NDWI) y de otras variables topográficas empleadas como variables auxiliares en la clasificación. Se obtuvieron distintas bases de datos auxiliares, del Sistema de Información sobre Ocupación del Suelo de España, (SIOSE, 2005, 2009, 2011, 2014), lo que sirvió para obtener áreas de verdad-terreno candidatas. En base al análisis de la firma espectral y temporal de las áreas candidatas, se identificaron y analizaron distintos tipos de errores e inconsistencias, que sirvieron de base para la definición de cinco reglas de filtrado basadas en el NDVI de las propias imágenes empleadas en la clasificación. Su efectividad se puso de manifiesto a partir de las clasificaciones obtenidas mediante el algoritmo *kNN*, el cual calcula la distancia euclidiana entre cada píxel a clasificar y los pixeles de referencia asignados a una categoría. Posteriormente se consideran los *k* vecinos más próximos, cuyo valor modal determina la categoría temática que se asigna al píxel a clasificar. Además, la implementación de MiraMon provee de métricas de calidad como la *incertidumbre* con la que cada píxel es clasificado de acuerdo con las áreas de entrenamiento derivadas. Se emplearon ortofotografías del Plan Nacional de Ortofotografía Aérea, (PNOA), e información sobre la composición de las especies forestales de las parcelas inventariadas en las bases de datos del Inventario Forestal Nacional (IFN) en la supervisión de la calidad de las áreas obtenidas. Información más detallada de las reglas de filtrado se describen en el artículo 2.

A pesar de los esfuerzos a la hora de definir áreas de verdad-terreno de calidad para cada categoría, generalmente existen situaciones en las cuales se combinan señales espectrales mixtas, como por ejemplo en los píxeles de borde entre categorías, cuya afectación se hace más manifiesta, si cabe, cuando existen errores geométricos entre las imágenes utilizadas, más evidentes éstos, cuanto más antiguas son las imágenes. Ello es algo que todo investigador en esta área debe tener presente.

Durante la fase de generación cartográfica, los principales errores puntuales detectados se asociaron a la existencia de píxeles clasificados como categorías agrícolas (leñosas de secano) en áreas ajenas a cultivos agrícolas (zonas urbanizadas, cubiertas naturales), o píxeles clasificados como suelo urbano en áreas ajenas a áreas antropizadas. Para resolver estas inconsistencias, se diseñaron estratégicas semiautomáticas que permitían clasificar

aquellas localizaciones problema, excluyendo la categoría temática problema de las áreas de entrenamiento. Por ejemplo, píxeles erróneos de 'suelo urbano' distribuidos generalmente sobre cubiertas naturales, se clasificaron excluyendo la categoría 'suelo urbano' de las áreas de entrenamiento. Como resultado, estas áreas resultaron clasificadas correctamente como suelo desnudo, categoría con la que suelo urbano presenta similitud espectral. De otro lado, a lo largo de los bordes de los cursos fluviales y embalses se producía una mezcla de respuestas espectrales asociadas con las oscilaciones en el nivel del agua a lo largo del año, resultando clasificadas con categorías diversas, distintas a masas de agua. Una solución simple fue aplicar una máscara de agua que aunara las máscaras individuales de cada imagen satélite utilizada en la clasificación, empleando para ello el *Normalized Difference Snow Index*, (NDSI), índice que combina la banda del infrarrojo de onda corta y longitudes de onda del visible y que en este caso tiene una aplicación más allá de la cartografía de superficies innivadas. Por último, la aparición del efecto de "sal y pimienta" característico de las clasificaciones por píxel, se resolvió aplicando un filtro selectivo sobre aquellas agrupaciones menores a 3 píxeles contiguos, reasignados en base a la categoría modal determinada sobre una ventana de convolución de 3×3, una solución mucho más efectiva, más elegante y menos lesiva que los filtros de moda indiscriminados. De forma efectiva, estas soluciones permitieron corregir los errores puntuales ocurridos sobre extensas áreas, como son las escenas Landsat, previamente a su utilización para el análisis de dinámicas de usos y cubiertas del suelo.

Una vez recopilada toda la información requerida para establecer un conjunto de variables predictoras, así como aunado el conocimiento para generar mapas de usos y cubiertas multitemporales de calidad, se aborda el análisis de los factores implicados en la expansión forestal a lo largo de un transecto Norte-Sur de Landsat sobre la PI en varios momentos separados en el tiempo.

De forma previa al análisis de la expansión forestal, se llevó a cabo una fase exploratoria que permitió investigar cuestiones tales como (i) la respuesta de distintos métodos estadísticos a las dinámicas de las cubiertas, (ii) el diseño de estrategias para la extracción de posiciones de cambio basadas en trayectorias consolidadas, o (iii) la aplicación de filtros de incertidumbre a las posiciones de cambio. Todo ello en el contexto de las escenas 200–030 y 200–031 caracterizadas con ocho clasificaciones temporales generadas (1982, 1987, 1992, 1997, 2002, 2007, 2012 y 2017) y diversas trayectorias de cambio evaluadas (intensificación agrícola, conversiones entre tipos fisionómicos de bosque, perturbaciones y expansión forestal). Este análisis exploratorio sirvió para establecer las bases metodológicas desarrolladas en el análisis de la expansión forestal que se describen a continuación.

El análisis de la expansión forestal a lo largo de un transecto Norte-Sur de Landsat (escenas 200-030 a 200-034) se dividió en tres fases: Una primera fase de generación de los mapas de usos y cubiertas (1987, 2002 y 2017, puesto que se consideró suficiente la visión basada en saltos de 15 años), empleando las metodologías desarrolladas en el artículo 2. Una segunda fase de extracción de posiciones de cambio y la aplicación de estrategias de muestreo: (i) la aplicación de filtros de incertidumbre (derivados de la cartografía temática), permitiría excluir del análisis posiciones que superaban un umbral determinado; (ii) el muestreo de las posiciones de ausencia de acuerdo a la densidad local de las presencias, reduciría el sesgo existente entre las posiciones de presencia y ausencia; (iii) la reducción de la autocorrelación espacial; (iv) la segmentación espacial en función de su caracterización bioclimática, que evitaría considerar posiciones de presencia y ausencia distantes y sin

relación espacial. Finalmente, se consideraron todas las trayectorias que parten de categorías de cultivos agrícolas y cubiertas naturales/seminaturales (6 categorías), que se convierten en bosques (3 categorías), desagregadas en ocho regiones bioclimáticas, y a lo largo de dos periodos, lo que implicó una considerable dimensionalidad del estudio (Figura 1).
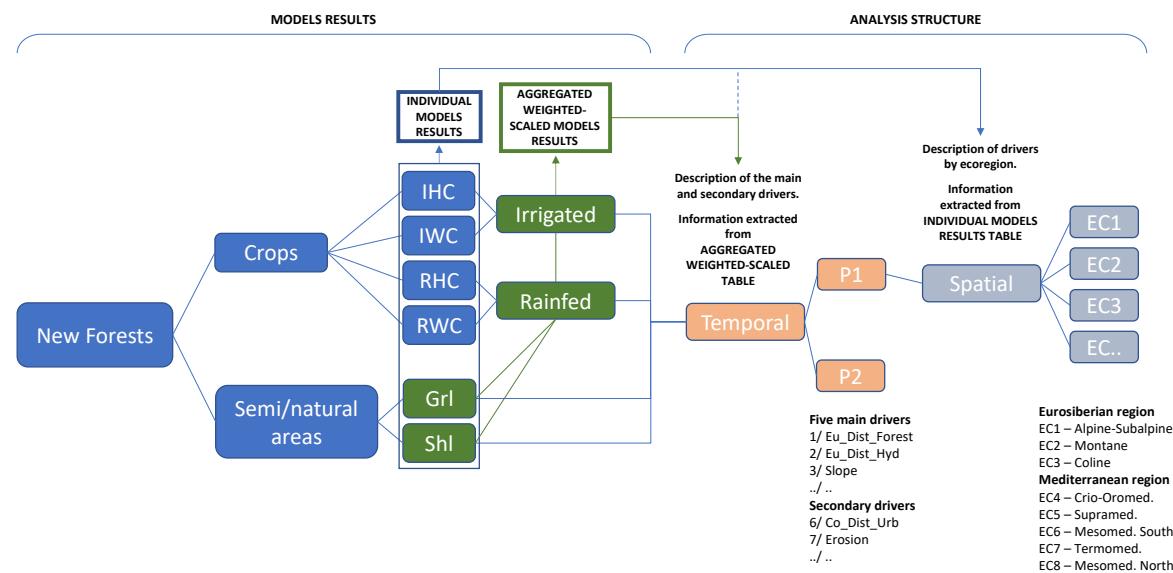
Figura 1. Esquema procedimental para el análisis de la expansión forestal.

De entre los distintos métodos estadísticos, una de las aproximaciones más ampliamente utilizadas en el análisis de cambios de usos y cubiertas del suelo se basa en la estimación de la función de la "regresión logística", que describe la probabilidad de ocurrencia de una categoría o la probabilidad de que en una localización se transicione desde una categoría a otra. No obstante, presenta limitaciones tales como la presunción de existencia de linealidad entre las variables predictoras y la variable respuesta, ya que, con frecuencia, los efectos presentan un comportamiento no lineal. A fin de relajar esta presunción, diferentes modelos no lineales han sido utilizados para describir los cambios de usos y cubiertas del suelo, por ejemplo, *generalized additive models* (Hastie and Tibshirani, 1990), o *artificial neural networks* (Pijanowski et al., 2002). Estas aproximaciones, no obstante, presentan limitaciones en el contexto de grandes volúmenes de datos (minería de datos). Un salto significativo que permite solventar estas limitaciones es la técnica *boosting*, que permite combinar múltiples modelos permitiendo un manejo más eficiente de grandes conjuntos de variables. Además, una variedad de modelos basados en técnicas de *machine learning* vienen siendo desarrolladas en el análisis de cambios de usos y cubiertas del suelo (Wang et al., 2022).

Otro tipo de técnicas son las basadas en árboles de decisión, que combinada con la técnica *boosting*, determina el algoritmo *boosted regression trees* (BRT) (Friedman, 2001). Esta técnica ha sido ampliamente utilizada por su alta capacidad de predicción y presenta ventajas respecto a otras aproximaciones: no asumen un tipo de distribución de los datos *a priori*, lo que facilita la interacción entre distintos tipos variables (binarias, cuantitativas discretas/continuas o variables categóricas con distintos niveles de clasificación); identifica los principales predictores y sus interacciones; permite representar gráficamente la relación entre la variable respuesta y los predictores (gráficas de dependencia parcial), mostrando las condiciones o el rango de valores de la variable donde es más favorable el cambio o la dinámica de cubierta analizada; además, muestra menor sensibilidad a valores atípicos y a

predictores poco explicativos. *Boosting* es un método que mejora el rendimiento del modelo mediante la combinación de un número elevado de modelos en un conjunto ensamblado. A diferencia de otras técnicas relacionadas (*model averaging* o *bagging*), *boosting* es secuencial, lo que significa que nuevos árboles de regresión son añadidos de forma aditiva, ajustando los residuales del árbol anterior (Hastie et al., 2009). En cada iteración, una muestra aleatoria (sin reemplazamiento) de los datos de entrenamiento es seleccionada para el ajuste de los modelos, lo que proporciona mayor velocidad computacional (Friedman, 2001) y robustez frente a problemas de sobreajuste del modelo (Friedman, 2002; Hastie et al., 2009). En esta Tesis se emplean modelos BRT para el análisis de la expansión forestal, empleándose una estrategia novedosa, basada en tres pasos.

Para llevar a cabo este estudio se desarrollaron extensos procesos de automatización para la producción cartográfica, generación de variables predictoras, la extracción de las localizaciones de análisis, así como las distintas metodologías y análisis de sensibilidad llevados a cabo, junto con gráficas y tablas de agregación de resultados, en un contexto de estudio de alta multidimensionalidad (Figura 1). Todo ello desarrollado en *scripts* basados en el lenguaje de programación del *software* R, además del uso, y desarrollo también de *scripts* cuando fue necesario, de los *softwares* MiraMon 9.1, ArcGIS 10.7 y SAGA v7.5.0.

Estos y otros aspectos quedan extensamente desarrollados en el artículo 3, así como en los materiales suplementarios que lo acompañan.

AVANCES EN EL COMPLETADO DE LAS SERIES CLIMÁTICAS

2. AVANCES EN EL COMPLETADO DE LAS SERIES CLIMÁTICAS

2.1. Artículo 1: Does the gap-filling method influence long-term (1950-2019) temperature and precipitation trend analyses?

Resumen: Las series climáticas incompletas requieren de enfoques de relleno de lagunas de información para que puedan ser usados en el análisis homogéneo de tendencias espaciotemporales a largo plazo. La base de datos mensual de temperatura Media (MT) y Precipitación (PR) de las estaciones meteorológicas de la Península Ibérica presenta un alto porcentaje de datos ausentes: 80.21 % y 73.25 % para el periodo 1950–1979 (P1), y 61.82 % y 58.03 % para el periodo 1980–2019 (P2). Se emplearon los diferentes métodos de relleno de datos faltantes del software *Emmental* para determinar su rendimiento y si el método de relleno influye en el análisis de las tendencias. El enfoque no paramétrico de Theil-Sen y la prueba de Mann-Kendall evaluaron la magnitud de la tendencia y su significación. Los resultados mostraron (i) patrones similares entre los métodos evaluados, pero con (ii) diferencias espaciales, especialmente durante P1. (iii) La comparación entre las series normalizadas completadas y no completadas no mostró diferencias significativas para la MT y la PR, aunque en el primer caso (completadas) se produjo una reducción de la variabilidad de las tendencias. (iv) La temperatura media de verano mostró la mayor tendencia al calentamiento (0.27 °C/década), mientras que la menor tuvo lugar en otoño (0.21 °C/década) (datos medios para P1 y P2). En general, se produjo un incremento de 1.45 °C en todo el período (mediana anual). (v) La PR no mostró una tendencia clara en ningún mes considerando todo el período. Esta investigación ha demostrado cómo las tendencias climáticas pueden verse afectadas por la reducción de variabilidad de los datos debida a la aplicación de métodos de relleno de datos ausentes. Tener en cuenta la variabilidad de los datos es de crucial importancia para análisis climáticos, pero ignorar las discontinuidades en las superficies climáticas derivadas causa mayores inconsistencias espaciotemporales en los productos climáticos derivados.

Palabras clave: Relleno de datos faltantes; series temporales; estaciones meteorológicas; análisis de las tendencias climáticas a largo plazo, temperatura media, precipitación, Península Ibérica.

Geofocus es una revista indizada/resumida en las bases de datos de:

- ESCI, Emerging Sources Citation Index
- REDIB, Portal de revistas científicas electrónicas y buscador de recursos
- ISOC, Geografía, Urbanismo y Arquitectura. CINDOC, Consejo Superior de Investigaciones Científicas, España
- GEOREF, American Geological Institute
- GOOGLE ACADEMICO

Índices de impacto y evaluación de calidad de Geofocus

- IN-RECS, Índice de impacto de revistas científicas, Universidad de Granada, España.
- LATINDEX, Sistema Regional de Información en Línea para Revistas Científicas de América Latina, el Caribe, España y Portugal.
- DURSI, Sistema de información para la identificación y evaluación de revistas, Generalitat de Catalunya, España.
- Listas CARHUS con nivel de valoración.
- MIAR, Matriz de Información para el Análisis de Revistas.
- CIRC, Clasificaión Integrada de Revistas Científicas.

Portales y repositorios científicos que incluyen a Geofocus

- Dialnet
- DOAJ, Directory of Open Access Journals, Lund University Libraries
- Geoscience e-Journals
- RECOLECTA, Recolector de ciencia abierta. Ministerio de Ciencia y Competitividad (España), FECYT. Colab. CRUE y REBIUN

Sponsors

GeoFocus es la revista del Grupo de Tecnologías de la Información Geográfica de la Asociación de Geógrafos Españoles. Recibe soporte institucional y técnico de RedIRIS (Red Española de I+D soportada por el Gobierno de España), de la FECYT (Fundación Española para la Ciencia y la Tecnología) y Grumets (Grupo de Investigación Métodos y Aplicaciones en Teledetección y Sistemas de Información Geográfica).

- Spanish Geographers Association
- RedIRIS
- Universitat Autònoma de Barcelona

DOES THE GAP-FILLING METHOD INFLUENCE LONG-TERM (1950–2019) TEMPERATURE AND PRECIPITATION TREND ANALYSES?

Mario Padial-Iglesias[1,a], Xavier Pons[1,b], Pere Serra[1,c], Miquel Ninyerola[2,d]
[1] Grumets Research Group, Departament de Geografia, Edifici B. Universitat Autònoma de Barcelona. 08193, Bellaterra, Catalonia, Spain
[2] Grumets Research Group, Departament de Biologia Animal, Biologia Vegetal i Ecologia, Edifici C. Universitat Autònoma de Barcelona. 08193 Bellaterra, Catalonia, Spain
[a]mario.padial@uab.cat, [b]xavier.pons@uab.cat, [c]pere.serra@uab.cat, [d]miquel.ninyerola@uab.cat

ABSTRACT

Incomplete climatic series require gap-filling approaches so they can be used in homogeneous long-term spatiotemporal trend analyses. Monthly mean Temperature (MT) and Precipitation (PR) databases from the meteorological stations of the Iberian Peninsula have a high percentage of data gaps: 80.21 % and 73.25 % for the period 1950–1979 (P1), and 61.82 % and 58.03 % for the period 1980–2019 (P2). The different gap-filling methods of the *Emmental* software were tested to determine their performance and whether the gap-filling method influences these trend analyses. The nonparametric Theil-Sen approach and the Mann-Kendall test were used to assess the trend magnitude and its significance. The results showed (i) similar patterns between the evaluated methods, but with (ii) spatial differences, especially during P1. (iii) The comparison between standardized gap-filled and unfilled series did not show significant differences for MT and PR, although a reduction in the trend variability occurred in the first case (filled). (iv) Summer mean temperatures showed the largest warming trend (0.27 °C/decade), while autumn showed the smallest (0.21 °C/decade) (median data for P1 and P2). Overall, an increase of 1.45 °C occurred in the entire period (annual median). (v) PR did not show any clear trend in any month in the entire period. This research has shown how climate trends can be affected by a reduction in data variability due to the application of gap filling methods. Although accounting for variability is of crucial importance for climate analysis, ignoring discontinuities in derived climatic surfaces causes greater spatiotemporal inconsistencies in derived climate products.

Keywords: gap-filling; time series; meteorological stations; long-term climate trend analysis; mean temperature; precipitation; Iberian Peninsula.

¿INFLUYE EL MÉTODO DE RELLENO DE DATOS FALTANTES EN LOS ANÁLISIS DE TENDENCIAS DE TEMPERATURA Y PRECIPITACIÓN A LARGO PLAZO (1950–2019)?

RESUMEN

Las series climáticas incompletas requieren de enfoques de relleno de lagunas de información para que puedan ser usados en el análisis homogéneo de tendencias espaciotemporales a largo plazo. La base de datos mensual de Temperatura Media (MT) y Precipitación (PR) de las estaciones meteorológicas de la Península Ibérica presenta un alto porcentaje de datos ausentes: 80.21 % y 73.25 % para el periodo 1950–1979 (P1), y 61.82 % y 58.03 % para el periodo 1980–2019 (P2). Se emplearon los diferentes métodos de relleno de datos faltantes del software *Emmental* para determinar su rendimiento y si el método de relleno influye en el análisis de las tendencias. El enfoque no paramétrico de Theil-Sen y la prueba de Mann-Kendall evaluaron la magnitud de la tendencia y su significación. Los resultados mostraron (i) patrones similares entre los métodos evaluados, pero con (ii) diferencias espaciales, especialmente durante P1. (iii) La comparación entre las series normalizadas completadas y no completadas no mostró diferencias significativas para la MT y la PR, aunque en el primer caso (completadas) se produjo una reducción de la variabilidad de las tendencias. (iv) La temperatura media de verano mostró la mayor tendencia al calentamiento (0.27 °C/década), mientras que la menor tuvo lugar en otoño (0.21 °C/década) (datos medios para P1 y P2). En general, se produjo un incremento de 1.45 °C en todo el período (mediana anual). (v) La PR no mostró una tendencia clara en ningún mes considerando todo el período. Esta investigación ha demostrado cómo las tendencias climáticas pueden verse afectadas por la reducción de variabilidad de los datos debida a la aplicación de métodos de relleno de datos ausentes. Tener en cuenta la variabilidad de los datos es de crucial importancia para análisis climáticos, pero ignorar las discontinuidades en las superficies climáticas derivadas causa mayores inconsistencias espaciotemporales en los productos climáticos derivados.

Palabras clave: Relleno de datos faltantes; series temporales; estaciones meteorológicas; análisis de las tendencias climáticas a largo plazo, temperatura media, precipitación, Península Ibérica.

1. Introduction

Monitoring climate change requires observational datasets of long-time periods, which should be as complete as possible to ensure a consistent time series analysis, the comparison between different series, the detection of breakpoints, and the generation of multitemporal surfaces to derive climate change metrics, such as the climate velocity (Loarie *et al.*, 2009; Dobrowski and Parks, 2016; Brito-Morales *et al.*, 2018). Furthermore, the development of societal and environmental climate change mitigation and adaptation strategies depends on the quality of the climate data. However, missing values (data gaps) in the series are common, and there are very few stations with a complete long-term series, which is a big problem when the geographical variability of the climate is a major feature. For instance, the number of observatories recording meteorological variables has increased gradually in the Iberian Peninsula between 1860 and 2019; however, the number of stations has increased significantly since 1975. The sudden installation of new stations and the increasing number of professional staff to make the observations were administrative responses to the need for a more densely distributed climatic network for climate monitoring. Thus, the time series dataset structure differs in spatiotemporal coverage, with scarce and spatially distanced stations in the first decades and more densely distributed stations in the recent ones (Figure 1). In terms of the temporal structure of the datasets, the observations are more densely concentrated over the last four decades (Figure A1 in Appendix 1).

There are diverse reasons for the gaps, ranging from human-induced errors caused by not reporting records or misinterpretation during data transcription (manual stations) or due to malfunctions of electronic/mechanic instruments (automatic stations), information transmission, or storage. Furthermore, meteorological instruments are occasionally replaced or renewed, introducing temporal discontinuities in the series. Frequently these changes are hardly reported in the metadata associated with the stations.

All these effects result in incomplete series with data gaps ubiquitously distributed throughout them. Thus, various studies have proposed different gap-filling approaches to identify an appropriate method that is adapted to a target variable. As a result, many gap-filling techniques have been developed, varying in complexity and ranging from simple to extremely complex approaches. The most simple methods are based on the imputation of data gaps according to the information contained in the same time series, assigning the data before or after the gap, or applying the local or the sample average of the series (Pappas *et al.*, 2014; Gil-Guirado and Pérez-Morales, 2019). Another technique widely used in the reconstruction of the precipitation datasets is the Normal Ratio (Paulhus and Kohler, 1952; Longman *et al.*, 2018;). Others, such as the kNN weighted averaging method, consist in generating reference series in a location formed by the weighted average of the data observed in neighboring stations (Beguería *et al.*, 2019). Yet other approaches consider multiple linear regression models (Mora *et al.*, 2014; Tardivo and Berti, 2014; Serrano-Notivoli *et al.*, 2017), the Inverse Distance Weighting algorithm (Bielenki Junior *et al.*, 2018; Lu and Wong, 2008; Armanuos *et al.*, 2020) and, more recently, strategies such as tree based methods and machine learning algorithms (Körner *et al.*, 2018; Bellido-Jiménez *et al.*, 2021), or the combination of several gap-filling methods (Armanuos *et al.*, 2020; Longman *et al.*, 2020).

Generally, gap-filling approaches focus on minimizing the error (*e.g.*, the Root Mean Square Error, RMSE) using a leave-one-out cross-validation method that allows observed and estimated values to be compared, or approaches maximizing the goodness of fit in regression models for example through the coefficient of determination, R^2 (Teegavarapu and Chandramouli, 2005; Vicente-Serrano et al., 2009; Singh and Xiaosheng, 2019).

Given the different available techniques and results, this study examines the effect of four gap-filling approaches on the long-term temperature and precipitation trends in the Iberian Peninsula. We assessed the trend magnitude and significance, and analyzed the spatiotemporal patterns, focusing on how the different gap-filling methods influence the completion of the climatic dataset, the long-term trend, and the spatiotemporal patterns. The research applies the *Emmental* program implemented in the MiraMon software (Pons, 2004) to large datasets of month-to-month records of these two major climatic variables in the Iberian Peninsula (Spain, Portugal, and Andorra), as described in the methodology section.

We hypothesize that (i) temperature and precipitation variables will exhibit different gap-filling method parametrizations according to their dataset structure and spatiotemporal irregularity (with a denser spatiotemporal network for precipitation). (ii) The gap-filling method will influence the magnitude and significance of long-term trends in temperature and precipitation according to the method itself and the spatiotemporal structure of the datasets. And (iii) the proportion of data gaps in the dataset may condition the performance of the gap-filling methods according to the structure of the dataset.

2. Materials and methods

2.1. Study area

The study area is defined by the Iberian Peninsula, comprising Spain, Portugal, and Andorra, a context located in the border region between tropical and semi-tropical climates, which offers ideal conditions to evaluate climate change in the northern hemisphere. This context is characterized by a significant climatic variability, with dry conditions in the southeast Mediterranean, continental regimes towards the center, and humid conditions in the north-west Atlantic context. Furthermore, due to its location, global warming is expected to become especially evident in the peninsula due to its sensitivity to climate change. Therefore, climate monitoring is essential to adopt appropriate climate change adaptation measures.

2.2. Climatic datasets

Datasets of monthly mean temperature (MT) (in d°C) and precipitation (PR) (in dmm) were compiled from observations provided by the Spanish (Agencia Estatal de Meteorología (AEMET)) and the Andorran (Servei Meteorològic Nacional) meteorological services. Furthermore, additional stations were collected from the Sistema Nacional de Informação de Recursos Hídricos (SNIRH) of Portugal. As a result, large datasets were generated for each climatic variable. We selected stations with observations spanning from January 1950 to December 2019 for each climatic variable, a seventy-year period during which the number of observatories and observations significantly varied. Details about the spatial distribution are provided in Figure 1 while Figure A1 in Appendix 1 provides details of the temporal distribution of the observations. A higher proportion of gaps was concentrated in the first decades of the period.
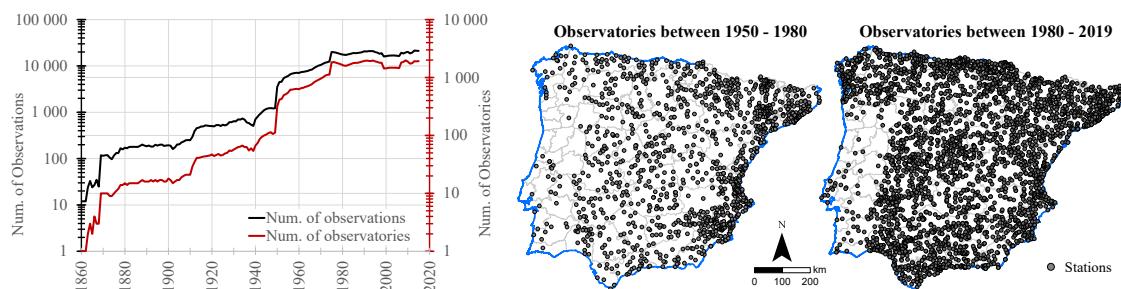
Figure 1. Mean temperature dataset structure: spatiotemporal distribution of observatories in the Iberian Peninsula

As shown in Table 1, almost 30 % of the MT dataset corresponds to observations, and 70 % are data gaps. Precipitation (PR) improves these proportions, with nearly 35 % observations and 65 % gaps. Furthermore, the table shows that if we divide the whole dataset into two periods, P1:1950–1979 and P2:1980–1979, the percentage of gaps in P1 (30 years of observations) was more prominent than in P2 (40 years of observations), with no differences between months.

The analysis periods could be established according to the year when new stations notably appeared (1975) or when the climatic trend was reported to change (1980). In this study we preferred to use the last of these to analyze the implications of the methods evaluated in this article, because the general interest in the scientific community is more focused on this aspect.

Table 1. Structure of the climatic datasets (upper part) and gap distributions by month and aggregation of annual observations (lower part).

Var.	Period	Stations	No. Observ.	Completeness	No.Gaps	Gaps (%)
MT	(P1) 1950–1979	1889	256 845	19.59 %	1 054 275	80.41 %
	(P2) 1980–2019	3364	667 427	38.18 %	1 080 733	61.82 %
	(P3) 1950–2019	3642	924 272	30.21 %	2 135 008	69.79 %
PR	(P1) 1950–1979	5374	736 581	26.75 %	2 016 699	73.25 %
	(P2) 1980–2019	7158	1 540 808	41.97 %	2 130 232	58.03 %
	(P3) 1950–2019	7648	2 277 389	35.45 %	4 146 931	64.55 %

Var	Period	Jan	Feb	Mar	Apr	May	Jun	Jul	Aug	Sep	Oct	Nov	Dec	Ann
MT	P1 [1]	6.71	6.72	6.70	6.69	6.69	6.69	6.72	6.73	6.70	6.70	6.68	6.69	7.20
	P2	5.14	5.12	5.15	5.14	5.14	5.15	5.15	5.19	5.16	5.16	5.13	5.19	6.23
	P3	5.81	5.80	5.81	5.80	5.80	5.81	5.82	5.85	5.82	5.82	5.80	5.83	6.65
PR	P1	6.12	6.11	6.09	6.08	6.08	6.10	6.15	6.14	6.10	6.10	6.07	6.10	6.90
	P2	4.81	4.78	4.80	4.78	4.78	4.85	4.90	4.94	4.85	4.81	4.85	4.87	6.37
	P3	5.37	5.35	5.36	5.34	5.34	5.39	5.44	5.45	5.39	5.36	5.37	5.40	6.59

[1] Values represent the split of percentages of gaps by months, while the annual percentage is estimated when all month values are available. All percentages in the table are referred to the maximum possible observations in each period.

2.3. Data preparation and filtering

In an initial exploratory phase, time series were quality controlled by testing data coherence within the series and with close neighbors, excluding outliers. During the filling stage, the stations with less than 240 observations (28.5% of a potential of 70 years x 12 months = 840 observations) only served as data providers, and were not completed during the filling process (Figure 2). Therefore, we considered the stations with more than 20 years of monthly data to evaluate the choice of the filling method in the long-term spatiotemporal climatic trend analysis. This threshold was used based on the assumption of filling stations with a reasonable level of missing data to be reconstructed. However, further analysis would be required to evaluate the repercussions of considering a higher percentage of unfilled stations in the research. Other authors have excluded data series with less than 15 years for reconstruction (Vicente-Serrano *et al.*, 2009).
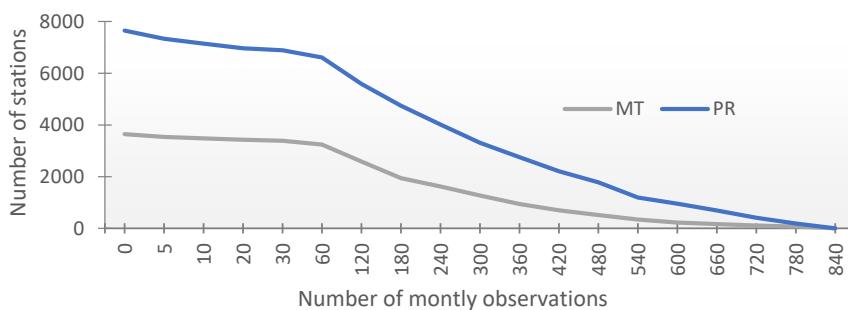
Figure 2. Frequency of stations with a number of monthly observations.

2.4. *Emmental* gap-filling approaches

The *Emmental* gap filling program is implemented in the MiraMon Geographic Information System and Remote Sensing software (Pons, 2004), providing four strategies to fill time series with associated parametrization.

The **MONTH** method ('*M_*' suffix in parameters) considers other months of neighbor years of the same station. Thus, the main parameter to be set by the user is the maximum number of months of neighbor years to the gap—*i.e.*, as a temporal buffer—used to estimate the filling value (*M_YESTIM*). Then the average or the median of the neighbor years (as local approximates) can be used to approximate the gap value.

The **SIMILAR** method ('*S_*' suffix in parameters) explores the most similar series among spatially nearest stations. The similarity is computed between pairs of 'n' dates time series formed by the problem station and each station of a set of nearest neighbor stations. The main parameters to be set are the number of years—*i.e.*, a temporal buffer—from the gap and among the neighbor years (*S_YESTIM*) and the maximum number of nearest neighbor stations—*i.e.*, a spatial buffer—used in the similarity analysis (*S_N_NEARST*). The root-mean-square (RMS) and the R^2 can be used to perform the similarity analysis between series: in the first case, the station with the lower RMS provides the value for the gap in the problem station (*S_SUBMET=m*), with the possibility of applying a bias correction, computed as the mean of the differences between the common values for the years compared between stations (*S_SUBMET=o*). However, in the second case, the station with the strongest correlation, R^2 (assuming a minimum R^2 threshold of 0.6) provides the value after applying a linear model fitted with the common values for the years compared between the pair of stations (*S_SUBMET=r*).

In addition, for the MONTH and SIMILAR methods, an extra parameter controls the minimum number of years that will make the gap value estimation reliable (*M_MIN_YESTIM* and *S_MIN_YESTIM*), conditioning the presence of data gaps in the range of selected values, and hence the continuity and contiguity of the selected values around the gap. No gaps are allowed in the temporal selection when *S_YESTIM = S_MIN_YESTIM*.

The **REGRES** method ('*R_*' suffix in parameters) uses the nearest stations with data available in the gap year and month at the problem station. A multiple linear regression model is generated with the gap value as the dependent variable, regressed considering a set of independent variables. The user defines the covariates (*VAR_1*, *VAR_2*,...) and the maximum number of nearest neighbor stations (*R_N_NEARST*) included in the regression model. The covariates in this study were the Euclidean distance to the coast (as a measure of continentality), the potential solar radiation (evaluated as the annual average following Pons and Ninyerola, (2008)), the latitude, the longitude, and the altitude.

Finally, the **IDW** method ('*I_*' suffix in parameters) estimates the gap value by interpolating the available data from the nearest stations, considering the Inverse Distance Weighting algorithm. The importance of the data from the nearest stations for the interpolated gap is set by the IDW power parameter (*I_IDW*).

Emmental filling methods have the /TEST parameter, which makes it possible to assess the performance of filling methods in time series datasets and to approximate the parametrizations of the optimum filling method. In test mode, each real observation in a station is considered a gap and simulated according to the rest of the observations and the user's specified parametrizations. According to Table 1,

about one-third of the whole dataset corresponded to available observations, which were used to derive the best filling parametrizations applied to fill the real gaps in the dataset, representing approximately two-thirds of the whole dataset (white spaces in Figure A1 in Appendix 1). Comparing estimated *vs.* real observations allows us to calculate evaluation statistics for each station and the global dataset: error statistics (*i.e.*, the minimum, maximum, and mean error, and the global RMSE), the goodness of fit of the residuals (the coefficient of determination, R^2, in the SIMILAR submethod), as well as the parametrization filling capacity performed. Nevertheless, there is a trade-off between minimizing RMSE and the filling capacity of the parametrizations, especially in the SIMILAR filling method, and parametrizations with the best performance (minimum RMSE) coincide with a relatively low percentage of gaps filled. It is important to note that SIMILAR uses parameters to control the temporal and spatial buffer, which can compromise the filling capacity according to the parametrizations. This particularity led us to explore an iterative gap-filling strategy, in which the best parametrizations obtained in the test mode were applied to fill the gaps iteratively, ordered by an increasing RMSE. Moreover, the percentage of gaps filled differed in the test mode (one-third of the dataset) from the filling mode (two-thirds of the dataset) due to the dataset structure. Thus, one-third of the real observations were used to fill two-thirds of the real gaps, using the parametrizations that minimize the RMSE estimated with around one-third of the data. Therefore, in the first stage, several testbeds were performed to estimate the optimal parametrizations (minimizing the RMSE) for each filling method, used in the second stage to fill the gaps in the climatic datasets.

2.5. Long-term trend assessment.

In this approach, the long-term trend was estimated in three temporal periods: two separated subperiods (P1: 1950–1979 and P2: 1980–2019), taking into account the splitting points found in previous research (Almarza and Luna, 2016; Carnicer et al., 2019), and the whole period (P3: 1950–2019). The magnitude and significance of the trend were evaluated monthly (*e.g.*, all January's observations, all February's observations), seasonally (*e.g.*, winter determined by averaging: December, January, and February), and annually (assessed averaging 12 months, when available for the year). Month-to-month linear regression was not considered due to the repercussions of the seasonal component for the magnitude and significance of the trend, and thus time series had to be previously de-seasonalized, as was tested. The nonparametric Theil-Sen (Sen, 1968; Theil, 1992) estimator was used to derive the trend magnitude, while the Mann-Kendall (Kendall, 1975; Mann, 1945) test was used to quantify the trend significance. These statistics have been used in several case studies (Alemu and Dioha, 2020; Beguería *et al.*, 2019; Gocic and Trajkovic, 2013; Teegavarapu and Nayak, 2017). The advantages of using nonparametric statistics are that they do not require data to be normally distributed, they have low sensitivity to breaks in inhomogeneous series, and there are abnormal values (Sayemuzzaman *et al.*, 2014). The Mann-Kendall test null hypothesis assumes that there is no trend in the data (random and independently ordered observations), which is tested against the alternative hypothesis, i.e., assuming there is a trend in the data.

The trend magnitude and significance were estimated for each climatic variable, period (*e.g.*, 1950–1979) and data aggregation (*e.g.*, January, spring, or Annual) for the original and filled series, considering at least five available observations. All station trends were considered when filling methods were compared without applying significance restrictions. However, before assessing the trends and significance, the time series were standardized to compare MT and PR patterns. Lastly, applying significance restrictions made it possible to analyze the climatic rate of change in the period. Gap-filling computations were performed with

the *Emmental* program, and the statistics and trend analysis were programmed in R language, version 4.1.1 (R Core Team, 2022).

3. Results

3.1. Assessment of the Filling method parametrization

The testbeds performed in the test mode provided the best parametrizations, which minimized the overall RMSE and were used to fill the gaps. In the MONTH method, we tested the maximum number of years (*M_YESTIM*) from the year of the gap and among the neighbor years in the problem station, combined with the parameter (*M_MIN_YESTIM*) that sets the minimum number of years that makes the estimated value reliable. For instance, considering *M_YESTIM*=10 neighbor years from the year of the gap and *M_MIN_YESTIM*=6 years, means that at least six dates were available to approximate the gap value, while four or less were data gaps (*e.g.*, o–o–o–x–x–[simulated gap]–x–o–o–o–x, where 'o' denotes real observations and 'x' are gaps). The previous parameters ranged from 5 to 30 neighbor years, considering the mean and the median to approximate the gap. The results showed that the local average performed slightly better than the local median for MT and PR. Furthermore, the gap-filling capacity of the parametrization increased at the expense of degrading the overall RMSE when data gaps were allowed in the selected values through the *M_MIN_YESTIM* parameter (the lack of continuous and contiguous observations to approximate the simulated value increases the estimated error). For MT, a minimum RMSE of 14.5 d°C (*i.e.*, 1.45°C) was achieved with a *M_YESTIM* ranging between 10 and 18 years and filling between 72.13 and 86.81 % of gaps. For precipitation, a minimum RMSE of 477.7 dmm (*i.e.*, 47.77 mm) was achieved with a *M_YESTIM* of 30 years, filling 62.51% of gaps. This last result suggests that the larger the number of years, the lower the RMSE and the gap-filling capacity (Figure 3). It is essential to note that the RMSE corresponded to the overall evaluated dataset, with almost a million observations for MT and more than two million for PR (Table 1), which justified minimizing the overall dataset RMSE (see the RMSE spatial distribution in Figure 7).

The parametrizations were ordered by increasing RMSE and decreasing temporal buffer (Δ RMSE; ∇ YESTIM) and used to fill the real gaps iteratively. With this strategy, we preferentially used parametrizations providing the lower RMSE (long-length series), reducing the temporal buffer in the later iterations.
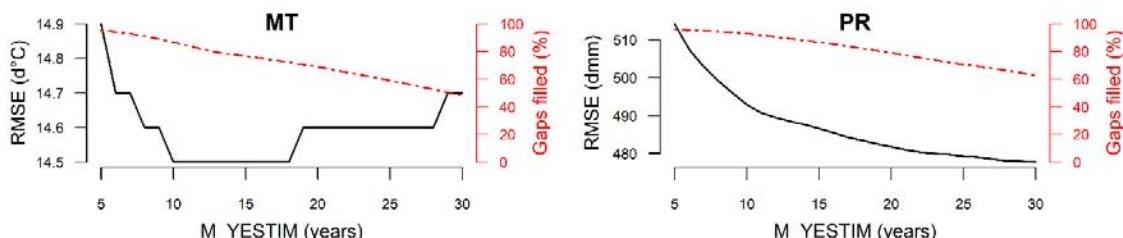
Figure 3. MONTH 'test' mode RMSE and gap-filling results, estimated considering 'n' neighbor years from the gap. The period 1950–2019 series is used.

In the SIMILAR method, the following parameter combinations were evaluated: *S_YESTIM*, *S_MIN_YESTIM* (with the same definitions as for the MONTH method), and *S_N_NEARST*, which sets the number of the nearest neighbor stations used to estimate the similarity. We also used three submethods ('r', 'o' and 'm') to assign the gap value in the problem station. The results showed that the 'r' submethod obtained the lowest overall RMSE, followed by 'o' and 'm'. For MT, the lowest RMSE of 7.1 d°C was obtained when similarity was evaluated considering long-length series of between 25 and 30 years around the year of the gap and within 5 nearest neighbor stations, resolving between 11.51 and 18.23 % of the gaps. The maximum filling capacity, over 95.30 %, was achieved when similarity was evaluated considering a short-length series of 5 years within 150 nearest stations. For PR, analogous patterns were observed. With a long series of 23 years around the gap and 5 nearest stations, the overall RMSE was minimized to 207.2 dmm, resolving 34.72 % of the simulated gaps. The maximum filling capability of 95.47 % was achieved considering short-length series of 5 years evaluated within the 150 nearest stations. In the upper part of Figure 4, the *S_N_NEARST* is fixed to 5 nearest stations for MT and PR. The RMSE and gap-filling capacity decreased when the temporal buffer (*S_YESTIM*) was increased. In the lower part of the figure, the temporal buffer (*S_YESTIM*) was fixed to 25 years, increasing the RMSE and the gap-filling capacity when the number of nearest stations considered to evaluate similarity was increased.

Similarly to the previous MONTH method, parametrizations were ordered by increasing RMSE, decreasing the temporal buffer, and increasing the newly added spatial buffer (Δ RMSE; ∇ YESTIM; Δ NEARST). Thus, parametrizations with a long-length temporal buffer and near the problem station were preferentially used, reducing the temporal and increasing the spatial buffer in the later iterations. During the process, it is important to note that short-length stations, tagged as data providers, were iteratively restituted to their original form, thus avoiding data propagation through them.
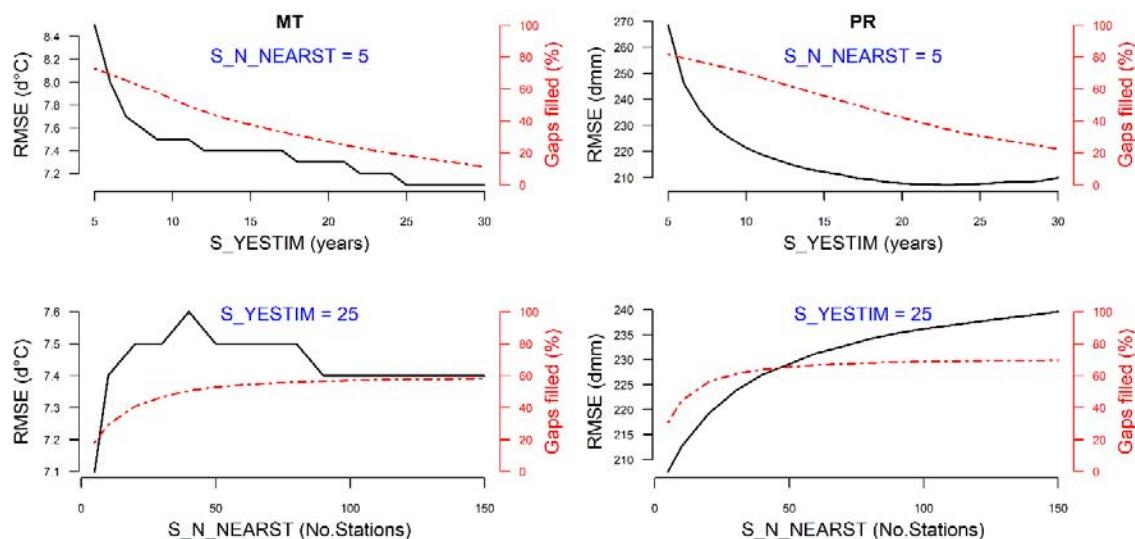
Figure 4. SIMILAR 'test' mode RMSE and gap-filling estimates, considering 'n' neighbor years from the gap and 'm' nearest stations. Results for the best submethod ('r') are shown.

The REGRES method requires the stations to be intersected with a set of predictors to generate a multiple linear regression model (the Euclidean distance to the coast, the potential solar radiation, the latitude, the longitude and the altitude, in our case). We tested the model performance considering the variables and the *R_N_NEARST* parameter (same definition as for the SIMILAR method). All variables were included in the model, and each predictor value was weighted according to its relative contribution to the overall prediction. The least-squares estimator ensures the maximal prediction of the gap to be filled from the set of variables used. The main difference with the previous methods was that the filling capacity was not compromised, and each parametrization filled 100 % of the gaps. Thus, the method showed an asymptotical RMSE decrease, achieving a minimum RMSE of 10.5 d°C for the 45 nearest stations in the case of temperature and a RMSE of 236.3 dmm for the 35 nearest stations in the case of PR (Figure 5).
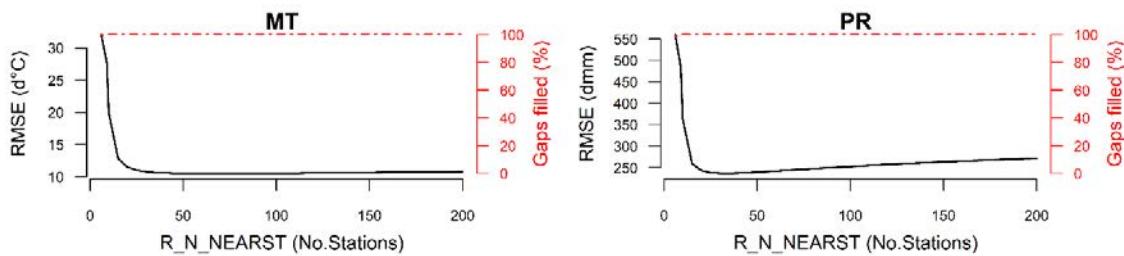
Figure 5. REGR 'test' mode RMSE and gap-filling results, estimated considering a set of covariates and 'm' nearest stations.

Finally, the IDW method was tested considering all the parameter combinations of a set of exponent values (*EXP=1,2,3*) and the *I_N_NEARST* parameter (same definition as in SIMILAR). Similarly to REGR, the filling capacity of the method was not compromised, as parametrizations filled 100 % of the gaps. Therefore, the results showed a minimum RMSE of 13.2 d°C for MT and 221.5 dmm for PR, considering parameters of *EXP=1* and 7 nearest stations (Figure 6).
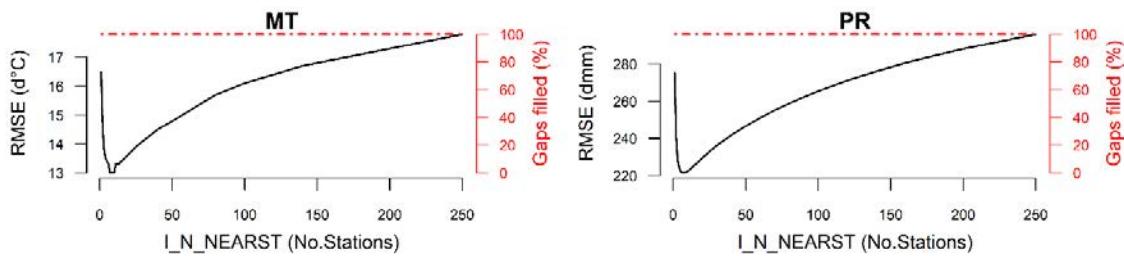
Figure 6. IDW 'test' mode RMSE and gap-filling results, estimated considering 'x' exponent values and 'm' nearest stations.

Figure 7 shows the RMSE spatial distribution. MONTH was the method with the highest overall RMSE, followed by IDW, REGR, and SIMILAR for temperature. REGR, and especially IDW, showed higher estimated errors in mountain areas, especially in the Iberian Peninsula's Atlantic, center and Mediterranean contexts. Likewise, MONTH had the largest overall RMSE for precipitation, and lower

differences were observed between IDW, REGR, and SIMILAR. Unexpectedly, the north-west Atlantic context showed a higher overall RMSE compared with the Mediterranean. This pattern suggests that areas with high precipitation rates derived the larger errors, mainly associated with the high spatial variability of the precipitation.
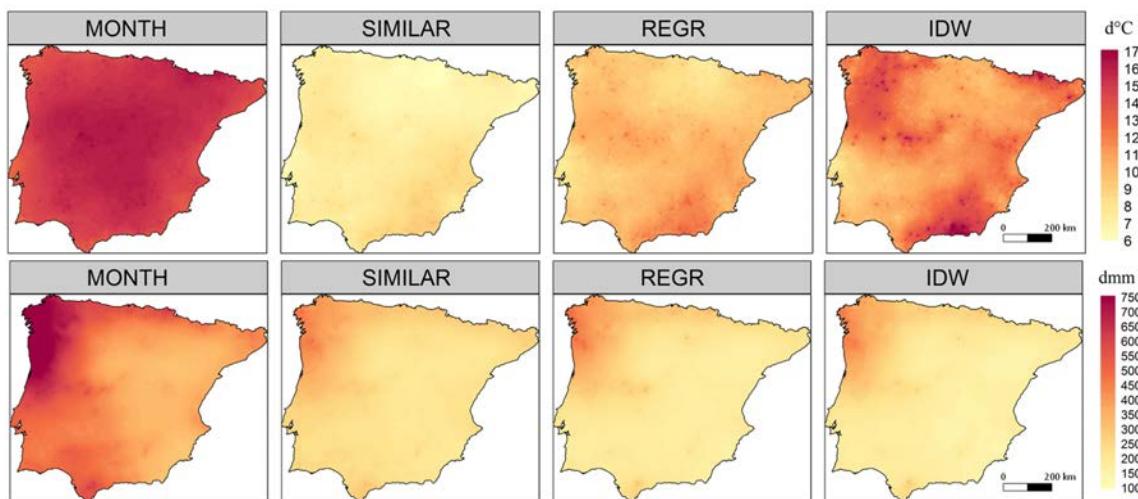
Figure 7. RMSE spatial distribution for temperature (upper) and precipitation (lower).

Table 2 shows the summary of the different parametrizations explained. In the ranking, SIMILAR clearly provides the best performance for MT even though it exhibits a trade-off between minimizing RMSE and the percentage of gaps filled, followed by REGR, IDW, and MONTH. Equally for PR, SIMILAR provides the best performance, followed by IDW, REGR, and MONTH.

Table 2. Parameterizations estimated in "test mode". Three different cases are shown: minimizing the overall RMSE (white rows), maximizing the filling percentage (dark gray), and a trade-off between the two (light gray). Filled percentages correspond to simulated gaps (see section 2.4.)

	VAR	SUBMET	YESTIM	MIN_YESTIM	Filled (%)	RMSE (d°C)‖(dmm)
MONTH	MT	m	18	18	72.13	14.5
		m	7	7	92.93	14.7
		m	5	5	95.35	14.9
	PR	m	30	30	62.51	477.7
		m	9	9	93.95	496.0
		m	5	5	96.13	514.2

	VAR	SUBMET	YESTIM	MIN_YESTIM	N_NEARST	Filled (%)	RMSE (d°C)‖(dmm)
SIMILAR	MT	r	30	30	5	11.51	7.1
		r	6	6	70	94.27	8.5
		r	5	5	150	95.35	9.9

		r	23	23	5	34.72	207.2
	PR	r	7	7	90	94.60	284.3
		r	5	5	150	95.47	361.8

	VAR	VARIABLES	N_NEARST	Filled (%)	RMSE (d°C)‖(dmm)
REGR	MT	Latitude+Longitude+Altitude+	45	100.00	10.5
	PR	Dist.Coast+Solar radiation	35	100.00	236.3

	VAR	EXP	N_NEARST	Filled (%)	RMSE (d°C)‖(dmm)
IDW	MT	1	7	100.00	13.2
	PR	1	7	100.00	221.5

3.2. Assessment of the completed datasets

The parametrizations described were applied to fill the gaps in the climatic datasets. MONTH and SIMILAR parametrizations were sorted and used iteratively to fill the climatic datasets. They achieved a high level of gap filling, comparable to that obtained through IDW and REGR; detailed lists are in Table A3, Appendix 1. The dataset completion almost achieved a complete filling: in the case of MT, the percentage was 99.98 % with MONTH and 99.95 % with SIMILAR, while in the case of PR, MONTH and SIMILAR completed 100 % of the gaps. Finally, the REGR and IDW methods completed 100 % of the MT and PR datasets.

The iterative gap-filling strategy showed different behaviors (Figure 8). MONTH increased the quantile 5 % (Q05) and decreased the quantile 95 % (Q95) for both MT and PR. For MT, the mean (MEAN) and the standard deviation (SD) decreased. Nevertheless, for PR, the mean showed an irregular pattern, but the standard deviation decreased. With SIMILAR, in the case of PR, the extreme quantiles (Q05, Q95) and the mean increased while the standard deviation decreased. However, for MT, the extreme quantiles and the mean decreased, but the standard deviation showed an irregular pattern. The number of gaps filled (NrOBS) increased progressively to a maximum around the 60th iteration, significantly contributing to the first iterations (ItOBS) in the filling process.

3.3. Repercussions of the filling method for climate trend analysis

The repercussions of the filling methods for long-term trends were evaluated considering stations with more than 20 years of original observations. The trend magnitude and significance were assessed using the Theil-Sen and Mann-Kendall estimators for the analysis periods.

According to Figure 9, all methods showed a similar behavior except MONTH, which showed a flattening pattern related to the method itself. The method uses the observations in the problem station to approximate the gap value by the local mean or median. Due to the lower number of observations in P1, the flattening effect was more intense than in P2. The propagation of values during iterations reduced the data variance, particularly in P1. This pattern was observed both for MT and PR. This can also be seen in the increase in the Q05 and the decrease in the Q95 in the MT and PR values (Figure 8).
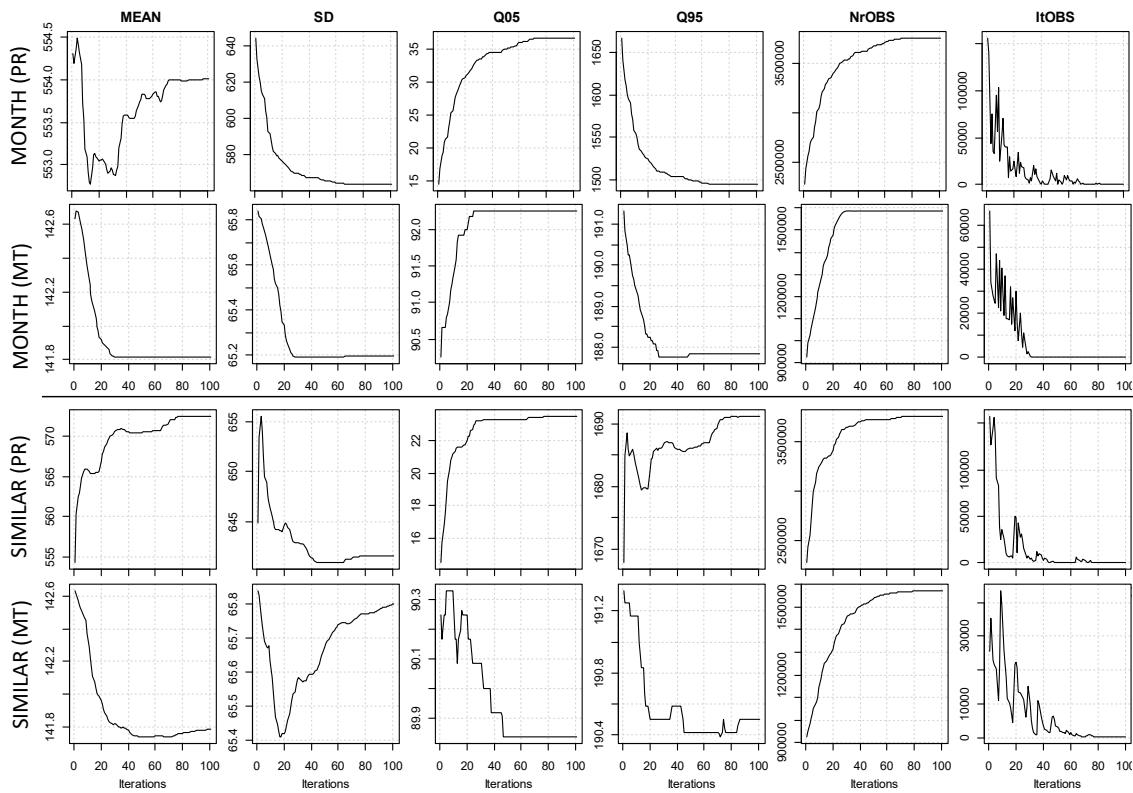
Figure 8. Monitoring the evolution of statistics during the iterative gap-filling. The whole dataset (1950–2019) is monitored. On the vertical axis, units are d°C for MT and dmm for PR.

Conversely, long-term trends denoted equal patterns in the other methods, but a higher dispersion between methods was observed in P1 (Table A2, Appendix 1). IDW in P1 showed a slightly higher dispersion than the other methods (the standard deviation of the trend was ± 0.45 for IDW, ± 0.25 for MONTH, ± 0.33 REGR, and ± 0.34 SIMILAR). For PR, larger differences were expected between filling methods due to the larger RMSE observed in the test mode. However, all the methods except MONTH predict equal climatic trends as in the case of MT. Detailed correlation matrices between the filled datasets are shown in Table A1 in Appendix 1. This similar pattern is consistent in all monthly trends.

Interestingly, when the spatial representation of the trends was analyzed (Figure 10), differences in the spatial patterns increased. In the case of MT and during P1, MONTH denoted the same flattening effect previously observed. However, IDW systematically showed larger trends in mountain range contexts, contrasting with REGR and SIMILAR. Moreover, similarities between IDW and REGR patterns were also observed. However, the methods differ from each other most significantly in the months August and September. Minor spatial differences between methods in all months were observed during P2. For instance, the IDW singular pattern in mountain contexts disappeared. Conversely, for PR, the spatial patterns observed in both periods were similar for the different methods, except for MONTH, which also occurred

in the case of MT. The lack of a clear trend in the spatial patterns was associated with an alternation between wetter and dryer years in the series, which produced a more similar spatiotemporal pattern between methods.

We analyzed standardized series to compare MT and PR long-term trends. Figure 11 allowed us to identify a clear reduction in the dispersion (interquartile range) of the assessed trends between the original unfilled series and the SIMILAR selected filled dataset. We used the SIMILAR method for comparisons as it had the best performance during the 'test mode' stage. Trend patterns derived from the original and filled datasets were consistent between them. The most significant dispersion occurred in P1. When the MT and PR trends were compared, the MT denoted the largest dispersion. The trend variability was larger in the original series and smaller in the filled series. Moreover, a more significant reduction in the trend variability was observed in the entire period.

3.4. Climatic trend analysis.

We compared long-term trends considering all the stations without significance filter application for the whole period (1950–2019). In Table 3, a reduction in the number of stations was observed. For temperature, the reduction was less critical, as 71 % were significative trends. However, only 28 % were significative for precipitation. Therefore, even though the sign of the trend was equal (with and without the application of the significance filter), the magnitude of the trend of the significant series was logically larger. Considering the magnitude of the temperature trend, summer was the season with the largest trend (0.276 °C/decade), while autumn showed the lowest (0.211 °C/decade). Overall, an increase of 1.46 °C occurred in the whole period (0.21 °C/decade), considering the annual tendency. On the other hand, precipitation showed different seasonal patterns. A significant decrease was detected for winter (-18.746 mm/decade) and spring (-14.363 mm/decade), and an increase for autumn (6.894 mm/decade). Overall, figures showed a decrease of -233.748 mm (*i.e.*, -31.964 mm/decade × 7 decades = -233.748 mm) in the whole period considering the annual trend (Table 3).

Temperature patterns can be observed in Figure 11. Thus, winter followed a similar pattern during P1 and P2, with January and February tending to be warmer, but December did not have a clear tendency. In the case of spring and summer, a clear cooling tendency was observed in P1, but this pattern was inverted in P2. Regarding autumn, September showed no clear changes between periods, but October significantly inverted to a warmer trend in P2. Lastly, November showed a cooling pattern in P1 but was slightly warmer during P2. From an annual point of view, P1 showed a clear cooling trend, inverting the trend to a warmer one in P2. Finally, considering the whole period, all months showed an overall warming tendency.

In the case of precipitation, in winter, the patterns observed were similar in both periods, but February showed a slight decrease in P2. In spring, a wide variability was observed: March inverted from a negative tendency in P1 to a positive one in P2; May showed the opposite pattern, and April showed no clear tendency in any case. Summer showed no tendencies in either of the two periods. Autumn had an increasing tendency in all months in P2. From an annual point of view, no changes in the trends between periods were observed. Finally, no clear increasing or decreasing tendency was reported for any of the months considering the whole period.
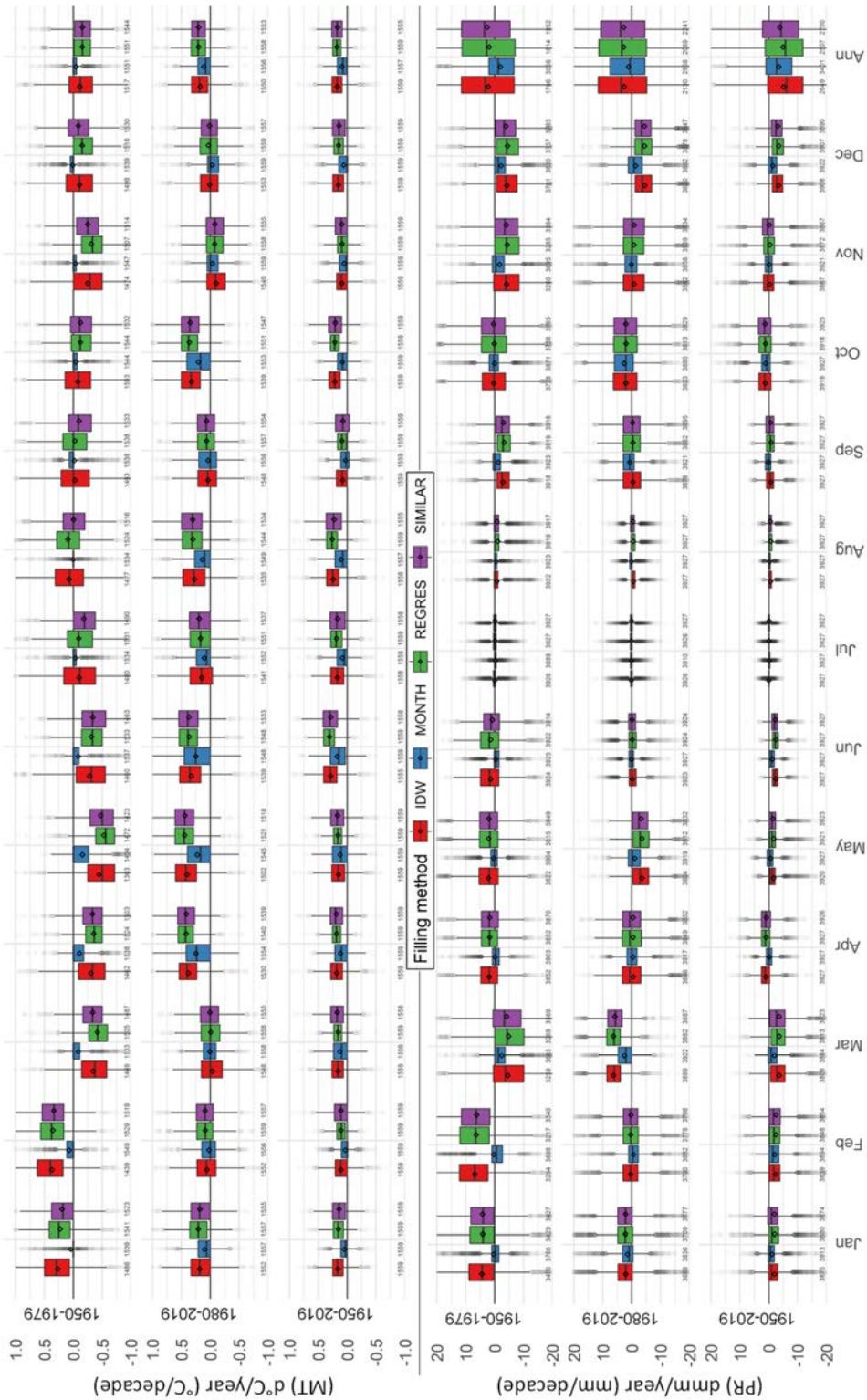
Figure 9. Mean temperature and precipitation long-term trend patterns evaluated for each filling method, temporal aggregation, and time period. Figures under the boxes refer to the number of gap-filled stations considered in each case. In the vertical axis, d°C/year and °C/decade (MT), and dmm/year and mm/decade (PR) are equivalents.
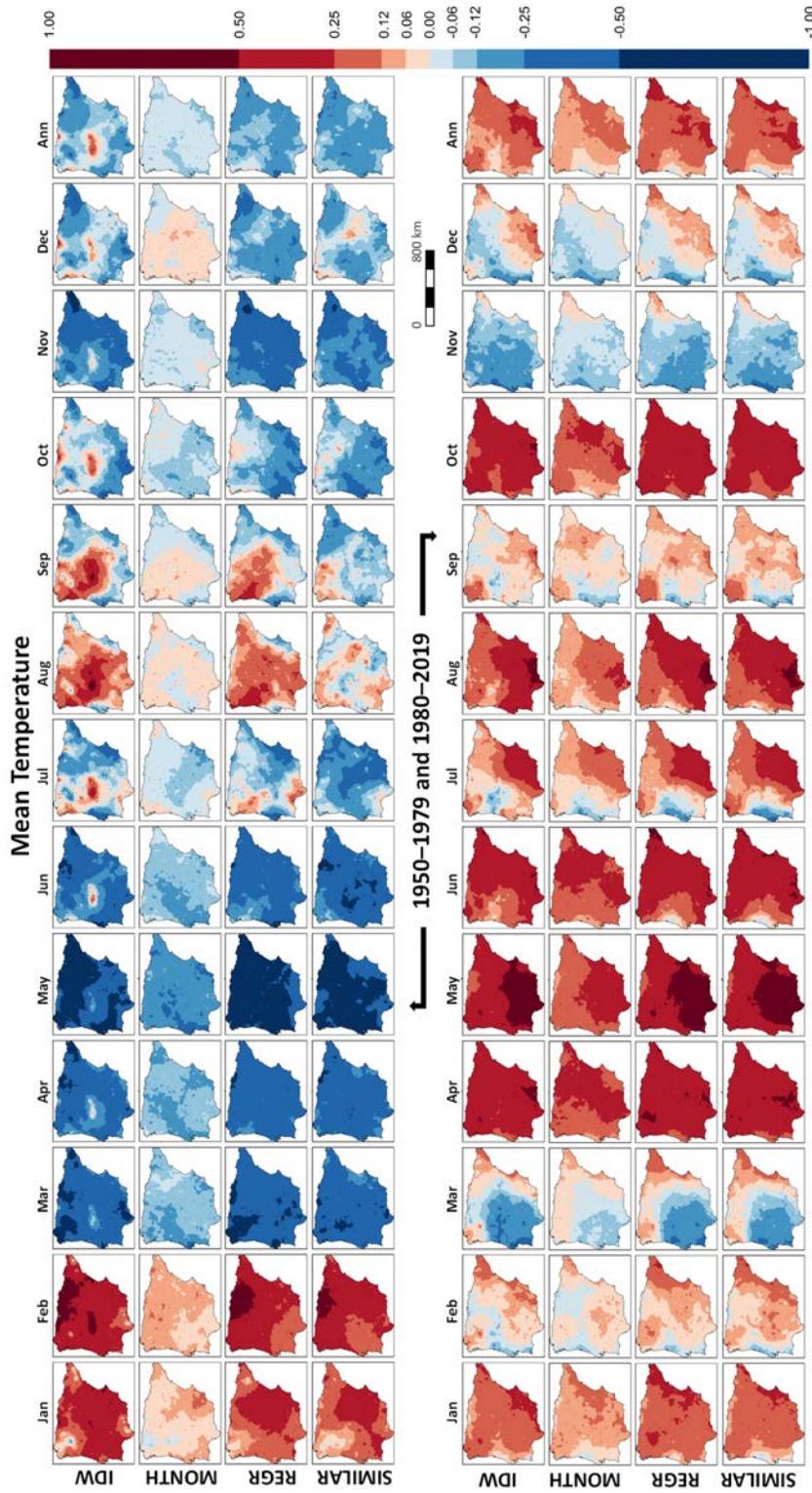
Figure 10. Mean temperature spatiotemporal trend patterns between 1950–1979 and 1980–2019, evaluated for each filling method. Trend values (not standardized, without MK filter) in d°C/year (°C/decade).
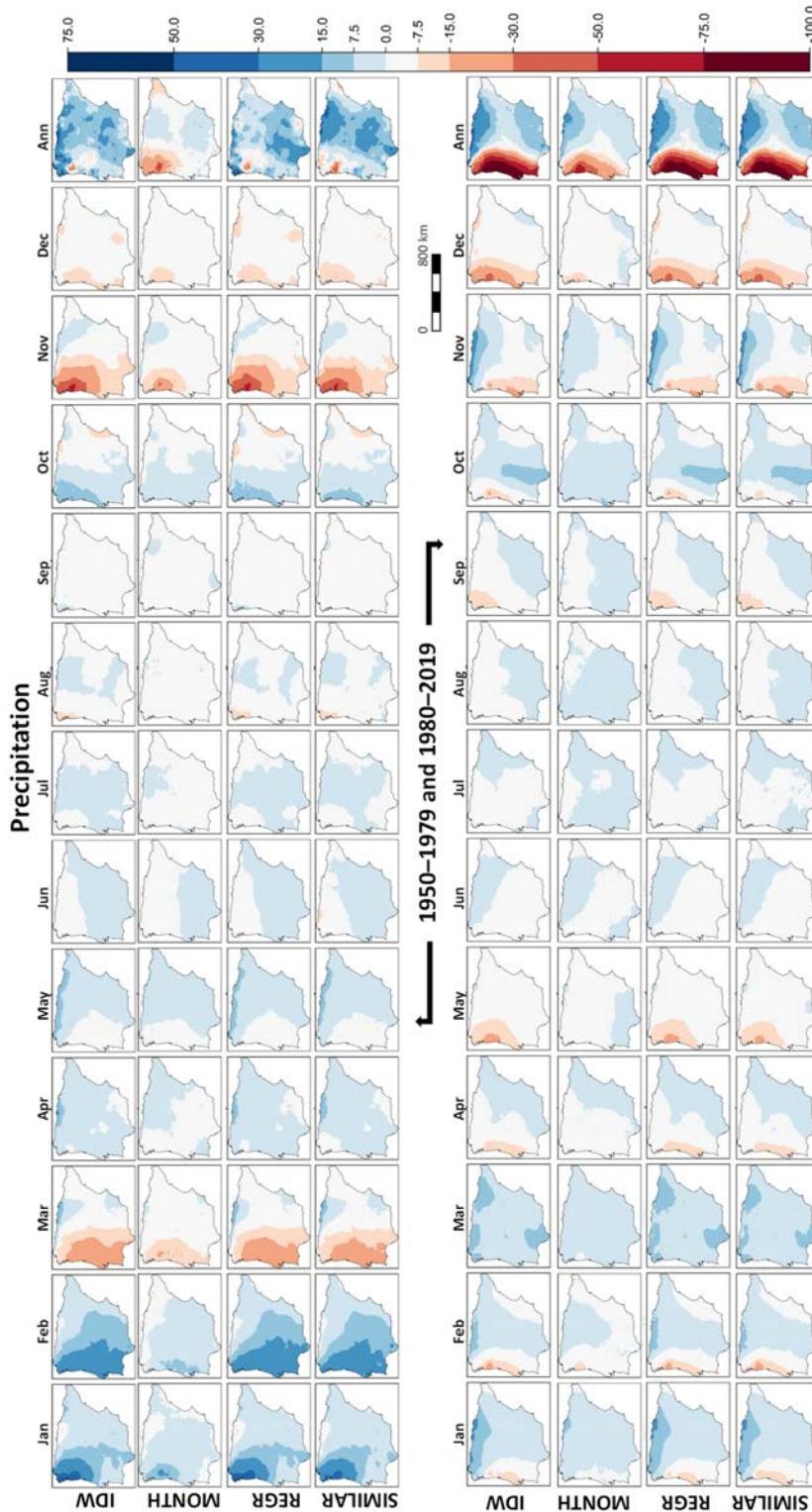
Figure 10 cont. Precipitation spatiotemporal trend patterns between 1950–1979 and 1980–2019, evaluated for each filling method. Trend values (not standardized, without MK filter) in dmm/year (mm/decade).
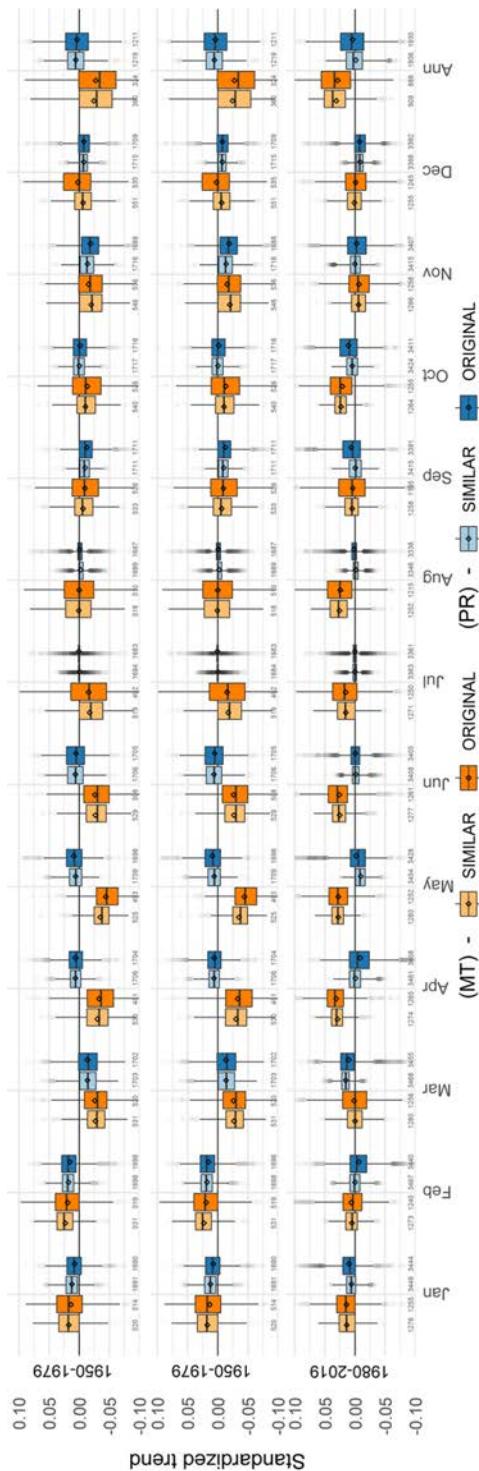
Figure 11. Mean temperature and precipitation standardized trend comparison between original series and SIMILAR gap filled series (without MK filter).

Table 3. Long-term trend comparisons between filled series using SIMILAR with and without a significance filter (MK filter at 0.05 significance). The period 1950–2019 is represented.

Var.	Filtering	Stations	Winter	Spring	Summer	Autumn	Annual	Trend °C||mm/period
MT	All stations	1557	0.133	0.191	0.233	0.135	0.176	1.232
MT	MK ≤ 0.05	1103	0.215	0.243	0.276	0.211	0.208	1.456
PR	All stations	3927	-7.519	-2.428	-2.556	1.094	-8.890	-62.230
PR	MK ≤ 0.05	1112	-18.746	-14.363	-4.424	6.894	-31.964	-223.748

4. Discussion

Incomplete series and data gaps are common in climatic series and must be filled before the series can be analyzed. Gap-filling strategies can resolve this issue in different ways, inducing changes in the spatiotemporal structure of the filled dataset and hence in the related analysis (such as in long-term trends of climate change). For instance, a well-known effect is a reduction in the variance, so that the extreme values of the variable are compressed, which is of decisive importance for the analysis of extreme events phenomena (Acero *et al.*, 2014; Teegavarapu and Nayak, 2017). However, despite the importance of using gap-filling strategies, the consequences and implications of the methods for trends have been analyzed very little considering large climatic datasets, which are mainly affected by structural changes in space and time, such as an increasing number of stations over time (Table 1). In this framework, we analyzed the influence of four gap-filling methods on long-term (1950–2019) temperature and precipitation trends at monthly, seasonal, and annual temporal aggregations in three subperiods (1950–1979, 1980–2019, 1950–2019).

The gap-filling methods showed similar trend patterns at different temporal aggregation and periods. Only MONTH depicted a contrasting pattern related to the filling method itself. The iterative process propagated, by averaging, the observations in the stations and reduced the variability of the observed trends based on the completed dataset. The decrease in the variance in reconstructed datasets has been extensively reported in other research (Serrano-Notivoli *et al.*, 2017; Teegavarapu and Nayak, 2017; Beguería *et al.*, 2019). Thus, MONTH should be used to fill short-length gaps but not to fill a whole dataset, which seems logical. Singh and Xiaosheng (2019) reported filling small gaps using the averaging nearest neighbor, reconstructing long-term gridded daily rainfall time series. Nevertheless, for the rest of the gap-filling methods, similar patterns in the interquartile range were observed (Figure 9).

Although none of the gap-filling methods had large repercussions on the long-term trends, there were spatial differences, especially in P1 (1950–1979). During this period, the number of stations and observations was limited, and the IDW method differs from the others, especially in areas with contrasting elevations. Thus, in a temporal context with a limited number of stations in mountain areas, the nearest stations had a greater influence than those far apart, even more influenced when considering stations geographically more distanced (plain areas) and with more contrasting climatic patterns. The reason why the other methods did not show similar patterns in this context has not been identified.

It is important to note that the long-term trend was determined considering stations with more than 20 years of data in the whole period. However, the distribution of the observations could be uneven in the periods 1950–1979 and 1980–2019 at monthly, seasonal and annual data aggregations. Since five minimum observations was the limit considered to assess trends (which could be a considerably low threshold), this could have affected the larger trend variability observed in the unfilled series in the period 1950–1979. The existence of a larger proportion of short-length time series could lead to the large trend variability. However, gap-filled series showed more coherent trends in this period.

The influence of neighborhood stations was decisive for maximizing the goodness of fit of the models but resolved in a wide variability of cases: 35 and 45 predictor stations for REGR, 7 stations in the case of IDW and SIMILAR showing a better model performance at shorter distances (even though the gap-filling capacity was minimized). This suggests that there is no clear criterium, and testbeds are needed to explore each particular situation. Previous research has found specific solutions for approximating this value (Tardivo and Berti, 2014). Furthermore, the number of years (*i.e.*, temporal buffer) for similarity

comparisons was decisive. Thus, the goodness of fit is maximized as the temporal buffer becomes more extensive, but this limits the gap-filling capacity of the MONTH and SIMILAR methods.

We expected a stronger influence of the number of available observations in the datasets when long-term trends were compared between periods; however, long-term trend patterns seemed to be hardly affected. One possible reason for this concern is how the N_NEARST parameter works. Each station is provided with a list in which the rest of the stations in the dataset are ranked by proximity. Thus, a problem station always has a candidate nearest station. Filling gaps in periods with a low number of stations and observations can be performed—i.e., only if there are observations at the gap date in the neighborhood—since no geographical restrictions are applied in the models.

Differences between long-term trends of temperature and precipitation were also expected due to the significant differences between the spatiotemporal dataset structures. We found a similar reduction in the trend variability associated with MONTH, with minor differences between the other methods. However, a larger dispersion in the trend was observed in P1, which is associated with a larger proportion of data gaps in the period.

The iterative gap-filling strategy was useful for applying parametrizations ordered according to the patterns observed in the test mode. This was a solution for the exiting trade-off between maximizing model performance and the gap-filling capacity. It also allowed us to explore the evolution of the spatiotemporal structure of the dataset throughout the process. Additional analyses are necessary for identifying differences in filled datasets when parametrizations that are ordered differently are used. Descriptive statistics measures, such as minimum, maximum, mean, and extreme quantiles, monitor the dataset structure during the gap-filling process.

A question not addressed in this article is the change observed in the spatial pattern of temperature and precipitation trends between Portugal and Spain, which are more intensive for precipitation (Figure 9). This effect could be attributable to the existence of differences between the meteorological networks and the possible differences in the data processing carried out by the different climate agencies. The observed effect requires an in-depth analysis to elucidate differences between climatic networks.

Standardized long-term trend comparisons between unfilled and filled series (SIMILAR) found very few differences. Nevertheless, the trend of reducing the variability in temperature and precipitation could be seen again. Focusing on precipitation, this variable has a high interannual variability, implying that regression methods are not the most suitable for detecting climatic trends. Previous research has reported that there is no clear tendency in precipitation and a high spatial and temporal variability (Gonzalez-Hidalgo *et al.*, 2009). This suggests that regression methods have limitations for evaluating the differences between gap-filling methods for precipitation and, therefore, for comparing gap-filling methods based on long-term trends. Thus, it could be of interest to explore other filling approaches. In our analysis, only 28 % of the precipitation trends were significant considering a gap-filled dataset with SIMILAR.

The climate trend in temperature showed a rate of change of 1.46 °C (0.21 °C/decade) in the whole period (1950–2019), slightly inferior to the reported in Luna et al. (2011). Summer was the season with the strongest warming trend and autumn and winter had the lowest. These results are in line with Bilbao *et al.* (2019), who evaluated trends from nine stations from 1950–2011. During the period 1950–1979, a decreasing trend was observed mainly in the spring months, and this pattern was inverted significantly in 1980–2019. In the case of precipitation, no clear trend was reported from an annual point of view. This has also been reported in other studies, which identified no significant trend in the 20th century in annual,

seasonal, or monthly data (González-Hidalgo *et al.*, 2010). However, an increase in precipitation for autumn and early spring in the period 1980–2019, compared with the period 1950–1979 was observed, which is in line with previous studies by Rodriguez-Puebla *et al.* (1998). In accordance with the authors, a scarcity of rain in summer months rains was observed. However, the highest rainfalls were observed in winter in the period 1950–1979 (in the northwest part of the Iberian Peninsula), evolving towards lower rainfalls in the period 1980–2019 in the entire context.

Considering our first hypothesis, we found that temperature and precipitation exhibited analogous long-term trend behaviors with small singularities. Considering our second hypothesis, we found that only the MONTH method showed a different behavior from the others in terms of the magnitude and significance of trends. Spatial differences between the methods were observed, especially for IDW in the period 1950–1979. This period is characterized by lower availability of observations and stations. However, gap-filling methods were hardly sensitive to the spatiotemporal structure of the data, which can be related to the robustness of the applied filling methods. Regarding the third hypothesis, we found that the proportion of data gaps has not significantly conditioned the adjustment of the gap-filling methods but a more significant variability of the trends was observed, especially in P1, when the patterns depicted greater spatial diversity.

Several aspects of our results require additional research to bring light to some considerations arising from this work. It is necessary to (i) perform gap-filling approaches in which the temporal structure of the gaps (distribution of the gaps regarding their temporal length) is considered, researching the repercussions of the gap-filling methods for them. In addition, (ii) the changes that occurred in 1975 at the administrative level in the datasets could have had an effect on the long-term trend analyzed; therefore, future studies could focus on thoroughly analyzing the repercussions of these changes.

5. Conclusions

The following conclusions can be highlighted about the different gap-filling methods used and their influence on long-term (1950–2019) temperature and precipitation trends. The methods behave in a similar way with regard to IDW, REGR, and SIMILAR, but contrast with MONTH due to its autocompletion scheme. The spatialization (maps) of the trends depicts the differences between methods, which cannot be seen in the boxplots, where the methods do not significantly differ from each other. Another aspect that should be highlighted is that the gap-filling process induced a clear reduction in the variability of the trends.

To conclude, the gap-filling series has a clear interest for generating continuous surfaces that reduce spatiotemporal discontinuities associated with data gaps. However, climate analyses can be affected by the aforementioned reduction in the data variability derived from the gap-filling processes, leading to a clear tendency towards flattening the derived trends, although they are perhaps more reliable.

6. Acknowledgements

References

Acero, F.J., García, J.A., Gallego, M.C., Parey, S., Dacunha-Castelle, D., (2014). "Trends in summer extreme temperatures over the Iberian Peninsula using nonurban station data". *Journal of Geophysical Research*. 119, 39–53. https://doi.org/10.1002/2013JD020590

Agencia Estatal de Meteorología (AEMET), http://www.aemet.es/en/portada (accessed 5.1.21).

Alemu, Z.A., Dioha, M.O., (2020). "Climate change and trend analysis of temperature: the case of Addis Ababa, Ethiopia". *Environmental Systems Research*. 9, 27. https://doi.org/10.1186/s40068-020-00190-5

Almarza, C., Luna, M.Y., (2016). "Homogeniedad y variabilidad de la precipitación y la temperatura en zonas climaticamente homogeneas de la peninsula iberica". *Servicio de Desarrollos Climatológicos. Instituto Nacional de Meteorología*. 1–7.

Armanuos, A.M., Al-Ansari, N., Yaseen, Z.M., (2020). "Cross Assessment of Twenty-One Different Methods for Missing Precipitation Data Estimation". *Atmosphere*. 11, 389. https://doi.org/10.3390/atmos11040389

Beguería, S., Tomas-Burguera, M., Serrano-Notivoli, R., Peña-Angulo, D., Vicente-Serrano, S.M., González-Hidalgo, J.C., (2019). "Gap filling of monthly temperature data and its effect on climatic variability and trends". *Journal of Climate*. 32, 7797–7821. https://doi.org/10.1175/JCLI-D-19-0244.1

Bellido-Jiménez, J.A., Gualda, J.E., García-Marín, A.P., (2021). "Assessing Machine Learning Models for Gap Filling Daily Rainfall Series in a Semiarid Region of Spain". *Atmosphere*. 12, 1158. https://doi.org/10.3390/atmos12091158

Bielenki Junior, C., Santos, F.M. dos, Povinelli, S.C.S., Mauad, F.F., (2018). "Alternative methodology to gap filling for generation of monthly rainfall series with GIS approach". *Brazilian Journal of Water Resources*. 23. https://doi.org/10.1590/2318-0331.231820170171

Bilbao, J., Román, R., De Miguel, A., (2019). "Temporal and Spatial Variability in Surface Air Temperature and Diurnal Temperature Range in Spain over the Period 1950–2011". *Climate* 7, 16. https://doi.org/10.3390/cli7010016

Brito-Morales, I., García Molinos, J., Schoeman, D.S., Burrows, M.T., Poloczanska, E.S., Brown, C.J., Ferrier, S., Harwood, T.D., Klein, C.J., McDonald-Madden, E., Moore, P.J., Pandolfi, J.M., Watson, J.E.M., Wenger, A.S., Richardson, A.J., (2018). "Climate Velocity Can Inform Conservation in a Warming World". *Trends in Ecology and Evolution*. https://doi.org/10.1016/j.tree.2018.03.009

Carnicer, J., Domingo-Marimon, C., Ninyerola, M., Camarero, J.J., Bastos, A., López-Parages, J., Blanquer, L., Rodríguez-Fonseca, B., Lenton, T.M., Dakos, V., Ribas, M., Gutiérrez, E., Peñuelas, J., Pons, X., (2019). "Regime shifts of Mediterranean forest carbon uptake and reduced resilience driven by multidecadal ocean surface temperatures". *Global Change Biology*. 25, 2825–2840. https://doi.org/10.1111/gcb.14664

Dobrowski, S.Z., Parks, S.A., (2016). "Climate change velocity underestimates climate change exposure in mountainous regions". *Nature Communications*. 7, 12349. https://doi.org/10.1038/ncomms12349

Gil-Guirado, S., Pérez-Morales, A., (2019). "Variabilidad climática y patrones termopluviométricos en Murcia (1863-2017). Técnicas de análisis climático en un contexto de cambio global". *Investigaciones Geográficas*. 27–54. https://doi.org/10.14198/INGEO2019.71.02

Padial-Iglesias, M., Pons, X., Serra, P., Ninyerola, M. (2022). Does the gap-filling method influence long-term (1950–2019) temperature and precipitation trend analyses? *GeoFocus, Revista Internacional de Ciencia y Tecnología de la Información Geográfica*, 29, 5–33. https://dx.doi.org/10.21138/GF.773

Gocic, M., Trajkovic, S., (2013). "Analysis of changes in meteorological variables using Mann-Kendall and Sen's slope estimator statistical tests in Serbia". *Global and Planetary Change*. 100, 172–182. https://doi.org/10.1016/j.gloplacha.2012.10.014

González-Hidalgo, J.C., Brunetti, M., Stepanek, P., de Luis Arrillaga, M., (2010). "La base de datos mopredas (monthly precipitatioon database of spain) y el análisis subregional de las tendencias de la precipitación mensual en españa (periodo 1945-2005)". *Asociación Española de Climatología*.

Gonzalez-Hidalgo, J.C., Lopez-Bustins, J.-A., Štepánek, P., Martin-Vide, J., de Luis, M., (2009). "Monthly precipitation trends on the Mediterranean fringe of the Iberian Peninsula during the second-half of the twentieth century (1951-2000)". *International Journal of Climatology*. 29, 1415–1429. https://doi.org/10.1002/joc.1780

Kendall, M.G., (1975). Rank correlation measures, 4th editio. ed. Charles Griffin, London, U.K.

Körner, P., Kronenberg, R., Genzel, S., Bernhofer, C., (2018). "Introducing Gradient Boosting as a universal gap filling tool for meteorological time series". *Meteorologische Zeitschrif,* 27, 369–376. https://doi.org/10.1127/metz/2018/0908

Loarie, S.R., Duffy, P.B., Hamilton, H., Asner, G.P., Field, C.B., Ackerly, D.D., (2009). "The velocity of climate change". *Nature* 462, 1052–1055. https://doi.org/10.1038/nature08649

Longman, R.J., Giambelluca, T.W., Nullet, M.A., Frazier, A.G., Kodama, K., Crausbay, S.D., Krushelnycky, P.D., Cordell, S., Clark, M.P., Newman, A.J., Arnold, J.R., (2018). Compilation of climate data from heterogeneous networks across the Hawaiian Islands. *Scientific Data,* 5, 180012. https://doi.org/10.1038/sdata.2018.12

Longman, R.J., Newman, A.J., Giambelluca, T.W., Lucas, M., 2020. "Characterizing the Uncertainty and Assessing the Value of Gap-Filled Daily Rainfall Data in Hawaii". *Journal of Applied Meteorology and Climatology*. 59, 1261–1276. https://doi.org/10.1175/JAMC-D-20-0007.1

Lu, G.Y., Wong, D.W., (2008). "An adaptive inverse-distance weighting spatial interpolation technique". *Computers & Geosciences*. 34, 1044–1055. https://doi.org/10.1016/j.cageo.2007.07.010

Luna, M.Y., López, J.A., Guijarro, J.A., (2011). "Tendencias observadas en España en precipitacion y temperatura". *Revista Española de Fisica*. 26, 1–13.

Mann, H.B., (1945). "Nonparametric Tests Against Trend". Econometrica 13, 245. https://doi.org/10.2307/1907187

Mora, D., Wyseure, G., Willems, P., (2014). "Gap Filling Based on a Quantile Perturbation Factor Technique". CUNY Academic Works.

Pappas, C., Papalexiou, S.M., Koutsoyiannis, D., (2014). "A quick gap filling of missing hydrometeorological data". *Journal of Geophysical Research*. 119, 9290–9300. https://doi.org/10.1002/2014JD021633

Paulhus, J.L.H., Kohler, M.A., (1952). "Interpolation of missing precipitation records". *Monthly Weather Review*. 80, 129–133. https://doi.org/10.1175/1520-0493(1952)080<0129:IOMPR>2.0.CO;2

Padial-Iglesias, M., Pons, X., Serra, P., Ninyerola, M. (2022). Does the gap-filling method influence long-term (1950–2019) temperature and precipitation trend analyses? *GeoFocus, Revista Internacional de Ciencia y Tecnología de la Información Geográfica*, 29, 5–33. https://dx.doi.org/10.21138/GF.773

Pons, X., (2004). MiraMon. Sistema d'Informació Geogràfica i software de Teledetecció. Centre de Recerca Ecològica i Aplicacions Forestals, CREAF. Bellaterra. ISBN:84-931323-4-9. https://www.miramon.cat.

Pons, X., Ninyerola, M., (2008). "Mapping a topographic global solar radiation model implemented in a GIS and refined with ground data". *International Journal of Climatology*. 28, 1821–1834. https://doi.org/https://doi.org/10.1002/joc.1676

R Core Team, (2022). R: A Language and Environment for Statistical Computing.

Rodriguez-Puebla, C., Encinas, A.H., Nieto, S., Garmendia, J., (1998). "Spatial and temporal patterns of annual precipitation variability over the Iberian Peninsula". *International Journal of Climatology*. 18, 299–316. https://doi.org/10.1002/(SICI)1097-0088(19980315)18:3<299::AID-JOC247>3.0.CO;2-L

Sayemuzzaman, M., Jha, M.K., Mekonnen, A., Schimmel, K.A., (2014). "Subseasonal climate variability for North Carolina, United States". *Atmospheric Research*. 145–146, 69–79. https://doi.org/10.1016/j.atmosres.2014.03.032

Sen, P.K., (1968). "Estimates of the Regression Coefficient Based on Kendall's Tau". *Journal of the American Statistical Association*. 63, 1379–1389. https://doi.org/10.1080/01621459.1968.10480934

Serrano-Notivoli, R., de Luis, M., Saz, M., Beguería, S., (2017). "Spatially based reconstruction of daily precipitation instrumental data series". *Climate Research*. 73, 167–186. https://doi.org/10.3354/cr01476

Servei Meteorològic Nacional, https://www.meteo.ad/en (accessed 5.1.21).

Singh, V., Xiaosheng, Q., (2019). "Data assimilation for constructing long-term gridded daily rainfall time series over Southeast Asia". *Climate Dynamics*. 53, 3289–3313. https://doi.org/10.1007/s00382-019-04703-6

Sistema Nacional de Informação de Recursos Hídricos (SNIRH), https://snirh.apambiente.pt/ (accessed 5.1.21).

Tardivo, G., Berti, A., (2014). "The selection of predictors in a regression-based method for gap filling in daily temperature datasets". *International Journal of Climatology*. 34, 1311–1317. https://doi.org/10.1002/joc.3766

Teegavarapu, R.S.V., Chandramouli, V., (2005). "Improved weighting methods, deterministic and stochastic data-driven models for estimation of missing precipitation records". *Journal of Hydrology*. 312, 191–206. https://doi.org/10.1016/j.jhydrol.2005.02.015

Teegavarapu, R.S.V., Nayak, A., (2017). "Evaluation of long-term trends in extreme precipitation: Implications of in-filled historical data use for analysis". *Journal of Hydrology*. 550, 616–634. https://doi.org/10.1016/j.jhydrol.2017.05.030

Theil, H., (1992). A Rank-Invariant Method of Linear and Polynomial Regression Analysis. pp. 345–381. https://doi.org/10.1007/978-94-011-2546-8_20

Vicente-Serrano, S.M., Beguería, S., López-Moreno, J.I., García-Vera, M.A., Stepanek, P., (2009). "A complete daily precipitation database for northeast Spain: reconstruction, quality control, and homogeneity". *International Journal of Climatology*. 30, 1146–1163. https://doi.org/10.1002/joc.1850

APPENDIX 1
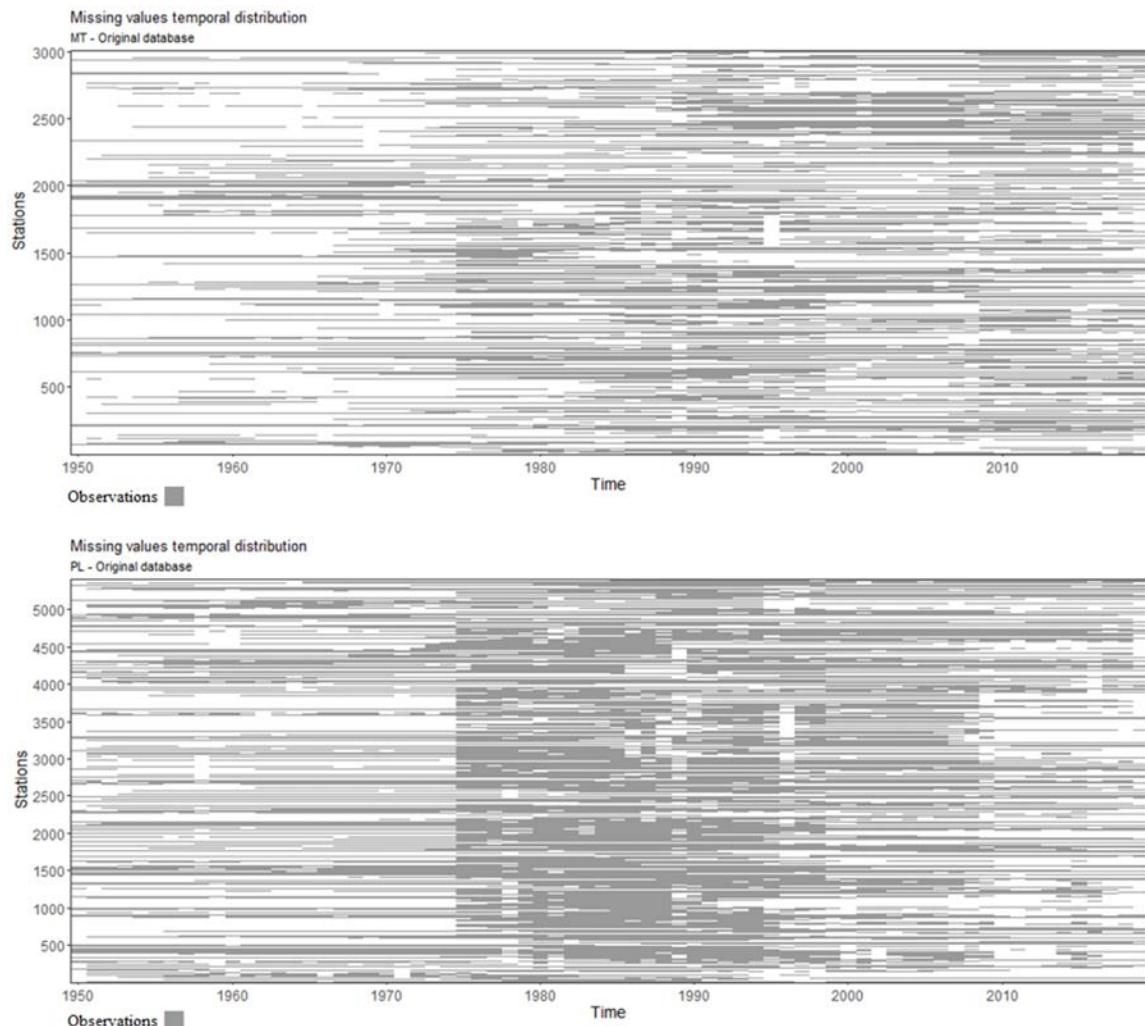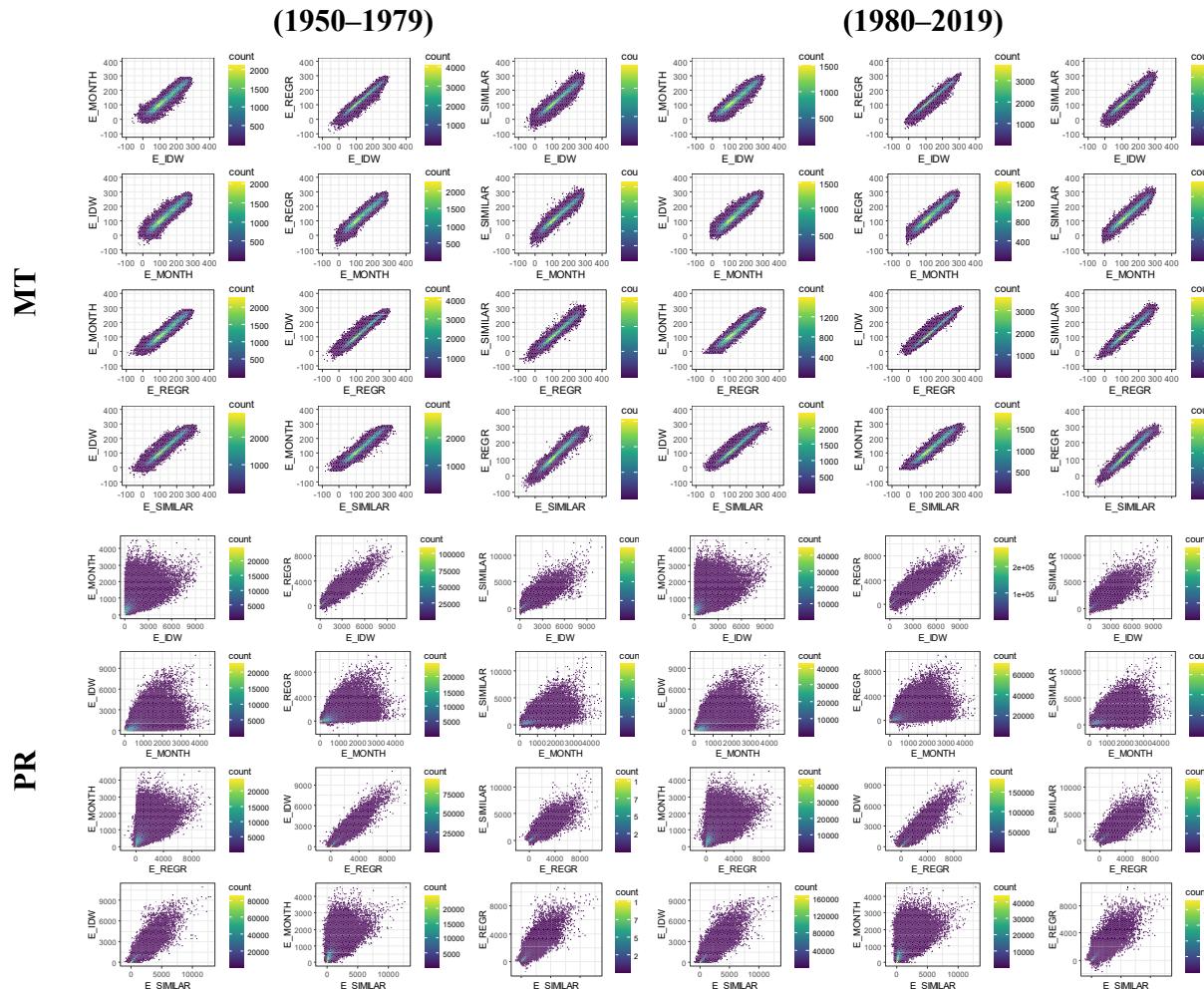
Figure A1. The temporal structure of the mean temperature (MT) and precipitation (PR) datasets. White spaces refer to data gaps.

Table A1. Pearson correlation evaluated for the different methods and periods, beside the related plots. Lower values in bold.

Period\Method		IDW	MONTH	REGR	SIMILAR		IDW	MONTH	REGR	SIMILAR
1950–1979										
IDW	MT	1.000	0.956	0.985	0.973	PR	1.000	**0.590**	0.963	0.915
MONTH		-	1.000	0.965	0.973		-	1.000	**0.590**	**0.658**
REGR		-	-	1.000	0.980		-	-	1.000	0.897
SIMILAR		-	-	-	1.000		-	-	-	1.000
1980–2019										
IDW	MT	1.000	0.959	0.989	0.979	PR	1.000	**0.542**	0.962	0.917
MONTH		-	1.000	0.968	0.974		-	1.000	**0.545**	**0.600**
REGR		-	-	1.000	0.986		-	-	1.000	0.898
SIMILAR		-	-	-	1.000		-	-	-	1.000

(1950–1979) **(1980–2019)**

Table A2. Mean trend and Std. Deviation disaggregated by variable, temporal aggregation, period, and filling method.

Climatic Variable	Temporal Aggreg.	IDW P1*	IDW P2**	MONTH P1	MONTH P2	REGR P1	REGR P2	SIMILAR P1	SIMILAR P2
MT (d°C/year (°C /decade))	Jan	0.30 ± 0.43	0.19 ± 0.26	0.05 ± 0.25	0.11 ± 0.20	0.24 ± 0.33	0.21 ± 0.24	0.22 ± 0.34	0.19 ± 0.24
	Feb	0.42 ± 0.45	0.06 ± 0.28	0.08 ± 0.23	0.02 ± 0.22	0.37 ± 0.31	0.09 ± 0.24	0.36 ± 0.33	0.09 ± 0.25
	Mar	-0.40 ± 0.45	-0.04 ± 0.31	-0.10 ± 0.28	0.01 ± 0.21	-0.44 ± 0.30	-0.01 ± 0.26	-0.37 ± 0.35	0.01 ± 0.26
	Apr	-0.35 ± 0.45	0.39 ± 0.29	-0.12 ± 0.26	0.25 ± 0.24	-0.37 ± 0.30	0.43 ± 0.23	-0.36 ± 0.34	0.42 ± 0.24
	May	-0.54 ± 0.47	0.43 ± 0.33	-0.20 ± 0.35	0.24 ± 0.26	-0.56 ± 0.32	0.46 ± 0.27	-0.53 ± 0.37	0.46 ± 0.27
	Jun	-0.32 ± 0.48	0.34 ± 0.32	-0.10 ± 0.28	0.26 ± 0.28	-0.32 ± 0.34	0.37 ± 0.27	-0.39 ± 0.39	0.38 ± 0.28
	Jul	-0.10 ± 0.50	0.15 ± 0.35	-0.05 ± 0.26	0.11 ± 0.24	-0.10 ± 0.39	0.17 ± 0.30	-0.21 ± 0.41	0.20 ± 0.30
	Aug	0.12 ± 0.48	0.28 ± 0.33	0.01 ± 0.25	0.14 ± 0.25	0.11 ± 0.38	0.31 ± 0.28	0.00 ± 0.38	0.31 ± 0.29
	Sep	-0.01 ± 0.47	0.04 ± 0.29	-0.02 ± 0.28	0.04 ± 0.26	-0.02 ± 0.36	0.06 ± 0.24	-0.10 ± 0.38	0.06 ± 0.25
	Oct	-0.08 ± 0.43	0.34 ± 0.28	-0.05 ± 0.25	0.21 ± 0.27	-0.13 ± 0.31	0.37 ± 0.23	-0.13 ± 0.34	0.35 ± 0.25
	Nov	-0.29 ± 0.43	-0.11 ± 0.27	-0.05 ± 0.24	-0.04 ± 0.20	-0.34 ± 0.34	-0.08 ± 0.23	-0.27 ± 0.34	-0.08 ± 0.24
	Dec	-0.12 ± 0.43	0.01 ± 0.28	0.01 ± 0.25	-0.03 ± 0.20	-0.17 ± 0.34	0.03 ± 0.25	-0.10 ± 0.34	0.02 ± 0.25
	Win	0.31 ± 0.42	0.10 ± 0.26	0.06 ± 0.22	0.04 ± 0.19	0.26 ± 0.31	0.12 ± 0.23	0.24 ± 0.29	0.11 ± 0.23
	Spr	-0.44 ± 0.44	0.29 ± 0.29	-0.15 ± 0.28	0.18 ± 0.20	-0.47 ± 0.29	0.33 ± 0.23	-0.43 ± 0.30	0.33 ± 0.22
	Sum	-0.06 ± 0.47	0.27 ± 0.32	-0.04 ± 0.23	0.18 ± 0.23	-0.07 ± 0.35	0.30 ± 0.27	-0.16 ± 0.33	0.32 ± 0.26
	Aut	-0.10 ± 0.42	0.09 ± 0.26	-0.04 ± 0.22	0.07 ± 0.20	-0.15 ± 0.30	0.11 ± 0.22	-0.15 ± 0.30	0.11 ± 0.21
	Ann	-0.12 ± 0.40	0.18 ± 0.26	-0.05 ± 0.20	0.11 ± 0.17	-0.15 ± 0.27	0.20 ± 0.21	-0.16 ± 0.26	0.20 ± 0.20
PR (dmm/year (mm/decade))	Jan	7.92 ± 13.48	2.70 ± 8.85	1.68 ± 9.08	1.97 ± 5.80	7.52 ± 13.54	2.76 ± 8.84	7.23 ± 12.69	2.52 ± 9.12
	Feb	10.34 ± 11.17	-0.17 ± 7.89	1.71 ± 9.07	-0.74 ± 4.93	10.24 ± 11.54	-0.31 ± 7.92	9.42 ± 10.93	-0.31 ± 7.78
	Mar	-7.20 ± 13.59	6.45 ± 4.43	-4.14 ± 9.34	2.57 ± 4.03	-7.24 ± 13.40	6.55 ± 4.60	-6.62 ± 12.85	6.07 ± 4.70
	Apr	2.41 ± 6.33	-0.99 ± 6.84	-0.04 ± 4.06	-0.41 ± 4.14	2.21 ± 6.22	-0.92 ± 6.74	2.04 ± 6.06	-0.86 ± 6.68
	May	2.69 ± 7.10	-4.33 ± 6.33	0.30 ± 4.20	-1.06 ± 3.95	2.61 ± 7.10	-4.26 ± 6.10	2.34 ± 6.72	-3.79 ± 5.82
	Jun	1.42 ± 5.15	-0.21 ± 3.29	-0.35 ± 3.15	0.11 ± 2.23	1.38 ± 5.20	-0.17 ± 3.30	0.77 ± 5.13	-0.07 ± 3.22
	Jul	0.01 ± 2.17	0.15 ± 2.02	-0.23 ± 1.39	0.14 ± 1.35	-0.13 ± 2.17	0.18 ± 2.05	-0.09 ± 2.30	0.10 ± 1.87
	Aug	-0.77 ± 3.57	-0.57 ± 2.00	-0.52 ± 2.12	0.10 ± 1.58	-1.06 ± 3.58	-0.53 ± 1.99	-0.88 ± 3.48	-0.37 ± 1.99
	Sep	-2.92 ± 4.20	-0.72 ± 5.77	-1.22 ± 3.54	0.67 ± 3.94	-3.30 ± 4.17	-0.65 ± 5.76	-3.10 ± 4.36	-0.47 ± 5.35
	Oct	0.65 ± 9.13	1.46 ± 8.32	0.13 ± 5.77	2.86 ± 6.00	0.16 ± 9.21	1.44 ± 8.33	0.18 ± 8.72	1.88 ± 7.69
	Nov	-9.27 ± 17.18	-0.21 ± 11.57	-3.98 ± 12.16	0.56 ± 6.12	-9.37 ± 17.28	-0.18 ± 11.49	-8.47 ± 16.47	-0.47 ± 11.59
	Dec	-4.82 ± 7.46	-7.08 ± 10.92	-2.90 ± 6.09	-1.85 ± 6.49	-5.13 ± 7.83	-7.08 ± 10.97	-4.58 ± 7.41	-6.62 ± 10.60
	Win	16.88 ± 30.69	-9.31 ± 25.60	2.02 ± 18.29	-3.03 ± 13.84	15.83 ± 31.67	-9.27 ± 26.02	15.24 ± 27.56	-9.08 ± 25.21
	Spr	-2.07 ± 24.78	1.55 ± 16.72	-3.49 ± 15.09	-0.09 ± 8.68	-2.25 ± 24.68	1.63 ± 16.42	-1.96 ± 22.71	1.43 ± 15.62
	Sum	0.97 ± 8.65	-1.87 ± 5.73	-0.71 ± 5.39	-0.17 ± 3.62	0.37 ± 8.98	-1.78 ± 5.68	0.44 ± 8.37	-1.46 ± 5.29
	Aut	-9.90 ± 18.59	-3.36 ± 20.81	-3.42 ± 13.84	2.12 ± 9.58	-10.57 ± 18.09	-3.32 ± 20.80	-9.48 ± 17.86	-2.90 ± 18.91
	Ann	10.20 ± 54.04	-9.35 ± 63.93	-3.76 ± 33.49	-2.02 ± 30.16	7.60 ± 54.35	-9.00 ± 63.18	9.08 ± 44.14	-8.98 ± 58.73

P1* refers to 1950–1979, and P2** refers to the 1980–2019 period.

Table A3. SIMILAR and MONTH parametrizations used for filling temperature datasets. Only the first parametrizations are shown.

METHOD	M_SUBMET	M_YESTIM	M_MIN_YESTIM		% Filled	RMSE
MONTH	m	18	18		72.13	14.5
MONTH	m	17	17		73.67	14.5
MONTH	m	16	16		75.13	14.5
MONTH	m	15	15		76.58	14.5
MONTH	m	14	14		78.00	14.5
MONTH	m	13	13		84.04	14.5
MONTH	m	13	12		79.24	14.5
MONTH	m	12	12		86.45	14.5
MONTH	m	12	11		81.60	14.5
MONTH	m	11	11		89.36	14.5
MONTH	m	11	10		83.93	14.5
MONTH	m	10	10		91.84	14.5
MONTH	m	10	9		86.81	14.5
MONTH	m	28	28		52.66	14.6
MONTH	m	27	27		54.83	14.6
MONTH	m	26	26		60.94	14.6
MONTH	m	26	25		56.94	14.6
METHOD	S_SUBMET	S_YESTIM	S_MIN_YESTIM	S_N_NEARST	% Filled	RMSE
SIMILAR	r	30	30	5	11.51	7.1
SIMILAR	r	29	29	5	12.66	7.1
SIMILAR	r	28	28	5	14.03	7.1
SIMILAR	r	27	27	5	15.39	7.1
SIMILAR	r	26	26	5	16.78	7.1
SIMILAR	r	25	25	5	18.23	7.1
SIMILAR	r	24	24	5	19.66	7.2
SIMILAR	r	23	23	5	21.28	7.2
SIMILAR	r	22	22	5	23.07	7.2
SIMILAR	r	21	21	5	25.02	7.3
SIMILAR	r	20	20	5	26.99	7.3
SIMILAR	r	19	19	5	29.14	7.3
SIMILAR	r	18	18	5	31.18	7.3
SIMILAR	r	29	29	10	21.00	7.4
SIMILAR	r	28	28	10	23.00	7.4
SIMILAR	r	27	27	10	24.98	7.4
SIMILAR	r	26	26	10	53.77	7.4
SIMILAR	r	25	25	10	27.11	7.4

Table A3 cont. SIMILAR and MONTH parametrizations used for filling the precipitation dataset. Only the first parametrizations are shown.

METHOD	M_SUBMET	M_YESTIM	M_MIN_YESTIM	% Filled	RMSE
MONTH	m	30	29	66.71	477.6
MONTH	m	30	28	69.99	477.7
MONTH	m	30	30	62.51	477.7
MONTH	m	29	28	68.53	477.7
MONTH	m	29	29	64.53	477.9
MONTH	m	28	28	66.29	478.0
MONTH	m	29	27	71.61	478.2
MONTH	m	28	27	70.13	478.2
MONTH	m	30	27	72.58	478.5
MONTH	m	27	27	67.83	478.5
MONTH	m	27	26	71.60	478.7
MONTH	m	28	26	73.09	478.8
MONTH	m	26	25	72.98	478.8
MONTH	m	27	25	74.48	478.9
MONTH	m	29	26	74.07	479.0
MONTH	m	26	26	69.26	479.0
MONTH	m	30	26	74.76	479.2

METHOD	S_SUBMET	S_YESTIM	S_MIN_YESTIM	S_N_NEARST	% Filled	RMSE
SIMILAR	r	23	23	5	34.72	207.2
SIMILAR	r	22	22	5	37.11	207.3
SIMILAR	r	24	24	5	32.43	207.4
SIMILAR	r	21	21	5	39.55	207.4
SIMILAR	r	25	25	5	30.68	207.6
SIMILAR	r	20	20	5	42.19	207.8
SIMILAR	r	26	26	5	28.96	208.0
SIMILAR	r	28	28	5	25.61	208.3
SIMILAR	r	19	19	5	44.77	208.3
SIMILAR	r	27	27	5	27.26	208.4
SIMILAR	r	29	29	5	24.00	208.9
SIMILAR	r	18	18	5	47.41	209.3
SIMILAR	r	17	17	5	50.05	209.9
SIMILAR	r	30	30	5	22.37	210.0
SIMILAR	r	16	16	5	52.84	211.2
SIMILAR	r	15	15	5	55.65	212.2
SIMILAR	r	28	28	10	38.07	212.4
SIMILAR	r	27	27	10	40.23	212.5

AVANCES PARA LA OBTENCIÓN DE MAPAS DE USOS Y CUBIERTAS DEL SUELO DE ALTA CALIDAD TEMÁTICA

3. AVANCES PARA LA OBTENCIÓN DE MAPAS DE USOS Y CUBIERTAS DEL SUELO DE ALTA CALIDAD TEMÁTICA

3.1. Artículo 2: A Framework of Filtering Rules over Ground Truth Samples to Achieve Higher Accuracy in Land Cover Maps.

Resumen: Las técnicas de clasificación digital de teledetección requieren muestras de verdad-terreno (VT) suficientes en número, precisas y distribuidas de forma ubicua. Las VT generalmente se consideran "verdaderas" *per se*; sin embargo, errores humanos, o diferencias de criterio a la hora de definir las categorías, entre otras razones, suelen limitar esta veracidad. Tener certeza de la calidad de las VT es tan decisivo que se deben definir protocolos para realizar controles de calidad adicionales antes de pasar a la etapa de clasificación. Afortunadamente, la naturaleza de las imágenes de teledetección permite establecer un marco de controles de calidad para mejorar la calidad en las VT, proponiendo un conjunto de reglas de filtrado basadas en la información de las propias imágenes. En esta investigación, se utilizaron dos conjuntos de datos de referencia preexistentes (rDS) para obtener píxeles candidatos de VT, sobre los cuales se identificaron distintas inconsistencias. Esto sirvió como base para inferir cinco reglas de filtrado basadas en el NDVI, un producto disponible en casi todos los instrumentos de teledetección. Se evaluó la aplicabilidad de las reglas en cuatro casos de estudio temporales y en dos áreas geográficas distintas. En cada caso, se extrajo un conjunto de muestras de VT a partir de los rDS y el conjunto se utilizó sin filtrar (original), y una vez filtrado de acuerdo con las reglas establecidas. Se demostró que las muestras filtradas de VT permitieron resolver problemas habituales en las categorías naturales y agrícolas. De hecho, las matrices de confusión revelaron, en promedio, un aumento en la precisión general del 10.9 puntos porcentuales, una disminución en el error de omisión de 16.8 puntos porcentuales y una disminución en el error de comisión de 14.0 puntos porcentuales. Las reglas de filtrado corrigieron las inconsistencias existentes en las muestras de VT extraídas del rDS, considerando diferencias inter-anuales e intra-anuales existentes, problemas de escala, comportamientos múltiples a lo largo del tiempo, así como asignaciones erróneas de etiquetado. Por ello, aunque se han detectado algunas limitaciones intrínsecas (como en los bosques mixtos), el protocolo permite una cartografía mucho más precisa de las cubiertas gracias al uso de muestras de verdad-terreno más robustas, algo especialmente importante en un contexto multitemporal en el cual la consideración de la fenología es esencial.

Palabras clave: cartografía de cambios de las cubiertas del suelo; Landsat; clasificación digital de imágenes; muestras de verdad-terreno; reglas de filtrado

Article

A Framework of Filtering Rules over Ground Truth Samples to Achieve Higher Accuracy in Land Cover Maps

Mario Padial-Iglesias [1,*]**, Pere Serra** [1]**, Miquel Ninyerola** [2] **and Xavier Pons** [1]

1   Grumets Research Group, Departament de Geografia, Edifici B. Universitat Autònoma de Barcelona, 08193 Bellaterra, Catalonia, Spain; pere.serra@uab.cat (P.S.); xavier.pons@uab.cat (X.P.)
2   Departament de Biologia Animal, Biologia Vegetal i Ecologia, Edifici C. Universitat Autònoma de Barcelona, 08193 Bellaterra, Catalonia, Spain; miquel.ninyerola@uab.cat
*   Correspondence: mario.padial@uab.cat

Abstract: Remote Sensing (RS) digital classification techniques require sufficient, accurate and ubiquitously distributed ground truth (GT) samples. GT is usually considered "true" per se; however, human errors, or differences in criteria when defining classes, among other reasons, often undermine this veracity. Trusting the GT is so crucial that protocols should be defined for making additional quality checks before passing to the classification stage. Fortunately, the nature of RS imagery allows setting a framework of quality controls to improve the confidence in the GT areas by proposing a set of filtering rules based on data from the images themselves. In our experiment, two pre-existing reference datasets (rDS) were used to obtain GT candidate pixels, over which inconsistencies were identified. This served as a basis for inferring five key filtering rules based on NDVI data, a product available from almost all RS instruments. We evaluated the performance of the rules in four temporal study cases (under backdating and updating scenarios) and two study areas. In each case, a set of GT samples was extracted from the rDS and the set was used both unfiltered (original) and filtered according to the rules. Our proposal shows that the filtered GT samples made it possible to solve usual problems in wilderness and agricultural categories. Indeed, the confusion matrices revealed, on average, an increase in the overall accuracy of 10.9, a decrease in the omission error of 16.8, and a decrease in the commission error of 14.0, all values in percent points. Filtering rules corrected inconsistencies in the GT samples extracted from the rDS by considering inter-annual and intra-annual differences, scale issues, multiple behaviours over time and labelling misassignments. Therefore, although some intrinsic limitations have been detected (as in mixed forests), the protocol allows a much better Land Cover mapping thanks to using more robust GT samples, something particularly important in a multitemporal context in which accounting for phenology is essential.

Keywords: land-cover change mapping; Landsat; digital image classification; ground truth samples; filtering rules

1. Introduction

Historically, land cover mapping (LCM) has provided specific information for monitoring environmental impacts related, for instance, to soil degradation, deforestation, water quality and biodiversity loss [1–5]. It also plays a decisive role in local, national and international management policies [6–8]. Aerial photography [9] was key for the start of a new era of LCM, a field nowadays strongly related to remote sensing (RS) in the task of providing land cover information for human needs [10,11]. In 1994, the "Land Use and Cover Change" project was launched to address how biophysical and anthropogenic factors impact land dynamics that produce environmental and social impacts [12]. Since then, LCM has substantially expanded due to the increasing demand for land cover information due to concern about global change and sustainability management, which are currently hot research topics within the scientific community. Studies based on LCM have been carried out practically all over the world (e.g., in Australia [13], Canada [14], China [15],

India [16], Iran [17], Kenya [18], Madagascar [19], Thailand [20], Uganda [21] or the United States of America [22–24], to cite only a few) and also in the global context [25–27]. Thus, RS provides data that improve our environmental understanding by making it possible to analyse time series of land cover change and the drivers involved in this. It contributes decisively to the definition of management strategies with a time perspective.

Current LCM focuses mainly on using RS data and machine learning classification algorithms [28]. The most relevant stages usually include: (1) the definition of the mapping approach, which includes establishing the purpose of the map, its thematic resolution (level of categorical detail), the geographic extent (local, regional or global scale), as well as the data and the processing algorithms to be used; (2) the data acquisition and pre-processing, including geometric and radiometric corrections; (3) the collection of a reliable dataset of ground truth (GT) samples to be used as training and test areas (TTA) in the classification stage; (4) the classification processing; (5) the post-classification phase, comprising generalisation or editing strategies to ensure consistency across the mapped area, re-examination of unclassified areas, etc.; and (6) a final stage of map accuracy assessment.

RS imagery has increased its availability since 2008 when the United States Geological Survey (USGS) adopted a free and open Landsat data policy [29], which has been highly beneficial to many segments of society, leading to new science applications and approaches within the scientific and technical community [30,31]. Since then, similar policies have been adopted worldwide, such as the joint European Commission and European Space Agency Copernicus programme [32], with Sentinel instruments that, from 2014 on, provide temporal continuity and systems compatibility with the Landsat and other satellite series [33]. Furthermore, the release of the Landsat Multispectral Scanner System (MSS) ESA archive adds a new collection of level 1 products acquired over European and North African countries as far back as 1975, enlarging Landsat and Copernicus Sentinel-2 satellite series [34].

During the last decades, technical advances have improved LCM production. For instance, satellite imagery has increased, especially in spatial, temporal and radiometric resolution capacities, and classification algorithms have led to more robust results, which frequently require larger datasets for training and validation purposes [35,36]. Furthermore, image processing systems supporting RS applications have increased in number and capabilities [37,38]. For instance, the Continuous Change Detection and Classification (CCDC) algorithm provides an efficient model capable of detecting land cover change continuously, using all the incorporated Landsat images and providing LCM at any time [39]. However, despite technological improvements, there are still some issues about deriving thematically precise and reliable GT samples for LCM production, mainly for large areas such as the ones covered by the above cited programmes [28] and when GT are not "perfect".

GT samples are a requisite for deriving LCM using most classification strategies. Several approaches are used to provide GT samples [40,41]: fieldwork campaigns [42], digitising polygons based on expert image photointerpretation of aerial photography and/or of the satellite imagery itself [43–45], crowdsourcing campaigns or citizen science initiatives [46], and data extraction from pre-existing reference datasets (rDS), including forest inventory data [47,48], or even a combination of them [49]. Recently, efforts have been made to analyse the influence of the quality of the GT samples during the classification processes used for LCM. For instance, in [50] the authors provide an overview of the repercussions of the training data error in machine learning algorithms. The research describes the main sources of error and the derived impacts. It also provides guidelines for accounting for and minimising errors. The sources of training data error are failure to adequately represent the spatial-temporal-spectral domains of the features of interest, including class balance, labelling accuracy, and class comprehensiveness; temporal unrepresentativeness; spatial co-registration problems; spatial resolution and scaling issues; and the lack of spatial representativeness due to uneven geographic contributions. These errors mainly come

from image misinterpretation, labelling mistakes, semantic ambiguity, intrinsic problems when pixels are labelled in transitional areas and geolocation inaccuracies.

In traditional Earth observation research, the uncertainty associated with TTA is generally unreported and it is often considered 100% accurate [50–52]. However, in the strategies for deriving GT samples, the map producer has to evaluate, among other aspects, the temporal consistency between the mapping classification imagery and the sources of rDS used. If an imperfect temporal consistency is assumed (which is usually the case), the map producer should define strategies to detect and exclude errors in GT samples, especially in highly dynamic categories such as those related to the wilderness and agriculture. In a classification context, the existence of errors in TTA is extremely relevant during the training phase of the classification stage and affects the resulting map accuracy. Moreover, thematic inconsistencies can produce error propagations towards products derived from LCM and subsequently have large repercussions in map-based decision making [53].

In LCM production, it is very common to derive GT samples using pre-existing rDS [54,55]. Examples of rDS are the CORINE land cover map at the European scale, and at country level, the *Sistema de Información sobre Ocupación del Suelo de España* (SIOSE), the *Land cover map for Great Britain* and the *Carte d'occupation des sols du France* (Table S1 provides other rDS examples and their characteristics). These rDS cartographies were generated at a certain scale (spatial resolution in raster format), thematic resolution (legend) and temporal reference. The scale establishes a minimum mapping unit (MMU for land cover objects with cartographic representation [56]. Therefore, real objects that do not reach the MMU have no cartographic representation and are dissolved with dominant objects. For instance, traditional CORINE land cover maps were generated with a MMU of 25 ha (5 ha for change products) and a minimum mapping width (MMW) of 100 m, providing land cover information across Europe at a 1:100,000 scale [57]. Another example is SIOSE with a MMU of 0.5, 1 or 2 ha (depending on the cover type) and 15 m of MMW for linear features. As a consequence of an established scale in the rDS, real phenomena with no cartographic representation coexist with others in the same cartographic object, and this is a potential source of error.

The thematic resolution refers to the level of detail of the geospatial information obtained in a particular cartographic representation [58,59]. It is a property of the rules defining the hierarchy of categories (when this hierarchy exists), the criteria used to describe them and the relationships between categories [60]. Historically, the RS community has produced several legend classification schemes [61–64]. For instance, in a hierarchical framework scheme [65], son-father-dependent relationships are established between classes. The more detail in the resolution in the source information, the more detail in the features (spatially and thematically) that can be interpreted. Classification schemes contain a discrete number of thematic levels (e.g., the CORINE land cover map distinguishes five classes at the first level, which are disaggregated into 15 classes at the second level and 44 detailed classes at the third level [66]). The rDS with hierarchical classification schemes can lead to potential sources of error, which are larger in the most extensive class levels.

Finally, rDS usually define the temporal reference of the product. For instance, during the first version of the SIOSE project, high-resolution 2005 SPOT-5 images (at a 10×10 m^2 resolution), together with auxiliary data were produced from photointerpretation tasks. Ideally, the cartographic production is updated periodically, providing a temporal pseudo-continuity. Depending on the availability of an rDS that is temporally close to the imagery to be used for classification purposes, there will be time differences to a lesser or greater extent. The lack of temporal consistency between images and rDS can lead to phenological inconsistencies between the real spectral signatures and the rDS associated labelling. A previous study detected thematic inconsistencies and errors during the classification process when reliable GT samples were derived, both at the training and validation stages, considering older images with respect to a rDS (namely a backdating effect) [54]. This work proposed a strategy consisting of finding spectrally invariant pixels for the legend categories between the rDS date and the imagery date. The same strategy can be used

when images in the future are used with respect to a former rDS date (being an updating effect in this case).

In a time series analysis, the lack of temporal continuity in the rDS, due to a budget reduction or even to no interest in updating, restricts the information to specific dates. This leads to temporal lags between the imagery and rDS dates, besides the labelling errors intrinsic to almost any dataset. Moreover, similarly to producing a land cover map for a certain year, imagery from several months is used (due to phenology properties, and to avoid cloud or snow problems, etc), and it is intra-annually impossible to have GT samples that perfectly match a set of images that is multitemporal in nature. Consequently, TTA candidates derived from rDS should be tested and temporally updated to reduce the errors also caused by these inconsistencies.

With this perspective, we hypothesise that the application of some filtering rules may help to exclude issues from the TTA candidates. Therefore, this research proposes applying some filtering strategies to identify and exclude errors from the GT samples derived from an rDS (the SIOSE dataset in this case). In our experimental phase, we identified errors in GT samples associated with various issues: the inter-annual time difference between imagery for mapping and the rDS used for GT extraction; the intra-annual time variability within the mapping imagery; the scale problem related to the rDS scale and imagery resolution compatibility; the existence of multiple behaviours within selector polygons; and, finally, polygon labelling misassignments. We researched the design and application of a set of filtering rules using the most used vegetation index, the NDVI. We chose this index due to its simplicity, because only two bands are involved, and its availability, because red and near-infrared bands are very widespread in almost all Earth Observation instruments that are used for LCM. Therefore, our main aim is to define this framework of filtering rules that can be used to solve real and recurrent problems in GT samples and demonstrate that they enhance the thematic quality of the final maps. To accomplish these objectives, we explore the performance of rules in the context of four full Landsat scenes (from 200-030 to 200-033) in the Iberian Peninsula at four temporal moments (1987, 2002, 2012 and 2017 maps) and using rDS with different time differences between the rDS and the year of the classification imagery. This diverse test bed is aimed at providing information about the robustness of the proposed filtering rules.

2. Study Area

The study area is located in the Iberian Peninsula (Figure 1) and is defined by the Landsat scenes with path 200 and rows 030 to 033 of the Landsat Worldwide Reference System-2 (WRS-2), located between $-4°0'$W and $0°1'$E and $38°0'$N and $44°6'$N and covering about 126,000 km^2. The area comprises large part of the Spanish Autonomous Communities (NUTS 2) of Andalucía, Aragón, Castilla-La Mancha, Castilla y León, Euskadi, Navarra, La Rioja, some part of Madrid, Comunitat Valenciana and Murcia, and part of the French Pyrénées-Atlantiques department located in the southwest of France and the Nouvelle-Aquitaine region. The scenes cover a large sector of the Ebro hydrographic basin and the head of the Tagus, Jucar, Guadiana and Guadalquivir hydrographic systems.

Spatial heterogeneity characterises the geographical context in terms of its climatology, topography, geology and land cover. The Pyrenees mark its influence, extending between the Atlantic Ocean and the Mediterranean Sea, with an elevation that gradually increases from the Basque mountains near the Bay of Biscay to the central sector, where the highest elevations are reached. The Iberian System and the north of the Baetic System mark the limits of extensive valleys where agriculture activities have been developed historically.

The context is characterised by different rainfall and temperature regimes along longitudinal and latitudinal gradients. The total annual-accumulated precipitation varies from 450 to 1200 mm, a variation that determines a heterogeneous vegetation distribution in this context. The north-western extreme is under the oceanic influence, with high accumulated annual precipitations and relatively small differences between winter and summer temperatures. The humid conditions gradually diminish eastward and southward,

where semi-arid Mediterranean conditions prevail, while the central Pyrenees and Iberian System mainly have continental conditions [67]. The foreland Ebro Basin occupies around 85,000 km^2, where agricultural irrigation and industrial activities have historically taken place due to the water availability and soil fertility provided by the Ebro River [68].
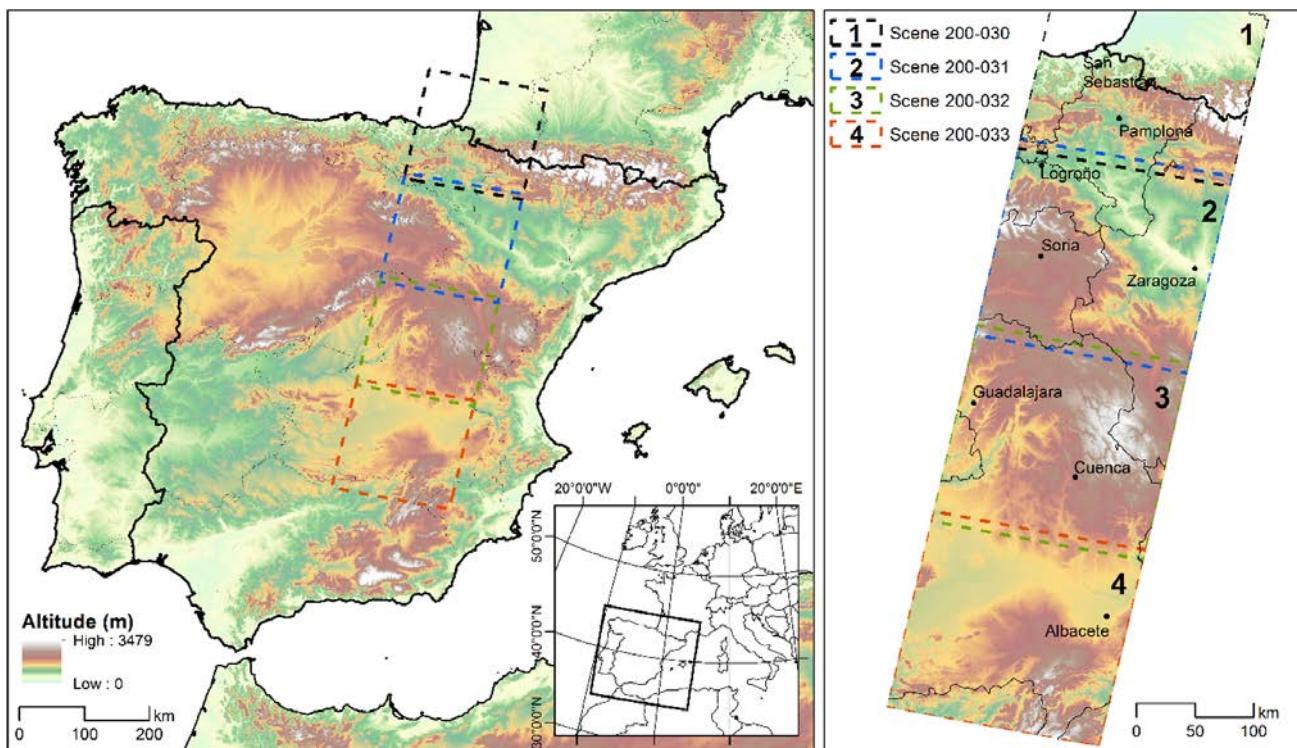
Figure 1. The spatial location of the Landsat scenes in the context of the Iberian Peninsula.

3. Materials

3.1. Remote Sensing Images

In this study, three temporal classification cases were generated in the context of a land cover time-series change analysis occupying the north scenes 200-030 and 200-031. The classification dates corresponded to 1987, 2002 and 2017 (LCM-1987, LCM-2002, LCM-2017), being the GT samples derived from the SIOSE 2005. Two additional classifications were developed to evaluate the sensitivity of the filtering rules. The first one considering another version of the SIOSE dataset (SIOSE 2011), deriving the LCM-2012 for the scenes 200-030 and 200-031. The second classification considering a new spatial context comprising the southern scenes 200-032 and 200-033. For this case, the SIOSE 2005 rDS was used together with imagery temporally close generating the LCM-2002 in these southern scenes.

Each classification was performed considering images temporally close to the reference date and distributed throughout the growing season. This temporal variability is required for gathering most of the phenological variation of crops and natural land covers (intra-annual phenological variability) in a multi-temporal perspective [69]. Therefore, images from the reference year were preferentially selected. However, in their absence (because of clouds), other images that were as temporally close as possible were selected. This decreased the disparities with the phenology of the vegetated land cover categories, a requirement that cannot always be assured in more dynamic categories, such as those with crop rotation. Nevertheless, if inconsistency does occur, it should be managed through filtering rules, as described in the following sections.

Level 1 terrain-corrected Landsat images, courtesy of the U.S. Geological Survey (USGS), were acquired throughout the USGS website portal (https://earthexplorer.usgs.gov/, accessed on 8 June 2021) [70] for the four temporal moments (1987, 2002, 2012 and 2017)

and the path-rows 200-030 to 200-033. Table S2 in the Supplementary Materials describes the set of images selected. Imagery corresponds to the Landsat 4–5 Thematic Mapper (TM), Landsat 7 Enhanced Thematic Mapper Plus (ETM+) and Landsat 8 Operational Land Imager (OLI).

3.2. Ancillary Data

Topography is a determinant factor that controls the total amount of energy incident on the Earth's surface [71]. This affects biophysical processes, water/energy balances, and acts as a driver in numerous ecological, physiological, and life processes [72]. Ancillary data, such as digital elevation and related models (slope, aspect, solar radiation), have been proven to enhance land cover type discrimination and increase the final accuracy of the digital data in RS classification [73–77]. In the study area, a 30 m spatial resolution Digital Elevation Model (DEM) was obtained through a 1:5000 lidar dataset from the Spanish National Plan for Aerial Orthophotography 2010 (PNOA, https://pnoa.ign.es/el-proyect o-pnoa-lidar, accessed on 5 July 2021) [78]. Two auxiliary variables were generated from the DEM of the area, using the free MiraMon GIS & RS software [79]:

(1)   A summer solar radiation surface (10 kJ/(m^2 × day × μm)), following the procedure described in Pons and Ninyerola [80] and implemented in the *InsolDia* module of MiraMon.
(2)   A slope surface (in degrees), using the *Pendent* module.

Summer solar radiation and slope were used as independent variables in the classification process as they were useful in previous LCM [81].

3.3. Ground Truth from a Reference Dataset (rDS)

The Land Occupation Information System of Spain (SIOSE) dataset was considered to derive reasonably robust GT samples, divided into training and test area (TTA) subsets. The SIOSE dataset is produced by photointerpretation at a reference scale of 1:25,000, with 5 m of planimetric accuracy, following the INSPIRE principles and techniques. During the first version of the SIOSE project, high-resolution 2005 SPOT-5 images (10 × 10 m^2 resolution), auxiliary Landsat 5 TM (thematic mapper) images (30 × 30 m^2) and orthophotographs (0.25 × 0.25 m^2 resolution) of the PNOA were collected for photointerpretation tasks. Other auxiliary datasets, such as cadastral information, helped to characterise land-use regimes (dry/irrigated) in agriculture plots. SIOSE is updated periodically, and there are versions available at the time of this paper for reference dates: 2005, 2009, 2011, and 2014. High-resolution 2014 and 2017 products are under production.

The SIOSE project adopted an object-oriented data model [82] where the polygon is the spatial unit that stores every present and displayable land cover enclosed in it, occupying at least 5% of the total area of the polygon. Every defined land cover type is a continuous and homogeneous spatial region characterised by its attributes. It can be described as "*simple*", or "*composite*" in the case of a combination of two or more simple units. *Simple* land covers are bare soils (SDN), pastures/grasslands (PST), shrublands (MTR), broadleaf deciduous forest (FDC), broadleaf evergreen forest (FDP), coniferous (CNF), rice/not rice herbaceous crops (CHA/CHL), and vineyard/olive groves/citrus fruit trees (LVI/LOL/LFC). Furthermore, the land covers can be characterised by "*attributes*" that confer additional information (i.e., sc (rainfed; CHLsc), rr (irrigated; CHLrr), pl (plantation forest; CNFpl)).

The SIOSE_CODE database field describes the polygon composition according to the type of land cover, the cover fraction (percentage of areal occupation within a polygon), and the spatial distribution/aggregation form (association (A), irregular mosaic (I) and regular mosaic (R)) in the case of *composite* land cover polygons. For instance, the SIOSE_CODE (A(70CNF_20PST_10MTR)) denotes an association of 70% coniferous, 20% grasslands and 10% shrublands, adding up to 100% all together. Thereby SIOSE_CODE served to extract polygons based on the desired characteristics. Table 1 provides examples of the polygon labelling definition and its visual correspondence over high-resolution orthophotography,

denoting multiple land cover types coexisting in the *composite* land cover polygons, being the more problematic ones to be served as GT for RS imagery classification.

Table 1. Land cover composition and spatial distribution labelling within SIOSE polygons.

Land Cover Composition	SIOSE_CODE Database Field	Visual Example
Simple	CHLsc [1]	
Composite in **R**egular Mosaic	**R**(55FDP_45CHLsc) [2]	
Composite in **I**rregular Mosaic	**I**(50CHLsc_35FDP_15PST) [2]	
Composite in **A**ssociation	**A**(40CNF_40PST_20MTR) [2]	

A figure to define the percentage occupation is not required in [1] *simple* land cover polygons since the land cover occupies 100% of the total area. Any form of [2] *composite* land cover polygons is characterised by a mixture of land covers (potentially different phenological responses), which could derive into error-prone GT areas.

Due to the scarceness of *simple* land cover polygons and the dominance of *composite* land cover polygons, there is a strong need to define filtering rules to select locations agreeing with target category phenology and to exclude other behaviours, besides serving as updating/backdating information for other temporal moments. The proposed filtering rules should be applied to *composite* land cover polygons and are extendible to *simple* land cover polygons as an error protection measure (human errors, etc.). The filtering strategies are assessed in Section 4.2.

4. Methods

This study develops a framework to enhance land cover classification accuracy through quality control of GT areas based on a set of filtering rules. However, for these rules to be general and to fulfil the goal that other RS users achieve similar enhancement effects, it is important to explain the pre-processing of the imagery. The proposed filtering rules are based on analysing the NDVI time series. Choosing NDVI solves the usual GT reliability problems that occur in both the wilderness and crop categories, ensuring a likely phenological behaviour. This allows our method to be widely usable because the NDVI can be computed from almost all RS instruments. We evaluated the performance of the filtering rules through classification of study cases. The framework depicted in Figure 2 is divided into three main stages developed in the following subsections: (Section 4.1) image pre-processing and preparation of other auxiliary variables, (Section 4.2) ground truth (training and test samples) treatment, and (Section 4.3) classification process and accuracy assessment.

(A) PREPROCESSING (4.1 section)

LANDSAT L1T IMAGES

Auxiliary variables

DEM
SLOPE
SOLAR RADIATION

RADIOMETRIC CORRECTION

REFLECTANCE VALUES IMAGERY

SPECTRAL INDICES

NDVI
NDWI

CLOUDS, CLOUD SHADOWS AND SNOW MASKS

FINAL VARIABLES

(B) GROUND TRUTH (TRAINING AND TEST SAMPLES) TREATMENT (4.2 section)

SQL STATEMENTS → SIOSE 2005 GT REFERENCE DATASET

NEAREST NDVI SERIES → GT PIXEL CANDIDATES

SPECTRAL-TEMPORAL SIGNATURES

INCONSISTENCIES IDENTIFICATION ANALYSIS

INTER-ANNUAL TIME — INTRA-ANNUAL TIME — SCALE
MISASSIGNMENT — MULTI-BEHAVIOUR

NDVI FILTERING RULES

RULE [0]
RULE [1]
RULE [2]
RULE [...]
RULE [N]

(C) CLASSIFICATION PROCESS AND ACCURACY ASSESSMENT (4.3 section)

CLASSIFICATION (KNN)
LAND COVER MAP
ACCURACY ASSESSMENT

ROBUST GT TRAINING SAMPLES
ROBUST GT TEST SAMPLES

Figure 2. Methodology flowchart. Image pre-processing (**A**) provided the final variables used in the classification process and NDVI series to characterise the spectral-temporal signatures of the different classes. (**B**) Structured Query Language (SQL) statements applied to SIOSE 2005 rDS provided a set of polygon selectors which determined the initial GT candidate pixels. (**C**) The rules applied to GT candidate pixels provided a final set of robust GT samples, segregated into training and test area (TTA) subsets.

4.1. Image Pre-Processing

Satellite imagery was kept in the Universal Transverse Mercator 31 N zone, WGS84, spatial reference system in order to avoid introducing additional resampling problems. To generate a unified classification context, images captured on the same day (equal path/orbit) were mosaicked previously to any other process, using the *Mosaic* module of MiraMon. In other cases, a mosaic of neighbour dates was applied after radiometric correction to derive a coherent surface reflectance composition (see next point).

4.1.1. Geometric and Radiometric Correction

The satellite imagery had an L1TP level of processing (https://www.usgs.gov/core-science-systems/nli/landsat/landsat-levels-processing, accessed on 5 July 2021) based on ground control points and a DEM for topographic displacement correction. The average geometric Root Mean Square Error (RMSE) model was 5.55 m (median 5.26 m), 3.56 m for minimum and 10.39 m for maximum, for all images considered. Note that these figures mean an accuracy level clearly lower than half of a 30 m pixel.

Images were radiometrically corrected using pseudo-invariant areas following [83,84] the methods implemented in the *CorRad* module of MiraMon. The procedure obtains reflectance values from digital numbers through atmospheric and topographic corrections using, among other parameters, pseudo-invariant areas (PIA) derived from a long time-series of MODIS reference locations, sensor calibration parameters, solar illumination and cast-shadow models for each pixel and date.

4.1.2. Spectral Indices

Spectral indices are based on the properties of the spectral signatures that characterise the interaction of electromagnetic radiation with a specific surface. Combining several multispectral bands makes it possible to emphasise land cover characteristics, and identify where they dominate spatially. In this research, the legend was established based on previous studies [54], and describes thirteen categories: *coniferous forest* (CoF), *broadleaf deciduous forest* (BDF), *broadleaf evergreen forest* (BEF) *shrublands* (Shl), *grasslands* (Grl), *bare soils* (BrS), *water bodies* (WaB), *urban areas and infrastructures* (Urb), *irrigated herbaceous crops* (IHC), *dry herbaceous crops* (DHC), *irrigated woody crops* (IWC), *dry woody crops* (DWC) and, finally, *rice crops* (RiC). According to previous studies in the same geographical context, indices such as the Normalised Difference Vegetation Index (NDVI), the Normalised Difference Water Index (NDWI) or the Normalised Difference Snow Index (NDSI) have proven appropriate for emphasising vegetation phenological patterns, bare soils or water bodies, and also for excluding snow and cloud covers [54,81,85].

The NDVI [86] is the most widely used index for monitoring vegetation activity and its dynamics, and enables easy spatial and temporal comparisons. The index is derived as the difference values measured in red and near-infrared (NIR) bands, divided by their sum. The NDWI (NDWI$_3$ in [87]) is used for identifying water bodies in classification processing. It is computed as the difference values measured in shortwave-infrared (SWIR) and NIR bands, divided by the sum of them. For all the dates considered, the NDVI and NDWI were used to better characterise many of the land cover classes in the classification process. Furthermore, the NDVI series were used to derive the filtering strategies carried out in Section 4.2.

Cloud-cover and cloud-shadow masking are a time cost, but they are a necessary pre-processing task. These areas were identified using the *Fmask* algorithm [88]. However, a visual review and manual corrections over the automatic procedure were required, mainly when masking thin clouds, contrails and anomalous sensor behaviours, the last of these being more common in earlier images.

The Normalised Difference Snow Index (NDSI) has a long history in the context of snow classification and uses the combination of SWIR and visible wavelengths [89,90]. It is assessed as the difference values measured in Green and SWIR bands, divided by their sum. We defined a threshold of NDSI > 0.15, lower than the usual 0.40 value [90], to discriminate snow-covered areas in line with other authors [91–93]. Decreasing the threshold gave better results when snow cover was discriminated in the Pyrenees, which has a rugged/irregular terrain and snow with a patchy distribution or mixed with vegetation. Once cloud or snow masks were derived, they were applied to exclude these areas from the spectral bands.

4.2. Ground Truth (Training and Test Samples) Treatment

In this study, GT (training and test) samples were extracted considering the SIOSE 2005 and 2011 datasets (SIOSE, https://www.siose.es/, accessed on 5 July 2021) [94] as a GT reference dataset source. We established and applied a set of Structured Query Language (SQL) statements to the SIOSE_CODE database field. The purest and high-cover-fraction polygons were identified, avoiding those that mix certain types of land covers (see Table S3 in the Supplementary Materials). Polygons were eroded, applying a 30 m buffering corresponding to Landsat pixel size, diminishing the influence of mixed pixels (heterogeneous) and the planimetric error associated with imagery/vectors at the boundaries [95]. Furthermore, polygons with an area ≤1.0 ha were discarded because

of their low representativeness. The remaining polygons masked the initial set of GT candidate pixels evaluated for each category.

Given the extensive study area (four full Landsat scenes), some empirical tests were performed with different tile sizes (3 × 3, 5 × 5, 7 × 7 and 9 × 9) to define the best unit size of analysis, considering the trade-off between computation time and a better polygons subdivision. The selected option was partitioning polygons into tiles of 7 × 7 pixels (210 m wide) co-registered with the spatial pattern of the imagery. The *Fishnet* tool from the ArcGIS® 10.7 software (ESRI, Redlands, CA, USA) was used for tilling. This GIS ech-nique makes it possible to partition large polygons into homogeneous square-shaped sub-polygons for sampling purposes, reducing the spatial autocorrelation and increasing the homogeneity in the spatial distribution of the TTA subset used for modelling. For each category, we randomly selected 70% of the total area for training and preserved the remaining 30% for validation purposes, ensuring category representativeness in both sub-sets. Tiles were also helpful for estimating statistics locally (central tendency and statistical dispersion measures) to define filtering rules. Final polygon masks defined the initial GT candidate pixels for each category.

In the exploratory phase, the LCM-2002 imagery was selected because of its temporal proximity to SIOSE 2005 rDS. The classification imagery should describe the intra-annual phenology during the growing season of natural and agricultural land covers. Dates spanning from Spring to Autumn enhance the phenological contrasts of categories (Table S2). Images were pre-processed, cloud masked, and the radiometric correction performed before deriving the NDVI series.

As a form of sensitivity analysis, we evaluated the performance of the rules by using the SIOSE 2011, as a new rDS, and contemporary imagery, deriving the LCM-2012. Complementarily, rules performance was evaluated in a new spatial context, the scenes 200-032 and 200-033 considering SIOSE 2005 as rDS.

4.2.1. Spectral-Temporal Signatures

The training set of polygons (70% of the GT total area) were masked with the NDVI series, and their temporal dynamics were evaluated. The objective was to analyse pheno-logical patterns of each category in order to identify abnormal behaviours. Furthermore, analysing the temporal patterns served to formulate filtering rules and approximate the parametrisation of the rules.

Inconsistencies were identified through the temporal frequency distribution as in the plots in Figure 3. For instance, low NDVI values were observed in coniferous, broadleaf evergreen, and deciduous forest because of the associations among several categories within polygons.
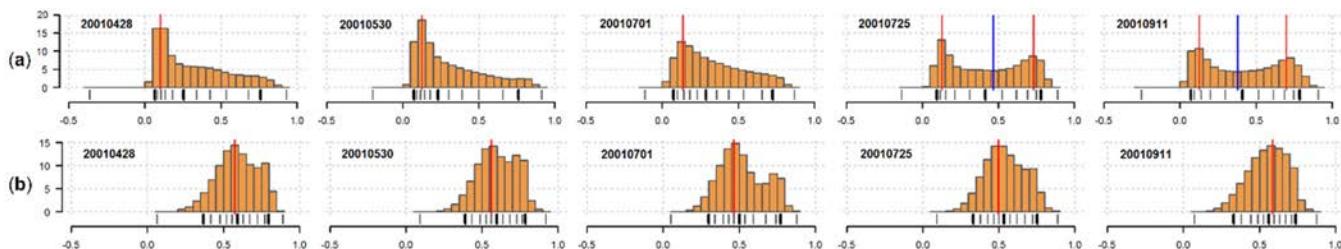
Figure 3. The temporal relative frequency distribution of the NDVI is displayed for (**a**) *irrigated herbaceous crops* and (**b**) *broadleaf evergreen forest* categories. Percentage values are shown in the vertical axis, while the NDVI range of values is presented in the horizontal axis. The red and blue vertical lines define modes (Mo) and antimodes (AMo), respectively; modelled locations are useful when multimodality is assessed [96]. Dates are in year-month-day format.

Furthermore, bimodal distributions were identified in the case of broadleaf evergreen forest and irrigated herbaceous crop categories. The inconsistencies were analysed, and filtering rules applied to exclude them. Histograms of the rest of the categories are detailed in Figure S1 in the Supplementary Materials.

4.2.2. Identification and Analysis of Inconsistencies

Historical PNOA orthophotography (dates between 1998–2003) and the imagery spectral bands supported phenological interpretation during the analysis. Furthermore, the National Forest Inventory (NFI) (version 2 (1986–1995) and version 3 (1997–2007)) provided robust information about forest species composition in the inventory plot locations over time [97]. SIOSE datasets provide particularly valuable and useful cartographic information for the Spanish territory; however, the complexity of the territory and land cover dynamics makes it necessary to have an appropriate set of filtering measures to avoid inconsistencies in the TTA. Some of the sources of the identified inconsistencies were:

(a) *The inter-annual time difference* between the rDS and imagery dates. There is a temporal lag between rDS and LCM-2002 imagery. Figure 4 depicts the NDVI temporal activity of several *irrigated herbaceous crop* patches (tiles) where no photosynthetic signal is detected during the summer dates of the years previous to 2005. Dry herbaceous crops or fallow practices were predominant in this area before irrigation plans were implemented in this geographic context. The set of patches occupies 787 ha, resulting in a significant error source that affects the identification of irrigated and dry herbaceous crop classes.

(b) *The intra-annual time series* collect annual phenology, which is constrained by the availability of the imagery. Some intra-annual events (forestry clear-cutting practices and fire disturbances) causes abrupt phenology changes at an intra-annual time scale. These events should be managed (selected/excluded/reclassified) in GT candidate samples. In Figure 5, a forestry clear-cutting practice in a coniferous plantation is shown; the coniferous phenological activity drops on 24 September 2000, affecting an area of 176 ha. The polygons that are not affected show a steady temporal profile.

(c) *Scale errors* are associated with the conflict between the rDS minimum mapping unit (SIOSE with values of 0.5, 1 or 2 ha, depending on the cover type) and the Landsat spatial resolution (30 m). SIOSE *composite* land cover polygons circumscribed different phenological responses in the imagery resolution, as shown in Table 1. Figure 6 shows a *composite* land cover polygon with an association of 70% coniferous, 20% pasture and 10% shrublands. Coniferous forest and sparsely vegetated plots can be identified in the orthophotography on 28 April, 2001, NDVI, where the lower values are pastures/grasslands.

(d) *Labelling errors* in rDS feature labels can be due to the subjectivity of photointerpretation or human errors when the polygons label are assigned. Figure 7 shows an almost pure polygon defined as an association of 95% broadleaf evergreen forest and 5% shrublands. Despite its definition, the observed phenology conforms to deciduous patterns. In (a), a dense forest structure can be recognised, which corresponds with dominant deciduous species (*Fagus sylvatica*, *Quercus pyrenaica*) inventoried in the NFI plots. In (b) and (c), 28 April 2001, and 25 July 2001, NDVI showed a clear increase in NDVI values between the dates. The polygon occupies 198 ha, which can become a source of characterisation errors between evergreen and deciduous forest classes.

(e) *Multiple (phenological) behaviours* are mainly associated with agriculture categories. Crop phenology is complex, and there is a large chance that two neighbouring crop fields within a polygon can be in very different phenological stages (active crops, fallow patterns), as well as belong to different categories (winter crops, summer crops or woody crops). Examples of multiple behaviours were detected in dry and irrigated herbaceous crop polygons. The latter is exemplified in Figure 8. Only part of the entire polygon is displayed due to the large area occupied by the irrigated crops in this area. In (a), the orthophotography depicts the spatial variability, different sizes

and phenological states of crop fields. In (b), 28 April 2001, NDVI denotes active winter (red rectangles), perennial crops and other inactive fields. In contrast, on 25 July 2001, NDVI denotes that (c) active summer crops (blue triangle) and inactive fields dominate the area. The contrasting phenological behaviours in large irrigated crop polygons become a source of error and confusion between winter/summer crop categories.
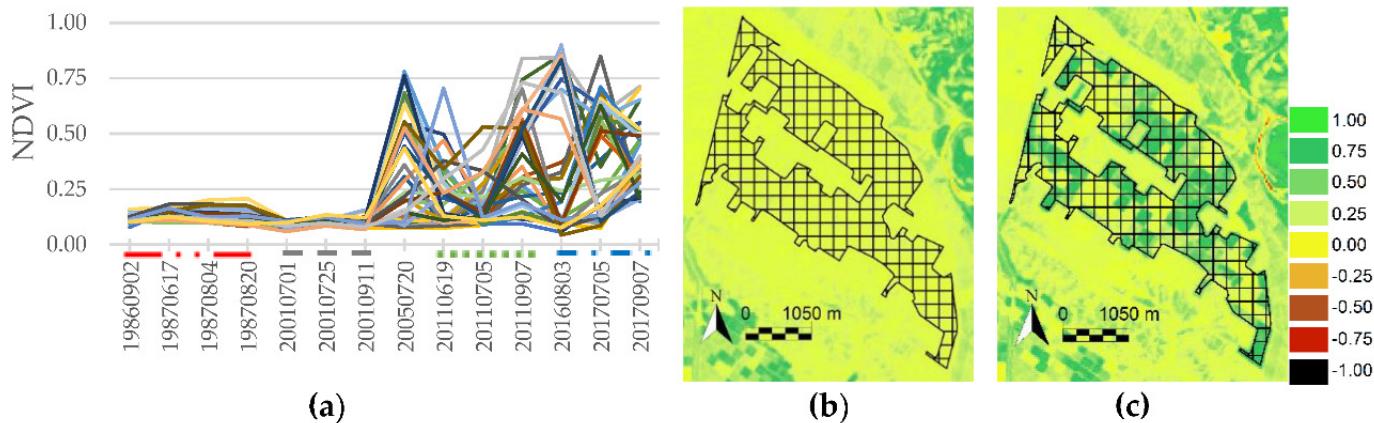
Figure 4. The NDVI summer multiannual profile of *irrigated herbaceous crops* is shown. Colour lines in (**a**) represent the median value of the pixels within polygon tiles. For the sake of simplicity, a random third of the tiles are represented. The red, grey, green and blue dotted lines over date figures denote the imagery (summer months), including 20 July 2005, as a date that is contemporary to the rDS. In (**b**,**c**), the polygon is represented in black over two summer dates NDVI (25 July 2001, and 20 July 2005). Note that during the first time period, the pattern is highly stable.
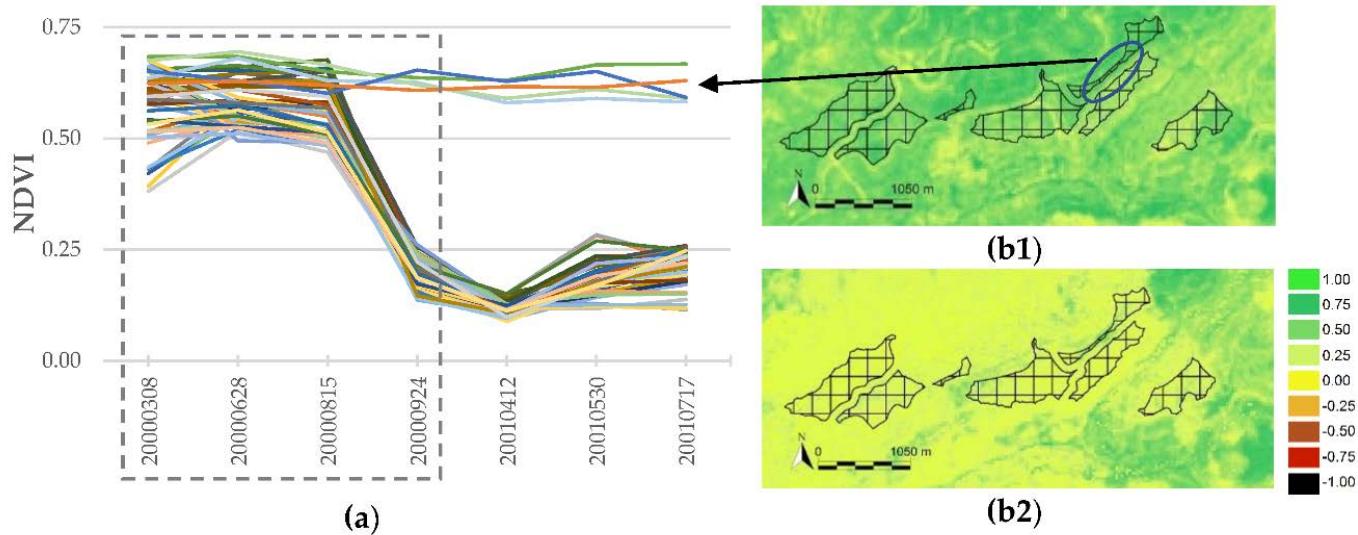
Figure 5. Intra-annual NDVI temporal profile over a coniferous plantation area. Colour lines in (**a**) represent the median values of the pixels in tile polygons displayed in (**b1**,**b2**), and the grey dotted rectangle denotes the intra-annual imagery dates. In (**b1**,**b2**), tile polygons are represented with black outlines over 15 August 2000, and 24 September 2000, NDVI.
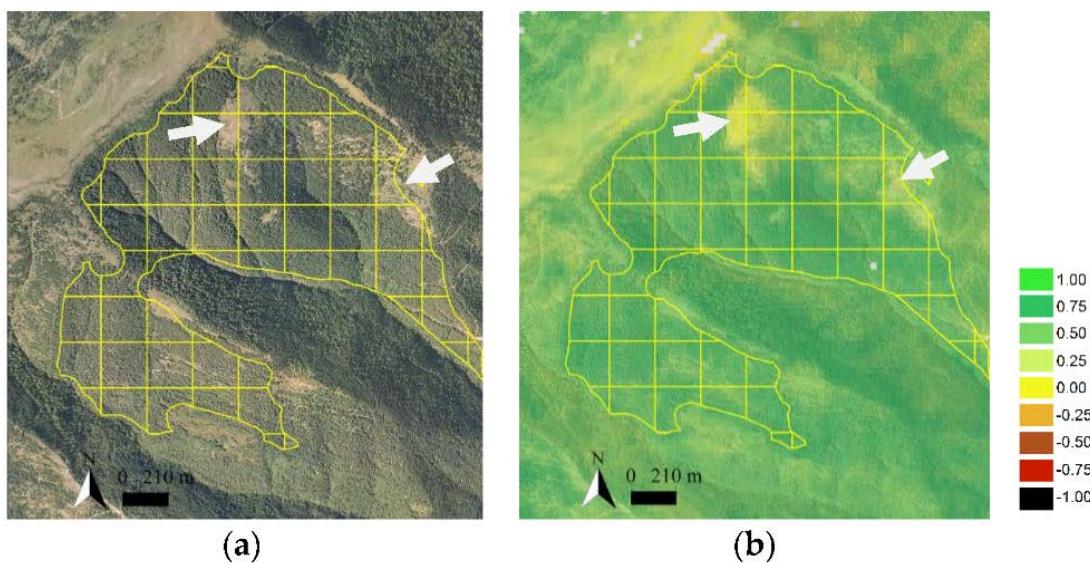
Figure 6. *Composite* land cover polygon tiles are shown with a yellow outline. Arrows in (**a**,**b**) identify the sparsely vegetated plots.
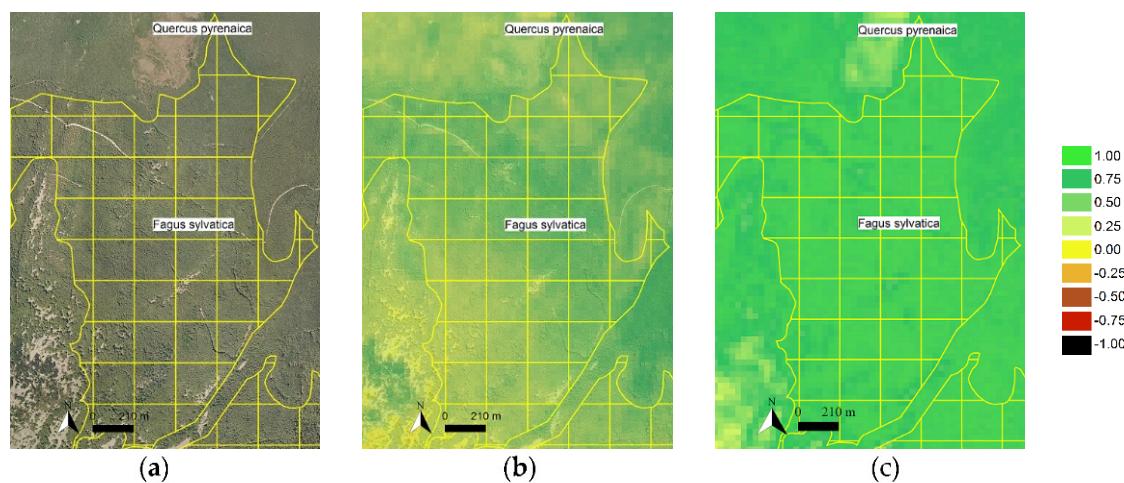
Figure 7. An example of a mislabelled polygon, depicted in yellow over the orthophotography (**a**), 28 April 2001 NDVI (**b**) and 25 July 2001 NDVI (**c**).
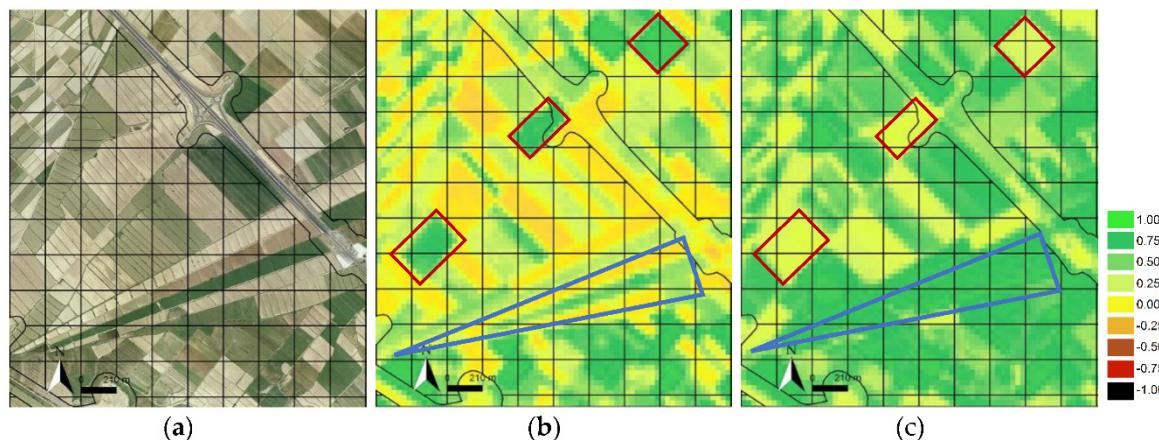
Figure 8. A *simple* land cover polygon defined as *irrigated herbaceous crops* is shown in a black tile outline. Multiple phenological behaviours can be identified between spring and summer NDVI responses (**a**–**c**).

4.2.3. NDVI Filtering Rules

Filtering rules aim to minimise the impact of errors in GT samples used for classification. The rules were generated to deal with issues observed during the exploratory phase and were constructed based on the previous analysis of spectral-temporal signatures, which serve to identify the phenological patterns of each category. The phenological patterns were analysed considering NDVI, but other vegetation indices could be used if their usage suggests an even better behaviour. We considered the LCM-2002 imagery in the examples of the rules below.

Rule 1: Maximum NDVI temporal response

This rule serves to select pixel locations with the maximum NDVI temporal response, dynamically and in each tiled polygon. The rule is defined as:

$$\text{NDVImax} \geq | \leq (\text{Max r1\_μ\_tile} \pm \text{Max r1\_σ\_tile}), \text{r1\_μ} \in [-1,1], \text{r1\_σ} \in [0,1] \quad (1)$$

where NDVImax is the maximum value per each pixel in the imagery series and is taken as a reference value in a per-pixel evaluation form. Individual pixels are evaluated regarding two statistics calculated at a tile-polygon level; (1) the r1_μ_tile is a central tendency measure (e.g., median (MED)) evaluated for each tile-polygon and date; the maximum of the central tendency of the series determines the Max r1_μ_tile value; (2) the r1_σ_tile is a dispersion measure (e.g., the standard deviation (SDV) on the means of the absolute differences from the median) calculated for each tile-polygon and date; the maximum dispersion of the series determines the Max r1_σ_tile value. Therefore, each tile-polygon is characterised by the maximum central tendency value, the median, and the maximum dispersion measure, the dispersion measure for all the dates. Pure SIOSE *simple* land cover polygons are expected to be characterised by a median and a relatively low dispersion measure. However, in *composite* land cover polygons with a mixture of categories, the dispersion measure varies according to the tile composition variability. For a dispersion measure, the cut-off value defined by the Max r1_μ_tile ± Max r1_σ_tile can be displaced towards lower or upper NDVI values to determine the acceptable variability for the category.

For instance, we focus on a *composite* land cover polygon tile (e.g., A(65CNF_35MTR)), defined as an association of 65% coniferous and 35% shrubland in Figure 9. In this tile, coniferous pixels can be discriminated by selecting pixels with an (NDVImax ≥ MEDmax − (1 × SDVmax)). Complementarily, pixels with an (NDVImax ≤ MEDmax − (1 × SDVmax)) characterised low NDVI values associated with shrublands. In both statements, transitional values (red squares) would be incorrectly managed if they were not filtered out.

This rule is appropriate for wilderness land cover categories but is also extendable to agriculture categories. The rule makes it possible to discriminate forest categories (e.g., coniferous) from non-forest vegetation categories (e.g., shrublands), and also differentiate between the non-forest vegetation categories in the natural succession, especially in *composite* land cover polygons. Used together with Rule 2, it has the benefit of defining the range of NDVI values over which a category varies. Thus, this rule is useful for avoiding scale errors and intra-annual errors, specifically in *composite* land cover polygons where several categories and transitional NDVI values coexist. Some categories require selecting the lower NDVI response, such as bare soils, considering an NDVImax ≤ MEDmax + (1 × SDVmax).

Rule 1 is applied over a *composite* land cover polygon defined as an association of 70% coniferous and 30% shrubland depicted in Figure 10. The rule statement is defined as (NDVImax ≥ MEDmax − (1 × SDVmax)) to select the more densely forested areas. The orthophotography allows us to differentiate compact and densely forested plots from sparsely vegetated areas. Tile polygons are depicted with white outlines. The highest NDVI maximum values are shown from green to blue, whereas the values under ~0.40 are associated with scarce vegetation. The zoom details pixel exclusion in these areas. It is worth noting that for the tiles where lower NDVI maximum values predominate (e.g., tiles mixing coniferous and shrubland or those affected by a forest fire), it is essential to consider

a complementary condition statement to exclude lower NDVI responses, the minimum NDVI threshold detailed in Rule 2.
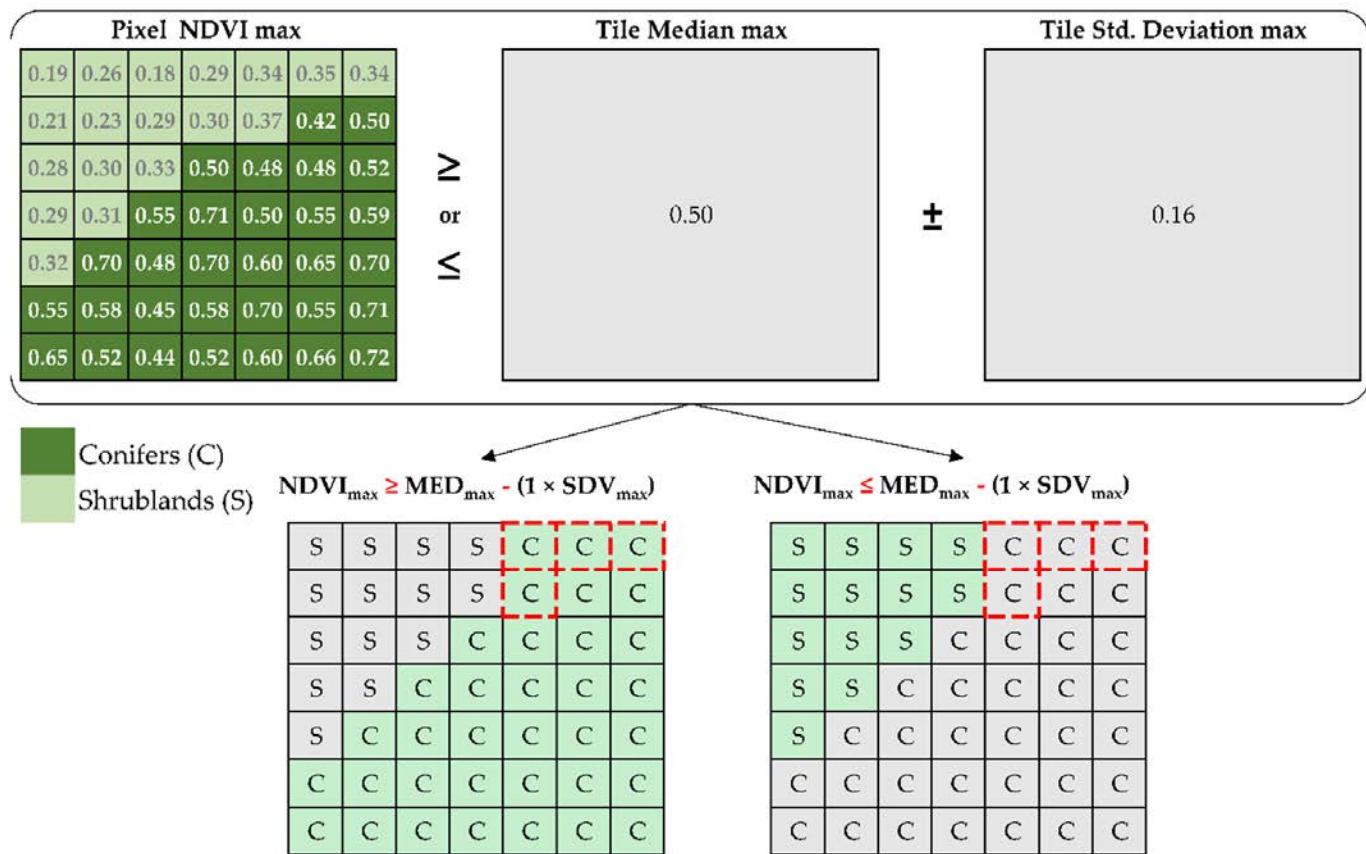
Figure 9. Rule 1 application in a tile polygon. Transitional locations (red squares) with anomalous NDVImax values were selected (green colour) in the left selection (**a**) but unselected in the right (**b**). Establishing additional NDVI thresholds (detailed in rule 2) makes it possible to better control the transitional values in *composite* land cover polygons.
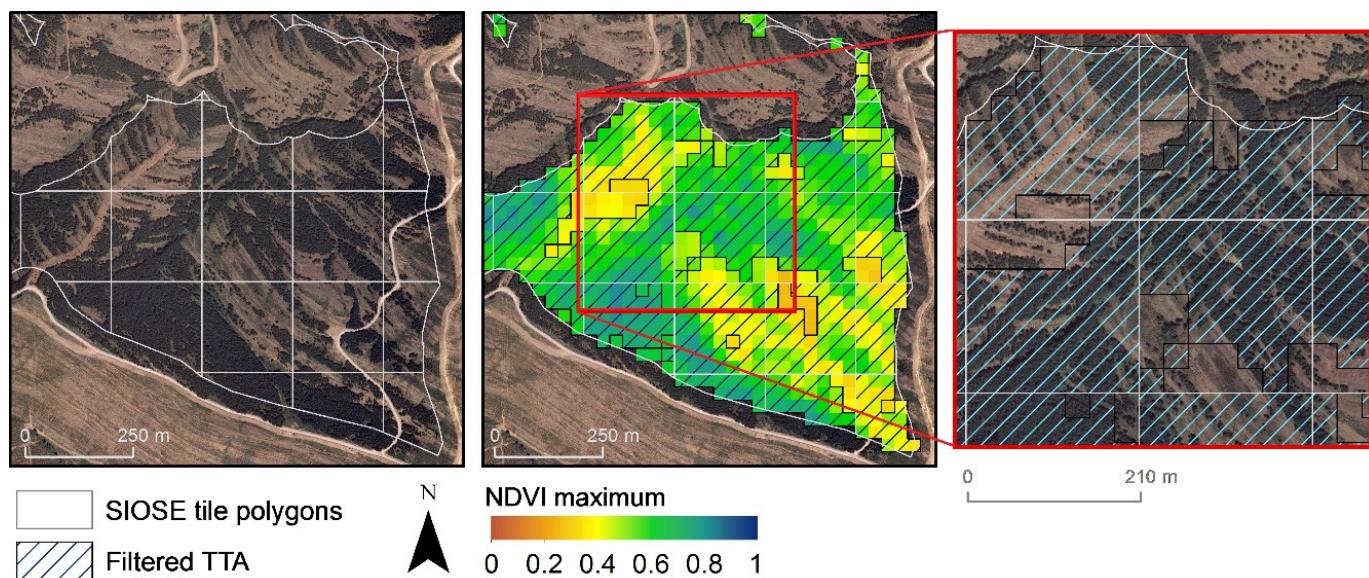
Figure 10. Rule 1 filtering applied over a polygon association.

Rule 2: NDVI range along with the 'n' dates

This rule determines the range of NDVI values over which a category varies along the 'n' dates considered. The rule is defined as:

$$\forall \text{ NDVI} \in [r2\_a, r2\_b]; \ r2\_a, r2\_b \in [-1,1] \qquad (2)$$

where r2_a, r2_b are the NDVI minimum and maximum values, respectively, which define the NDVI range of variation of a category. Considering the conceptual example shown previously in Figure 9, Rule 2 was added to manage transitional behaviours, which is exemplified in Figure 11. The sentence is defined as: (NDVImax $\geq$ | $\leq$ MEDmax $-$ ($1 \times$ SDVmax) AND ($\forall$ NDVI $\in$ [0.40,0.90])), where values outside the limit are excluded.

This rule complements Rule 1 but can also be used independently. Since the series of NDVImax is assumed as a reference value, a minimum NDVI threshold is necessary. The aim is to isolate positions that do not fit the category NDVI characteristic range in the initial set of GT candidate pixels, especially in *composite* land cover polygons. Moreover, intra-annual disturbance events (forestry clear-cuttings or fire events) in forested areas cause NDVI drops, for which pixels can also be isolated. Rule 2 used independently can be helpful to extract crop categories characterised with a specific NDVI range of values (e.g., rice crops NDVI range approximately between [-0.30,0.80]).

Locations in Figure 10 with low NDVI values were not adequately filtered. Rules 1 and 2 were applied in the exact location, and the results are displayed in Figure 12. Excluding non-forested locations and anomalous minimum values requires defining a threshold (NDVI minimum) in accordance with the category variability. The filtering statement is defined as (NDVImax $\geq$ MEDmax $-$ ($1 \times$ SDVmax) AND ($\forall$ NDVI $\in$ [0.40,0.90])). Those pixels under the NDVI < 0.40 are discarded (any disturbance events causing NDVI drops, sparsely vegetated or low-density forested areas, shrublands, pastures, bare soils or even water bodies), so that only densely forested plots remain.
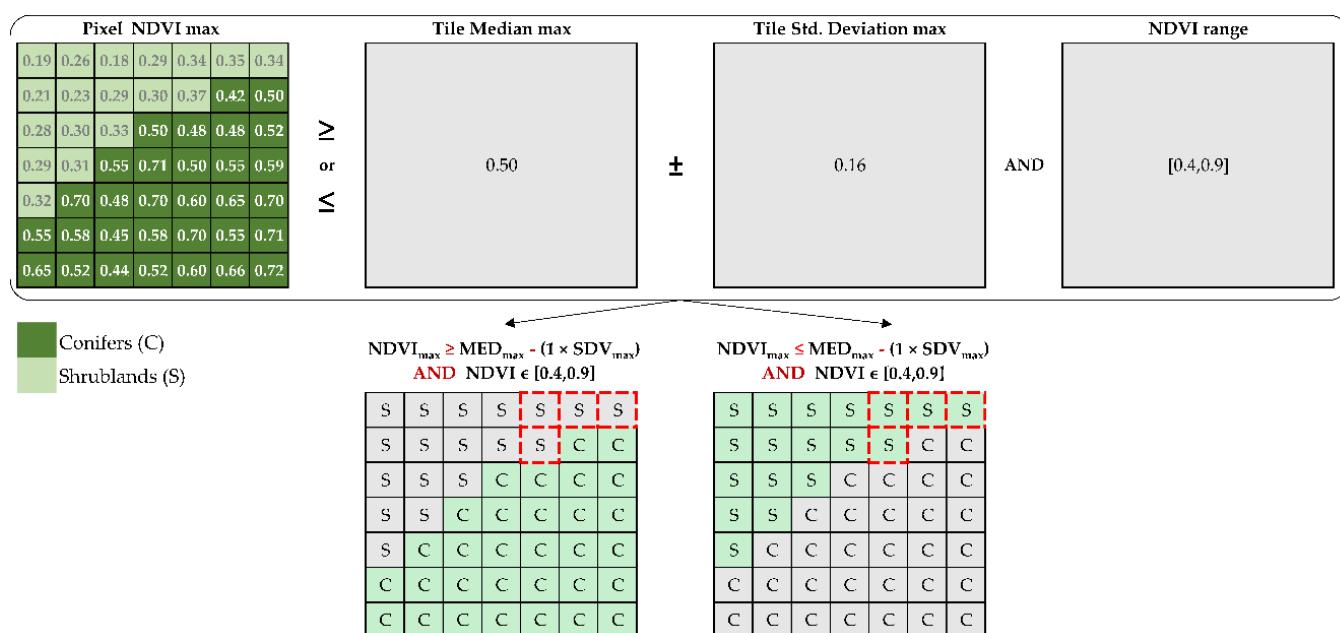
Figure 11. Rule 1 and 2 applied to a tile polygon. Transitional locations (red squares) in (**a**,**b**) with anomalous NDVImax values are correctly selected using Rule 2 restrictions.
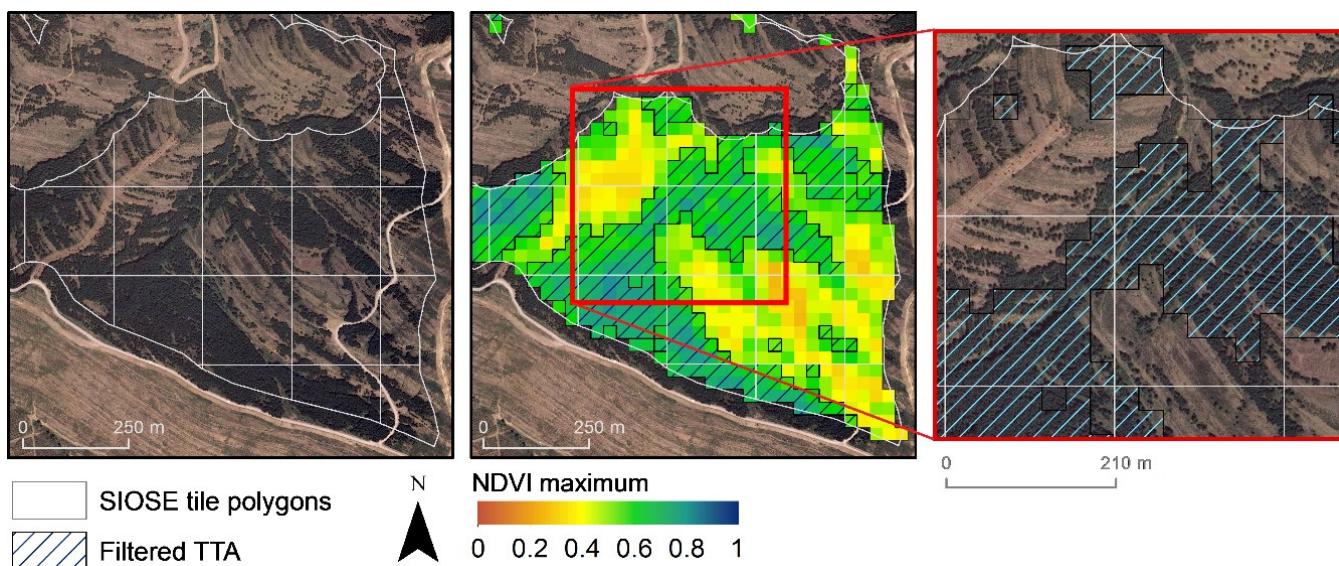
Figure 12. Rules 1 and 2 applied over a composite land cover polygon.

Rule 3: Photosynthetic activity for 'n' dates

This rule is a proxy of the total photosynthetic activity for a category considering the range of values over which the sum of 'n' dates NDVI variates. The rule is defined as:

$$\sum_{i=(1,n)} NDVI_i \in [r3\_a, r3\_b]; r3\_a, r3\_b \in [-n, n] \tag{3}$$

where r3_a and r3_b are the minimum and maximum values between which the total sum (NDVIsum) of 'n' NDVI varies for a category. It works at the individual pixel level.

The rule makes it possible to discriminate between active and non-active agriculture crop fields in herbaceous and woody crop categories. Since the rule amplifies the NDVI total signal, it enables better recognition between active/non-active crops within dry or irrigated crop categories in the SIOSE dataset. Defining thresholds to discriminate irrigation regimes favours deriving consistent TTA sets for LCM time series production, and hence, more reliable land cover change analysis in these categories, mainly in irrigated woody crops, where there is also a mixture with dry crops. For the forest categories, the rule is useful for distinguishing the most active broadleaf deciduous species, especially those located close to rivers.

We applied this rule in irrigated olive grove plantation polygons, shown in Figure 13. Orthophotography with a 2001 date can be used to identify consolidated and productive parcels close to recent plantation fields, besides their total photosynthetic activity correspondence values. Through visual interpretation, we defined the NDVI sum $\in [1.0, 2.0]$ to capture dense plantations, discarding the lower photosynthetic response associated with recent plantations and non-cultivated areas.

Rule 4: Contrast between $NDVI_{max}$ values of a group of dates

The intra-annual phenology variability is characteristic for each category. The rule is based on the NDVI maximum difference between the initial and final growing season, typically the summer and spring dates, but is adaptable to other dates or groups of dates. The rule is defined as:

$$\begin{aligned} NDVIdifference\ (NDVI_{max}\ Summer\ dates - NDVI_{max}\ Spring\ dates) \\ \in [r4\_a, r4\_b]; r4\_a, r4\_b \in [-2, 2] \end{aligned} \tag{4}$$

where r4_a, r4_b are the minimum and maximum values derived from the absolute difference between the NDVImax reached on the summer and spring dates. The NDVI difference can also be interpreted as the NDVI temporal gradient between two temporal moments.
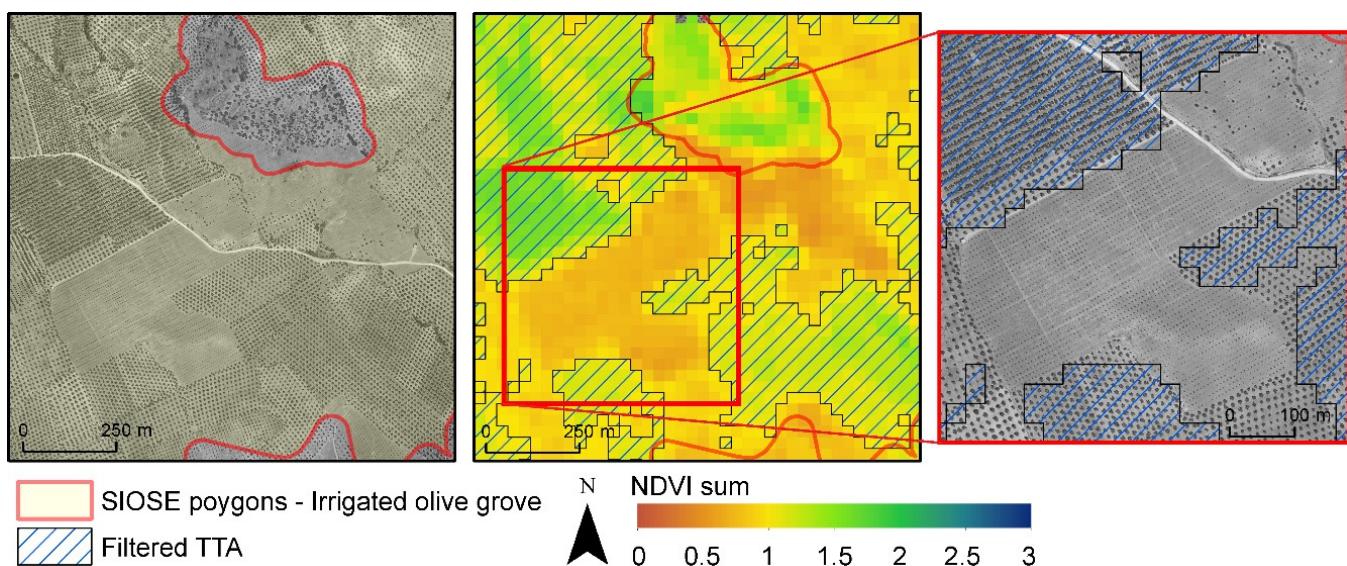
Figure 13. Rule 3 applied to irrigated olive grove polygons. Brown NDVI colours depict more recent plantations or low-density plantation schemes. The red square zoom details new plantation fields. The white line in the zoom is a road.

The rule makes it possible to control more dynamic agronomic classes and forest behaviours. Considering the summer and spring NDVI maximum differences, it is well known that there is a strong positive temporal gradient during the growing season, characteristic of summer crops (herbaceous or rice crops), deciduous forest species (*Fagus sylvatica* and sclerophyllous deciduous and pseudo-deciduous species) and some woody crops (vineyards). In contrast, the strong negative gradients are typically associated with winter crops or low-altitude pastures. Other categories (e.g., coniferous, broadleaf evergreen forest, shrublands or urbanised areas) depict a temporal response with no trend in the NDVI temporal profiles, which means close to zero NDVI temporal gradients. This rule distinguishes polarised phenological patterns as winter and summer crops or deciduous and evergreen forest patterns and allows each category to be characterised with the NDVI temporal gradient. However, the rule is limited when less contrasting patterns are discriminated (between bare soils and fallow lands or between coniferous and evergreen forest categories). Furthermore, the rule helps to define the NDVI temporal gradient patterns. This avoids labelling misassignment or other errors related to rDS and inter-annual time differences in imagery when rapid transformations occur (e.g., dry to irrigated regimes and forest conversion from evergreen to deciduous species, or vice-versa). The rule can also be used to discriminate mixed forest in regular pattern associations when deciduous with evergreen patterns coexist.

The example in Figure 14 illustrates a labelling inconsistency associated with the rDS and the inter-annual difference of the imagery. The polygon label is defined as *irrigated herbaceous crops*, while the real phenology revealed winter crops or fallow patterns related to agriculture practices of *dry herbaceous crops*. Rule 4 was established and applied to exclude the negative temporal patterns in the initial candidate pixels of *irrigated herbaceous crops*. We approximate the NDVI absolute difference range values between [0.05, 2] based on the local analysis of the pixels involved. Limits should not be restrictive since the aim is to only exclude the negative NDVI temporal gradients.
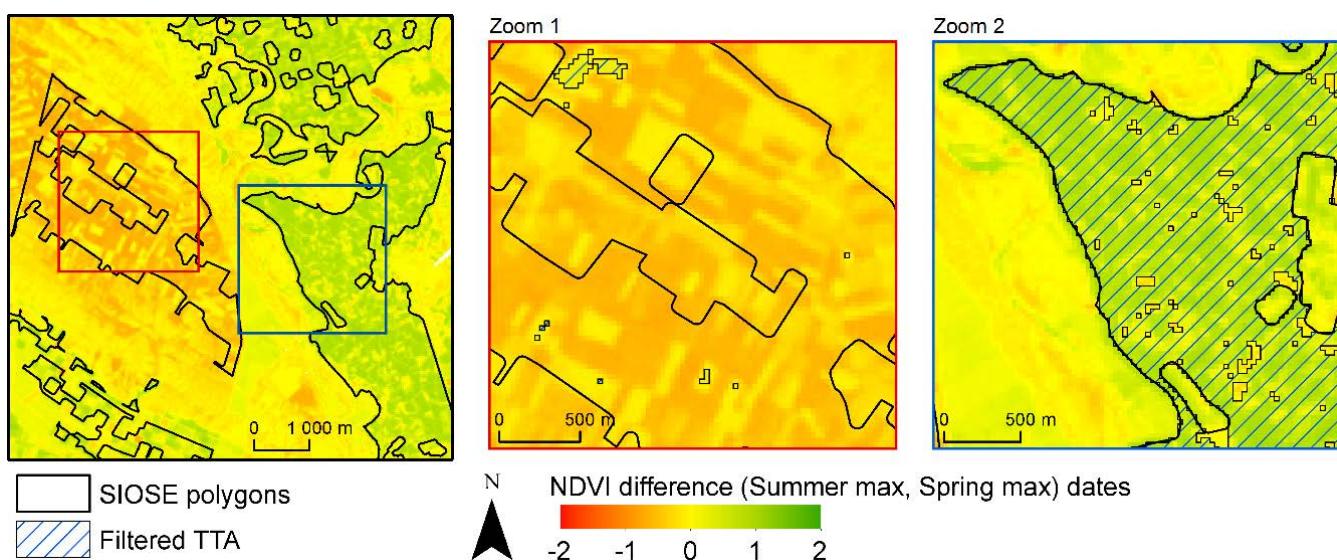
Figure 14. Rule 4 applied to *irrigated herbaceous crop* polygons. Brown NDVI depict negative NDVI temporal gradients; yellow is related to low contrasting patterns (fallows); green depicts positive NDVI temporal gradients. Positive and negative gradient domains are detailed in zooms 1 and 2.

Rule 5: Phenological moment

Establishing NDVI thresholds on specific dates or a group of dates or direct comparisons between dates or a group of dates may be required. Some casuistics are:

$$
\begin{aligned}
& \text{NDVI Spring date or, NDVI}_{max|min} \text{ Spring dates} \geq | \leq r5\_a \\
& \text{NDVI Summer date or, NDVI}_{max|min} \text{ Summer dates} \geq | \leq r5\_b \\
& \text{NDVI Autumn date or, NDVI}_{max|min} \text{ Autumn dates} \geq | \leq r5\_c \\
& \text{NDVI}_{max|min} \text{ Spring dates} \geq | \leq \text{NDVI}_{max|min} \text{ Summer dates} \\
& \text{NDVI}_{max|min} \text{ Summer dates} \geq | \leq \text{NDVI}_{max|min} \text{ Autumn dates} \\
& \text{NDVI}_{max|min} \text{ Spring dates} \geq | \leq \text{NDVI}_{max|min} \text{ Autumn dates,} \\
& \qquad\qquad r5\_a, r5\_b, r5\_c \in [-1,1]
\end{aligned}
\tag{5}
$$

where r5_a, r5_b, r5_c are specific NDVI thresholds in phenological moments defined for a particular date or group of dates. For instance, to detect rice fields, we can establish a threshold in NDVI spring dates ≤ 0.0 together with high activity during the NDVI summer dates ≥ 0.60. Direct comparisons (NDVImax spring dates $\geq$ NDVImax summer dates, useful for winter crop characterisation) between dates or a group of dates can also be used for better phenological control. It is a flexible rule that makes it possible to compare a free combination of NDVI thresholds between dates.

Specific situations require NDVI thresholds to analyse particularly tricky phenological patterns. For instance, when there are two relative minimum (or two maximum) NDVI values in an NDVI temporal profile. The rule helps establish specific NDVI thresholds to reproduce temporal profiles in specific categories on which the map producer focuses their interest. For instance, detecting the temporal pattern of double crops requires establishing an NDVI minimum at the moment of harvesting and two maximum values on early spring and later summer dates. Furthermore, this rule is helpful for managing vegetation senescence in temporal profiles.

Figure 15 represents examples where double crops and dry vineyard patterns were extracted from irrigated herbaceous crops and dry vineyard woody crop polygons. Rule 5 in double-crop patterns was defined as [NDVI$_{20010428} \geq 0.50$] AND [NDVImin summer ≤ 0.40] AND [NDVImax summer ≥ 0.50], which makes it possible to capture the variability of the crop in the summer dates. For characterising active dry vineyard plantation fields, Rule 5 was defined as [NDVI$_{20010428} \leq 0.15$] AND [NDVImax summer ≥ 0.30] AND

[NDVI$_{20010701}$ > NDVI$_{20010911}$], adapting the rule to capture the characteristic senescence period of the crop.
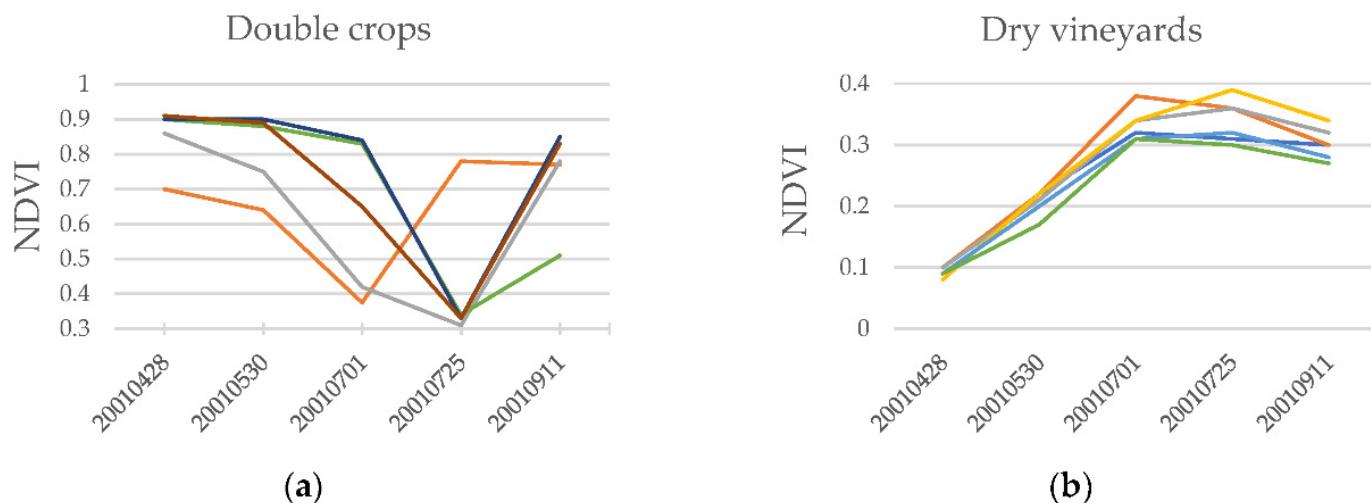
Figure 15. Rule 5 applied to irrigated herbaceous crops and vineyard crop polygons. Coloured lines depict the pixels selected as NDVI median values in polygons for (**a**) double crop filtered samples, and (**b**) dry vineyard woody crop field filtered samples.

We defined the statements of the filtering rules and proposed a parametrisation for each category, adapted to the geographical context, detailed in Table S4 in the Supplementary Materials. The initial set of candidate pixels was filtered based on the rules, deriving a robust set of TTA, which were randomly selected to be used in the classification stage.

4.3. Classification Process and Accuracy Assessment

We used the k-nearest neighbour (kNN) classifier implemented in MiraMon, parallelised for better performance, to derive LCM over which we evaluated the performance of the filtering rules. kNN is a supervised classification approach that relies on labelled input samples to learn and produce an output in the new given unlabelled data. The process is developed in two steps for each pixel in the image: (1) the algorithm determines the nearest neighbours by calculating a distance metric (e.g., the Euclidean distance) between the target pixel and each training area provided; then (2) the target pixel label is determined by selecting the kNN candidates (defined by the map producer), over which the modal category is calculated. The kNN parameter was fixed to 15, based on a previous work analysis and considering better robustness when the number of training samples is large [54], as it is in the context of two Landsat scenes.

The variables used in the classification process were Landsat TM and ETM+ bands 3, 4, 5 and 7, OLI bands 4, 5, 6 and 7 for each date, as well as two indices (NDVI, NDWI) and three topo-climatic variables (altitude, slope and summer potential solar radiation). Thermal bands were excluded, and Blue and Green bands were discarded because of their high correlation and the strong influence of atmospheric aerosols. The spectral bands, spectral indices, slope, altitude and summer potential solar radiation were all scaled to 0–100 so that values were all unified in the same range. In total, the classification dataset in all study cases was composed by thirty tree variables.

The map accuracy was assessed by evaluating the agreement between the map produced and the test areas, summarising the discrepancies by means of the confusion matrix [40,98,99]. The confusion matrix is essential for quantifying the impact of the TTA error on the map accuracy and the performance of the filtering rules. The unequal presence of classes in our map obliges us to adapt some computations. For instance, if the commission errors of *dry herbaceous crops* are associated with the *bare soils* category, but the number of herbaceous crop test samples is considerably larger than the bare soils test samples

(e.g., one order of magnitude as the first ones are much more frequent in the area), then the interpretation of the user's accuracy is incorrect. This could be balanced before the confusion matrix calculations; however, this implies losing test samples and deciding where to remove them. Alternatively, it can be corrected by a factor computed as follows:

$$\text{Factor i} = (\text{Map pixels i/Map total pixels})/(\text{Test pixels i/Test total pixels}) \qquad (6)$$

where, 'i' denotes each category. The factor computed for each category allows us to obtain a confusion matrix free from these imbalances.

5. Results

The LCM generated for the four temporal cases (LCM-1987, LCM-2002, LCM-2012 and LCM-2017) and the additional spatial case are shown in Figure S2, and their confusion matrices are detailed in Tables S5–S14 in the Supplementary Materials. For simplicity, only LCM-2002 results are detailed due to the coherence with the rest of the maps generated. The performance of the rules is detailed through visual examples, and their confusion matrices are interpreted in the following subsections.

5.1. The Performance of the Rules in Visual Examples

The visual examples in Figures 16 and 17 illustrate the performance of the rules in specific locations. The LCM-2002 classifications were compared before and after the rules were applied.

Example A in Figure 16 represents Rules 1 and 2 applied to coniferous polygons to prevent the scale and intra-annual time errors. Rule 1 selected all the most active positions in the period according to the (NDVImax ≥ MEDmax − 1SDVmax) evaluated in tiles, avoiding the lowest NDVI responses (*shrublands, grasslands, bare soils*) typically associated with SIOSE *composite* polygons. Rule 2 ensured that NDVI values varied within the range of variation allowed for the category (e.g., ∀ NDVI ∈ [0.40, 0.90] for coniferous forest) on all dates. The clear-cutting event was misclassified as *coniferous* forest using unfiltered TTA, but correctly classified as *shrublands* when the filtering rule was applied.

Example B in Figure 16 exemplifies a misassignment error, where pixels on a broadleaf evergreen forest polygon depict a clear deciduous pattern. Rule 4 served to exclude pixels with deciduous temporal patterns in the evergreen category. The statement rule concatenates three terms: (NDVImax ≥ MEDmax − 1SDVmax) AND (∀ NDVI ∈ [0.40, 0.90]) AND (NDVI difference ∈ [−0.15, 0.05]), which allow us to extract the most active forested areas (Rules 1 and 2), and avoid deciduous (positive NDVI gradients) patterns (Rule 4). The classification results showed a mixture of evergreen and deciduous forest classified pixels when unfiltered TTA was used, while the filtered set provided pixels correctly classified as deciduous forest.

Example C in Figure 17 illustrates an inter-annual time error. Several irrigated herbaceous crop polygons depicted phenological patterns associated with dry herbaceous crops. Rule 4 was used to characterise the irrigated crops: a positive NDVI gradient during the growing season, excluding any negative NDVI gradient associated with the dry crops. The rule statement was defined as (∀ NDVI ∈ [0.05, 0.90]) AND (NDVI difference ∈ [0.05, 2.00]), capturing the irrigated crops with a positive NDVI temporal gradient. The results showed the area misclassified as irrigated herbaceous crops when unfiltered TTA was used, while the filtered set correctly classified the area as dry herbaceous crops.

Example D in Figure 17 describes the existence of multiple behaviours in woody crop categories. In the example, dry vineyard woody crop polygons depict anomalously high photosynthetic activity (related to irrigated woody crops) with irrigation ponds located in parcels.
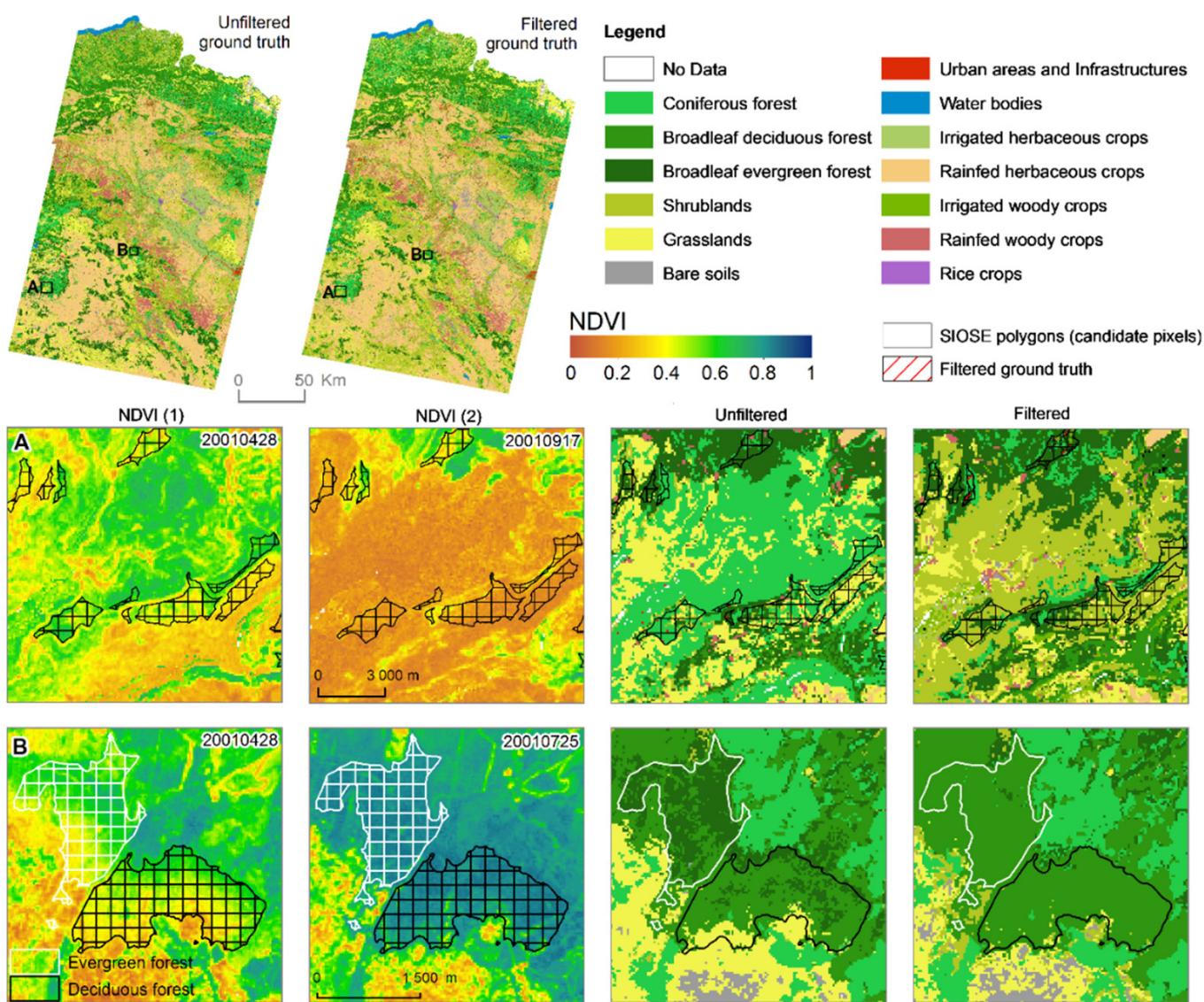
Figure 16. Examples of applying the filtering rules. In (**A**), coniferous polygons affected by clear-cutting forestry practices are shown (outlined in black). An intra-annual NDVI drop is produced. Unfiltered TTA misclassified the area as coniferous forest, while filtered TTA classified the area correctly as shrublands and grasslands. In (**B**), a mislabelled broadleaf evergreen forest (in white) polygon and a correctly labelled broadleaf polygon.

The rule statement defined for dry woody crops was ($\forall$ NDVI $\in$ [0.05, 0.60]) AND (NDVIsum $\in$ [0.30, 0.75]) AND (NDVIdifference $\in$ [0.15, 1.00]) AND ([NDVI max Spring] < [NDVI max Summer]). The first term made it possible to capture the NDVI range of variation; the second term, made it possible to determine the minimum total photosynthetic activity as a dry woody crop; and the third and fourth terms characterised the positive NDVI difference during the growing season. This made it possible to exclude any pixel contamination with herbaceous crops or pastures, which generally have negative NDVI difference patterns. Unfiltered TTA resulted in misclassifying the area as dry woody crops. Using filtered TTA, the level of NDVI total activity reached in these locations allowed us to classify them as irrigated woody crops.
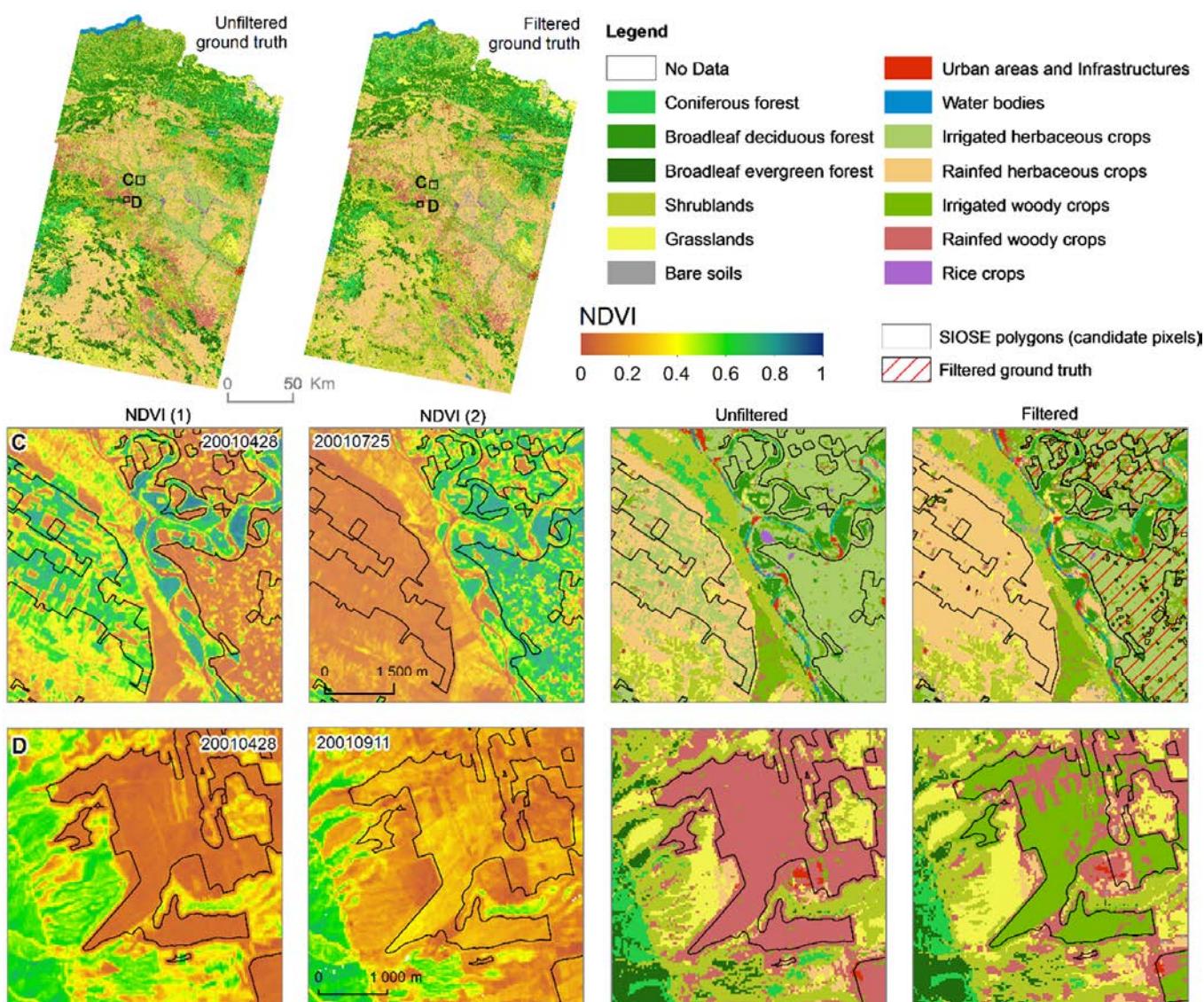
Figure 17. Examples of the application of filtering rules. In (**C**), irrigated and dry herbaceous crop patterns coexist within irrigated herbaceous crop polygons (outlined in black). Unfiltered TTA misclassified dry patterns as irrigated crops, while filtered TTA correctly discriminated between categories. In (**D**), an irregular, high NDVI activity is located in dry vineyard woody crop polygons (in black). Unfiltered TTA misclassified the crop fields as dry woody crops, while the filtered TTA correctly classified them as irrigated woody crops.

5.2. The Performance of the Rules in Confusion Matrices

The results of the confusion matrices, comparing unfiltered and filtered TTA for LCM-2002, are detailed in Tables 2 and 3. The LCM-2002 overall accuracy (OA) using unfiltered TTA was 83.8% and 88.6% when it was weighted by the ground truth area considering only classified pixels (OAw). For the filtered TTA, the OA reached 93.0%, and OAw obtained 96.0%. Therefore, matrices corroborated a better identification of categories when the filtering rules were applied, decreasing the confusion between classes and avoiding error inconsistencies. This pattern could also be seen in the rest of the LCM.

Figure 18 compares the omission error and the commission error resulting from the evaluation of the maps with and without applying the filtering rules. There is a clear reduction in OE and CE in all categories.

Table 2. Confusion matrix results derived from **unfiltered** ground truth samples from SIOSE 2005 rDS and imagery for LCM-2002.

Classified Map	Unfiltered Ground Truth Samples													Total	CE (%)	UA (%)
	CoF	BDF	BEF	Shl	Grl	BrS	Urb	WaB	IHC	DHC	IWC	DWC	RiC			
(CoF) Coniferous forest	**50,907**	823	1058	1612	295	34	31	25	11	55	15	29	1	54,895	7.3	92.7
(BDF) Broadleaf deciduous forest	1044	**67,728**	1403	1884	1077	91	0	11	163	173	59	0	0	73,634	8.0	92.0
(BEF) Broadleaf evergreen forest	5640	1644	**60,658**	7398	785	109	5	26	41	197	5	27	0	76,534	20.7	79.3
(Shl) Shrublands	3715	1587	3007	**115,688**	9356	938	160	105	301	2450	180	2154	7	139,649	17.2	82.8
(Grl) Grasslands	504	678	429	13,544	**86,142**	1135	39	18	824	8148	224	1252	11	112,948	23.7	76.3
(BrS) Bare soils	64	54	52	488	1214	**3545**	78	0	58	625	23	67	0	6268	43.4	56.6
(Urb) Urban areas and Infrastructures	1	3	0	66	53	57	**2802**	7	48	300	57	112	1	3507	20.1	79.9
(WaB) Water bodies	1	10	0	5	9	2	0	**1488**	1	22	0	4	0	1543	3.5	96.5
(IHC) Irrigated herbaceous crops	17	184	3	424	868	155	145	13	**37,114**	5524	1526	825	304	47,100	21.2	78.8
(DHC) Dry herbaceous crops	55	51	43	1647	1853	636	293	82	6709	**175,596**	984	2764	17	190,729	7.9	92.1
(IWC) Irrigated woody crops	26	146	12	274	231	101	226	12	2154	921	**9841**	4011	27	17,982	45.3	54.7
(DWC) Dry woody crops	99	11	22	1614	545	124	368	26	967	2748	3098	**29,232**	12	38,866	24.8	75.2
(RiC) Rice crops	5	11	0	20	12	1	6	4	667	34	10	2	**1494**	2267	34.1	65.9
NoData	31	120	51	84	111	149	0	0	0	0	0	0	0	547		
Total	62,110	73,049	66,739	144,748	102,552	7077	4153	1817	49,057	196,793	16,021	40,479	1875	766,469	OA = 83.8%	
OE (%)	18.0	7.3	9.1	20.1	16.0	49.9	32.5	18.1	24.3	10.8	38.6	27.8	20.3		OAw = 88.6%	
PA (%)	82.0	92.7	90.9	79.9	84.0	50.1	67.5	81.9	75.7	89.2	61.4	72.2	79.7		k = 0.7	

OE: omission error, CE: commission error, PA: producer's accuracy, UA: user's accuracy, k: kappa index of agreement, OA: overall accuracy, OAw: overall accuracy weighted by the ground truth area considering only classified pixels (unclassified pixels are not considered errors and are solved by spatial proximity). Figures in bold represent positions where the predicted label is equal to the true label.

Table 3. Confusion matrix results derived from **filtered** ground truth samples from SIOSE 2005 rDS and imagery for LCM-2002.

Classified Map	Filtered Ground Truth Samples													Total	CE (%)	UA (%)
	CoF	BDF	BEF	Shl	Grl	BrS	Urb	WaB	IHC	DHC	IWC	DWC	RiC			
(CoF) Coniferous forest	**46,959**	226	525	311	222	0	0	0	3	4	4	0	0	48,254	2.7	97.3
(BDF) Broadleaf deciduous forest	388	**83,499**	330	55	906	0	0	0	94	0	33	0	0	85,306	2.1	97.9
(BEF) Broadleaf evergreen forest	4891	934	**52,718**	3278	300	0	0	0	7	17	13	0	0	62,157	15.2	84.8
(Shl) Shrublands	1634	311	1889	**115,291**	6468	97	39	0	15	410	337	1178	0	127,670	9.7	90.3
(Grl) Grasslands	48	342	18	4281	**84,012**	32	13	0	66	3616	14	1481	0	93,924	10.6	89.4
(BrS) Bare soils	0	0	0	16	33	**10,379**	494	0	0	1711	0	60	0	12,692	18.2	81.8
(Urb) Urban areas and Infrastructures	0	0	0	4	1	79	**5678**	0	0	220	1	133	0	6117	7.2	92.8
(WaB) Water bodies	0	0	0	0	0	0	0	**1578**	0	0	0	0	0	1578	0.0	100.0
(IHC) Irrigated herbaceous crops	2	84	0	15	134	0	0	0	**27,676**	181	507	0	5	28,603	3.2	96.8
(DHC) Dry herbaceous crops	0	0	0	57	624	874	759	0	23	**189,497**	13	1344	0	193,191	1.9	98.1
(IWC) Irrigated woody crops	16	277	18	232	296	0	18	0	1640	183	**25,474**	90	0	28,244	9.8	90.2
(DWC) Dry woody crops	1	0	0	1422	1208	333	0	0	9	5266	96	**68,756**	0	77,090	10.8	89.2
(RiC) Rice crops	0	0	0	0	0	0	0	0	201	0	0	0	**958**	1159	17.3	82.7
NoData	0	0	0	0	0	0	0	0	0	0	0	0	0	0		
Total	53,939	85,672	55,499	124,963	94,204	11,794	7002	1578	29,735	201,105	26,492	73,042	963	765,986	OA = 93.0%	
OE (%)	12.9	2.5	5.0	7.7	10.8	12.0	18.9	0.0	6.9	5.8	3.8	5.9	0.5		OAw = 95.9%	
PA (%)	87.1	97.5	95.0	92.3	89.2	88.0	81.1	100.0	93.1	94.2	96.2	94.1	99.5		k = 0.9	

OE: omission error, CE: commission error, PA: producer's accuracy, UA: user's accuracy, k: kappa index of agreement, OA: overall accuracy, OAw: overall accuracy weighted by the ground truth area considering only classified pixels (unclassified pixels are not considered errors and are solved by spatial proximity). Figures in bold represent positions where the predicted label is equal to the true label.

(a)   (b)

Figure 18. Comparison of the omission (**a**) error (OE) and commission (**b**) error (CE) regarding unfiltered (uf.) and filtered (f.) ground truth areas. Figures refer to SIOSE 2005 and LCM-2002 imagery.

Wilderness land cover categories (*coniferous forest*, *broadleaf evergreen forest*, *broadleaf deciduous forest*, *shrublands*, *grasslands* and *bare soils*) showed a clear reduction in both OE and CE. This pattern was expected due to the more stable phenological patterns in wilderness categories and the effect of minor inter-annual time problems. The *coniferous forest* showed errors associated mainly with *broadleaf evergreen forest*, *shrublands*, and, to a lesser extent, *broadleaf deciduous forest*. The application of Rules 1 and 2 reduced the scale errors (the association of forest with the *shrubland*, *grassland*, and *bare soil* categories) and intra-annual errors (disturbance events), while Rule 4 served to exclude labelling misassignments (coniferous polygons mislabelled as deciduous forest). This led to a reduction in OE from 18.0% to 12.9% and in CE from 7.3% to 2.7%. However, the OE for *coniferous forest* and *broadleaf evergreen forest* remained, which shows that a mixture of the two categories in filtered TTA remains to a certain extent.

Broadleaf deciduous forest errors were associated with *broadleaf evergreen forest* and *shrublands*. Rules 1 and 2 were helpful for reducing the scale errors, and Rule 4 made it possible to exclude temporal responses without trend NDVI temporal patterns. This reduced the OE from 7.3% to 2.5% and the CE from 8.0% to 2.1%. *Broadleaf evergreen forest* errors were mainly related to *shrublands* and *broadleaf deciduous forest*. Rules 1 and 2 served to reduce the scale errors, and Rule 4 helped exclude deciduous patterns. When the filtering rules were applied, the confusion matrices reported that the OE dropped from 9.1% to 5.0% and the CE from 20.7% to 15.2%.

Shrublands were confused mainly with *grasslands* and *broadleaf evergreen forest*, *dry herbaceous* and *dry woody crops*. Confusion matrices revealed a decline in the OE from 20.1% to 7.7% and in the CE from 17.2% to 9.7%. *Shrublands* are characterized by high intraclass variability in the study context. The rules aim to capture the intraclass variability with Rules 1 and 2 and limit the NDVI temporal gradient with Rule 4, excluding deciduous

patterns associated with grasslands or deciduous forest species. Once the rules have been applied, there is still confusions with dry woody crops. *Grasslands* were confused mainly with *shrublands*, *dry herbaceous crops*, and *dry woody crops*. The confusion matrices revealed a reduction in the OE from 16.0% to 10.8% and in CE from 23.7% to 10.6%. Rules applied to *grasslands* were defined to capture humid and dry phenological patterns separately, where Rules 1 and 2 capture a wide range of variation and Rules 4 and 5 serve to define NDVI gradients and restrictions of phenological moments. Nevertheless, after the rules have been applied, there are still some confusions with the *dry woody crop* category.

The *bare soils* category was confused mainly with *grasslands, dry herbaceous crops* and *dry woody crops*. Rules 1 and 2 were applied to capture low NDVI responses, and Rule 4 to restrict the steady NDVI gradient. Confusion matrices showed a significant drop in the OE from 49.9% to 12.0% and in the CE from 43.4% to 18.2%. *Urban areas and infrastructures* were confused with *bare soils* and *dry herbaceous crops*. Confusion matrices showed a drop in the OE from 32.5% to 18.9% and in the CE from 20.1% to 7.2%. The *water bodies* category was confused with several categories, but due to their characteristic shortwave infrared absorption and negative NDVI values, Rule 2 was sufficient for filtering this category correctly. The OE dropped from 18.1% to 0.0% and the CE from 3.5% to 0.0%.

Irrigated herbaceous crops were confused mainly with *dry herbaceous crops* and *irrigated woody crops*. Error related to dry crops was associated with the inter-annual time difference between the rDS and the imagery date, so that the phenological patterns of the winter crops and summer crops are mixed in the polygons. Once pixels with the dry patterns were decreased using Rule 4, the OE dropped from 24.3% to 6.9% and the CE from 21.2% to 3.2%. Resolving this inconsistency in *irrigated herbaceous crops* also had an effect on the accuracy of classifying *dry herbaceous crops*. *Dry herbaceous crops* were confused with *irrigated herbaceous crops* and *grasslands* and to a lesser extent with *dry woody crops*. Once the inconsistencies with irrigated crops were decreased by using Rule 4, the OE dropped from 10.8% to 5.8% and the CE from 7.9% to 1.9%. *Rice crop* confusion errors were related to *irrigated herbaceous crops*, which share common phenological patterns (positive NDVI gradient and high photosynthetic activity). The OE dropped from 20.3% to 0.5%, while the CE decreased from 34.1% to 17.3%.

Irrigated woody crops and *dry woody crops* are characterised by mixtures of different photosynthetic activities and soil contributions in crop fields. Based on the proxy of the photosynthetic activity, Rule 3 aimed to bring order to the greenness level achieved in different types of woody crops. This strategy excluded new plantations or even cases of irrigation plans not established on the imagery date. The OE associated with *irrigated woody crops* dropped from 38.6% to 3.8%, and *dry woody crops* did the same from 27.8% to 5.9%. The CE dropped from 45.3% to 9.8% for *irrigated woody crops* and from 24.8% to 10.8% for *dry woody crops*. The figures show a reduction in confusion with categories other than woody crops but an increase in the commission error with *shrublands* and *grasslands*, which to a certain extent share common patterns with the spectral variability of *dry woody crops*.

The LCM-1987 and LCM-2017 were derived considering GT samples generated from the SIOSE 2005 rDS. The results in the confusion matrices depicted a similar reduction in OE and CE in the categories, and more significantly in crop categories. The LCM-1987 overall accuracy (OA) using unfiltered TTA was 77.5% and it was 92.5% when filtered TTA was considered. For LCM-2017, the overall accuracy (OA) using unfiltered TTA was 78.7% and 93.4% using filtered TTA. When unfiltered TTA was used, the OA in both classifications was lower than that obtained in LCM-2002, which is related to the temporal lag between the imagery and rDS. However, all three classifications depicted a similar OA, of around 93.0%, when filtered TTA was used.

In the additional temporal test, we evaluated the performance of the rules by using the SIOSE 2011 as a new rDS. A new set of unfiltered and filtered TTA was used with imagery contemporary to SIOSE 2011 to generate LCM-2012. The results showed an OA of 85.6% considering unfiltered TTA and 94.2% when filtered TTA was used. A reduction in OE and CE was observed in all categories, and was more significant in agriculture categories in

accordance with the previously observed pattern. The OA in LCM-2012 was higher than the OA obtained in LCM-2002. This could be related to the imagery dates selected with respect to the rDS reference date. For LCM-2012, the selected images were contemporaneous or later than those of the SIOSE 2011 reference date, while for LCM-2002, they were all previous to the SIOSE 2005. The results showed a lower temporal repercussion of filtering when imagery dates were contemporaneous or as near to the rDS selected as possible. In the case of the spatial test, rules were evaluated in the southern scenes comparing LCM-2002 confusion matrices without and with rules application. The results showed an OA of 85.1% considering unfiltered TTA and 92.3% when were filtered. Again, crops categories denoted a higher reduction in OE and CE in accordance with previous results.

6. Discussion

Collecting precise GT samples is a prerequisite for performing accurate supervised classifications. Insufficient and unrepresentative reference samples were recognised as the primary source of errors [50,100]. Despite the substantial progress in LCM production, the lack of an accurate and representative number of GT samples is still a challenge [101]. On most occasions, the origin and quality of the GT used during the classification process are not explained or are only mentioned briefly [52,102]. Usually, to derive robust GT samples, pre-existing reference datasets (rDS) are used as a source of information instead of field work [54]. However, from an extended multitemporal analysis, the lack of temporal continuity (due to budget or investment reductions or even a decrease in interest in updates) limits the rDS to specific dates, leading to temporal lags between the rDS and imagery dates. Furthermore, error always exists in rDS, and the repercussions are intensified as the temporal extent increases.

In this study, a large number of GT samples were extracted from the SIOSE dataset, over which filtering rules were applied to update pixel labelling to the imagery date, diminishing error inconsistencies during the classification. The concatenation of the rules adjusted for each thematic category allowed us to control quality and the updating of the original pixel assignation to the target imagery date. The filtering rules were helpful for reducing inter-annual (time lags), intra-annual (disturbances), scale (associations of several land covers in polygons), and labelling (misassignments) inconsistencies in filtered GT samples.

There was a significant decrease in errors in wilderness categories, but there was a greater decrease in agricultural categories (Figure 18). These results were expected due to the inner dynamics of crop categories, which are more affected by the inter-annual time problem that impacts large areas (i.e., a higher number of pixels involved), and the more stable temporal behaviour of wilderness categories. Crop phenology complexity implies that two neighbouring crop fields can be in very different phenological stages (active crops or fallow) or belong to different categories (fallow land or winter crop patterns within dry or irrigated herbaceous crops). Considering the four temporal cases and the spatial case analysed, the wilderness categories showed an error reduction, on average, of over 15.1 percentage points in OE and over 11.6 percentage points in the CE, whereas the reduction in agricultural categories was over 19.4 percentage points and 21.3 percentage points, respectively (Table 4).

From the rDS, GT candidate pixels of forest categories were initially associated erroneously with *shrublands*, *grasslands*, or *bare soils* due to the scale error problem and the scarceness of pure polygons. Rules 1 and 2 showed their effectiveness for selecting the most active positions (forests) in tiles on all the dates considered, excluding low NDVI responses associated with *shrublands*, *grasslands* and *bare soils*, and any disturbance event affecting the candidate pixels within the intra-annual period considered (Figure 16A).

Table 4. Summary statistics of the confusion matrices considering unfiltered and filtered GT samples derived from SIOSE 2005 and 2011 in three temporal cases and one spatial case.

	LCM-1987				LCM-2012				LCM-2017				LCM-2002 *			
	OE (%)		CE (%)		OE (%)		CE (%)		OE (%)		CE (%)		OE (%)		CE (%)	
	uf.	f.	uf.	f.	uf.	f.	uf.	f.	uf.	f.	uf.	f.	uf.	f.	uf.	f.
CoF	22.9	16.8	18.8	8.7	12.0	10.0	5.3	2.1	17.9	11.5	11.1	3.5	13.5	7.4	15.2	6.1
BDF	25.0	3.8	21.2	2.8	5.2	2.6	7.1	1.4	21.1	2.6	14.2	3.3	22.2	6.9	26.1	15.3
BEF	10.3	5.8	25.5	16.0	7.5	3.3	15.7	13.5	9.8	3.3	19.9	13.4	15.3	6.6	18.3	11.6
Shl	36.6	5.4	20.7	9.3	17.4	4.7	17.7	5.9	41.5	6.0	25.1	6.2	49.2	30.6	33.1	16.7
Grl	26.3	12.9	23.5	11.2	16.2	7.1	20.5	8.8	19.6	9.2	24.5	12.1	15.4	8.5	16.9	9.8
BrS	45.1	9.3	40.3	12.2	47.5	13.9	32.4	18.5	51.2	6.3	41.9	22.2	49.2	19.5	41.9	19.9
Urb	56.0	10.4	15.3	19.4	19.6	12.3	10.4	6.0	27.1	8.6	15.2	26.7	46.4	38.2	30.5	14.2
WaB	21.8	0.0	3.3	0.0	3.9	0.2	2.5	0.0	5.3	0.0	4.1	0.0	13.7	0	6.4	0
IHC	31.5	7.3	23.7	6.4	19.0	2.6	23.8	4.9	29.2	2.9	32.1	6.3	17.5	0.7	20.8	1.3
DHC	16.4	6.8	11.2	1.4	11.1	5.1	6.8	1.3	15.0	5.1	8.8	1.4	9.5	6.9	4.2	1.6
IWC	37.7	7.4	50.6	13.5	34.8	12.2	40.4	6.5	42.0	14.9	48.9	5.9	40.2	2.6	60.4	3.4
DWC	15.2	4.8	28.2	10.7	34.5	4.6	25.1	16.0	20.2	17.8	28.3	15.4	12.8	2.6	15.6	12.6
RiC	66.7	0.0	59.8	0.0	18.8	5.0	17.8	1.6	13.4	7.1	43.5	17.6	–	–	–	–
OA	77.5	92.5			85.6	94.2			78.7	93.4			85.1	92.3		
K	0.7	0.9			0.8	0.9			0.7	0.9			0.8	0.9		

OA = Overall accuracy, OE = omission error, PA = producer accuracy, CE = commission error, UA = user accuracy, K = Kappa statistic, uf. = unfiltered GT samples, f. = filtered GT samples. LCM-2002 * refers to spatial test assessed in the southern scenes (200-032 and 200-033).

In addition, these two rules used together provide interesting utilities when forested areas have a discontinuous or sparse distribution (e.g., in open woodlands, such as *dehesa*). The map producer can establish an NDVI minimum threshold (using Rule 2) over which a forest category can be defined, considering the lower values as previous successional stages (*shrublands* or *grasslands*) towards the forest categories. This approach has a crucial significance during LCM production and its related time-series change analysis because the classified categories (and the land cover dynamics) have been coherently derived. Rule 4 was also helpful for reducing the labelling misassignment errors in categories with contrasting phenological patterns (e.g., between evergreen and deciduous forest categories) (Figure 16B). It is worth noting that this rule applied to evergreen forest polygons led to better discrimination between sclerophyllous deciduous species (e.g., *Quercus faginea*, *Q. pyrenaica*) and sclerophyllous evergreen species (e.g., *Quercus ilex*) in the study area. Errors in polygon labelling were detected in rDS, which is understandable due to difficulties in differentiating between the textures of sclerophyllous species during photointerpretation tasks. It could be of interest to discriminate between deciduous and evergreen sclerophyllous species when species transitions, adaptation and plasticity are evaluated in a context of global change.

Grasslands and *shrublands* are categories closely related in the study area and coexist in very different bioclimatic regions. Broad climatic conditions lead to high intraclass variability, spanning from the humid North-Atlantic to the dry Mediterranean bioclimatic regions. The high-class variability could lead to a coexistence of categories under climatic conditions and other dynamics related to ecological succession processes (e.g., new forest plantation areas, the tree line afforestation and field abandonment), enhanced by the inter-annual time problem. The rules applied to *shrublands* aim to capture this intraclass variability by considering a wide range of variation in thresholds with Rules 1 and 2 as well as limiting the NDVI temporal gradient with Rule 4, excluding deciduous patterns associated with grasslands and deciduous forest species. However, these rules cannot differentiate succes-

sional transitions at the limit towards the evergreen forest. In *grasslands*, the rules were defined to capture humid North-Atlantic and dry Mediterranean phenological patterns separately, where Rule 1 and 2 captured a wide range of variation and Rule 4 and 5 served to define NDVI gradients and phenological time restrictions.

Bare soils represent the lower NDVI responses in wilderness categories but were typically confused with *urban areas and infrastructures* or crop categories, with a high soil contribution in the NDVI signal. Rules 1 and 2 were used to extract the lower NDVI responses, and Rule 4 to limit contrasting phenological patterns (mainly exclusion of grasslands). Confusion errors between *dry herbaceous crops* and *dry woody crops* remained after the filtering rules were applied, explained by the soil spectral influence during crop harvesting or fallow periods in dry conditions. In the case of *urban areas and infrastructures*, errors remained in association with *bare soils* and *dry herbaceous crops* because of their spectral similarity and soil influence in crop categories. Rule 2 and Rule 4 were applied to restrict the NDVI values and phenological contrast, respectively, which made it possible to exclude vegetated areas in urban areas or even industrial polygons defined in rDS but not built at the imagery date (urban expansion).

Irrigated herbaceous crops are a heterogeneous category with multiple phenological behaviours (e.g., fallows, winter crops, perennial crops, double crops and summer crops) coexisting within polygons. The main errors were related to inter-annual time issues as irrigation plan transformations that have occurred periodically, mixing irrigated and dry crop patterns in the same polygon (Figure 17C). The irrigation conversion identified in SIOSE 2005 rDS was consolidated in LCM-2017 but not in LCM-2002 and LCM-1987. In this sense, rule 4 was crucial for discriminating between irrigated (positive NDVI gradient) and dry (negative NDVI gradient) herbaceous crops in the LCM and could contribute also to examining agricultural land fragmentation, identifying the number of parcels per holding and evaluating land consolidation policies over time. The application of rules also contributed to better identifying the boundaries of land parcels, more significantly in irrigated areas, where the multiplicity of phenological behaviours predominates.

Rice crops were mainly confused with *irrigated herbaceous crops*. Due to their characteristic phenological evolution during the growing season, the rules (mainly 2, 4 and 5) allowed us to capture *rice crop* phenology, reducing almost any confusion with other categories. On the other hand, *dry herbaceous crops* showed a lower variety of phenological responses (e.g., winter crops, fallows) being the main errors related to *irrigated herbaceous crops*, *grasslands* and, to a lesser extent, to *dry woody crops*. Rule 4 was crucial for characterising its negative temporal gradient in active crops or almost steady temporal pattern in fallows.

Irrigated woody crops and *dry woody crops* showed inconsistencies related to the labelling misassignments in polygons. Since the SIOSE rDS uses complementary cadastral information to define woody crop categories, the two regimes can coexist within polygons. Visual inspection of orthophotography made it possible to identify different crop stages. Thus, new plantation fields coexisted with older and consolidated fields, besides the variety in plantation frames (traditional, intensive or superintensive, in most cases accompanied by irrigation ponds) in irrigated olive or vineyard crop fields. Rule 3 was used to discriminate between areas (Figure 17D) with a total photosynthetic activity for 'n' dates over or under a threshold, which is a value adjusted to the woody crop type. The additive effect of the sum of NDVI responses allowed a better threshold definition and avoided selecting a specific date in the growing season to establish the limit. Rule 2 was used to define the woody crop range of variation allowed, especially to establish the minimum NDVI whereas Rule 5 was used as an auxiliary rule when NDVI thresholds were defined in phenological moments. Therefore, the initial confusion between *dry woody crops* and *irrigated woody crops* was considerably decreased after the rules were applied. However, there remained CE with *dry herbaceous crops*, *shrublands* and *grasslands*, which shows that some mixtures with these categories were produced, and rules should be adjusted thoroughly, if possible. Nevertheless, there was a large reduction in confusion between categories, ensuring category consistency in land-cover time-series change analyses.

7. Limitations and Future Research

The SIOSE dataset provides high-quality information for the Spanish territory. Thus, it is a source of a large number of candidate pixels that can be updated by applying filtering rules to the imagery date. However, filtering rules in a context of high intraclass variability can eliminate some part of the class variability. In this sense, some studies suggest the possibility of dividing the territory into more homogenous bioclimatic regions or spatial stratification based on bioclimatic characteristics [103]. Dividing the territory into homogeneous eco-climatic regions would make it possible to adjust filtering rules more accurately and improve the final map accuracy since intraclass variability would be reduced. This approach is attractive in the context of a large-area classification but requires reference data for each region (stratum). In this context, filtering rules can be used to derive robust stratum GT based on expert knowledge of established biogeographic regions.

After applying the filtering rules, *shrublands* and *grasslands* showed a general decrease in confusion with other categories, but there were still errors between them, which can be explained by their high intraclass variability. However, CE increased with *dry woody crops*, which can be related to the phenological and the spectral similarity between them and *shrublands/pastures* with high intraclass variability. The filtering rules had also some limitations when coniferous and sclerophyllous forest categories were discriminated. New strategies for researching evergreen mixed forest associations are necessary when there is a lack of phenological contrast. When the OE of coniferous and evergreen forest in LCM-2002 was examined, error locations were detected within coniferous plantation polygons. Clear-cutting practices are carried out periodically in forest plantations. Therefore, depending on the time lag between the clear-cutting and the imagery date, coniferous GT pixels were in a successional stage between shrublands and coniferous forest, with an NDVI signal that was classified as broadleaf evergreen forest. At the same time, the application of the rules reduced the confusion of dry herbaceous crops with *irrigated herbaceous crops* but the mix up remained with *grasslands,* whereas errors with *bare soils* and *dry woody crops* increased slightly in relation to the soil contribution during harvesting or fallow periods.

Through the temporal and spatial sensitivity analysis performed, we have obtained robust results, clearly showing the goodness to apply a set of filtering rules to improve the GT samples quality. This methodology could be broadly extended and applied using other remote sensing images (at coarse, medium or high-resolution) providing vegetation indices. As a future research, we will investigate the application of this framework of filtering rules using other vegetation indices such as SAVI or EVI, among others.

8. Conclusions

The research objective in this paper was to propose and demonstrate the applicability of a set of filtering rules to control the quality of GT samples derived from an rDS, the SIOSE dataset in this study. We firstly identified errors in the GT samples associated with various issues: the inter-annual time difference between imagery and the rDS dates; the intra-annual time variability within the imagery dates; the scale problem related to the rDS scale and imagery resolution compatibility; the existence of multiple behaviours in rDS polygons; and, finally, labelling misassignments. Secondly, to deal with the error sources, we designed and applied a framework of filtering rules using the NDVI to reduce inconsistencies, adapting GT samples to the target imagery date. Thirdly, unfiltered and filtered sets of GT samples were used to derive LCM classifications for evaluating the performance of the filtering rules in four temporal study cases: LCM-1987, LCM-2002 and LCM-2017 considering SIOSE 2005, and LCM-2012 considering the SIOSE 2011 as an additional rDS. An additional spatial case was evaluated for LCM-2002 located in the southern scenes considering SIOSE 2005 as rDS.

There are several main conclusions: (i) the results of the confusion matrices in the five study cases yielded, on average, an increase in the overall accuracy of 10.9 percentage points, with a reduction in the omission error of 16.8 percent points and in the commission error of 14.0 percent points. Filtered GT samples depicted a clear reduction in the com-

mission and omission errors. The thirteen categories showed a decrease in error, which was more remarkable in agriculture categories due to their spatial heterogeneity and higher temporal sensitivity to the time lag between rDS and imagery dates compared to wilderness categories. Only a slight increase in the commission error of dry woody crops with first stages of the natural succession categories was detected. (ii) Filtering rules can be formulated to characterise the phenology of the categories, which is the basis for reducing the confusion between classes. Rule 1 together with Rule 2 effectively prevented scale and intra-annual time errors in wilderness categories. These rules made it possible to extract pixels in tiles with the maximum NDVI response and also restrict minimum NDVI values in the series. These two rules together are a decisive strategy for filtering candidate pixels and avoiding intra-annual time events (e.g., fire disturbances, forestry management practices) affecting wilderness categories in the target time. Rule 2 was useful for defining the NDVI range of variation values over which the categories vary. Rule 3 effectively avoided labelling misassignments in woody crop categories. This rule is helpful for discriminating multiple behaviours in irrigated woody crops, keeping pixels with the higher photosynthetic activity in the same class while reassigning samples with lower values to the dry woody crop category. Rule 4 allowed the temporal NDVI gradient to be characterised, avoiding mixtures of categories with contrasting temporal gradients (evergreen and deciduous forests, summer and winter crops). This rule prevented labelling misassignments in herbaceous crops where dry and irrigated phenological patterns coexist, and even more so in areas where irrigation planning changed over time. The rule also allowed distinguishing between deciduous and evergreen patterns in forest categories. Finally, Rule 5 served as an auxiliary rule when the phenology made it necessary to establish specific thresholds at certain phenological moments. This rule enables binary comparisons between dates and establishing a threshold value for specific moments.

In short, ideally, a good design of the classes would avoid or reduce the need of their quality control, but in most cases, reliable GT samples are not available, and some control of the quality should be applied. rDS availability is restricted and limited to specific reference dates. In cases of no temporal continuity or the lack of availability of an rDS on the map producer's date of interest, it is necessary to filter the samples extracted from the rDS, which is always discontinuous in time, from a past or future target time. Otherwise, erroneous GT samples will be included in the classification procedure and, as a consequence, LCM production for each date and also the derived time-series products will be much more unreliable.

Supplementary Materials: The following are available online at https://www.mdpi.com/article/10.3390/rs13142662/s1, Table S1: rDS examples in different geographic ambits, and at different thematic, spatial and temporal resolutions; Table S2: Details of the imagery considered for each LCM; Table S3: Examples of SQL queries for forest category polygon extraction of forest categories; Table S4: Parametrisation of rule statements defined for each category and geographical context; Table S5: Confusion matrix without the application of filtering rules. SIOSE 2005 rDS ground truth samples and LCM-1987 imagery; Table S6: Confusion matrix with the application of filtering rules. SIOSE 2005 rDS ground truth samples and LCM-1987 imagery; Table S7: Confusion matrix without the application of filtering rules. SIOSE 2005 rDS ground truth samples and LCM-2002 imagery; Table S8: Confusion matrix with the application of filtering rules. SIOSE 2005 rDS ground truth samples and LCM-2002 imagery; Table S9: Confusion matrix without the application of filtering rules. SIOSE 2005 rDS ground truth samples and LCM-2017 imagery; Table S10: Confusion matrix with the application of filtering rules. SIOSE 2005 rDS ground truth samples and LCM-2017 imagery; Table S11: Confusion matrix without the application of filtering rules. SIOSE 2011 rDS ground truth samples and LCM-2012 imagery; Table S12: Confusion matrix with the application of filtering rules. SIOSE 2011 rDS ground truth samples and LCM-2012 imagery; Table S13: Confusion matrix without the application of filtering rules. SIOSE 2005 rDS ground truth samples and LCM-2002 imagery (scenes 200-032–200-033); Table S14: Confusion matrix with the application of filtering rules. SIOSE 2005 rDS ground truth samples and LCM-2002 imagery (scenes 200-032–200-033); Figure S1: The temporal relative frequency distribution of the NDVI evaluated for each category; Figure S2:

Classification results considering unfiltered and filtered GT samples from SIOSE 2005 (LCM-1987, LCM-2002 and 2017), and SIOSE 2011 (LCM-2012).

References

1. Peraza-Castro, M.; Ruiz-Romera, E.; Meaurio, M.; Sauvage, S.; Sánchez-Pérez, J.M. Modelling the impact of climate and land cover change on hydrology and water quality in a forest watershed in the Basque Country (Northern Spain). *Ecol. Eng.* **2018**, *122*, 315–326. [CrossRef]
2. Rogger, M.; Agnoletti, M.; Alaoui, A.; Bathurst, J.C.; Bodner, G.; Borga, M.; Chaplot, V.; Gallart, F.; Glatzel, G.; Hall, J.; et al. Land use change impacts on floods at the catchment scale: Challenges and opportunities for future research. *Water Resour. Res.* **2017**, *53*, 5209–5219. [CrossRef] [PubMed]
3. Biro, K.; Pradhan, B.; Buchroithner, M.; Makeschin, F. Land Use/Land Cover Change Analysis And Its Impact On Soil Properties In The Northern Part Of Gadarif Region, Sudan. *Land Degrad. Dev.* **2013**, *24*, 90–102. [CrossRef]
4. Abd El-Kawy, O.R.; Rød, J.K.; Ismail, H.A.; Suliman, A.S. Land use and land cover change detection in the western Nile delta of Egypt using remote sensing data. *Appl. Geogr.* **2011**, *31*, 483–494. [CrossRef]
5. Rodríguez-Rodríguez, D.; Martínez-Vega, J.; Echavarría, P. A twenty year GIS-based assessment of environmental sustainability of land use changes in and around protected areas of a fast developing country: Spain. *Int. J. Appl. Earth Obs. Geoinf.* **2019**, *74*, 169–179. [CrossRef]
6. Heidrich, O.; Reckien, D.; Olazabal, M.; Foley, A.; Salvia, M.; de Gregorio Hurtado, S.; Orru, H.; Flacke, J.; Geneletti, D.; Pietrapertosa, F.; et al. National climate policies across Europe and their impacts on cities strategies. *J. Environ. Manag.* **2016**, *168*, 36–45. [CrossRef] [PubMed]
7. Reckien, D.; Salvia, M.; Heidrich, O.; Church, J.M.; Pietrapertosa, F.; De Gregorio-Hurtado, S.; D'Alonzo, V.; Foley, A.; Simoes, S.G.; Krkoška Lorencová, E.; et al. How are cities planning to respond to climate change? Assessment of local climate plans from 885 cities in the EU-28. *J. Clean. Prod.* **2018**, *191*, 207–219. [CrossRef]
8. Estrela, T.; Sancho, T.A. Drought management policies in Spain and the european union: From traditional emergency actions to drought management plans. *Water Policy* **2016**, *18*, 153–176. [CrossRef]
9. Colwell, R.N. (Ed.) *Manual for Photographic Interpretation*; The American Society of Photogrammetry: Washington, DC, USA, 1960.
10. Cihlar, J. Land cover mapping of large areas from satellites: Status and research priorities. *Int. J. Remote Sens.* **2000**, *21*, 1093–1114. [CrossRef]
11. Aplin, P. Remote sensing: Land cover. *Prog. Phys. Geogr.* **2004**, *28*, 283–293. [CrossRef]
12. Lambin, E.F.; Helmut, G. *Land-Use and Land-Cover Change: Local Processes and Global Impacts*; Springer: Berlin, Germany; New York, NY, USA, 2006; ISBN 978-3-540-32201-6.
13. Calderón-Loor, M.; Hadjikakou, M.; Bryan, B.A. High-resolution wall-to-wall land-cover mapping and land change assessment for Australia from 1985 to 2015. *Remote Sens. Environ.* **2021**, *252*, 112148. [CrossRef]
14. Pan, D.; Domon, G.; De Blois, S.; Bouchard, A. Temporal (1958–1993) and spatial patterns of land use changes in Haut-Saint-Laurent (Quebec, Canada) and their relation to landscape physical attributes. *Landsc. Ecol.* **1999**, *14*, 35–52. [CrossRef]
15. Chen, Y.; Zhang, X.; Fang, G.; Li, Z.; Wang, F.; Qin, J.; Sun, F. Potential risks and challenges of climate change in the arid region of northwestern China. *Reg. Sustain.* **2020**, *1*, 20–30. [CrossRef]
16. Mishra, P.K.; Rai, A.; Rai, S.C. Land use and land cover change detection using geospatial techniques in the Sikkim Himalaya, India. *Egypt. J. Remote Sens. Space Sci.* **2020**, *23*, 133–143. [CrossRef]
17. Azimi Sardari, M.R.; Bazrafshan, O.; Panagopoulos, T.; Sardooi, E.R. Modeling the Impact of Climate Change and Land Use Change Scenarios on Soil Erosion at the Minab Dam Watershed. *Sustainability* **2019**, *11*, 3353. [CrossRef]
18. Serneels, S.; Lambin, E.F. Impact of land-use changes on the wildebeest migration in the northern part of the Serengeti-Mara ecosystem. *J. Biogeogr.* **2001**, *28*, 391–407. [CrossRef]
19. Laney, R.M. A process-led approach to modeling land change in agricultural landscapes: A case study from Madagascar. *Agric. Ecosyst. Environ.* **2004**, *101*, 135–153. [CrossRef]
20. Crews-Meyer, K.A. Agricultural landscape change and stability in northeast Thailand: Historical patch-level analysis. *Agric. Ecosyst. Environ.* **2004**, *101*, 155–169. [CrossRef]

21. Gabiri, G.; Diekkrüger, B.; Näschen, K.; Leemhuis, C.; van der Linden, R.; Mwanjalolo Majaliwa, J.G.; Obando, J.A. Impact of climate and land use/land cover change on thewater resources of a tropical inland valley catchment in Uganda, East Africa. *Climate* **2020**, *8*, 83. [CrossRef]

22. Rogan, J.; Miller, J.; Stow, D.; Franklin, J.; Levien, L.; Fischer, C. Land-cover change monitoring with classification trees using Landsat TM and ancillary data. *Photogramm. Eng. Remote Sens.* **2003**, *69*, 793–804. [CrossRef]

23. MacDonald, G.M. Water, climate change, and sustainability in the southwest. *Proc. Natl. Acad. Sci. USA* **2010**, *107*, 21256–21262. [CrossRef]

24. Homer, C.G.; Huang, C.; Yang, L.; Wylie, B.K.; Coan, M. Development of a 2001 National Land Cover Database for the United States. *Photogramm. Eng. Remote Sens.* **2004**, *70*, 829–840. [CrossRef]

25. Gong, P.; Wang, J.; Yu, L.; Zhao, Y.; Zhao, Y.; Liang, L.; Niu, Z.; Huang, X.; Fu, H.; Liu, S.; et al. Finer resolution observation and monitoring of global land cover: First mapping results with Landsat TM and ETM + data. *Int. J. Remote Sens.* **2013**, *34*, 2607–2654. [CrossRef]

26. Song, X.-P.; Hansen, M.C.; Stehman, S.V.; Potapov, P.V.; Tyukavina, A.; Vermote, E.F.; Townshend, J.R. Global land change from 1982 to 2016. *Nature* **2018**, *560*, 639–643. [CrossRef] [PubMed]

27. Hansen, M.C.; Potapov, P.V.; Moore, R.; Hancher, M.; Turubanova, S.A.; Tyukavina, A.; Thau, D.; Stehman, S.V.; Goetz, S.J.; Loveland, T.R.; et al. High-Resolution Global Maps of 21st-Century Forest Cover Change. *Science* **2013**, *342*, 850–853. [CrossRef] [PubMed]

28. Gómez, C.; White, J.C.; Wulder, M.A. Optical remotely sensed time series data for land cover classification: A review. *ISPRS J. Photogramm. Remote Sens.* **2016**, *116*, 55–72. [CrossRef]

29. Woodcock, C.; Allen, R.; Anderson, M.; Belward, A.; Bindschadler, R.; Cohen, W.; Gao, F.; Goward, S.; Helder, D.; Helmer, E.; et al. Free Access to Landsat Imagery. *Science* **2008**, *320*, 1011. [CrossRef]

30. Zhu, Z.; Wulder, M.A.; Roy, D.P.; Woodcock, C.E.; Hansen, M.C.; Radeloff, V.C.; Healey, S.P.; Schaaf, C.; Hostert, P.; Strobl, P.; et al. Benefits of the free and open Landsat data policy. *Remote Sens. Environ.* **2019**, *224*, 382–385. [CrossRef]

31. Wulder, M.A.; Masek, J.G.; Cohen, W.B.; Loveland, T.R.; Woodcock, C.E. Opening the archive: How free data has enabled the science and monitoring promise of Landsat. *Remote Sens. Environ.* **2012**, *122*, 2–10. [CrossRef]

32. Jutz, S.; Milagro-Pérez, M.P. Copernicus program. In *Comprehensive Remote Sensing*; Elsevier: Oxford, UK, 2017; Volume 1, ISBN 9780128032206.

33. Wulder, M.A.; Coops, N.C.; Roy, D.P.; White, J.C.; Hermosilla, T. Land cover 2.0. *Int. J. Remote Sens.* **2018**, *39*, 4254–4284. [CrossRef]

34. Saunier, S.; Beaton, A.; Lavender, S.; Galli, L.; Ferrara, R.; Mica, S.; Biasutti, R.; Goryl, P.; Gascon, F.; Meloni, M. Bulk processing of the Landsat MSS/TM/ETM+ archive of the European Space Agency: An insight into the Level 1 MSS processing. In Proceedings of the Image and Signal Processing for Remote Sensing XXIII, Warsaw, Poland, 11–14 September 2017; Bruzzone, L., Ed.; 2017; Volume 10427, pp. 1–16. [CrossRef]

35. Lary, D.J.; Alavi, A.H.; Gandomi, A.H.; Walker, A.L. Machine learning in geosciences and remote sensing. *Geosci. Front.* **2016**, *7*, 3–10. [CrossRef]

36. Sishodia, R.P.; Ray, R.L.; Singh, S.K. Applications of Remote Sensing in Precision Agriculture: A Review. *Remote Sens.* **2020**, *12*, 3136. [CrossRef]

37. Tuia, D.; Camps-Valls, G. Recent advances in remote sensing image processing. *Proc. Int. Conf. Image Process. ICIP* **2009**, 3705–3708. [CrossRef]

38. Gómez, C.; Alejandro, P.; Hermosilla, T.; Montes, F.; Pascual, C.; Ruiz, L.A.; Álvarez-Taboada, F.; Tanase, M.; Valbuena, R. Remote sensing for the Spanish forests in the 21st century: A review of advances, needs, and opportunities. *For. Syst.* **2019**, *28*, eR001. [CrossRef]

39. Zhu, Z.; Woodcock, C.E. Continuous change detection and classification of land cover using all available Landsat data. *Remote Sens. Environ.* **2014**, *144*, 152–171. [CrossRef]

40. Olofsson, P.; Foody, G.M.; Herold, M.; Stehman, S.V.; Woodcock, C.E.; Wulder, M.A. Good practices for estimating area and assessing accuracy of land change. *Remote Sens. Environ.* **2014**, *148*, 42–57. [CrossRef]

41. Stehman, S.V.; Foody, G.M. Key issues in rigorous accuracy assessment of land cover products. *Remote Sens. Environ.* **2019**, *231*. [CrossRef]

42. Millard, K.; Richardson, M. On the Importance of Training Data Sample Selection in Random Forest Image Classification: A Case Study in Peatland Ecosystem Mapping. *Remote Sens.* **2015**, *7*, 8489–8515. [CrossRef]

43. Rozenstein, O.; Karnieli, A. Comparison of methods for land-use classification incorporating remote sensing and GIS inputs. *Appl. Geogr.* **2011**, *31*, 533–544. [CrossRef]

44. Gašparović, M.; Zrinjski, M.; Gudelj, M. Automatic cost-effective method for land cover classification (ALCC). *Comput. Environ. Urban Syst.* **2019**, *76*, 1–10. [CrossRef]

45. Mellor, A.; Boukir, S.; Haywood, A.; Jones, S. Exploring issues of training data imbalance and mislabelling on random forest performance for large area land cover classification using the ensemble margin. *ISPRS J. Photogramm. Remote Sens.* **2015**, *105*, 155–168. [CrossRef]

46. Fritz, S.; McCallum, I.; Schill, C.; Perger, C.; See, L.; Schepaschenko, D.; van der Velde, M.; Kraxner, F.; Obersteiner, M. Geo-Wiki: An online platform for improving global land cover. *Environ. Model. Softw.* **2012**, *31*, 110–123. [CrossRef]

47. Rodriguez-Galiano, V.F.; Ghimire, B.; Rogan, J.; Chica-Olmo, M.; Rigol-Sanchez, J.P. An assessment of the effectiveness of a random forest classifier for land-cover classification. *ISPRS J. Photogramm. Remote Sens.* **2012**, *67*, 93–104. [CrossRef]

48. Shao, Y.; Lunetta, R.S. Comparison of support vector machine, neural network, and CART algorithms for the land-cover classification using limited training data points. *ISPRS J. Photogramm. Remote Sens.* **2012**, *70*, 78–87. [CrossRef]

49. Griffiths, P.; Kuemmerle, T.; Baumann, M.; Radeloff, V.C.; Abrudan, I.V.; Lieskovsky, J.; Munteanu, C.; Ostapowicz, K.; Hostert, P. Forest disturbances, forest recovery, and changes in forest types across the carpathian ecoregion from 1985 to 2010 based on landsat image composites. *Remote Sens. Environ.* **2014**, *151*, 72–88. [CrossRef]

50. Elmes, A.; Alemohammad, H.; Avery, R.; Caylor, K.; Eastman, J.R.; Fishgold, L.; Friedl, M.A.; Jain, M.; Kohli, D.; Bayas, J.C.L.; et al. Accounting for training data error in machine learning applied to earth observations. *Remote Sens.* **2020**, *12*, 1034. [CrossRef]

51. Ye, S.; Pontius, R.G.; Rakshit, R. A review of accuracy assessment for object-based image analysis: From per-pixel to per-polygon approaches. *ISPRS J. Photogramm. Remote Sens.* **2018**, *141*, 137–147. [CrossRef]

52. Foody, G.M. Assessing the accuracy of land cover change with imperfect ground reference data. *Remote Sens. Environ.* **2010**, *114*, 2271–2285. [CrossRef]

53. Fuller, R.M.; Smith, G.M.; Devereux, B.J. The characterisation and measurement of land cover change through remote sensing: Problems in operational applications? *Int. J. Appl. Earth Obs. Geoinf.* **2003**, *4*, 243–253. [CrossRef]

54. Vidal-Macua, J.J.; Zabala, A.; Ninyerola, M.; Pons, X. Developing spatially and thematically detailed backdated maps for land cover studies. *Int. J. Digit. Earth* **2017**, *8947*, 1–32. [CrossRef]

55. Ghorbanian, A.; Kakooei, M.; Amani, M.; Mahdavi, S.; Mohammadzadeh, A.; Hasanlou, M. Improved land cover map of Iran using Sentinel imagery within Google Earth Engine and a novel automatic workflow for land cover classification using migrated training samples. *ISPRS J. Photogramm. Remote Sens.* **2020**, *167*, 276–288. [CrossRef]

56. Sankey, T.T. Scale, Effects. In *Encyclopedia of GIS*; Shekhar, S., Xiong, H., Eds.; Springer US: Boston, MA, USA, 2008; pp. 1021–1026, ISBN 978-0-387-35973-1.

57. Bossard, M.; Feranec, J.; Otahel, J. CORINE Land Cover Technical Guide: Addendum 2000. In *CORINE Land Cover Technical Guide*; European Environment Agency: Copenhagen, Denmark, 2000; ISBN 9282625788.

58. Buyantuyev, A.; Wu, J. Effects of thematic resolution on landscape pattern analysis. *Landsc. Ecol.* **2007**, *22*, 7–13. [CrossRef]

59. Lechner, A.M.; Rhodes, J.R. Recent Progress on Spatial and Thematic Resolution in Landscape Ecology. *Curr. Landsc. Ecol. Rep.* **2016**, *1*, 98–105. [CrossRef]

60. De Fries, R.S.; Hansen, M.; Townshend, J.R.G.; Sohlberg, R. Global land cover classifications at 8 km spatial resolution: The use of training data derived from Landsat imagery in decision tree classifiers. *Int. J. Remote Sens.* **1998**, *19*, 3141–3168. [CrossRef]

61. Anderson, J.R.; Hardy, E.E.; Roach, J.T.; Witmer, R.E. *A Land Use and Land Cover Classification System for Use with Remote Sensor Data*; U.S. Geological Survey Professional Paper 964; U.S. Geological Survey: Reston, VA, USA, 1976; 28p.

62. Federal Geographic Data Committee National Vegetation Classification Standard. Available online: https://www.fgdc.gov/standards/projects/vegetation/standards/projects/vegetation/vegclass.pdf (accessed on 11 January 2021).

63. Scott, J.M.; Jennings, M.D. Large-Area Mapping of Biodiversity. *Ann. Mo. Bot. Gard.* **1998**, *85*, 34–47. [CrossRef]

64. Gregorio, A.D.; Jansen, L.J.M. Land Cover Classification System (LCCS): Classification Concepts and User Manual. *FAO* **2000**, *53*, 179.

65. Silla, C.N.; Freitas, A.A. A survey of hierarchical classification across different application domains. *Data Min. Knowl. Discov.* **2011**, *22*, 31–72. [CrossRef]

66. European Environment Agency Corine Land Cover Update 2000-Technical Guidelines. Available online: https://land.copernicus.eu/user-corner/technical-library/techrep89.pdf (accessed on 5 July 2021).

67. Del Barrio, G.; Creus, J.; Puigdefabregas, J. Thermal seasonality of the high mountain belts of the Pyrenees. *Mt. Res. Dev.* **1990**, *10*, 227–233. [CrossRef]

68. Comín, F.A. Management of the Ebro River Basin: Past, present and future. *Water Sci. Technol.* **1999**, *40*. [CrossRef]

69. Sangüesa-Barreda, G.; Camarero, J.J.; García-Martín, A.; Hernández, R.; De la Riva, J. Remote-sensing and tree-ring based characterization of forest defoliation and growth loss due to the Mediterranean pine processionary moth. *For. Ecol. Manag.* **2014**, *320*, 171–181. [CrossRef]

70. USA Geological Survey EarthExplorer. Available online: https://earthexplorer.usgs.gov/ (accessed on 8 June 2021).

71. Dubayah, R.; Rich, P.M. Topographic solar radiation models for GIS. *Int. J. Geogr. Inf. Syst.* **1995**, *9*, 405–419. [CrossRef]

72. Olpenda, A.S.; Stereńczak, K.; Będkowski, K. Modeling Solar Radiation in the Forest Using Remote Sensing Data: A Review of Approaches and Opportunities. *Remote Sens.* **2018**, *10*, 694. [CrossRef]

73. Eiumnoh, A.; Shrestha, R.P. Application of DEM data to Landsat image classification: Evaluation in a tropical wet-dry landscape of Thailand. *Photogramm. Eng. Remote Sens.* **2000**, *66*, 297–304.

74. Hutchinson, C.F. Techniques for combining Landsat and ancillary data for digital classification improvement. *Photogramm. Eng. Remote Sens.* **1982**, *48*, 123–130.

75. Jones, A.R.; Settle, J.J.; Wyatt, B.K. Use of digital terrain data in the interpretation of SPOT-1 HRV multispectral imagery. *Int. J. Remote Sens.* **1988**, *9*, 669–682. [CrossRef]

76. Palacio-Prieto, J.L.; Luna-González, L. Improving spectral results in a GTS context. *Int. J. Remote Sens.* **1996**, *17*, 2201–2209. [CrossRef]

77. Bahadur, K.C.K. Improving Landsat and IRS Image Classification: Evaluation of Unsupervised and Supervised Classification through Band Ratios and DEM in a Mountainous Landscape in Nepal. *Remote Sens.* **2009**, *1*, 1257–1272. [CrossRef]

78. Aerial Orthophotography National Plan (PNOA). Available online: https://pnoa.ign.es/el-proyecto-pnoa-lidar (accessed on 10 February 2021).

79. Pons, X. 2004. MiraMon. Geographic Information System and Remote Sensing Software. Centre de Recerca Ecològica i Aplicacions Forestals, CREAF. Bellaterra. Available online: https://www.miramon.cat/Index_usa.htm (accessed on 5 July 2021).

80. Pons, X.; Ninyerola, M. Mapping a topographic global solar radiation model implemented in a GIS and refined with ground data. *Int. J. Climatol.* **2008**, *28*, 1821–1834. [CrossRef]

81. González-Guerrero, O.; Pons, X. The 2017 Land Use/Land Cover Map of Catalonia based on Sentinel-2 images and auxiliary data. *Rev. Teledetec.* **2020**, *55*, 81–92. [CrossRef]

82. Egenhofer, M.; Frank, A. Object-Oriented Modeling for GIS. *URISA J.* **2001**, *4*, 3–19.

83. Pons, X.; Pesquer, L.; Cristóbal, J.; González-Guerrero, O. Automatic and improved radiometric correction of landsat imagery using reference values from MODIS surface reflectance images. *Int. J. Appl. Earth Obs. Geoinf.* **2014**, *33*, 243–254. [CrossRef]

84. Padró, J.-C.; Pons, X.; Aragonés, D.; Díaz-Delgado, R.; García, D.; Bustamante, J.; Pesquer, L.; Domingo-Marimon, C.; González-Guerrero, Ò.; Cristóbal, J.; et al. Radiometric Correction of Simultaneously Acquired Landsat-7/Landsat-8 and Sentinel-2A Imagery Using Pseudoinvariant Areas (PIA): Contributing to the Landsat Time Series Legacy. *Remote Sens.* **2017**, *9*, 1319. [CrossRef]

85. Griffiths, P.; van der Linden, S.; Kuemmerle, T.; Hostert, P. A Pixel-Based Landsat Compositing Algorithm for Large Area Land Cover Mapping. *IEEE J. Sel. Top. Appl. Earth Obs. Remote Sens.* **2013**, *6*, 2088–2101. [CrossRef]

86. Tucker, C.J. Red and photographic infrared linear combinations for monitoring vegetation. *Remote Sens. Environ.* **1979**, *8*, 127–150. [CrossRef]

87. Ouma, Y.; Tateishi, R. A water index for rapid mapping of shoreline changes of five East African Rift Valley lakes: An empirical analysis using Landsat TM and ETM + data. *Int. J. Remote Sens.* **2006**, *27*, 3153–3181. [CrossRef]

88. Zhu, Z.; Wang, S.; Woodcock, C.E. Improvement and expansion of the Fmask algorithm: Cloud, cloud shadow, and snow detection for Landsats 4–7, 8, and Sentinel 2 images. *Remote Sens. Environ.* **2015**, *159*, 269–277. [CrossRef]

89. Kyle, H.L.; Curran, R.J.; Barnes, W.L.; Escoe, D. A cloud physics radiometer. In Proceedings of the Third Conference on Atmospheric Radiation, Davis, CA, USA, 28–30 June 1978; pp. 107–109.

90. Dozier, J. Spectral signature of alpine snow cover from the landsat thematic mapper. *Remote Sens. Environ.* **1989**, *28*, 9–22. [CrossRef]

91. Herrero, J.; Polo, M.J.; Losada, M. Snow evolution in Sierra Nevada (Spain) from an energy balance model validated with Landsat TM data. *Proc. SPIE Int. Soc. Opt. Eng.* **2011**, *8174*. [CrossRef]

92. Klein, A.G.; Hall, D.K.; Riggs, G.A. Improving snow cover mapping in forests through the use of a canopy reflectance model. *Hydrol. Process.* **1998**, *12*, 1723–1744. [CrossRef]

93. Negi, H.S.; Kulkarni, A.V.; Semwal, B.S. Estimation of snow cover distribution in Beas basin, Indian Himalaya using satellite data and ground measurements. *J. Earth Syst. Sci.* **2009**, *118*, 525–538. [CrossRef]

94. Land Occupation Information System of Spain (SIOSE). Available online: https://www.siose.es/ (accessed on 5 July 2021).

95. Serra, P.; Pons, X.; Saurí, D. Post-classification change detection with data from different sensors: Some accuracy considerations. *Int. J. Remote Sens.* **2003**, *24*, 3311–3340. [CrossRef]

96. Ameijeiras-Alonso, J.; Crujeiras, R.M.; Rodríguez-Casal, A. Multimode: An R Package for Mode Assessment. *arXiv* **2018**, arXiv:1803.00472.

97. Nunes, L.; Moreno, M.; Alberdi, I.; Álvarez-González, J.G.; Godinho-Ferreira, P.; Mazzoleni, S.; Castro Rego, F. Harmonized Classification of Forest Types in the Iberian Peninsula Based on National Forest Inventories. *Forests* **2020**, *11*, 1170. [CrossRef]

98. Pontius, R.G.; Millones, M. Death to Kappa: Birth of quantity disagreement and allocation disagreement for accuracy assessment. *Int. J. Remote Sens.* **2011**, *32*, 4407–4429. [CrossRef]

99. Congalton, R.G. A review of assessing the accuracy of classifications of remotely sensed data. *Remote Sens. Environ.* **1991**, *37*, 35–46. [CrossRef]

100. Amani, M.; Brisco, B.; Afshar, M.; Mirmazloumi, S.M.; Mahdavi, S.; Mirzadeh, S.M.J.; Huang, W.; Granger, J. A generalized supervised classification scheme to produce provincial wetland inventory maps: An application of Google Earth Engine for big geo data processing. *Big Earth Data* **2019**, *3*, 378–394. [CrossRef]

101. Friedl, M.A.; Sulla-Menashe, D.; Tan, B.; Schneider, A.; Ramankutty, N.; Sibley, A.; Huang, X. MODIS Collection 5 global land cover: Algorithm refinements and characterization of new datasets. *Remote Sens. Environ.* **2010**, *114*, 168–182. [CrossRef]

102. Xie, Z.; Chen, Y.; Lu, D.; Li, G.; Chen, E. Classification of land cover, forest, and tree species classes with Ziyuan-3 multispectral and stereo data. *Remote Sens.* **2019**, *11*, 164. [CrossRef]

103. Inglada, J.; Vincent, A.; Arias, M.; Tardy, B.; Morin, D.; Rodes, I. Operational High Resolution Land Cover Map Production at the Country Scale Using Satellite Image Time Series. *Remote Sens.* **2017**, *9*, 95. [CrossRef]

3.2. Artículo 2: Supplementary materials

Padial-Iglesias, M.; Serra, P.; Ninyerola, M.; Pons, X. A Framework of Filtering Rules over Ground Truth Samples to Achieve Higher Accuracy in Land Cover Maps. *Remote Sensing.* 2021, *13*, 2662. https://doi.org/10.3390/rs13142662 (Journal Impact Factor (JIF): 4.848, Q1: 27/200 (2020) [Geosciences, Multidisciplinary]).

Hipervínculo: https://www.mdpi.com/2072-4292/13/14/2662/s1

Supplementary Material

Table S1. rDS examples in different geographic ambits, and at different thematic, spatial and temporal resolutions.

rDS	Ambit	DB model	Thematic resolution	Scale/ spatial resolution	Temporal resolution	Main methodology
Global Land Cover 2000 database	Global	HI	22 classes (global detail)	1000 m	2000	AC
GlobCover	Global	HI	22 classes (global detail)	300 m	2005–2006, 2009	AC
CORINE	Europe	HI	44 classes (max. level)	1:100000	1990, 2000, 2006, 2012, 2018	Ph
Land Cover Map for Great Britain	Country (Great Britain)	HI	21 classes	25 m	1990, 2000, 2007, 2015, 2017, 2018, 2019	AC
SIOSE	Country (Spain)	OO	41 s.c 44 p.c.c	1:25000	2005, 2009, 2011, 2014	Ph
Land Use and Vegetation Cover Map of Andalusia	Regional (Andalusia)	HI	144^{I}, 166^{II} Classes	$1:50000^{I}$, $1:25000^{II}$	1991^{I}, 1995^{I}, 1999^{I} and 1999^{II}, 2003^{II}, 2007^{II}	Ph
Land Cover Map of Catalonia	Regional (Catalonia)	HI	21^{III}, 61^{IV}, 241^{V} classes	$1:3000^{III}$, $1:1500^{IV}$, $1:1000^{V}$,	1993^{III}, $2000–2002^{IV}$, $2005–2007^{V}$, 2009^{V}	Ph

Database (DB) models are Hierarchical (HI) or Object-Oriented (OO). SIOSE thematic resolution "s.c" and "p.c.c" stands for "simple coverages" and "predefined compound coverages". The main methodology used is based on Automatic Classification (AC) or Photo interpretation (Ph). Superindices refer to the version of each thematic, scale or temporal resolution.

Table S2. Details of the imagery considered for each LCM.

Classification	200-030	200-031	Platform-Sensor
LCM-1987	30 April 1987	14 April 1987	L5-TM
	17 June 1987	17 June 1987	L5-TM
	4 August 1987	4 August 1987	L5-TM
	20 August 1987	20 August 1987	L5-TM
	2 September 1986	2 September 1986	L5-TM
LCM-2002	28 April 2001	28 April 2001	L7-ETM+
	30 May 2001	30 May 2001	L7-ETM+
	1 July 2001 & 5 July 2000	1 July 2001	L7-ETM+
	25 July 2001	25 July 2001	L5-TM
	17 September 2003	11 September 2001	L5-TM
LCM-2012	7 March 2014	7 March 2014	L8-OLI
	19 June 2011	19 June 2011	L5-TM
	5 July 2011	5 July 2011	L5-TM
	11 August 2013	11 August 2013	L8-OLI
	7 September 2011	7 September 2011	L5-TM
LCM-2017	15 March 2017	15 March 2017	L8-OLI
	19 April 2018	19 April 2018	L8-OLI
	19 June 2017	19 June 2017	L8-OLI
	5 July 2017	5 July 2017	L8-OLI
	3 August 2016	3 August 2016	L8-OLI
	22 August 2017	22 August 2017	L8-OLI
	7 September 2017	7 September 2017	L8-OLI
Classification	**200-032**	**200-033**	**Platform-Sensor**
LCM-2002	8 March 2000	8 March 2000	L7-ETM+
	12 April 2001	12 April 2001	L7-ETM+
	30 May 2001	30 May 2001	L7-ETM+
	28 June 2000	28 June 2000	L7-ETM+
	17 July 2001	17 July 2001	L7-ETM+
	15 August 2000	15 August 2000	L7-ETM+
	24 September 2000	24 September 2000	L5-TM

The pair of images corresponding to each WRS-2 scene (200-030 and 200-031) was mosaicked to obtain a unified classification ambit. The mosaic of images with the same path-row, but different dates, is indicated with the '&' symbol. L5-TM: Landsat 5 satellite and Thematic Mapper instrument; L7-ETM: Landsat 7 satellite and Enhanced Thematic Mapper Plus instrument; L8-OLI: Landsat 8 satellite and Operational Land Imager instrument. The same procedure was extended to the scenes 200-032 and 200-033.

Table S3. Examples of SQL queries for polygon extraction of forest categories.

Category	SQL statement
CNF	("CNFpl" >= 70 OR "CNF" >= 70 OR "SIOSE_CODE"='CNF') AND ("SIOSE_CODE" NOT LIKE '%FDP%' AND "SIOSE_CODE" NOT LIKE '%FDC%' AND "SIOSE_CODE" NOT LIKE '%ALG%' AND "SIOSE_CODE" NOT LIKE '%LAA%' AND "SIOSE_CODE" NOT LIKE '%LOL%' AND "SIOSE_CODE" NOT LIKE '%LFN%' AND "SIOSE_CODE" NOT LIKE '%CHL%' AND "SIOSE_CODE" NOT LIKE '%LFC%' AND "SIOSE_CODE" NOT LIKE '%LVI%' AND "SIOSE_CODE" NOT LIKE '%LOC%' AND "SIOSE_CODE" NOT LIKE '%CHA%')
FDC	("FDCpl" >= 70 OR "FDCfr" >= 70 OR "FDC" >= 70 OR "SIOSE_CODE"='FDC') AND ("CNF" <= 5 AND "CNFpl" <= 5 AND "FDP" <= 5) AND ("SIOSE_CODE" NOT LIKE '%ALG%' AND "SIOSE_CODE" NOT LIKE '%LAA%' AND "SIOSE_CODE" NOT LIKE '%LOL%' AND "SIOSE_CODE" NOT LIKE '%LFN%' AND "SIOSE_CODE" NOT LIKE '%CHL%' AND "SIOSE_CODE" NOT LIKE '%LFC%' AND "SIOSE_CODE" NOT LIKE '%LVI%' AND "SIOSE_CODE" NOT LIKE '%LOC%' AND "SIOSE_CODE" NOT LIKE '%CHA%')
FDP	("FDP" >= 65 OR "SIOSE_CODE"='FDP') AND ("CNF" < 10 AND "CNFpl" < 10 AND "FDC" < 10) AND ("SIOSE_CODE" NOT LIKE '%ALG%' AND "SIOSE_CODE" NOT LIKE '%LAA%' AND "SIOSE_CODE" NOT LIKE '%LOL%' AND "SIOSE_CODE" NOT LIKE '%LFN%' AND "SIOSE_CODE" NOT LIKE '%CHL%' AND "SIOSE_CODE" NOT LIKE '%LFC%' AND "SIOSE_CODE" NOT LIKE '%LVI%' AND "SIOSE_CODE" NOT LIKE '%LOC%' AND "SIOSE_CODE" NOT LIKE '%CHA%')

SQL statements were generated to extract candidate pixels from the SIOSE 2005 and 2011 datasets. Queries were formulated to identify preferentially pure and high cover fraction polygons. The examples show SQL statements applied to forest categories. The first line defines the minimum cover fraction of the category of interest, followed by a set of limiting or excluding predicates that restrict categories not compatible with the main one. Full category labels can be found in Tables S5-12 and in Section 3.3 of the manuscript.

Table S4. Parametrisation of rule statements defined for each category and geographical context.

Category	Rule 1	Rule 2	Rule 3	Rule 4	Rule 5
CoF	$NDVI_{max} \geq (MED_{max} - 1SDV_{max})$	0.40,0.90	--	0.15, 0.30	--
BDF	$NDVI_{max} \geq (MED_{max} - 1SDV_{max})$	0.50,0.90	--	0.10, 1.00	$(NDVI_{max\ Spring}) < (NDVI_{max\ Summer})$
BEF	$NDVI_{max} \geq (MED_{max} - 1SDV_{max})$	0.40,0.90	--	-0.15, 0.05	--
Shl	$NDVI_{max} \geq (MED_{max} - 1SDV_{max})$	0.15,0.65	--	-0.10,0.10	--
Grl[1]	$NDVI_{max} \geq (MED_{max} - 1SDV_{max})$	0.10,0.60	--	-0.10,0.60	$(NDVI_{max\ Spring}) > (NDVI_{max\ Summer})$
BrS	$NDVI_{max} \leq (MED_{max} + 1SDV_{max})$	-0.05,0.05	--	-0.10,0.05	--
WaB	--	-1.00,0.15	--	0.10,2.00	--
Urb	--	-0.15,0.15	--	0.05,0.15	--
IHC	--	0.05,0.90	1.00,4.50	0.20,1.00	--
DHC	--	0.05,0.90	0.30,4.50	-1.00,-0.05	$(NDVI_{max\ Spring}) > (NDVI_{max\ Summer})$
IWC[3]	--	0.15,0.90	0.75,4.50	0.15,1.00	$(NDVI_{max\ Spring}) < (NDVI_{max\ Summer})$
DWC[4]	--	0.10,0.60	1.00,4.50	0.10,0.10	--
RiC	--	-0.70,0.90	1.50,4.50	0.40,1.00	$(NDVI_{max\ Spring} < 0.05)$ AND $(NDVI_{max\ Summer} > 0.60)$

Rule 1 is the Maximum NDVI temporal response; **Rule 2** is the NDVI range along 'n' dates; **Rule 3** is the Photosynthetic activity for 'n' dates; **Rule 4** is the Contrast between the NDVImax values of the group of dates; **Rule 5** controls Phenological moments. Grl[1] refers to low altitude grasslands; IWC[3] refers to irrigated vineyard woody crops; DWC[4] denotes dry olive groves. Filtering rules are applied to the category candidate pixels derived from purer and high cover fraction SIOSE polygons. Full category labels can be found in Tables S5-12 and in Section 3.3 of the manuscript.

LCM-1987 imagery and SIOSE 2005 as rDS (scenes 200-030–200-031).

Table S5. Confusion matrix **without** the application of filtering rules. SIOSE 2005 rDS ground truth samples and LCM-1987 imagery.

Classified map	Ground truth samples													Total	CE (%)	UA (%)
	CoF	BDF	BEF	Shl	Grl	BrS	Urb	WaB	IHC	DHC	IWC	DWC	RiC			
(CoF) Coniferous forest	**65 624**	2 388	4 232	4 071	3 883	163	52	54	23	166	0	139	0	80 797	18.8	81.2
(BDF) Broadleaf deciduous forest	1 914	**39 012**	494	568	7 263	10	3	10	17	191	0	0	0	49 482	21.2	78.8
(BEF) Broadleaf evergreen forest	11 401	5 841	**72 633**	3 044	3 974	107	6	86	18	306	0	127	0	97 544	25.5	74.5
(Shl) Shrublands	2 619	565	2 046	**47 325**	4 650	394	33	29	29	820	35	1 140	0	59 685	20.7	79.3
(Grl) Grasslands	1 237	1 212	925	12 021	**79 822**	1 091	37	44	340	6 720	215	684	0	104 349	23.5	76.5
(BrS) Bare soils	22	6	4	656	1 350	**3 613**	32	3	26	314	0	25	0	6 051	40.3	59.7
(Urb) Urban areas and Infrastructures	1	0	0	35	21	30	**898**	3	12	41	7	13	0	1 061	15.3	84.7
(WaB) Water bodies	0	16	7	5	0	0	1	**1 660**	0	16	0	13	0	1 716	3.3	96.7
(IHC) Irrigated herbaceous crops	120	592	11	173	1 312	53	165	29	**31 467**	3 950	2 162	1 190	0	41 224	23.7	76.3
(DHC) Dry herbaceous crops	223	35	96	1 149	2 176	343	183	108	6 652	**162 202**	2 030	5 965	1 544	182 705	11.2	88.8
(IWC) Irrigated woody crops	127	282	15	349	612	71	117	19	3 547	4 958	**15 196**	3 900	1 544	30 738	50.6	49.4
(DWC) Dry woody crops	619	36	258	4 687	1 784	260	447	67	2 844	13 826	4 573	**74 867**	0	104 269	28.2	71.8
(RiC) Rice crops	33	11	0	173	178	61	69	9	959	406	187	215	**1 544**	3 845	59.8	40.2
NoData	1 129	2 047	276	345	1 238	381	0	0	0	19	0	0	0	5 436		
Total	85 070	52 044	80 997	74 600	108 265	6 575	2 043	2 122	45 934	193 935	24 405	88 278	4 632	768 901	OA = 77.5%	
OE (%)	22.9	25.0	10.3	36.6	26.3	45.1	56.0	21.8	31.5	16.4	37.7	15.2	66.7		OAw = 92.3%	
PA (%)	77.1	75.0	89.7	63.4	73.7	54.9	44.0	78.2	68.5	83.6	62.3	84.8	33.3		k = 0.7	

OE: omission error, CE: commission error, PA: producer's accuracy, UA: user's accuracy, *k*: kappa index of agreement, OA: overall accuracy, OAw: overall accuracy weighted by the ground truth area considering only classified pixels (unclassified pixels are not considered errors and are solved by spatial proximity).

LCM-1987 imagery and SIOSE 2005 as rDS (scenes 200-030–200-031).

Table S6. Confusion matrix **with** the application of filtering rules. SIOSE 2005 rDS ground truth samples and LCM-1987 imagery.

Classified map	Ground truth samples												Total	CE (%)	UA (%)
	CoF	BDF	BEF	Shl	Grl	BrS	Urb	WaB	IHC	DHC	IWC	DWC			
(CoF) Coniferous forest	**41 259**	559	933	994	1 419	0	0	0	3	12	5	0	45 183	8.7	91.3
(BDF) Broadleaf deciduous forest	739	**80 022**	485	81	891	0	0	0	99	0	2	0	82 321	2.8	97.2
(BEF) Broadleaf evergreen forest	5 295	1 355	**46 933**	1 568	671	0	0	0	1	43	20	0	55 886	16.0	84.0
(Shl) Shrublands	1 989	338	1 437	**116 342**	6 105	123	9	0	17	784	322	855	128 322	9.3	90.7
(Grl) Grasslands	302	469	24	2 805	**77 660**	83	19	0	34	5 104	30	900	87 428	11.2	88.8
(BrS) Bare soils	0	0	0	56	72	**13 486**	157	0	0	1 366	0	222	15 359	12.2	87.8
(Urb) Urban areas and Infrastructures	0	0	0	3	1	90	**2 047**	0	0	132	0	267	2 541	19.4	80.6
(WaB) Water bodies	0	0	0	0	0	0	0	**1 543**	0	0	0	0	1 543	0.0	100.0
(IHC) Irrigated herbaceous crops	1	154	1	4	137	0	0	0	**27 995**	238	1 387	0	29 916	6.4	93.6
(DHC) Dry herbaceous crops	0	0	0	57	1 076	422	43	0	40	**193 282**	15	1 093	196 029	1.4	98.6
(IWC) Irrigated woody crops	10	308	5	307	279	2	6	0	2 019	457	**22 638**	127	26 159	13.5	86.5
(DWC) Dry woody crops	0	0	0	747	850	668	3	0	0	5 904	27	**68 454**	76 653	10.7	89.3
NoData	0	0	0	0	0	0	0	0	0	0	0	0	0		
Total	49 595	83 205	49 818	122 964	89 161	14 874	2 284	1 543	30 207	207 321	24 447	71 920	747 340	OA = 92.6%	
OE (%)	16.8	3.8	5.8	5.4	12.9	9.3	10.4	0.0	7.3	6.8	7.4	4.8		OAw = 95.9%	
PA (%)	83.2	96.2	94.2	94.6	87.1	90.7	89.6	100.0	92.7	93.2	92.6	95.2		k = 0.9	

OE: omission error, CE: commission error, PA: producer's accuracy, UA: user's accuracy, k: kappa index of agreement, OA: overall accuracy, OAw: overall accuracy weighted by the ground truth area considering only classified pixels (unclassified pixels are not considered errors and are solved by spatial proximity).

LCM-2002 imagery and SIOSE 2005 as rDS (scenes 200-030–200-031).

Table S7. Confusion matrix **without** the application of filtering rules. SIOSE 2005 rDS ground truth samples and LCM-2002 imagery.

Classified map	Ground truth samples													Total	CE (%)	UA (%)
	CoF	BDF	BEF	Shl	Grl	BrS	Urb	WaB	IHC	DHC	IWC	DWC	RiC			
(CoF) Coniferous forest	**50 907**	823	1 058	1 612	295	34	31	25	11	55	15	29	1	54 895	7.3	92.7
(BDF) Broadleaf deciduous forest	1 044	**67 728**	1 403	1 884	1 077	91	0	11	163	173	59	0	0	73 634	8.0	92.0
(BEF) Broadleaf evergreen forest	5 640	1 644	**60 658**	7 398	785	109	5	26	41	197	5	27	0	76 534	20.7	79.3
(Shl) Shrublands	3 715	1 587	3 007	**115 688**	9 356	938	160	105	301	2 450	180	2 154	7	139 649	17.2	82.8
(Grl) Grasslands	504	678	429	13 544	**86 142**	1 135	39	18	824	8 148	224	1 252	11	112 948	23.7	76.3
(BrS) Bare soils	64	54	52	488	1 214	**3 545**	78	0	58	625	23	67	0	6 268	43.4	56.6
(Urb) Urban areas and Infrastructures	1	3	0	66	53	57	**2 802**	7	48	300	57	112	1	3 507	20.1	79.9
(WaB) Water bodies	1	10	0	5	9	2	0	**1 488**	1	22	0	4	0	1 543	3.5	96.5
(IHC) Irrigated herbaceous crops	17	184	3	424	868	155	145	13	**37 114**	5 524	1 526	825	304	47 100	21.2	78.8
(DHC) Dry herbaceous crops	55	51	43	1 647	1 853	636	293	82	6 709	**175 596**	984	2 764	17	190 729	7.9	92.1
(IWC) Irrigated woody crops	26	146	12	274	231	101	226	12	2 154	921	**9 841**	4 011	27	17 982	45.3	54.7
(DWC) Dry woody crops	99	11	22	1 614	545	124	368	26	967	2 748	3 098	**29 232**	12	38 866	24.8	75.2
(RiC) Rice crops	5	11	0	20	12	1	6	4	667	34	10	2	**1 494**	2 267	34.1	65.9
NoData	31	120	51	84	111	149	0	0	0	0	0	0	0	547		
Total	62 110	73 049	66 739	144 748	102 552	7 077	4 153	1 817	49 057	196 793	16 021	40 479	1 875	766 469	OA = 83.8%	
OE (%)	18.0	7.3	9.1	20.1	16.0	49.9	32.5	18.1	24.3	10.8	38.6	27.8	20.3		OAw = 88.6%	
PA (%)	82.0	92.7	90.9	79.9	84.0	50.1	67.5	81.9	75.7	89.2	61.4	72.2	79.7		*k* = 0.7	

OE: omission error, CE: commission error, PA: producer's accuracy, UA: user's accuracy, *k*: kappa index of agreement, OA: overall accuracy, OAw: overall accuracy weighted by the ground truth area considering only classified pixels (unclassified pixels are not considered errors and are solved by spatial proximity).

LCM-2002 imagery and SIOSE 2005 as rDS (scenes 200-030–200-031).

Table S8. Confusion matrix with the application of filtering rules. SIOSE 2005 rDS ground truth samples and LCM-2002 imagery.

Classified map	Ground truth samples													Total	CE (%)	UA (%)
	CoF	BDF	BEF	Shl	Grl	BrS	Urb	WaB	IHC	DHC	IWC	DWC	RiC			
(CoF) Coniferous forest	**46 959**	226	525	311	222	0	0	0	3	4	4	0	0	48 254	2.7	97.3
(BDF) Broadleaf deciduous forest	388	**83 499**	330	55	906	0	0	0	94	0	33	0	0	85 306	2.1	97.9
(BEF) Broadleaf evergreen forest	4 891	934	**52 718**	3 278	300	0	0	0	7	17	13	0	0	62 157	15.2	84.8
(Shl) Shrublands	1 634	311	1 889	**115 291**	6 468	97	39	0	15	410	337	1 178	0	127 670	9.7	90.3
(Grl) Grasslands	48	342	18	4 281	**84 012**	32	13	0	66	3 616	14	1 481	0	93 924	10.6	89.4
(BrS) Bare soils	0	0	0	16	33	**10 379**	494	0	0	1 711	0	60	0	12 692	18.2	81.8
(Urb) Urban areas and Infrastructures	0	0	0	4	1	79	**5 678**	0	0	220	1	133	0	6 117	7.2	92.8
(WaB) Water bodies	0	0	0	0	0	0	0	**1 578**	0	0	0	0	0	1 578	0.0	100.0
(IHC) Irrigated herbaceous crops	2	84	0	15	134	0	0	0	**27 676**	181	507	0	5	28 603	3.2	96.8
(DHC) Dry herbaceous crops	0	0	0	57	624	874	759	0	23	**189 497**	13	1 344	0	193 191	1.9	98.1
(IWC) Irrigated woody crops	16	277	18	232	296	0	18	0	1 640	183	**25 474**	90	0	28 244	9.8	90.2
(DWC) Dry woody crops	1	0	0	1 422	1 208	333	0	0	9	5 266	96	**68 756**	0	77 090	10.8	89.2
(RiC) Rice crops	0	0	0	0	0	0	0	0	201	0	0	0	**958**	1 159	17.3	82.7
NoData	0	0	0	0	0	0	0	0	0	0	0	0	0	0		
Total	53 939	85 672	55 499	124 963	94 204	11 794	7 002	1 578	29 735	201 105	26 492	73 042	963	765 986	OA = 93.0%	
OE (%)	12.9	2.5	5.0	7.7	10.8	12.0	18.9	0.0	6.9	5.8	3.8	5.9	0.5		OAw = 95.9%	
PA (%)	87.1	97.5	95.0	92.3	89.2	88.0	81.1	100.0	93.1	94.2	96.2	94.1	99.5		k = 0.9	

OE: omission error, CE: commission error, PA: producer's accuracy, UA: user's accuracy, k: kappa index of agreement, OA: overall accuracy, OAw: overall accuracy weighted by the ground truth area considering only classified pixels (unclassified pixels are not considered errors and are solved by spatial proximity).

LCM-2017 imagery and SIOSE 2005 as rDS (scenes 200-030–200-031).

Table S9. Confusion matrix **without** the application of filtering rules. SIOSE 2005 rDS ground truth samples and LCM-2017 imagery.

Classified map	Ground truth samples													Total	CE (%)	UA (%)
	CoF	BDF	BEF	Shl	Grl	BrS	Urb	WaB	IHC	DHC	IWC	DWC	RiC			
(CoF) Coniferous forest	75 220	1 644	2 194	3 279	1 569	87	51	8	35	185	13	284	8	84 578	11.1	88.9
(BDF) Broadleaf deciduous forest	2 164	46 233	748	922	3 721	5	0	7	22	84	2	0	0	53 907	14.2	85.8
(BEF) Broadleaf evergreen forest	5 869	3 087	60 513	4 299	1 275	98	7	1	14	244	0	95	0	75 503	19.9	80.1
(Shl) Shrublands	2 531	836	2 444	40 383	5 566	316	38	5	44	565	36	1 129	8	53 900	25.1	74.9
(Grl) Grasslands	1 483	2 956	535	12 854	88 801	2 039	203	6	414	6 045	149	2 109	0	117 594	24.5	75.5
(BrS) Bare soils	26	11	5	585	920	3 494	149	1	138	541	76	71	0	6 018	41.9	58.1
(Urb) Urban areas and Infrastructures	5	0	0	41	43	114	3 665	8	112	206	22	103	0	4 320	15.2	84.8
(WaB) Water bodies	1	6	0	5	18	0	11	2 351	14	36	0	8	0	2 450	4.1	95.9
(IHC) Irrigated herbaceous crops	177	363	20	318	1 207	38	56	10	37 276	11 288	1 997	1 816	299	54 867	32.1	67.9
(DHC) Dry herbaceous crops	82	34	66	705	1 605	251	118	9	7 517	160 165	1 038	3 957	17	175 563	8.8	91.2
(IWC) Irrigated woody crops	216	691	34	343	1 373	33	94	9	3 692	2 252	15 878	6 381	91	31 087	48.9	51.1
(DWC) Dry woody crops	596	66	176	4 770	2 236	267	569	22	1 941	6 188	8 134	63 415	17	88 396	28.3	71.7
(RiC) Rice crops	11	40	1	9	62	0	2	14	1 450	472	51	79	2 843	5 034	43.5	56.5
NoData	3 196	2 653	375	508	2 094	420	67	34	0	94	0	16	0	9 457		
Total	91 578	58 619	67 113	69 021	110 491	7 162	5 031	2 483	52 669	188 367	27 395	79 463	3 284	762 674	OA = 78.7%	
OE (%)	17.9	21.1	9.8	41.5	19.6	51.2	27.1	5.3	29.2	15.0	42.0	20.2	13.4		OAw = 89.9%	
PA (%)	82.1	78.9	90.2	58.5	80.4	48.8	72.9	94.7	70.8	85.0	58.0	79.8	86.6		k = 0.7	

OE: omission error, CE: commission error, PA: producer's accuracy, UA: user's accuracy, OA: overall accuracy, OAw: overall accuracy weighted by the ground truth area considering only classified pixels (unclassified pixels are not considered errors and are solved by spatial proximity), k: kappa index of agreement.

LCM-2017 imagery and SIOSE 2005 as rDS (scenes 200-030–200-031).

Table S10. Confusion matrix **with** the application of filtering rules. SIOSE 2005 rDS ground truth samples and LCM-2017 imagery.

Classified map	Ground truth samples													Total	CE (%)	UA (%)
	CoF	BDF	BEF	Shl	Grl	BrS	Urb	WaB	IHC	DHC	IWC	DWC	RiC			
(CoF) Coniferous forest	**60 146**	365	642	793	250	0	0	0	33	17	82	0	0	62 328	3.5	96.5
(BDF) Broadleaf deciduous forest	981	**80 755**	174	21	1 372	0	0	0	125	0	49	0	0	83 476	3.3	96.7
(BEF) Broadleaf evergreen forest	4 329	311	**56 333**	3 482	481	0	0	0	6	75	27	0	0	65 044	13.4	86.6
(Shl) Shrublands	2 141	263	1 016	**140 197**	2 638	330	64	0	70	1 039	1 007	774	0	149 537	6.2	93.8
(Grl) Grasslands	360	976	78	3 304	**59 121**	10	22	0	129	2 273	309	657	0	67 239	12.1	87.9
(BrS) Bare soils	0	0	0	447	15	**13 443**	493	1	0	2 080	17	788	0	17 284	22.2	77.8
(Urb) Urban areas and Infrastructures	0	0	0	7	8	84	**6 790**	0	0	376	56	1 942	0	9 263	26.7	73.3
(WaB) Water bodies	0	0	0	0	0	0	0	**1 922**	0	0	0	0	0	1 922	0.0	100.0
(IHC) Irrigated herbaceous crops	9	177	0	104	246	0	0	0	**39 467**	555	1 570	0	11	42 139	6.3	93.7
(DHC) Dry herbaceous crops	0	0	1	178	636	159	45	0	160	**190 102**	214	1 285	0	192 780	1.4	98.6
(IWC) Irrigated woody crops	19	40	2	145	78	0	11	0	624	312	**20 168**	29	0	21 428	5.9	94.1
(DWC) Dry woody crops	1	0	0	431	246	315	3	0	2	3 417	202	**25 342**	0	29 959	15.4	84.6
(RiC) Rice crops	0	0	0	0	0	0	0	0	29	0	0	0	**138**	168	17.6	82.4
NoData	0	0	0	0	0	0	0	0	0	0	0	0	0	0		
Total	67 984	82 886	58 246	149 110	65 091	14 341	7 428	1 922	40 646	200 245	23 702	30 816	149	742 566	OA = 93.5%	
OE (%)	11.5	2.6	3.3	6.0	9.2	6.3	8.6	0.0	2.9	5.1	14.9	17.8	7.1		OAw = 96.0%	
PA (%)	88.5	97.4	96.7	94.0	90.8	93.7	91.4	100.0	97.1	94.9	85.1	82.2	92.9		k = 0.9	

OE: omission error, CE: commission error, PA: producer's accuracy, UA: user's accuracy, IA: producer's accuracy, UA: user's accuracy, OA: overall accuracy, OAw: overall accuracy weighted by the ground truth area considering only classified pixels (unclassified pixels are not considered errors and are solved by spatial proximity).

LCM-2012 imagery and SIOSE 2011 as rDS (scenes 200-030–200-031).

Table S11. Confusion matrix **without** the application of filtering rules. SIOSE 2011 rDS ground truth samples and LCM-2012 imagery.

Classified map	Ground truth samples													Total	CE (%)	UA (%)
	CoF	BDF	BEF	Shl	Grl	BrS	Urb	WaB	IHC	DHC	IWC	DWC	RiC			
(CoF) Coniferous forest	**74 750**	551	1 020	1 818	501	32	43	7	30	149	11	37	0	78 949	5.3	94.7
(BDF) Broadleaf deciduous forest	558	**105 845**	2 338	2 110	2 406	39	13	14	70	365	76	41	0	113 874	7.1	92.9
(BEF) Broadleaf evergreen forest	5 515	2 052	**78 566**	5 252	1 285	101	7	0	11	352	7	47	0	93 195	15.7	84.3
(Shl) Shrublands	3 482	1 316	2 349	**140 989**	13 887	2 166	445	16	653	3 633	253	2 188	5	171 383	17.7	82.3
(Grl) Grasslands	394	1 284	473	15 741	**123 122**	1 995	172	58	1 059	9 369	173	1 081	0	154 920	20.5	79.5
(BrS) Bare soils	25	17	18	1 227	810	**6 763**	180	21	43	747	13	139	0	10 004	32.4	67.6
(Urb) Urban areas and Infrastructures	4	0	0	61	54	265	**7 358**	12	137	255	8	54	2	8 211	10.4	89.6
(WaB) Water bodies	0	11	0	13	51	0	0	**3 661**	0	14	0	0	2	3 753	2.5	97.5
(IHC) Irrigated herbaceous crops	46	244	33	699	1 564	302	299	7	**57 684**	10 258	2 784	1 165	650	75 735	23.8	76.2
(DHC) Dry herbaceous crops	128	76	70	1 934	2 303	1 046	286	5	8 254	**220 416**	281	1 775	26	236 601	6.8	93.2
(IWC) Irrigated woody crops	7	216	20	194	445	41	119	0	2 092	686	**12 349**	4 495	39	20 703	40.4	59.6
(DWC) Dry woody crops	67	3	7	720	531	126	233	5	645	1 746	2 933	**20 975**	2	27 995	25.1	74.9
(RiC) Rice crops	0	21	7	11	12	9	0	7	500	47	63	3	**3 145**	3 827	17.8	82.2
NoData	0	0	0	0	0	0	0	0	0	0	0	0	0	0		
Total	84 977	111 636	84 903	170 772	146 972	12 884	9 156	3 811	71 179	248 036	18 952	32 001	3 872	999 150	OA = 85.6%	
OE (%)	12.0	5.2	7.5	17.4	16.2	47.5	19.6	3.9	19.0	11.1	34.8	34.5	18.8		OAw = 94.2%	
PA (%)	88.0	94.8	92.5	82.6	83.8	52.5	80.4	96.1	81.0	88.9	65.2	65.5	81.2		_k_ = 0.8	

OE: omission error, CE: commission error, PA: producer's accuracy, UA: user's accuracy, OA: overall accuracy, OAw: overall accuracy weighted by the ground truth area considering only classified pixels (unclassified pixels are not considered errors and are solved by spatial proximity). _k_: kappa index of agreement.

LCM-2012 imagery and SIOSE 2011 as rDS (scenes 200-030–200-031).

Table S12. Confusion matrix with the application of filtering rules. SIOSE 2011 rDS ground truth samples and LCM-2012 imagery.

Classified map	Ground truth samples													Total	CE (%)	UA (%)
	CoF	BDF	BEF	Shl	Grl	BrS	Urb	WaB	IHC	DHC	IWC	DWC	RiC			
(CoF) Coniferous forest	**61 433**	244	520	412	142	0	0	0	11	1	2	0	0	62 765	2.1	97.9
(BDF) Broadleaf deciduous forest	100	**81 034**	39	83	836	0	0	0	50	1	24	0	0	82 168	1.4	98.6
(BEF) Broadleaf evergreen forest	4 720	503	**56 536**	3 014	505	0	0	0	5	36	9	0	0	65 327	13.5	86.5
(Shl) Shrublands	1 838	544	1 336	**142 670**	2 259	315	67	0	91	1 262	1 010	257	0	151 651	5.9	94.1
(Grl) Grasslands	130	723	19	2 132	**60 686**	41	8	0	42	2 360	63	299	0	66 505	8.8	91.2
(BrS) Bare soils	0	0	0	483	30	**12 399**	615	0	0	1 508	0	173	0	15 209	18.5	81.5
(Urb) Urban areas and Infrastructures	0	0	0	2	0	169	**6 540**	3	0	224	0	19	0	6 957	6.0	94.0
(WaB) Water bodies	0	0	0	0	0	0	0	**1 925**	0	0	0	0	0	1 925	0.0	100.0
(IHC) Irrigated herbaceous crops	1	112	0	76	114	0	0	0	**39 728**	155	1 577	0	7	41 772	4.9	95.1
(DHC) Dry herbaceous crops	0	0	0	160	446	907	215	1	128	**190 777**	53	0	0	193 313	1.3	98.7
(IWC) Irrigated woody crops	5	24	5	200	63	0	8	0	732	390	**20 892**	33	0	22 352	6.5	93.5
(DWC) Dry woody crops	0	0	0	412	242	562	0	0	2	4 247	156	**29 519**	0	35 141	16.0	84.0
(RiC) Rice crops	0	0	0	0	0	0	0	0	2	0	0	0	**142**	144	1.6	98.4
NoData	0	0	0	0	0	0	0	0	0	0	0	0	0	0		
Total	68 228	83 183	58 455	149 645	65 324	14 392	7 455	1 929	40 792	200 963	23 787	30 927	149	745 229	OA = 94.2%	
OE (%)	10.0	2.6	3.3	4.7	7.1	13.9	12.3	0.2	2.6	5.1	12.2	4.6	5.0		OAw = 96.7%	
PA (%)	90.0	97.4	96.7	95.3	92.9	86.1	87.7	99.8	97.4	94.9	87.8	95.4	95.0		*k* = 0.9	

OE: omission error, CE: commission error, PA: producer's accuracy, UA: user's accuracy, *k*: kappa index of agreement, OA: overall accuracy, OAw: overall accuracy weighted by the ground truth area considering only classified pixels (unclassified pixels are not considered errors and are solved by spatial proximity).

LCM-2002 imagery and SIOSE 2005 as rDS (scenes 200-032–200-033).

Table S13. Confusion matrix **without** the application of filtering rules. SIOSE 2005 rDS ground truth samples and LCM-2002 imagery.

Classified map	Ground truth samples												Total	CE (%)	UA (%)
	CoF	BDF	BEF	Shl	Grl	BrS	Urb	WaB	IHC	DHC	IWC	DWC			
(CoF) Coniferous forest	**139 100**	1 129	14 789	2 731	4 159	593	17	382	71	442	15	575	164 002	15.2	84.8
(BDF) Broadleaf deciduous forest	568	**15 453**	3 486	373	876	17	0	2	34	68	10	11	20 897	26.1	73.9
(BEF) Broadleaf evergreen forest	14 228	2 411	**179 708**	7 410	12 771	273	8	2	40	317	58	2 818	220 046	18.3	81.7
(Shl) Shrublands	1 454	128	2 820	**21 941**	5 561	171	6	2	2	153	62	504	32 804	33.1	66.9
(Grl) Grasslands	2 461	420	8 327	9 404	**200 089**	2 142	123	16	215	13 651	181	3 690	240 720	16.9	83.1
(BrS) Bare soils	57	8	87	253	1 719	**6 163**	71	4	23	1 504	23	705	10 615	41.9	58.1
(Urb) Urban areas and Infrastructures	26	0	5	3	121	154	**1 703**	0	1	163	21	253	2 448	30.5	69.5
(WaB) Water bodies	0	0	0	0	121	0	0	**2 640**	2	59	0	0	2 821	6.4	93.6
(IHC) Irrigated herbaceous crops	7	51	14	21	363	17	14	0	**27 246**	6 410	94	183	34 420	20.8	79.2
(DHC) Dry herbaceous crops	312	13	160	168	6 619	1 455	102	6	3 934	**392 302**	764	3 473	409 306	4.2	95.8
(IWC) Irrigated woody crops	127	13	87	67	484	107	179	2	348	1 412	**12 498**	16 234	31 558	60.4	39.6
(DWC) Dry woody crops	1 438	233	2 583	767	3 456	994	955	2	1 123	16 958	7 175	**193 142**	228 827	15.6	84.4
NoData	1 044	10	192	80	140	55	0	0	0	0	0	13	1 534		
Total	160 823	19 867	212 256	43 217	236 479	12 142	3 177	3 058	33 040	433 439	20 901	221 601	1 400 000	OA = 85.1%	
OE (%)	13.5	22.2	15.3	49.2	15.4	49.2	46.4	13.7	17.5	9.5	40.2	12.8		OAw = 93.3%	
PA (%)	86.5	77.8	84.7	50.8	84.6	50.8	53.6	86.3	82.5	90.5	59.8	87.2		k = 0.7	
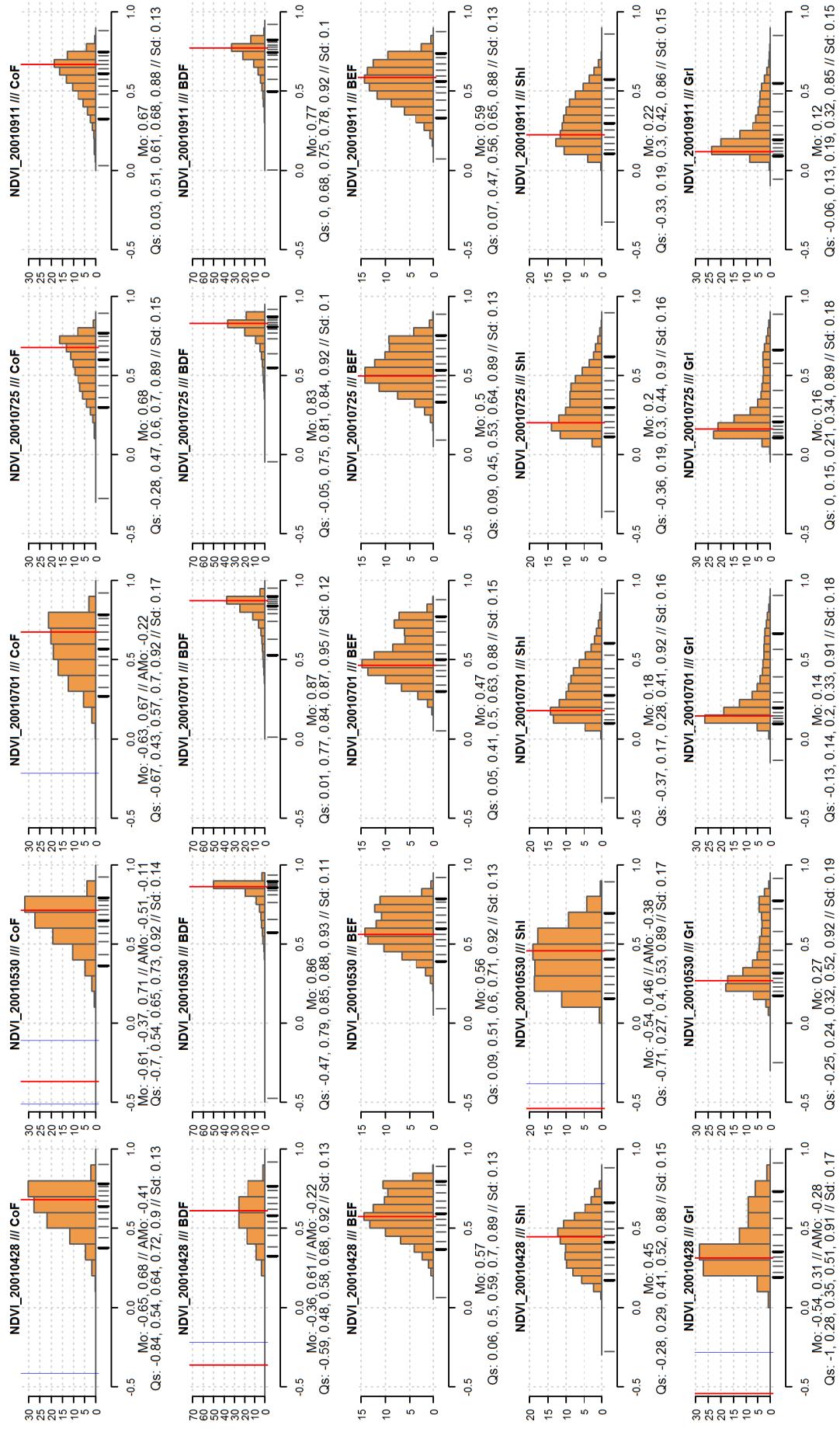
OE: omission error, CE: commission error, PA: producer's accuracy, UA: user's accuracy, k: kappa index of agreement, OA: overall accuracy, OAw: overall accuracy weighted by the ground truth area considering only classified pixels (unclassified pixels are not considered errors and are solved by spatial proximity).
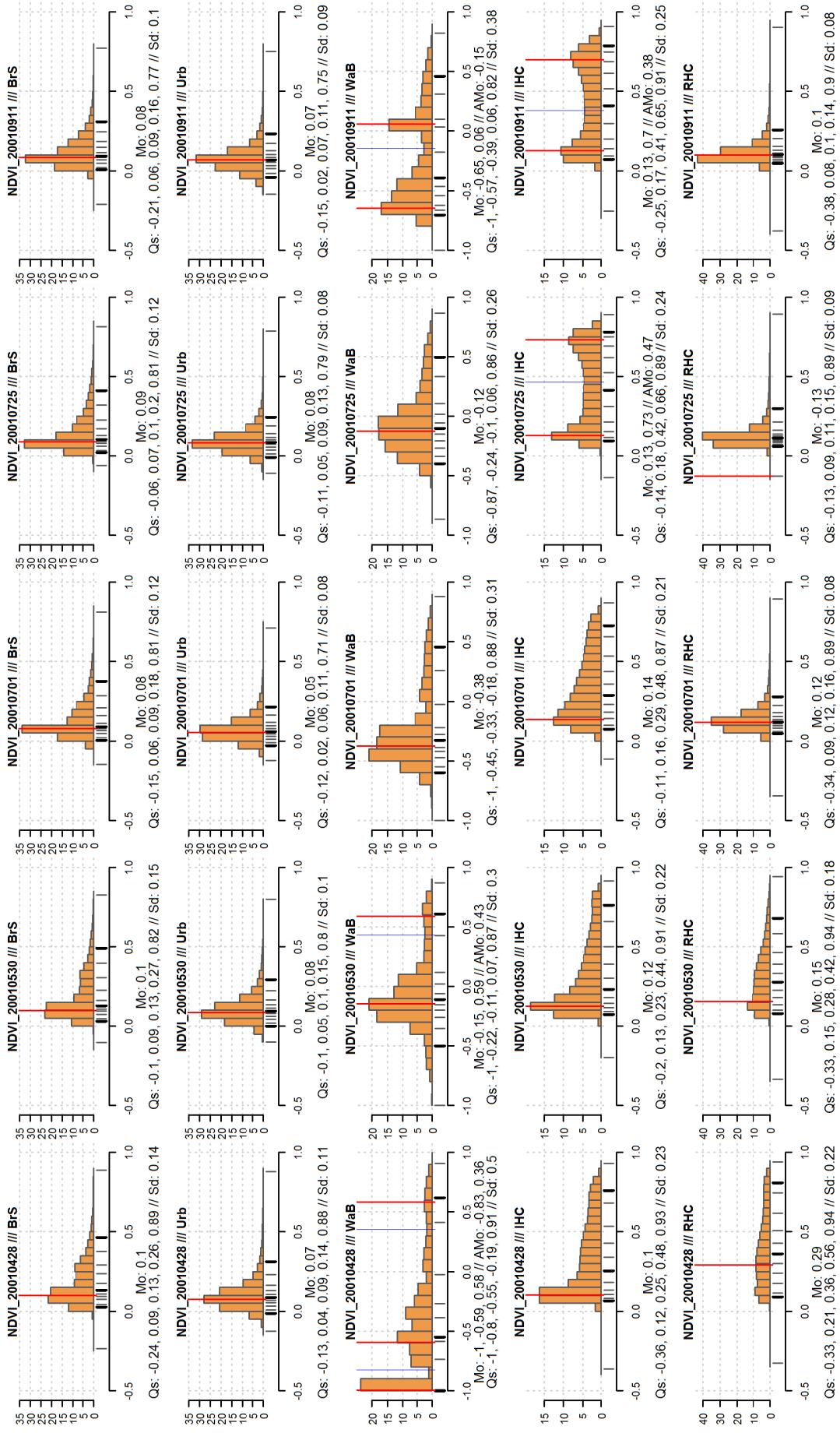
LCM-2002 imagery and SIOSE 2005 as rSD (scenes 200-032-200-033).

Table S14. Confusion matrix **with** the application of filtering rules. SIOSE 2005 rDS ground truth samples and LCM-2002 imagery.

Classified map	Ground truth samples												Total	CE (%)	UA (%)
	CoF	BDF	BEF	Shl	Grl	BrS	Urb	WaB	IHC	DHC	IWC	DWC			
(CoF) Coniferous forest	**121 586**	239	6 133	893	581	0	0	0	0	2	46	0	129 480	6.1	93.9
(BDF) Broadleaf deciduous forest	308	**16 620**	2 253	190	225	0	0	0	24	0	0	0	19 619	15.3	84.7
(BEF) Broadleaf evergreen forest	8 481	920	**177 990**	7 293	5 483	0	0	0	6	75	1 048	0	201 295	11.6	88.4
(Shl) Shrublands	757	30	1 622	**41 975**	5 342	159	4	0	0	33	433	58	50 414	16.7	83.3
(Grl) Grasslands	140	11	1 663	9 199	**217 645**	1 299	20	0	6	9 604	99	1 619	241 305	9.8	90.2
(BrS) Bare soils	0	0	0	190	2 615	**22 713**	115	0	0	1 917	0	810	28 361	19.9	80.1
(Urb) Urban areas and Infrastructures	0	0	0	0	0	169	**1 958**	0	0	71	0	86	2 283	14.2	85.8
(WaB) Water bodies	0	0	0	0	0	0	0	**3 680**	0	0	0	0	3 680	0.0	100.0
(IHC) Irrigated herbaceous crops	0	21	0	8	89	0	0	0	**23 975**	121	69	0	24 282	1.3	98.7
(DHC) Dry herbaceous crops	0	0	0	22	3 763	1 041	26	0	14	**422 871**	0	2 083	429 819	1.6	98.4
(IWC) Irrigated woody crops	78	9	918	491	380	0	18	0	123	292	**65 878**	10	68 195	3.4	96.6
(DWC) Dry woody crops	0	0	0	201	1 809	2 826	1 026	0	4	19 427	46	**175 928**	201 267	12.6	87.4
NoData	0	0	0	0	0	0	0	0	0	0	0	0	0		
Total	131 349	17 850	190 580	60 461	237 932	28 206	3 166	3 680	24 152	454 412	67 618	180 594	1 400 000		OA = 92.3%
OE (%)	7.4	6.9	6.6	30.6	8.5	19.5	38.2	0.0	0.7	6.9	2.6	2.6			OAw = 96.4%
PA (%)	92.6	93.1	93.4	69.4	91.5	80.5	61.8	100.0	99.3	93.1	97.4	97.4			k = 0.9

OE: omission error, CE: commission error, PA: producer's accuracy, UA: user's accuracy, k: kappa index of agreement, OA: overall accuracy, OAw: overall accuracy weighted by the ground truth area considering only classified pixels (unclassified pixels are not considered errors and are solved by spatial proximity).
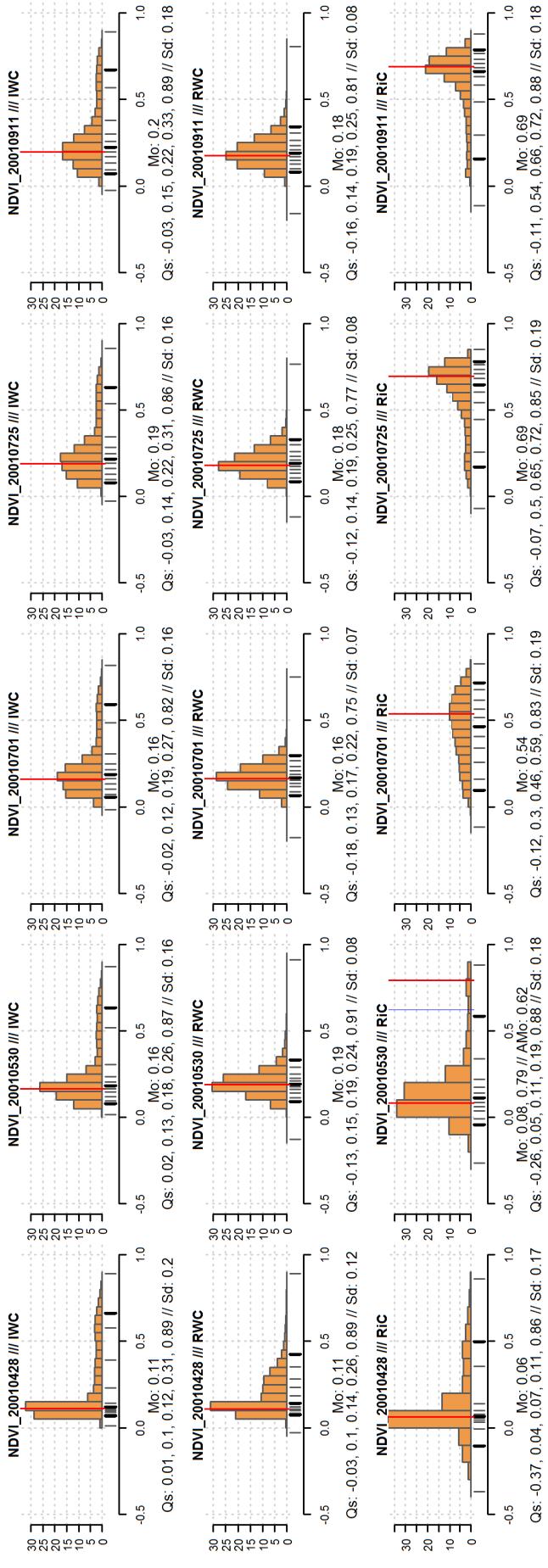
Figure S1. The temporal relative frequency distribution of the NDVI evaluated for each category. Percentage values are shown on the vertical axis, while the NDVI value range is shown on the horizontal axis. The red and blue vertical lines define *modes* (Mo) and *antimodes* (AMo), respectively [92]. The "Qs" values represent 0, 25, 50, 75 and 100% quantiles; "Sd" is the standard deviation.

Figure S2. Classification results considering unfiltered and filtered GT samples from SIOSE 2005 (LCM-1987, LCM-2002 and 2017), and SIOSE 2011 (LCM-2012).

MODELIZACIÓN DE LOS FACTORES DETERMINANTES DE LA EXPANSIÓN FORESTAL

4. MODELIZACIÓN DE LOS FACTORES DETERMINANTES DE LA EXPANSIÓN FORESTAL EN LA PENÍNSULA IBÉRICA

4.1. Artículo 3: Driving Forces of Forest Expansion Dynamics across the Iberian Peninsula (1987–2017): A Spatio-Temporal Transect.

Resumen: Este estudio analiza la dinámica espaciotemporal de los factores determinantes de la expansión forestal en la Península Ibérica para los períodos 1987-2002-2017 a través de un transecto Norte-Sur de Landsat de 185 km de ancho. El análisis ha considerado una gran variedad de regiones biogeográficas [0–3500 m.s.n.m., precipitaciones anuales 150–2200 mm] y 30 variables explicativas. Una rigurosa producción cartográfica a una resolución de 30 m, que incluye métodos de filtrado detallados y la gestión de la incertidumbre a escala de píxel, proporcionó mapas de usos y cubiertas del suelo de alta calidad. Las principales trayectorias de expansión forestal se relacionaron con variables explicativas utilizando *Boosted Regression Trees*. La proximidad a áreas forestales preexistentes fue un factor común clave para la expansión forestal en todos los tipos fisionómicos de bosque, además de otros factores, como la distancia a la red hidrográfica, la temperatura y la precipitación para los bosques de frondosas caducifolias (BDF), la precipitación, la temperatura y la radiación solar para los bosques de frondosas perennifolias (BEF) y la precipitación, la distancia a las capitales de provincia y la radiación solar para los bosques de aciculifolias (NEF). Los resultados además mostraron un contraste en las trayectorias de expansión forestal y factores determinantes en las regiones biogeográficas, con un alto dinamismo de los pastizales hacia nuevos bosques en las regiones eurosiberiana y áreas montañosas mediterráneas, una mayor importancia de los cultivos como origen de nuevos bosques en el la región mesomediterránea, y una importancia creciente a lo largo del tiempo de los factores socioeconómicos (empleados en el sector industrial, superficie agrícola utilizada) en la región supramediterránea, mostrando un patrón opuesto en la región mesomediterránea sur. Por otro lado, tasas más bajas de precipitación favorecieron la expansión de NEF a partir de matorrales en la región termomediterránea que, junto con la mesomediterránea norte, mostraron las tasas relativas más altas de expansión forestal. Estos hallazgos proporcionan información fiable para desarrollar políticas que consideren los impactos ecológicos y sociales del abandono de la tierra y la posterior expansión forestal.

Palabras clave: nuevos bosques; fuerzas inductoras; abandono agrícola; *boosted regression trees*.

Driving Forces of Forest Expansion Dynamics across the Iberian Peninsula (1987–2017): A Spatio-Temporal Transect

Mario Padial-Iglesias [1],[*] , Miquel Ninyerola [2] , Pere Serra [1] , Òscar González-Guerrero [1] , Josep Maria Espelta [3],[4] , Joan Pino [3],[4] and Xavier Pons [1]

1   Grumets Research Group, Departament de Geografia, Edifici B. Universitat Autònoma de Barcelona, 08193 Bellaterra, Catalonia, Spain; pere.serra@uab.cat (P.S.); oscar.gonzalez.guerrero@uab.cat (Ò.G.-G.); xavier.pons@uab.cat (X.P.)

2   Grumets Research Group, Departament de Biologia Animal, Biologia Vegetal i Ecologia, Edifici C. Universitat Autònoma de Barcelona, 08193 Bellatera, Catalonia, Spain; miquel.ninyerola@uab.cat

3   Centre de Recerca Ecològica i Aplicacions Forestals (CREAF), 08193 Bellaterra, Catalonia, Spain; josep.espelta@uab.cat (J.M.E.); joan.pino@uab.cat (J.P.)

4   Departament de Biologia Animal, Biologia Vegetal i Ecologia, Edifici C. Universitat Autònoma de Barcelona, 08193 Bellaterra, Catalonia, Spain

*   Correspondence: mario.padial@uab.cat

Abstract: This study analyzes the spatio-temporal dynamics of the drivers of forest expansion in the Iberian Peninsula for the periods 1987–2002–2017 through a 185 km-wide north–south Landsat scene transect. The analysis has considered a variety of biogeographical regions [0–3500 m.a.s.l, annual rainfalls 150–2200 mm] and 30 explanatory variables. A rigorous map production at 30 m resolution, including detailed filtering methods and uncertainty management at pixel scale, provided high-quality land cover maps. The main forest expansion trajectories were related to explanatory variables using boosted regression trees. Proximity to previous forests was a key common factor for forest encroachment in all forest types, with other factors being distance to the hydrographic network, temperature and precipitation for broadleaf deciduous forests (BDF), precipitation, temperature and solar radiation for broadleaf evergreen forests (BEF) and precipitation, distance to province capitals, and solar radiation for needleleaf evergreen forests (NEF). Results also showed contrasting forest expansion trajectories and drivers per biogeographic region, with a high dynamism of grasslands towards new forest in the Eurosiberian and the mountainous Mediterranean regions, a high importance of croplands as land cover origin of new forest in the Mesomediterranean, and increasing importance over time of socioeconomic drivers (such as those employed in the industry sector and the utilized agricultural area) in the Supramediterranean region but the opposite pattern in the Southern Mesomediterranean. Lower precipitation rates favored new NEF from shrublands in the Thermomediterraean region which, together with the Northern Mesomediterranean, exhibited the highest relative rates of new forests. These findings provide reliable insights to develop policies considering the ecological and social impacts of land abandonment and subsequent forest expansion.

Keywords: new forests; driving forces; land abandonment; boosted regression trees

1. Introduction

In the last decades, evidence of decreasing the net forest loss has been manifested globally, even though deforestation continues to increase unequally distributed around the globe [1]. In the five-year period 2010–2015, the tropical forest area declined, temperate forest expanded, and little net change was observed in the boreal and sub-tropical forest. The forest area expanded in the European countries, East and Western-Central Asia, North America, and the Caribbean, and declined in Central and South America, South Asia, and Africa. In fact, Africa surpassed South America in the rate of forest loss during the last decade [1–3]. In Europe, the forest area even increased during the past century due

to policies favoring tree planting or the spontaneous forest establishment on croplands suffering the land abandonment syndrome [2,4–7]. Indeed, in recent decades, the collapse of many rural economies of Europe has triggered profound changes in the territory, causing significant land use and cover changes, especially in mountainous regions [8,9]. Furthermore, from rural to more urbanized areas, general population movements have occurred, concentrating inhabitants in some inner cities and coastal regions, provoking agriculture abandonment processes followed by forest succession, mainly in areas with more biophysical constraints [10–12].

The Iberian Peninsula (IP) is a representative area of diversity, ecological value, and vulnerability of the Eurosiberian and Mediterranean terrestrial ecosystems. Its complex relief (mean elevation around 614 m a.s.l. extracted from the ASTER Digital Elevation Model and large areas, i.e., 18,810 km^2, above 1 500 m a.s.l.) creates a heterogenous climatic mosaic, with the usual conditions found on the northern rim of the Mediterranean Basin, combined with elevation-driven climatic gradients in mountain ranges [13]. In this context, forest increase has been observed in recent decades [14,15], with the cropland abandonment as the primary land source [10,16–18]. Vidal-Macua et al. [19] found that 20% of shrublands became forest in the 1987–2012 period in three Landsat representative scenes. Recently, Gelabert et al. [20] estimated an overall area proportion of 66% affected by woody encroachment on former pastures and croplands in the Pyrenees. Despite indicating a progressive increase in forest cover over the past century, official data do not provide enough robust information to ascertain the spatial pattern of this increase and its links to other processes and to the potential drivers, although this situation is changing [19,21]. More detail about the spatial patterns of the driving forces associated with the main sources of new forests is fundamental for landscape management and planning. Nevertheless, this information is often limited by the availability of accurate land cover (LC) map series for large areas [22]. In this sense, a study considering remote-sensing of medium–high spatial resolution imagery, providing spatio-temporal completeness (30 recent years of land use and LC changes along a wide transect) and covering a vast part of the climatic variability of the IP, can help shed light on these issues.

In any case, forest increase simultaneously occurs in areas with strong and heterogeneous changes in climate. Minimum and maximum temperatures increased in Spain during the 1951–2010 period, and the warming rate was highly dependent on the area and the length of the period analyzed [23]. For example, the summer warming trend is specifically significant in the western peninsula from the mid-1920s to 1959 and from the mid-1970s onwards. In contrast, the CLIVAR [24] report suggests no significant decrease in rainfall, although other research found some different trends for some specific regions and periods [25,26]. Furthermore, research demonstrates an increase in solar radiation since the 1980s [27,28]. The extent of climate change compromising forest expansion in the IP, together with its spatio-temporal variability, is still unknown.

Research works have analyzed the LC changes following the abandonment of traditional activities, using various LC change information sources and explanatory variables. Some examples, including aerial photographs and topographic maps [29], cartographic resources (e.g., CORINE) [30–32], and remote-sensing classification techniques [4,20,33,34], have been widely used for the analysis of vegetation transitions. Furthermore, other strategies use satellite imagery time series to detect LC changes, extracting the spectral trajectories and evaluating their temporal segmentation [20,35] or the Continuous Change Detection and Classification (CCDC) algorithm, which uses all available Landsat dataset to dynamically detect LC changes over time [36,37].

Researchers have collected different explanatory variables or driving forces (e.g., topographic, climatic, distances and accessibility, or socioeconomic) for LC change modeling using statistical approaches or techniques to relate them. Some examples are generalized linear models (GLM) and their derivatives as (simple/multiple) logistic regression or the linear discriminant analysis [38–43]. Moving beyond linearity assumption, regression splines, or generalized additive models are examples of replacing standard linear mod-

els [38,44,45]. Other lines of techniques are the tree-based methods, which include decision trees and methods, such as bagging, random forests, and boosting, which can enhance the predictive performance of the models [30,33,36,46–49]. Furthermore, unsupervised learning methods provide information on the sample structure and subgroups among the predictors or the observations [50].

In this study, the terms "forest expansion" and "new forest" have been used interchangeably, considered as the expansion of forest on land, implying a transformation of land cover from non-forest to forest [1]. Boosted regression trees (BRTs), a non-linear machine learning method, were used to explore the complex relationship and interactions between new forest (NF) dynamics and explanatory variables. The origin of NF regarding their primary sources in LC dynamics will be analyzed, attending to determine the drivers involved and their spatio-temporal patterns along a north–south transect in the IP's Eurosiberian and Mediterranean context.

Three main hypotheses will be contrasted in this spatio-temporal research: (i) a latitudinal transect along the Iberian Peninsula may reveal the significant patterns in the origin and drivers of NF dynamics in this representative area between the Eurosiberian and the Mediterranean regions, and can serve as a scenario to illustrate the role of topography and climate in a context of climate change; (ii) forest expansion processes have been concentrated in rural areas with low accessibility and weak industrialization, where the abandonment of traditional agricultural and livestock activities has been historically more intense; and (iii) forest expansion dynamics may reveal different temporal patterns, principally associated with the socioeconomic historical conditionings and/or the different climatic conditionings (the impact of climate change).

In order to contrast the key hypotheses, our main objectives in this study will be focused on (1) the identification of the principal forest expansion trajectories from the main LC sources (crops and natural/seminatural categories) for the main forests types across the represented bioclimatic regions; (2) the main drivers involved in these transitions; and (3) the spatial and temporal patterns of these drivers along with the bioclimatic regions within the transect.

2. Materials and Methods

2.1. Study Area

The study area corresponds to a transect of around 185 km wide and 755 km long crossing north–south of the IP and covering 120,190 km^2 (Figure 1). The transect allows us to study an important bioclimatic gradient where both the Eurosiberian and the Mediterranean biogeographical regions are represented [51]. The south Mediterranean context is characterized by dry conditions where the higher mean annual temperature (19 °C) and the lowest annual rainfall (150 mm) occur, evolving into continental regimes towards the center of the IP. In contrast, more humid and mountainous climatic regimes characterize the North Eurosiberian region, where the lowest mean annual temperatures (2 °C) and the highest annual rainfall (over 2200 mm) are reached. Figure S5 in the Supplementary Materials provide details about the topoclimatic variation along the transect.

The landscape can be divided into two geomorphological scenarios: large depressions drained by the main Iberian rivers (i.e., Ebro, Douro, Tagus, Guadiana, Guadalquivir, and a set of smaller basins) and bounded by mountain ranges of the alpine geological domain (i.e., the Baetic System, the Iberian System, and the Pyrenees). The extensive valleys are covered by recent quaternary materials favorable for agriculture activity.

A high latitudinal gradient characterizes the study ambit regarding climate, topography, and socioeconomic characteristics. Therefore, we subdivided the study area into bioclimatic regions (BRs) (Figure S1) to analyze the NF in local climatic detail. The averaged mean temperature surfaces comprising the 1987–2017 period and the BRs formulation [51] were used to subdivide the transect according to its climatic characteristics. A general overview of BRs is detailed in Figure S4. As will be shown later in the 'results' section,

regions 1, 4, and 7 (in P1) will not be analyzed as the remaining forest surface was not representative for robust modeling (Figure S6a).

The Spanish National Forest Inventory (NFI 2, 1986–1995 and NFI 3, 1997–2007) was used to identify the predominant forest species in each BR to better understand the forest composition in each region, which is detailed in Table 1. Thus, the broadleaf evergreen forests (BEF) and needleleaf evergreen forests (NEF) were predominant and widely distributed along the transect, while broadleaf deciduous forests (BDF) dominate in the humid Northern Eurosiberian context.
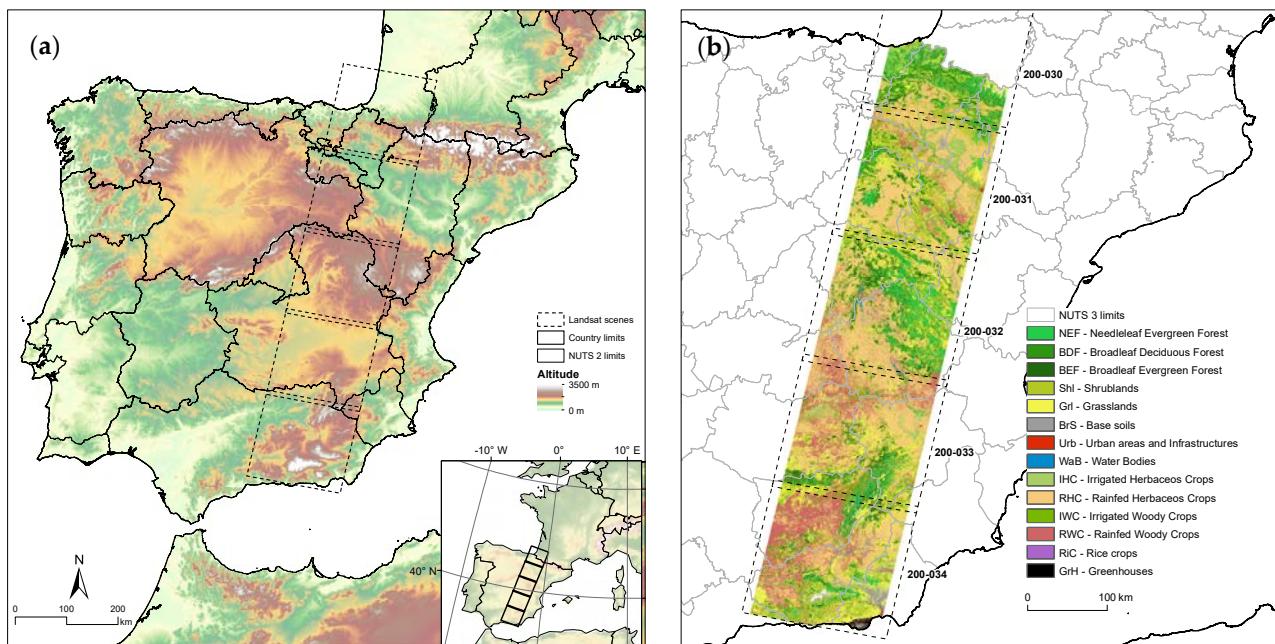
Figure 1. The transect along the Iberian Peninsula used in this study is shown in (**a**) and the land cover map (LCM) of 1987 in (**b**).

Table 1. Main forest species in BRs surveyed in the transect. BR numbers are related to other figures in the text.

Biogeographical Region		Bioclimatic Region (BR)	Main Forest Species [1]
Eurosiberian	(1)	Alpine	-
		Subalpine	*Pinus uncinata, P. sylvestris* (NEF)
	(2)	Montane	*Fagus sylvatica* (BDF), *P. sylvestris* (NEF), *Quercus pubescens* (BDF), *P. nigra* (NEF), *Q. pyrenaica* (BDF), *Q. petraea* (BDF).
	(3)	Coline	*P. radiata* (NEF), *Q. robur* (BDF), *F. sylvatica* (BDF), *Q. rubra* (BDF), *Castanea sativa* (BDF).
Mediterranean	(4)	Cryoromediterranean	-
		Oromediterranean	*P. uncinata, P. sylvestris* (NEF)
	(5)	Supramediterranean	*Q. ilex* (BEF), *P. nigra, P. sylvestris, P. pinaster* (NEF) *Q. pyrenaica* (BDF), *Q. faginea* (BDF), *Juniperus thurifera* (NEF), *P. halepensis* (NEF).
	(6,8)	Mesomediterranean	*Q. ilex* (BEF); *P. halepensis, P. pinaster, P. pinea, P. nigra* (NEF).
	(7)	Thermomediterranean	*P. halepensis* (NEF); *Q. ilex* and *Olea europea* (BEF).

[1] The list of species is shorted by dominance in each BR and considering the NFI 3 dataset.

2.2. Methodological Framework

The methodological framework followed in this study is shown in Figure 2, and it is divided into three main stages developed in the following subsections.
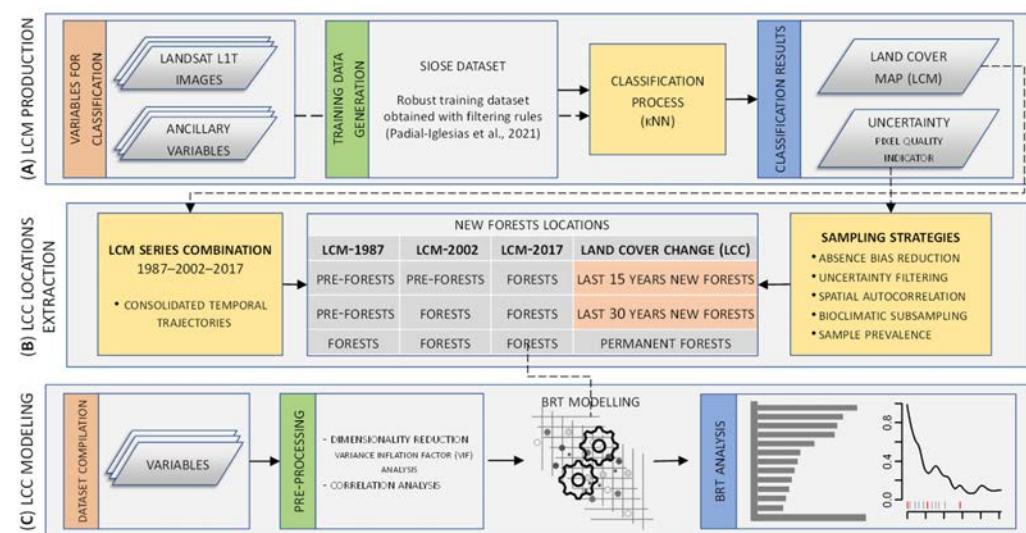
Figure 2. Methodological workflow. LCM processing (**A**) provided three temporal thematic maps and their associated uncertainty layers. In (**B**), locations of forest expansion from crops, shrublands, and grasslands (PRE-FORESTS) were extracted considering sampling strategies. Boosted regression trees (BRTs) were used to analyze the drivers involved (**C**) in NF occurrence.

2.2.1. Land Cover Map Production

Three LCMs were produced by remote sensing digital classification from 1987 and every 15 years (LCM-1987, LCM-2002, and LCM-2017). LCM have a spatial resolution of 30 m, according to the Landsat imagery series, courtesy of the U.S. Geological Survey (USGS); images were acquired through the website portal (https://earthexplorer.usgs.gov/ (accessed on 16 August 2021)) [52]. The k-nearest neighbor (kNN) classifier was implemented and parallelized in MiraMon GIS and remote sensing software [53]. The classification process followed the methodology detailed in [54–56]. In Padial-Iglesias et al. [54], the authors generated accurate ground truth areas using the SIOSE database and filtering rules based on the inner imagery NDVI data to correct inconsistencies in the initial samples by considering inter-annual and intra-annual differences, scale issues, multiple behaviors over time, and labelling misassignments. Furthermore, the authors considered phenologically representative imagery, image preprocessing lines, and auxiliary variables estimation for the classification process. These strategies were crucial for high-quality LCM series achievement, improving the temporal consistency required for LC change analysis.

The MiraMon kNN classifier provides complementary outputs associated with each classified map (e.g., the uncertainty of classified pixels). The uncertainty metric measures the degree to which no class clearly stands out above the others in the assessment of class membership of a pixel. In other words, it expresses complement to one of the degree of commitment to the targeted class relative to the largest possible commitment that can be made. Values range between 0 and 1, where 0 denotes the lowest level of uncertainty and, hence, the most likely accurate thematic pixel assignation. It was used as a filtering strategy to exclude pixels overcoming a level of uncertainty. Its formulation is defined as:

$$\text{Uncertainty} = 1 - (\text{MAX}_{\text{membership}} - \text{SUM}_{\text{membership}}/N)/(1 - 1/N), \tag{1}$$

where the 'MAX$_{\text{membership}}$' argument denotes the maximum set membership value for the pixel, the 'SUM$_{\text{membership}}$' is the total sum of the set membership values for the pixel, and 'N' is the total number of the classes considered.

2.2.2. New Forests' Occurrence Extraction, Sampling on Each BR, and Filtering

In order to model NF locations, explicitly consolidated temporal trajectories were considered. Once a category becomes a forest, it has to remain in later periods to be considered an NF. Similarly, absence locations were those of stable locations in all maps. Furthermore, any presence within fire perimeters polygons was excluded (as explained in Section 2.2.3 and the explanatory variables in the Supplementary Materials) to minimize areas affected by heavy disturbance events along periods.

For text simplicity, this section continues to be explained in a section with the same name in the Supplementary Materials part that gathers the complementary information to the main text. Further references cited in the Section 2.2.2. section that follows in the Supplementary Materials are [4,33,47,48,51,54,57–63].

2.2.3. Land Cover Change Modeling

The spatio-temporal distribution of forest expansion along the transect and the main drivers involved were analyzed by comparing every two consecutive LCM, i.e., 1987–2002 as the first period (P1) and 2002–2017 as the second period (P2). Dates were defined considering the initials (the mid-1980s) and the most recent Landsat images available at the moment of LC production (2017). The central date (2002) divides the period into two equal 15-year subperiods, coinciding with the auxiliary database date (SIOSE) used to extract training areas [54]. In both periods, each NF dynamic was modeled at the maximum desegregated categorical level (i.e., Grl/Shl to BDF/BEF/NEF and from crop categories to BDF/BEF/NEF), considering a binary presence–absence modeling scheme. The modeling process involved: (1) determining variables that may have potentially impacted the NF occurrence; (2) a dimensionality reduction in predictors, and (3) the model processing itself, developed in the following subsections.

Explanatory Variables

Spatial determinants potentially driving the past NF transitions are listed in Table 2. The selection of biophysical, climatic, distance and accessibility, geology, thematic and socioeconomic determinants was based on a literature review focusing on LC change analysis [4,19,30,57,64–70]. Selected determinants included variables collected from administrative-level historical statistics and spatially explicit pixel-level data. Details about sources and methods to extract these explanatory variables are given in the Supplementary Materials 'Explanatory variables' section. Further references cited in the Section 2.2.3 that follows in the Supplementary Materials are [71–83].

Collinearity Analysis

The collinearity between predictors was evaluated to exclude variables influenced by other predictors from analysis before modeling, thus reducing model overfitting and time computing. Thus, the level of correlation between predictors was assessed through the variance inflation factor (VIF), considering a VIF threshold of 5 [49]. The process iteratively excludes multicollinearity variables since all the remaining variables had a VIF score below the threshold considered. When two highly correlated variables were detected, the one that depicted a better interpretation behavior in the model and showed a smaller correlation (Pearson's coefficient) with the other explanatory variables was selected. The process was helpful in reducing dimensionality, especially in socioeconomic, distance-related, and drought-related variables. Subsequently, non-informative zero variance predictors were excluded, and the Pearson correlation coefficients were estimated for the remaining predictors. Lastly, the available presence–absence sample generated was intersected with the predictor variables, resulting in point features with data included in the attribute table.

Table 2. Explanatory variables used for modeling forest expansion in the study area. Variables collected at different temporal moments have a value in each period (P1, P2).

Group	Variable	Abbreviation	Units
Topoclimatic	Slope	Slope	Degrees
	General curvature	General_Curv	Dimensionless
	Potential radiation in winter solstice	Pot_Rad_Wint	$10 \text{ kJ}/(\text{m}^2 \times \text{day} \times \mu\text{m})$
	Averaged annual accumulated rainfall	Ac_Rain	dmm
	Averaged mean annual temperature	Av_Me_Temp	d °C
	Number of drought episodes (DE*)	DE*_S3/6/12	Counts
	Number of humid episodes (HE*)	HE*_S3/6/12	Counts
Distances and accessibility	Euclidean dist. to forests	Eu_Dist_Forests	Meters
	Euclidean dist. to hydrography	Eu_Dist_Hyd	Meters
	Euclidean dist. to protected areas	Eu_Dist_Protect	Meters
	Cost dist. to provincial capitals	Co_Dist_Cap	Meters
	Cost dist. to urban areas	Co_Dist_Urb	Meters
	Cost dist. to main roads	Co_Dist_M_Roads	Meters
	Cost dist. to secondary roads	Co_Dist_S_Roads	Meters
Geology	Lithological substrate	Lithology	Acidic, mixed, alkaline
	Sheet and rill erosion	Soil_Erosion	$\text{Mg}/(\text{ha} \times \text{year})$
Socioeconomic	Protected areas	Protect_Areas	Protected-Non protected
	Total population	Inhabitants	Inh
	Population density	Pop_Density	inh/km^2
	% of population 0–16 years	Pop_0_16y	0–16/inh * 100
	% of population 16–64 years	Pop_16_64y	16–64/inh * 100
	% of population >64 years	Pop_65y	>65/inh * 100
	Ageing index	Ageing_index	>65/(0–16) * 100
	% of agriculture workers	W_Agriculture	W_A/inh * 100
	% of industry workers	W_Industry	W_I/inh * 100
	% of building workers	W_Building	W_B/inh * 100
	% of services workers	W_Services	W_S/inh * 100
	Annual work units	AWU	Work Units
	Number of holdings	Num_Hold	No. of holdings
	Livestock units	LSU	Animals
	Utilized agricultural area	UAA	Hectares

Data Analysis: Boosted Regression Trees

The LC changes associated with NF transitions were assessed using boosted regression trees (BRTs). BRTs, which coincide with stochastic gradient boosting, are used within a non-parametric regression technique that combine the strengths of decision trees and the boosting ensemble technique [84]. BRTs do not assume any data distribution a priori, which facilitates multiple interactive variables. They also help to identify relevant determinants and their interactions, characterizing their partial dependence. BRTs are currently used in many fields, including remote sensing [33,47], LULC change analysis [46], ecology [4,49,85], hydrogeology [86,87], or marine spatial management [88]. Boosting is sequential, which means that new trees are additively included in a stagewise process and fitted to the residuals of the previous tree [89].

Model Fitting and Parametrization

We applied BRT [84] using the 'gbm()' function [48,90] available in the 'caret' package [91] in R software [92]. The BRT outputs essentially depend on the settings of four main hyperparameters: the 'tree complexity', which is the number of branches or splits for fitting each regression tree; the 'number of trees', which defines the number of models composing the final ensemble; the 'shrinkage', which is a regularization parameter that controls the model's influence within the ensemble [89]; and the 'minimum observations in node', which define the minimum number of training samples in a node to commence

splitting, providing, together with interaction depth, more control on the complexity of the weak learners. Furthermore, the 'gbm()' function has two additional parameters: the 'distribution' parameter, which defines the loss function, and was set as *Bernoulli* for binary response variables; and the 'bag fraction', which determines the fraction of the observations in a randomly selected training set to fit each weak learner (0.5 for stochastic gradient boosting) [84,89].

We assessed model sensitivity by testing all the combinations of tree complexity levels with the number of trees, the shrinkage, and the minimum number of node observations. A 10-fold cross-validation procedure for each parameter combination determined the optimal configuration to derive the final model. A test subset was used to evaluate the final model performance. The area under the receiver operating curve (AUC) and the accuracy rate measured the model performance [93–96].

A modeling strategy was performed to extract the five most important drivers (based on the 'relative importance') involved in NF dynamics. It was based on three steps. In the first step, an initial model is generated considering the whole set of variables, providing an overall perspective of the most important drivers. The second step gave a new model, considering all predictors but excluding the most important one in the first model. Thus, the repercussion of the first model's main determinant is excluded, allowing other predictors and their relationships to be evaluated, an exclusion of rising necessity the more significant the variable's relative importance. Lastly, a final model combines the most important variable of the first model and the four most important of the second one.

The reliability of the final models' results was evaluated for each NF dynamic. The aim was to corroborate the consistency in the results. We randomly partitioned the available sample into three independent subsets to achieve this sensitivity analysis. Each subset served to derive a training and test subsample used for modeling. The AUC score was used to evaluate model performance, the drivers' relative importance score, and their partial dependence plots pattern. The results reported similar model performance and main drivers' relative importance values, as well as PDPs (detailed in the next section) with similar patterns within the five most significant predictors. However, the order of drivers and PDP patterns varied when the subsample size was limited (i.e., <200 points). The results reported consistency and confident interpretations derived from them when the sample size exceeded the minimum estimated sample size.

Model Inference

The BRT technique provides tools for exploring the relationships between explanatory and response variables, estimating the 'relative importance' (RI) of the predictors in the model [84,97]. The RI measures the number of times a variable is selected for splitting, weighted by the squared improvement of each split in the model, and averaged over all trees [97]. It is subsequently scaled from 1 to 100 to express the individual contributions as percentages. The RI was calculated for all of the variables in the evaluated models.

To display the results, we estimated the partial dependencies that describe the relationships between the response variable and one explanatory variable while accounting for the average effect of the other predictors [84,97]. This calculus derived partial dependence plots (PDPs) that depict the relationship between the response variable in the space of the predictor and specify the suitable conditions for the LC transition. For each NF dynamic and analysis period model, the five final selected variables were considered to evaluate their importance across time and space (BRs), in addition to their PDPs for pattern interpretation.

As a complement to this, to provide a global perspective of the main drivers involved in each NF dynamics, their predictors' RI values were aggregated (the sum of the existing individual RI values of a predictor along the BRs), weighted by a factor, and finally scaled from 0 to 100. The factor was estimated as the number of times that a predictor was selected in different BRs divided by the maximum number of BRs where the LC dynamic was modeled; then, it was scaled between [0.5,1] (not between 0 and 1) to avoid a harsh penalization of those predictors selected just in a few BRs.

3. Results

3.1. New Forests Occurrence over the Last Thirty Years

Evaluating all forest land cover trajectories showed that forest expansion exceeds deforestation in extension, implying a positive net forest gain. In the whole transect, forests have increased in the last thirty years mainly at the expense of decreasing shrublands (e.g., 4160.1 km^2 between 1987 and 2017) and grasslands (e.g., 1934.6 km^2 between 1987 and 2017) and secondarily croplands (e.g., 349.0 km^2 of IWC between 1987 and 2017), as detailed in Figure 3. Furthermore, disaggregated details by BRs are shown in Figure S6 in the Supplementary Materials.

Category		1987	2002	2017
NEF	Needleleaf evergreen forests	6 737.6	7 792.9	9 204.4
BDF	Broadleaf deciduous forest	3 892.2	4 197.0	5 227.8
BEF	Broadleaf evergreen forest	7 932.3	9 909.5	11,139.3
Shl	Shrublands	4 160.1	2 096.2	-
Grl	Grasslands	1 934.6	1 035.8	-
BrS	Bare Soil	50.2	14.3	-
IHC	Irrigated herbaceous crops	102.2	48.3	-
RHC	Rainfed herbaceous crops	191.3	103.8	-
IWC	Irrigated woody crops	349.0	191.6	-
RWC	Rainfed woody crops	201.8	166.0	-

(a)   (b)

Figure 3. (**a**) Chord diagram showing NF trajectories between 1987 and 2017 in the whole transect. (**b**) Table detailing the occupation of each category implied in NF consolidated trajectories. All figures are shown in km^2.

Numerically, NF occurrence affected 701,156 ha in the transect (334,031 ha during the first period and 367,125 ha in the second). As seen in Figure 4, the two primary source categories converted into NF areas were related to natural/semi-natural categories (shrublands and grasslands) and cropland abandonment (irrigated/rainfed herbaceous and woody crops) processes.
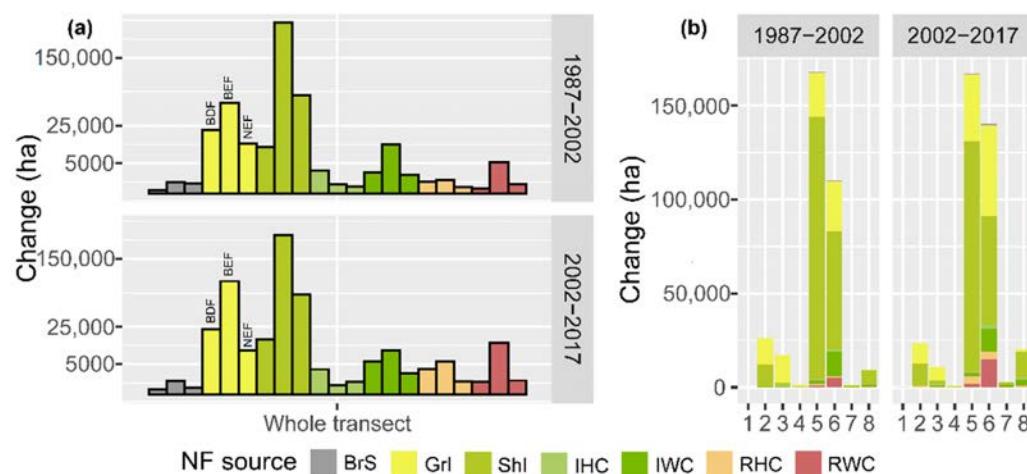
Figure 4. (**a**) NF transitions change area by source category and forest type for the whole transect. Colors denote source categories (e.g., yellow = grasslands), while the three consecutive bars represent each target forest (BDF, BEF, and NEF). (**b**) NF transition area disaggregated by BR, referenced by the numbers in Table 1.

According to Table 3, the NF spatial distribution varied according to BRs, but in general terms, grasslands dominated over shrublands as land donors in the Eurosiberian and

the mountainous Mediterranean regions, while the opposite occurred in the Mediterranean area. Crop categories dominated in the Mediterranean, especially in the Mesomediterranean BR. Broadleaf evergreen forests were the principal target forest category (66.3% of NF appearances), and they were mostly concentrated in the Supramediterranean and Southern Mesomediterranean regions. They are followed by needleleaf evergreen forests (20.2%) occupying a wide variability of conditions (from the upper mountain to the driest BRs) and by broadleaf deciduous forests (13.5%) principally located in the Montane and Coline. In absolute terms, the Supramediterranean and Southern Mesomediterranean BRs concentrated afforested areas (47.8% and 35.8%, respectively) due to their extension and geomorphological variability. However, the highest relative afforestation rates were observed in the Thermomediterranean and Northern Mesomediterranean regions.

Table 3. New forest dynamics in absolute and relative values. The source categories' transitioning area (all figures in ha) towards the target NF group categories (in the upper part of the table) is detailed and disaggregated by the finally modeled BRs and analysis period (P1, P2). In the lower part of the table, figures related to all forests are given to provide final relative figures.

Bio.Region	BR.2		BR.3		BR.5		BR.6		BR.7	BR.8	
Target Cat.	P1	P2	P1	P2	P1	P2	P1	P2	P2	P1	P2
NEF	4856.6	4488.8	7933.3	6425.6	31,413.3	24,529.0	18,379.1	20,186.6	1247.8	5743.6	13,973.4
BDF	11,924.0	12,806.6	8128.4	4250.1	15,163.6	25,039.0	3089.3	6451.8	1229.9	1742.3	4817.6
BEF	9434.1	6220.0	1333.9	314.4	121,223.1	117,453.6	88,802.9	114,093.5	323.9	2049.7	2157.9
Abs. Δ NF [1]	**26,214.7**	**23,515.4**	**17,395.6**	**10,990.1**	**167,800.0**	**167,021.6**	**110,271.3**	**140,731.9**	**2801.6**	**9535.6**	**20,948.9**
Source cat.	↑	↑	↑	↑	↑	↑	↑	↑	↑	↑	↑
Shl	11,969.0	11,773.8	1035.2	1715.7	139,591.7	122,779.5	62,408.0	57,933.2	1042.4	7069.1	13,814.9
Grl	13,860.7	10,759.6	14,732.6	7196.9	23,158.9	35,400.5	26,647.5	48,429.4	143.6	400.7	1086.5
BrS	1.4	3.7	9.8	6.8	594.7	418.6	691.5	897.7	44.2	10.0	24.8
IHC	96.3	47.3	974.7	810.2	770.2	739.8	1347.5	1881.2	54.9	402.5	1294.9
RHC	129.0	690.0	5.5	235.5	871.1	4468.6	693.6	4054.6	18.9	190.4	906.6
IWC	87.9	118.4	474.4	775.4	2020.4	1578.8	13,322.3	12,447.4	1288.2	1202.1	2946.9
RWC	-	0.1	-	0.7	748.7	1551.2	5084.0	14,748.0	147.8	18.2	151.9
Others	70.5	122.5	163.4	248.9	44.4	84.6	76.9	340.3	61.6	242.6	722.4
All forests	388,843.3	375,619.7	89,993.1	92,705.1	1,154,511.0	1,269,076.1	591,780.2	646,504.6	5261.0	58,641.8	57,578.7
NEF	97,215.0	108,544.5	41,852.3	48,364.0	439,790.3	465,941.1	173,548.1	169,650.5	3424.0	43,307.5	39,989.2
BDF	219,789.8	202,775.8	31,018.7	33,119.4	188,810.0	181,902.2	31,272.1	24,467.9	412.9	6108.2	6777.3
BEF	71,838.5	64,299.4	17,122.1	11,221.7	525,910.7	621,232.8	386,960.0	452,386.2	1424.1	9226.1	10,812.2
Shl	78,474.5	68,619.4	5341.4	11,045.0	1,011,593.4	908,174.3	458,904.8	446,259.5	33,579.5	242,900.8	271,144.4
Grl	77,531.0	100,007.2	43,718.1	37,472.8	657,331.5	629,819.3	907,027.6	813,254.9	86,335.2	103,983.7	131,507.4
Brs	988.1	847.5	122.1	169.8	53,807.0	54,331.7	135,633.7	130,237.9	38,382.1	53,041.3	49,668.7
IHC	5871.7	1092.4	14,494.5	8412.7	11,197.8	8053.4	165,911.8	104,488.2	7209.4	127,504.4	108,455.7
RHC	49,705.1	53,484.9	202.4	3787.7	793,903.2	816,432.4	1,878,760.7	1,995,948.0	19,286.3	598,332.8	552,903.8
IWC	1054.2	1646.1	7911.3	7514.0	8755.8	7762.4	271,217.7	246,390.4	32,907.6	88,430.6	100,804.7
RWC	25.3	50.2	0.5	4.7	40,612.4	37,109.3	1,202,153.8	1,217,517.8	142,547.0	110,433.6	100,577.1
Others	1808.7	2934.3	2915.1	3586.9	7206.5	8159.9	35,334.7	46,123.4	37,645.0	28,340.7	38,969.1
Rel. Δ NF [2]	**6.7%**	**6.3%**	**19.3%**	**11.9%**	**14.5%**	**13.2%**	**18.6%**	**21.8%**	**53.3%**	**16.3%**	**36.4%**

"Others" includes categories (Urb, WaB, RiC, and Grh) with lower representativeness in NF transitions. [1] represents the NF absolute increase; [2] the relative increase regarding the total forested area (All forests) disaggregated by forest group, and the rest of categories for each BR and period. The main NF dynamics in absolute and relative terms are highlighted in red.

On the other hand, afforestation was similar in both studied time periods but slightly higher during the second. The afforestation area was higher in the first period in the Montane, Coline, and Supramediterranean regions, and in the second period in the Mesomediterranean (Northern and Southern) and Thermomediterranean regions.

The results were derived from the LCMs, obtained with an overall accuracy—weighted by the ground truth area considering only classified pixels—of 97.2%, 92.2%, and 96.9% at each reference date (1987, 2002, and 2017). The average user and producer accuracy of the

natural categories (forest categories, shrublands, and grasslands) were 91.2% and 91.4%, respectively, while the same indicators were 94.8% and 94.3% for crop categories. The confusion matrices of the LCMs and the imagery series considered are detailed in Tables S1–S4 in the Supplementary Materials.

3.2. Model Validation

Table 4 shows the main drivers' aggregated, weighted, and scaled RI values detailed for each source category and target forest category. This table includes a total of 77 models (28 for BDF, 25 for BEF, and 24 for NEF new forests groups), considering those dynamics in the BRs providing enough samples for modeling. On average, the accuracy obtained in all models was 0.81 ± 0.06 for all the dynamics evaluated. Models in the first period provided an average accuracy of 0.83 ± 0.05 and slightly lower 0.79 ± 0.05 in the second period, mainly related to the higher variability in the NF locations during this period. Regarding source categories, the average values for natural categories were 0.83 ± 0.06 in the first period and 0.78 ± 0.06 in the second. Crop categories showed slightly higher average accuracy, being 0.84 ± 0.04 in the first period and 0.79 ± 0.07 in the second (Table S7).

3.3. New Forests' Main Drivers
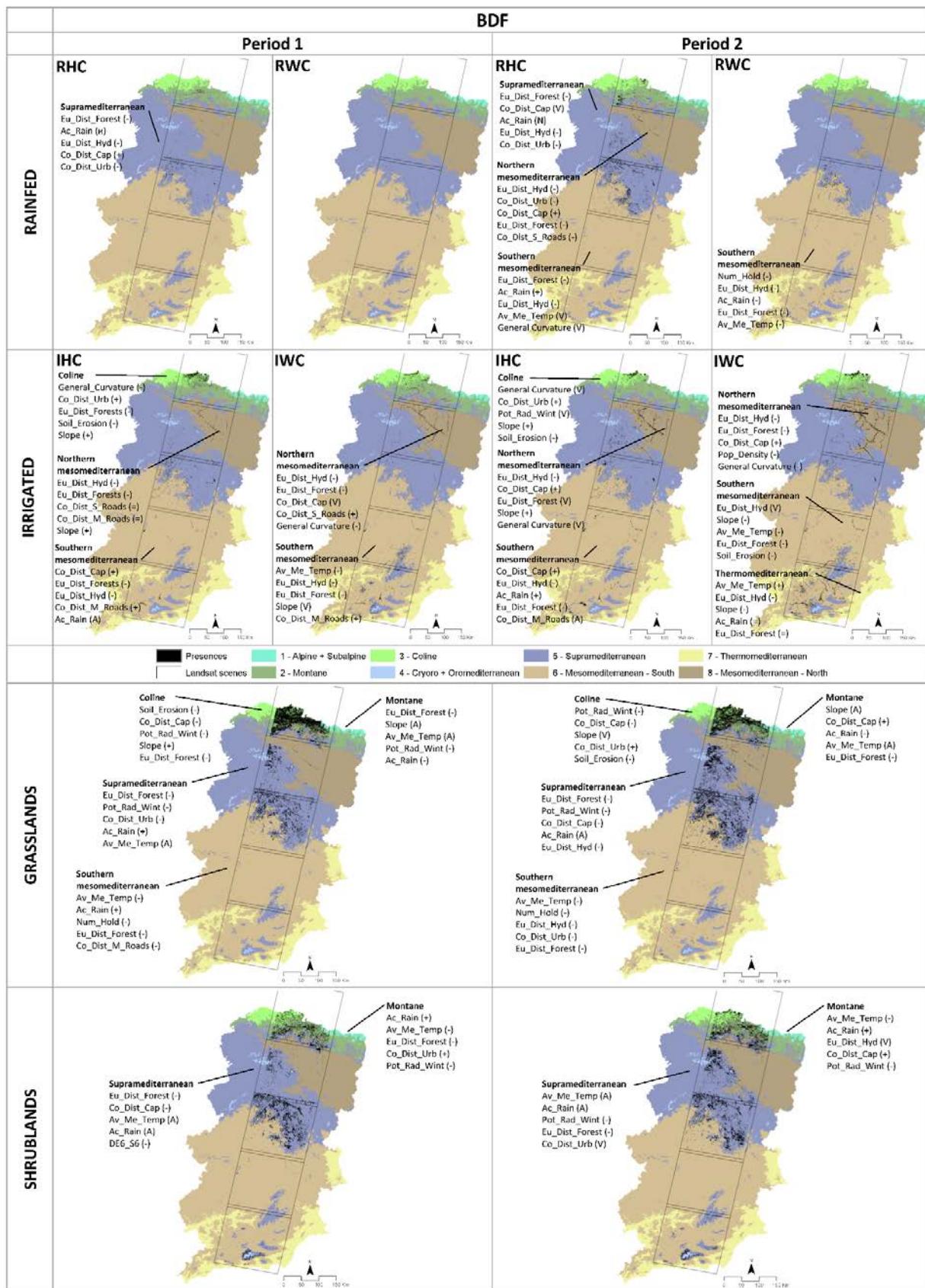
The NF driving forces were analyzed by LC source categories (rainfed crop categories, irrigated crops categories, grasslands, and shrublands). From the initial set of variables, twenty-five different variables were among the five main predictors in the models. The maps datailed in Figure 5a–c describe the drivers' temporal and spatial variation characteristics, detailed by period and BR. Moreover, Table 4 summarizes the driver's importance for each source category and target forest group. In this section, drivers are listed by their relative importance, accompanied by a symbol (in brackets) denoting the partial dependence main pattern. For instance, the (+grad) means that the transition probability increases with the variable, the (−grad) represents the opposite, and the (≠grad) means that there is not a clear positive or negative tendency. The (A-shape) indicates that the higher suitable conditions occur between two low values, while the (V-shape) denotes two high suitable conditions between a minimum. The (*u*-shape) depicts relatively suitable conditions in low values that sharply decrease, then increase to a second peak, and finally decrease at larger values. Lastly, the (±grad) is used in the case of different patterns of a driver when aggregating BRs.

A detailed description of the results section is provided in the Supplementary Materials for readers seeking more information, continuing the main text with the discussion of the principal results.

126

Table 4. Aggregated, weighted, and scaled relativ importance values are detailed for each predictor, source category, and new forests' target category. The "Irrigated" label groups are IHC and IWC, while "Rainfed" groups are RHC and RWC categories.

Target Forest Categories →	BDF								BEF								NEF							
Source Categories →	Rainfed		Irrigated		Grasslands		Shrublands		Rainfed		Irrigated		Grasslands		Shrublands		Rainfed		Irrigated		Grasslands		Shrublands	
Periods → / Variable ↓	P1	P2	P1	P2	P1	P2	P1	P2	P1	P2	P1	P2	P1	P2	P1	P2	P1	P2	P1	P2	P1	P2	P1	P2
Slope	-	-	5.9	6.9	7.9	7.2	-	-	9.7	5.3	-	18.1	8.3	3.3	9.0	2.4	-	-	-	-	5.5	14.2	4.5	11.9
General	-	1.0	4.3	5.2	-	-	-	-	-	-	-	-	-	-	-	-	-	-	-	-	-	-	-	-
Curvature	-	-	-	-	-	-	-	-	-	-	-	-	-	-	-	-	-	-	-	-	-	-	-	-
Pot_Rad_Wint	21.9	-	1.3	1.5	10.7	7.9	2.8	14.6	-	2.5	13.4	-	13.6	2.4	18.9	15.7	-	4.9	-	8.6	7.3	1.0	15.0	3.4
Ac_Rain	-	12.0	-	2.3	11.2	6.5	28.1	23.7	19.5	14.4	-	-	17.8	19.7	13.5	22.3	-	4.3	16.1	23.0	7.8	12.2	22.0	26.7
Av_Me_Temp	-	4.7	2.5	9.3	14.5	10.1	18.7	31.0	3.9	6.8	20.4	27.3	12.8	11.1	14.5	17.0	-	-	-	-	3.8	15.5	3.9	2.3
DE6_S6	-	-	-	-	-	-	3.3	-	-	-	-	-	-	-	-	-	-	-	-	-	-	-	-	1.7
DE9_S6	-	-	-	-	-	-	-	-	-	-	-	-	-	-	-	-	-	2.2	-	-	-	-	-	-
DE3_S12	-	-	-	-	-	-	-	-	-	1.5	-	-	-	-	-	-	-	-	-	-	-	-	-	-
DE3_S24	-	-	-	-	-	-	-	-	-	-	-	-	-	-	-	-	-	-	-	-	-	-	-	1.1
HE3_S12	-	-	-	-	-	-	-	-	-	-	-	-	-	-	-	-	-	-	-	-	-	-	-	1.2
Co_Dist_M_Roads	-	1.6	5.3	1.1	1.2	-	-	-	-	-	16.1	-	-	-	-	-	16.1	3.4	24.2	-	-	-	1.5	-
Co_Dist_S_Roads	-	5.8	2.2	-	-	-	-	-	-	-	-	-	-	-	-	1.2	-	4.3	-	2.1	-	-	-	-
Co_Dist_Urb	12.7	6.4	2.2	1.8	2.2	5.2	3.9	3.9	1.8	-	-	-	2.0	-	5.8	-	-	-	-	-	8.6	11.4	1.9	9.2
Co_Dist_Cap	18.7	20.9	6.9	8.7	2.8	12.8	4.8	3.6	35.1	35.7	21.2	20.7	24.3	27.7	-	12.6	31.5	30.6	-	20.7	8.0	17.2	2.0	18.5
Eu_Dist_Forest	26.0	24.7	18.9	11.8	22.5	10.5	24.1	4.2	2.0	4.9	-	-	-	8.9	30.9	14.0	20.9	20.1	-	3.6	28.6	1.9	30.3	-
Eu_Dist_Hyd	20.6	-	25.9	21.3	-	5.6	-	3.8	-	-	28.9	16.7	4.4	3.1	-	-	5.8	-	10.5	-	-	-	4.0	1.0
Soil Erosion	-	-	1.6	2.9	3.0	1.8	-	-	5.4	4.8	-	-	-	-	-	-	12.3	-	24.4	3.6	-	-	1.5	-
Protected_Areas	-	-	-	-	-	-	-	-	-	-	-	-	-	-	-	-	-	-	-	-	0.8	-	-	-
Pop_density	-	-	-	1.0	-	-	-	-	2.3	2.5	-	17.1	-	-	-	-	-	-	-	-	-	-	-	-
W_Building	-	-	-	-	-	-	-	-	2.2	1.7	-	-	-	-	-	-	-	-	-	-	-	-	-	-
W_Services	-	-	-	-	-	-	-	-	-	-	-	-	-	-	-	-	-	-	-	-	-	-	-	-
W_Industry	-	4.9	-	-	1.9	2.5	-	-	-	-	-	-	-	1.9	-	-	-	-	-	-	-	4.4	-	-
Num_Hold	-	-	-	-	-	-	-	-	-	-	-	-	1.9	2.4	-	-	19.3	-	21.9	3.5	-	-	-	-
LSU	-	-	-	-	-	-	-	-	-	-	-	-	-	-	-	-	-	-	13.4	2.7	-	-	-	-
UAA	-	-	-	-	-	-	-	-	1.7	-	-	-	-	-	-	-	-	-	-	-	3.2	3.1	-	-
Num. BRs Grouped	1	4	5	6	4	4	2	2	4	4	1	1	4	3	4	4	1	2	1	3	3	3	4	5
BRs Grouped (distinct)	5	5,6*,8	3,6*,8*	3,6*,7,8*	2,3,5,6	2,3,5,6	2,5	2,5	5*,6*	5*,6*	6	6	2,3,5,6	2,5,6	2,5,6,8	2,5,6,8	6	6,8	6	6,8*	2,5,6	2,5,6	2,5,6,8	2,5,6,7,8

* Values with an asterisk denote BRs appearing twice (for herbaceous and woody crops) in grouped categories.

(**a**)

Figure 5. *Cont.*
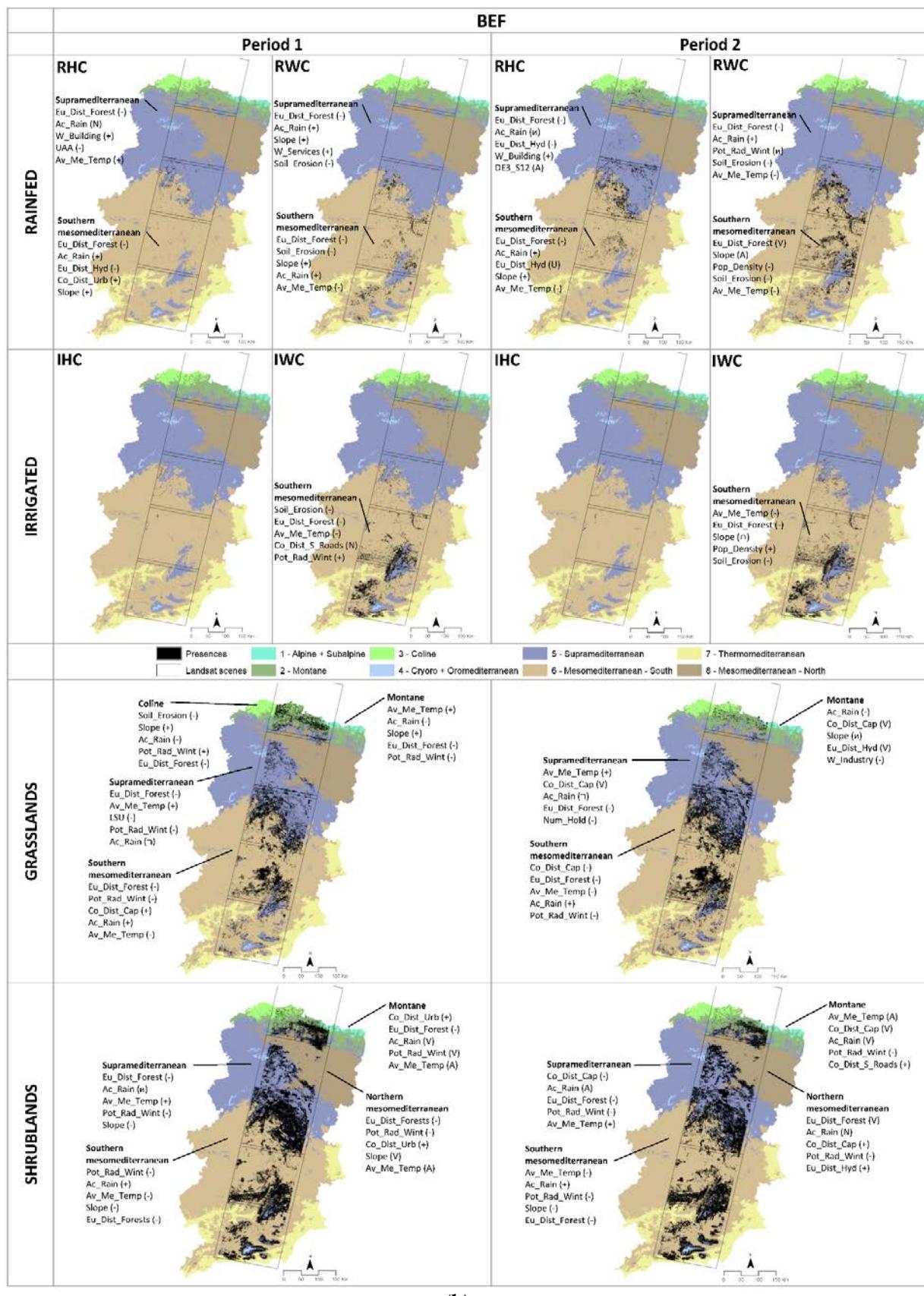
Figure 5. *Cont.*
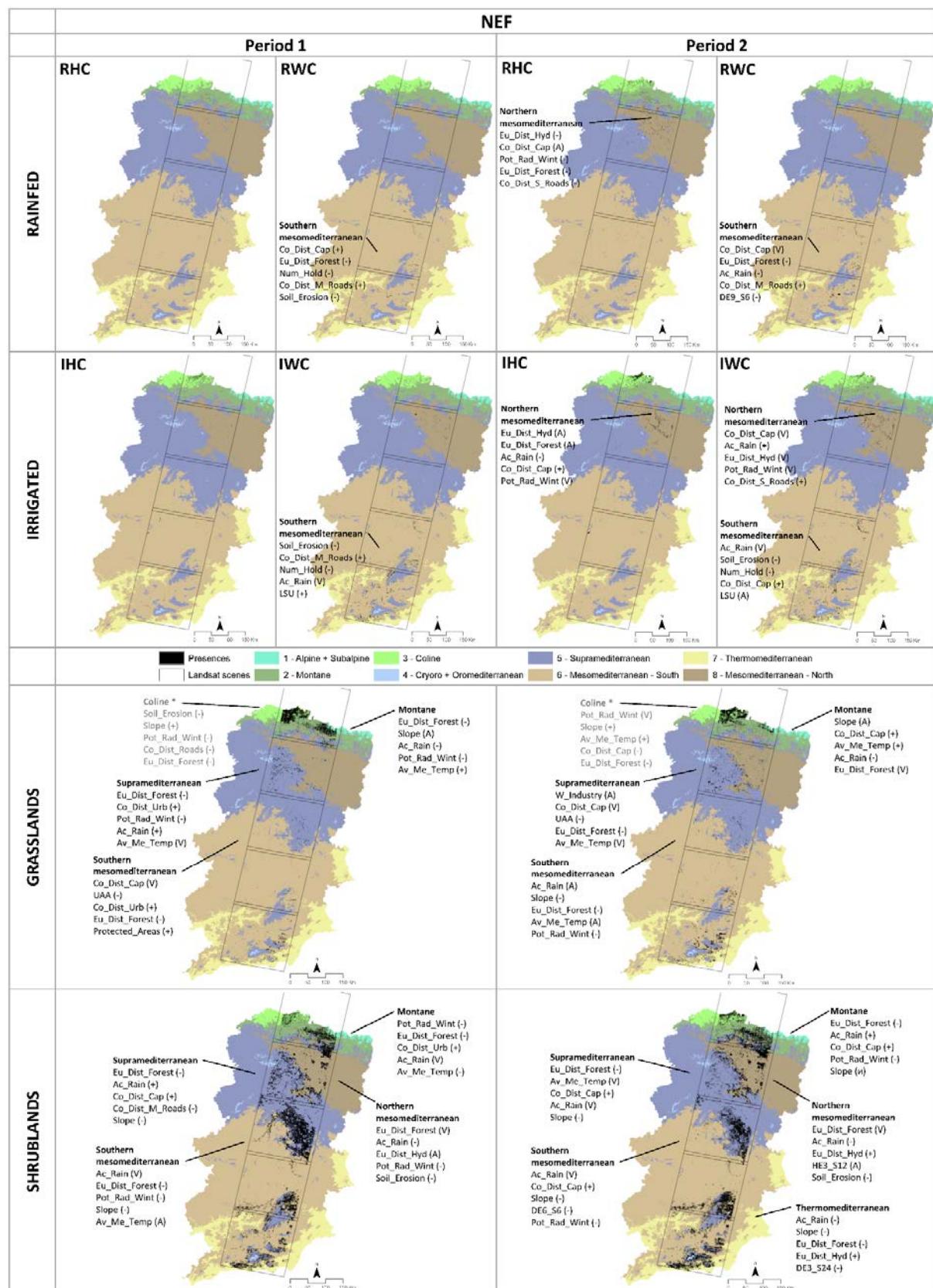
Figure 5. (**a**) Main drivers derived for each target forest, source category and period. Drivers are listed in order of importance. (**b**) Figure continuation. (**c**) Figure continuation.

4. Discussion

This study used a sound methodological treatment, which is why we open this section with two subsections discussing its role and contribution. Afterwards, the second subsection continues by examining drivers for the different NF types.

4.1. Land Cover Change Locations Extraction and Sampling Strategies in the Methodological Framework

From a methodological point of view, the training data used during LCM were coherently derived for the whole transect and temporal references, using filtering strategies to enhance their reliability and the quality of their thematic assignment, which also derived in the reliability of the uncertainty threshold applied for the extraction of changing positions [54]. Thus, the filtering rules used to derive ground truth samples provided highly accurate LCM for LC change analysis, together with the uncertainty for each classified pixel. As a result, the maps attained an outstanding performance with an overall accuracy of 95.4% (overall accuracy weighted by the ground truth area considering only classified pixels), providing high-quality information to support the NF analysis.

The accuracy of LCM is frequently influenced by factors such as imagery positional misregistration or wrongly parameterized radiometric correction, deriving in misclassified information. Considering the uncertainty in the dependent variable (NF), it was decisive to use top-performing models. As expected, models' accuracy increased when pixels with uncertainty over a threshold were eliminated, which is in line with previous research works [57,58].

There are concerns over sampling absence locations and how it could affect the performance of the models, their interpretability, generalization, and transferability. In this sense, different authors show the existence of a bias when obtaining a representative sample of presences–absences in species distribution modeling, proposing various solutions [61,98,99]. Even though this could be an entirely new research line, we considered it necessary to define a sampling strategy to select absences according to the presences available within a spatial buffer, reducing the spatial bias of the absences. Thus, this solution generated a balanced presence–absence sample, assuring their local prevalence.

Finally, the spatial segmentation into BRs was crucial to extract presence–absence locations within similar climatic conditions, enhancing the study's coherence and avoiding any consideration of absence locations far apart and without spatial relation with the presences in the model.

4.2. Driving Forces Modeling

According to Borda-Niño et al. [66], recent remote-sensing research evaluating forest changes focuses more on deforestation dynamics, and less attention is given to forest increase dynamics. However, understanding the driving forces of NF attending to their source categories is challenging, but decesive to elucidate their contribution to each target forest category, and spatio-temporal patterns. In this research, both local topoclimatic and socioeconomic factors are combined to analyze forestation processes from contrasting LC categories along a representative Eurosiberian and Mediterranean North–South transect.

Studies quite often evaluate the drivers involved in LC dynamics focusing on a specific issue or complex phenomenon to be analyzed, unifying several categories from LC maps into a unique "label", i.e., forest regrowth, deforestation, and cropland abandonment, which constitutes the phenomenon as a target for analysis in research works [19,21,30,33]. The study also benefited from investigating NF appearance, disaggregated into three forest types, focusing on six main source categories for the sake of understanding the specific drivers involved.

The BRT modeling strategy was based on three steps, and was advantageous in cases where the primary driver in importance in itself explains a large proportion of the variance of the model, i.e., over ~50% of the relative importance. Thus, super dominant drivers, such as the topography, mask the contribution, pattern, and interaction of other predictors with

lower explanatory power, which are underrepresented in the resulting models [4,33]. In this research, a solution based on three iterative steps minimized this issue. In the last step, the main driver in the first model and the four most important ones obtained in the second are taken, configuring the final set of drivers that explain the new forest appearance.

In our study, in general terms, topoclimatic and distance drivers were more frequently selected to explain NF dynamics along the BRs than socioeconomics ones, which is a recurrent situation in previous research works [4,7,57]. The lower explanatory power of socioeconomic drivers may be related to their homogeneous spatial distribution into administrative units (municipality, census section). However, we minimized this issue by considering the spatial autocorrelation from the Moran index and a presence–absence balanced sample. Furthermore, statistical analyses are not independent of the spatial configuration or aggregated information scale, leading to severe methodological difficulties such as the modifiable areal unit problem (MAUP) [100–102].

4.2.1. Drivers of Forestation from Croplands

Studies of forest expansion associated with cropland abandonment dynamics in mountainous regions have been reported at the European ambit [8,10,103–108]. In our results, the appearance of new BDF from crop categories was closely associated with the proximity to rivers, streams, or torrents, where water availability and humidity allows BDF species to grow. Similarly, their expansion is associated with irrigated crops, and is also favored by the proximity to forested areas, producing a fulfilling process between or within the forested patches (small or isolated cultivated areas) or along their edges, where seed dispersal triggers early stages of natural succession [109]. Regarding the spatio-temporal behavior, new BDF from crops mainly appeared in large hydrographic basins close to hydrographic network (Northern and Southern Mesomediterranean BRs) and in the transitions to mountainous areas (Supramediterranean) where croplands are less competitive [110–112], affecting specially rainfed crops in our results.

The proximity to pre-existing forests as a driver has been reported in several works [7,30,66,113–115], and it has played a crucial role according to our research. Concerning the proximity to the hydrographic network, studies considered and stated it in their results [66,114,115]. This driver affecting riparian vegetation was likely involved in poplar intensification (e.g., *Populus nigra* L., *Populus canadensis* L., *Populus alba* L.) close to rivers and preexisting deciduous species forest plantations. In fact, European initiatives promote the cultivation of poplar tree species because of their sustainability and efficiency (fast-growing and high-carbon sequestration rates) in a context of the need for renewable raw materials and global climate change [116].

For many studies, remoteness has been considered a main driver of NF associated with farmland abandonment [19,30,33,114,115,117]. In our research, the main drivers were the distance to urban settlements, in general, and to provincial capitals, in particular. Thus, the further the distance, the more the likelihood of farmland abandonment. We have also unveiled that croplands further away and less accessible from capital cities were more likely abandoned, which is in line with other works and in other areas [30]. Contrary to initial expectations, the distance to main and secondary roads, as an indicator of remoteness, were not explicative drivers of cropland abandonment, i.e., an outcome similar to other works such as Abadie et al. [115]. In our work, the only exception was in the conversion from crops to NEF, mainly in the first period when the explanatory power of the distance to main roads was high [33]. One possible explanation could be the high correlation with the distance to provincial capitals, which displays more substantial explanatory power.

Our results showed that the main topoclimatic determinant of crop abandonment to new BDF was precipitation, mainly in the case of rainfed crops with an increasing positive tendency. In some studies, this variable was initially removed due to the correlation with other drivers [30,64], whereas in others, it appeared as the main one [21,66]. Other topoclimatic drivers obtained from our analysis were temperature and slope, with a negative (except for the Thermomediterranean region) and a positive gradient, respectively. These

drivers were included in other works [64]. In Spain, Peña-Angulo et al. [118] found rainfall and altitude in the Cameros Viejo region (Iberian System, Spain) as the main factors in deciduous forest appearance from cropland abandoned in mountainous areas. Moreover, Alonso-Sarría et al. [119] found that climatic drivers (precipitation and temperature) predominated over geomorphological drivers in land abandonment in the Murcia region (Spain). These findings align with our results since climatic drivers were more represented and of higher importance in the warmest and driest BRs.

Within the socioeconomic variables, rural depopulation has been associated with the abandonment of agricultural land and subsequent natural succession dynamics, especially in the European mountain areas [8,103,107,112,120]. However, in our results, the role of depopulation dynamics was of low importance and was associated with a lower population density driver. Nevertheless, variables related to the agricultural structure of the holding played an important role in the Southern Mesomediterranean BR. In this context, NFs were favored in areas with a lower number of holdings devoted to rainfed woody crops in the limit with the Supramediterranean region, where the number of holdings is lower compared to lowlands in the middle of the large basins and presumably smaller agriculture holdings due to terrain (slope, area) limitations. In this line, Zglobicki et al. [121] found that holding size can drive land abandonment in eastern Poland. Nevertheless, in general terms, population and the agricultural structure driving forces were scarcely represented in our model results.

In the case of new BEF from crop abandonment processes, the proximity to previously forested areas remained as the main driver in all the BRs involved (mainly located in the south of the transect), and the distance to the hydrographic network disappeared as a consequence of much lower water requirements of evergreen forest species. Regarding the spatio-temporal behavior, new BEF from crops mainly appeared in Supramediterranean and Southern Mesomediterranean BRs, and especially in the transition between them. Contrary to BDF and NEF, distances and accessibility drivers, such as the distance to provincial capitals, urban settlements, and roads, showed scarce importance. Why remoteness is less informative is unclear and will be of interest in future research.

The main topoclimatic driver of new BEF from crop abandonment was temperature, mainly in the case of abandoned irrigated crops, showing a decreasing negative tendency. Thus, the higher relative importance was associated with the warmest southern BRs. Another driver was precipitation, associated with a positive trend to rainfed crops, especially in the Southern Mesomediterranean region. This was interpreted as a NF in the upper limit of the BR at higher altitudes, where total accumulated precipitation is high. Therefore, water availability and temperature were major drivers in the warmest areas of the transect, which is in line with studies performed in semi-arid regions [119,122]. Lastly, NF appearance was favored by steeper slopes, a pattern also observed in several studies [115,123–125].

Soil erosion showed a significant role in irrigated woody crops, with a general negative tendency, meaning that NF occurred in areas showing scarcely erosive processes. According to previous research, the intensity of soil erosion is controlled by the vegetation cover and land uses, which is considered to be more critical than slope and precipitation intensity, even though the low-frequency and high-intensity precipitation extreme events are generally responsible for soil erosion [126,127]. The revegetation process after the land abandonment in mountain areas during the 20th century resulted in a reduction in soil erosion, whereas sheet erosion, piping, or gullying affected abandoned crop fields in semi-arid contexts [128,129]. This driver has been fairly well studied in LC change analysis, such as by Bakker et al. [130,131], where the authors found soil erosion as an important driver of land use changes, for instance, in agricultural de-intensification processes favoring the reduction in erosion and sediment movement.

Compared to BDF, from our results, socioeconomic drivers played a specific role in the Supramediterranean and the Southern Mesomediterranean BRs. NF appearance preferentially occurred in areas with a higher percentage of the population employed in building and service activities, as well as low/high (rainfed/irrigated woody crops)

densely populated locations, more prone to be abandoned. Similarly, Vidal-Macua et al. [19] identified crop abandonment in the central Pyrenees in areas with a higher proportion of population employed in the service and building activities, which are job opportunities generally outside the agriculture sector [7]. In the Sierra de Albarracín (Spain), Melendez-Pastor et al. [132] found a clear reduction in the population employed in the primary sector, stability in the secondary, and a significant increase in the tertiary sector related to the promotion of rural tourism.

In the case of new NEF from crop abandonment processes, the distance to provincial capitals, forests, and secondary roads predominated in all the BRs involved. Moreover, the number of holdings and the livestock units dominated in the southern region, and the distance to the hydrographic network dominated in the northern region. Regarding the spatio-temporal behavior, new NEF from crops appeared in the Northern and Southern Mesomediterranean BRs, areas characterized by dry conditions, where NEF species (e.g., *Pinus halepensis* Mill., *Pinus pinaster* Aiton, *Pinus pinea* L., and *Pinus nigra* J.F.Arnold) are better adapted to lower water requirements.

Remoteness played a significant role through the distance to provincial capitals (mainly) and the distance to roads, both with a positive tendency, i.e., a larger distance away from capital cities and roads signalled a higher likelihood of croplands being abandoned, as discussed in other works [30]. The proximity to pre-existing forests showed lower importance than in the case of new BDF and BEF.

The main topoclimatic driver of new NEF from crop abandonment was precipitation, with irregular (positive and negative) trends along BRs. Thus, in the Southern Mesomediterranean, the V-shape indicates a non-linear pattern related to occurrences in the plain areas (lower precipitation) and the BRs' upper limit (higher precipitation). Finally, soil erosion played a significant role in the IWC category (similar to new BEF), with a clear negative tendency, meaning that NF was again favored in areas showing scarcely erosive processes. Thus, spontaneous vegetation (meadow, pastures) can promote low erosive situations and act as protection cover in humid conditions.

Compared to BDF and BEF, socioeconomic drivers were significant in the Southern Mesomediterranean BR, where new NEF appearance was more prone in areas with a low number of holdings. This fact is interpreted as the lower availability of agriculture holdings in the upper limit of the BR, far from provincial capitals and main roads. In addition, remoteness and climatic constraints reduce the productivity of the land, increased by uncertainty in the regularity of rainfall, making farmers more likely to make decisions aimed at abandoning land [11,119,122]. Finally, a positive trend related to livestock units has been observed, a totally new contribution up to our knowledge.

4.2.2. Drivers of Forestation from Grasslands

Studies of forest expansion in mountainous regions are numerous, and there are plenty of examples which consider the whole European ambit [10,31,133,134], as well as regional studies in Albania and Romania [33], Colombia [69], Portugal [135], Spain [19,57,132,136], Russia [40], or Slovakia [112].

According to our results, the appearance of new BDF from grasslands was closely related to the proximity to forested areas, in addition to topoclimatic drivers such as temperature, solar radiation and precipitation, and distance drivers (such as the distance to provincial capitals). Regarding the spatio-temporal behavior, new BDF from grasslands appeared mainly in the more humid mountainous BRs, i.e., Montane, Coline, Supramediterranean, and Southern Mesomediterranean. The proximity to forested areas was the main driver in the Montane and Supramediterranean BRs and secondary in the others, indicating a homogenization and fulfilling process within the forested patches or along their edges, enhanced by seed dispersal triggering the early stages of natural succession [109]. This driver also was considered in other research works [7,30,114,115].

The main topoclimatic driver was temperature, showing high importance and a decreasing negative tendency in the Southern Mesomediterranean region, as well as moderate

importance and non-linear (A-shape) tendency in the Supramediterranean and Montane. Furthermore, precipitation appeared with temperature and showed a negative trend in the Montane BR and a positive trend in others. Moreover, a negative tendency in the solar radiation was generally observed, in addition to steeper slopes in the Montane and Coline BRs, which was also observed in previous research [115,123–125]. Lower solar radiation rates and humid conditions were also reported by Vidal-Macua et al. [4] for this LC dynamic, and Borda-Niño et al. [66] found the proximity to forests and slope as the main factors which can positively influence forest regrowth. In the Supramediterranean, higher precipitation and lower solar radiation favored the new BDF appearance, which is in line with Diaz-Delgado et al. [137], finding a significant negative correlation between the vegetation recovery (from fire disturbance) and solar radiation and a positive correlation with precipitation. Furthermore, Pérez-Luque et al. [138] analyzed *Quercus pyrenaica* colonization over abandoned cropland in the Sierra Nevada mountain range (Spain) in the rear edge of their distribution and near mature forest on mainly southern-oriented hillsides.

Remoteness has been considered a primary driver of NF associated with farmland abandonment and subsequent natural succession. In our results, remoteness indicators were mainly represented by the distance to provincial capitals, urban settlements, and secondarily main roads. Thus, new BDF from grasslands were generally more likely at a shorter distance to them in all BRs, except for the Montane region at a higher distance to provincial capitals. Similarly, farmlands located close to provincial capitals were more likely to be abandoned in the Polish Carpathians [7], a process explained by new job opportunities outside of the agricultural sector or even by the pressure to change agrarian land use in the suburban areas for residential promotion [139]. Similarly, other studies found forest and shrubland regeneration near roads and urban sectors, where more off-farm opportunities in the vicinity of roads can occur [114,140].

The structure of agricultural holdings played a secondary role in the Southern Mesomediterranean BR. In this context, NFs were favored in areas with a lower number of holdings on the limit with the Supramediterranean region, which coincided with the patterns observed in new BDF from rainfed woody crops. The similarity in patterns and spatial context suggest that crop fields abandoned at different ages coexist in this area, as grasslands signal the decay of tillage works and the initial natural succession process.

The appearance of new BEF from grasslands was associated with topoclimatic drivers, such as precipitation, temperature, and solar radiation, as well as distance drivers, such as the proximity to forested areas and the distance to provincial capitals. Regarding the spatio-temporal behavior, new BEF from grasslands appeared with lower density in the Montane and Coline and with more intensity in the Supramediterranean and Southern Mesomediterranean BRs, as was initially expected compared to BDF, due to the adaptability of broadleaf evergreen species (*Quercus ilex sensu lato*), through their high water-use efficiency, to drier conditions.

The main topoclimatic driving forces were precipitation, temperature, and solar radiation, showing different importance and patterns. For example, new BEF from grasslands in the Montane region were favored by higher temperature, lower precipitation, and solar radiation on steep slopes, which denote NFs establishing at lower altitudes on steep hillsides with lower humidity conditions. Similarly, these patterns were observed in the Coline BR but with a positive solar radiation tendency, where water availability is less restricted. However, temperature (together with precipitation) showed opposite patterns in the Supramediterranean and Southern Mesomediterranean BRs, with positive and negative tendencies, respectively.

In our results, remoteness was represented by the distance to provincial capitals. Thus, new BEF from grasslands were more likely to be closer to and further from the main provincial capitals, in the mountainous regions, i.e., the Montane and Supramediterranean. This double pattern can be associated with the pressure of change agrarian land use close to main urban areas [139] and related to the declining agricultural activities and the land abandonment of less productive and remote land fields [110,141]. Furthermore, in the

Southern Mesomediterranean, two temporal patterns were observed (Figure S7b3). In the first period, the new BEF from grasslands predominantly were further from provincial capitals, while in the second period, they were closer to them. This can be interpreted as a first wave of land abandonment process mainly in the high lands, and a second wave in lowlands closer to main capitals, which coincided with the temporal pattern of temperature, showing an increase in the mean temperature (lower altitude) in the second period.

Indeed, regarding the structure of agricultural holdings, a negative tendency in the livestock units (and the number of holdings) was observed in the Supramediterranean BR. This pattern is in line with the de-intensification of agricultural activities (livestock grazing reduction and cropland abandonment) and the forest expansion process in mountainous areas identified in previous research works [12,141,142].

Grasslands' successional dynamics towards NEF showed an intensive temporal dynamism. New NEF from grasslands were related to proximity to forested areas, as well as topoclimatic drivers (such as precipitation, slope, and temperature) and distance drivers (such as the distance to provincial capitals). Most of the occurrences were in the Montane, Supramediterranean, and the Southern Mesomediterranean BRs, with the last two being the most dynamic between periods. Similarly to BDF and BEF, the proximity to pre-existing forests was significant for new NEF from grasslands, especially in the Montane and Supramediterranean, and secondary in the Southern Mesomediterranean BRs.

Regarding proximity to forests, previous studies in the central Pyrenees (Spain) found that the tree line remained almost static, while the forest patch density increased in a context of climate warming and LC change [143,144]. Thus, areas near forests and declining grazing pressure have promoted natural succession dynamics in the central Pyrenees. In the Urbión Mountains (Iberian System, Spain), Sanjuán et al. [142] analyzed a subalpine belt affected by intense deforestation, leading pastures for grazing since the middle of the past century. Subsequently, declining livestock pressure and the depopulation process resulted in the encroachment of shrublands and the expansion of conifer forests at the expense of grasslands and shrublands.

Concerning topoclimatic drivers, slope steepness and lower solar radiation enhanced the likelihood of conversion from grasslands to forests, in line with previous research in mountainous areas [113]. Furthermore, precipitation showed a negative tendency in the Montane and a positive tendency in the Supramediterranean BR, suggesting lower humidity requirements for new NEF to be established in the Montane but higher humidity requirements in the Supramediterranean and Southern Mesomediterranean regions according to the BR's range of values. Remoteness in the form of the distance to urban settlements and the distance to provincial capitals showed a generally positive trend, in line with the main drivers of the extensification dynamics found by Pazúr et al. [30].

Furthermore, our results showed that drivers in the Supramediterranean BR evolved towards socioeconomic drivers during the second period, with laboring in industry, utilized agricultural area, and distance to provincial capitals being the main drivers. This pattern suggested a lower contribution of the distance to forests, distance to urban settlements, and solar radiation during the second period, allowing socioeconomic drivers to appear. In contrast, the Southern Mesomediterranean region was related to the distances and socioeconomic drivers, evolving during the second period to topoclimatic driving forces. This was interpreted as the larger contribution of remoteness and socioeconomic drivers in the highlands during the first period and topoclimatic in the lowlands in the second.

4.2.3. Drivers of Forestation from Shrublands

Studies of forest expansion associated with land abandonment and natural succession analyzing forest encroachment are numerous, but are also specifically limited for shrublands [4,41,114,124,142,145,146].

According to our results, the appearance of new BDF from shrublands was related to topoclimatic drivers (such as precipitation, temperature, and solar radiation) and distance drivers (such as the distance to forests and distance to provincial capitals). Regarding the

spatio-temporal behavior, new BDF from shrublands mainly appeared in the mountainous BRs, i.e., the Montane and Supramediterranean.

The main topoclimatic drivers were precipitation and temperature, and secondarily solar radiation. In the Montane BR, topoclimatic drivers were the main drivers; precipitation showed a positive tendency, while a negative tendency was observed for temperature and solar radiation. This pattern suggests that new BDF from shrublands was favored by high precipitation, low radiation, and temperature (higher altitude). This binomial of low temperature and low radiation was in line with higher altitude (lower temperature) and lower radiation, as found by Vidal-Macua et al. [4] in a similar geographic context. Furthermore, these patterns were maintained in the second period, suggesting similarities in climatic drivers over time. Meanwhile, in the Supramediterranean BR, temperature and precipitation followed a non-linear tendency (A-shape) in both periods, suggesting that the most likely conditions are maximized on shady hillsides with temperature and precipitation constraints. Complementarily, the occurrence of medium-term droughts (6-month SPEI timescale) of at least six consecutive months was negatively related in the first period, suggesting a lower tolerance of BDF species to drought.

The proximity to forested areas was the main driver in the Supramediterranean BR and the secondary driver in the Montane during the first period, indicating the homogenization and fulfilling process in forest patches and along their edges, even further during the second period. This driver was considered in previous research works [7,30,114,115].

Remoteness was represented by the distance to provincial capitals and to urban settlements, generally denoting a positive tendency in the Montane BR. However, the tendency was negative in the Supramediterranean, indicating more likely conditions in areas near urbanized areas, which coincide with research works focusing on the land abandonment process [7,41,43]. Furthermore, these patterns were similar to those observed in the case of BDF from grasslands.

The appearance of new BEF from shrublands was associated with distance drivers, such as the distance to forests and to provincial capitals, in addition to topoclimatic factors, such as precipitation, solar radiation, and temperature. Regarding the spatio-temporal behavior, new BEF from shrublands appeared more densely in the Montane, Supramediterranean, and Southern Mesomediterranean BRs, and with lower density in the Northern Mesomediterranean.

The distance to forests was the main driver in all BRs except in the Southern Mesomediterranean, with topoclimatic drivers predominating. It showed a negative trend in all cases. A general decrease in the relative importance in the second period suggests that the forest completion and fulfilling process observed in the first period continued at a greater distance in the second. Woody encroachment due to the expansion of forests and shrublands (at the expense of grasslands) has been reported in mountain areas, confirming densification and expansion through the tree line [147–149].

Remoteness was represented by the distance to urban settlements in the first period and by the distance to provincial capitals in the second. In the Montane and Northern Mesomediterranean BRs, the most suitable conditions occurred far from urban areas and near forested areas in both periods. However, the opposite pattern was found in Palmero et al. [105] for forest expansion in temperate and Mediterranean regions on a European scale. Moreover, a negative trend was observed in the Supramediterranean region for the distance to provincial capitals, which agrees with previous research [114]. Furthermore, NFs in the proximity to provincial capitals can be explained by the increase in new job opportunities outside the agricultural sector or by the pressure to change agrarian land use in the suburban areas for residential promotion in agricultural abandoned areas [139]. Farmland abandonment probability increases when employment redirection to other sectors occurs [8].

The main topoclimatic drivers were precipitation, solar radiation, and temperature with different tendencies in BRs. In the Montane, precipitation followed a positive trend, while temperature and solar radiation were negative. This pattern suggests that new BEF

from shrublands was favored by higher precipitation and lower radiation and temperature (higher altitude). Binomial low temperature and low radiation were both in line with higher altitude (lower temperature) and lower radiation, as reported by Vidal-Macua et al. [4] in a similar geographic context. Furthermore, these patterns were maintained in the second period, suggesting similarities in climatic drivers over time. Meanwhile, in the Supramediterranean BR, precipitation and solar radiation followed a negative tendency and a positive one for temperature, suggesting that the most likely conditions are maximized at a lower altitude and on shady hillsides with less water availability, as sclerophyllous forests are adapted to lower water requirements in this region. These patterns are consistent with previous studies analyzing land abandonment processes and natural succession at lower altitudes on north-oriented hillsides [150]. In the Southern Mesomediterranean BRs, temperature and solar radiation followed a negative tendency and positive one for precipitation, which coincides with the drivers' pattern in the southern Landsat scene spatial context analyzed by Vidal-Macua et al. [4]. It suggests that the most likely conditions occurred at higher altitudes, on shady hillsides with less water availability in the BR, corresponding to areas with lower slope values in the proximity to forested mountainous areas close to the upper BR limit (Supramediterranean).

Shrublands' successional dynamics towards NEF were related to the proximity to forested areas, topoclimatic drivers (such as precipitation, solar radiation, and slope), and accessibility drivers (such as the distance to provincial capitals). New NEF occurrences dominated in all BRs except for the Coline. Similarly to BEF, in the case of new NEF from shrublands, the proximity to forested areas played a major role, especially in the Montane, Supramediterranean, and Northern Mesomediterranean BRs. This pattern coincides with a homogenization, fulfilment, and expansion of the forested areas. Woody encroachment due to the expansion of forests and shrublands has been reported in mountain areas, confirming densification and expansion through the tree line [147–149].

Remoteness was represented by the distance to provincial capitals and urban settlements. The most suitable conditions occurred far from urban areas in both periods in the Montane, Supramediterranean, and Southern Mesomediterranean BRs. However, the opposite pattern of forest expansion was observed on the European scale [105]. On the other hand, the main topoclimatic drivers were precipitation, solar radiation with different tendencies in BRs, and the slope with an overall negative trend.

In Montane areas, precipitation followed a non-linear tendency (a general positive tendency falling at high precipitation values) and a negative trend for solar radiation and temperature. Thus, it suggests that NEF from shrublands were favored at lower and higher humidity regimes (up to a limit) on shady hillsides at higher altitudes, while NEF species (*Pinus sylvestris, P. nigra*) are better adapted. These findings agree with Vidal-Macua et al. [4] in the Pyrenean context, where transitions to coniferous forests were favored at higher altitudes (lower temperature) and a lower radiation.

In the Supramediterranean context, precipitation followed a positive tendency, a negative for slope. The results suggest that the higher precipitation rates, the lower slopes, and the absence of solar radiation as a driver promoted new NEF (*Pinus nigra, P. sylvestris*) in more plain areas at higher altitudes, where the higher precipitation occurs. Melendez-Pastor et al. [132] identified a clear forest regeneration (mainly pine forest) in the Sierra de Albarracín (North Iberian System, Spain), at the expense of mainly shrublands and farming areas for the first period of analysis. Furthermore, Sanjuán et al. [142] found clear patterns of shrublands and clear forests evolving towards dense forests of *Pinus sylvestris*, in south-facing and stepped slopes in the Urbión Mountains (Iberic System, Spain).

Similarly, in the Southern Mesomediterranean, precipitation followed a non-linear tendency denoting higher likelihood at low/high precipitation values according to dominant species. Indeed, a negative trend in slope and solar radiation, suggesting that new NEF appearances took place in the more xeric (*Pinus halepensis*) and humid (*P. pinaster, P. nigra*) context of the BR, was favored by shady conditions. These findings agree with the lower solar radiation and soil moisture dependence in the transition of shrublands to

conifers in a similar context of analysis analyzed by Vidal-Macua et al. [4]. Furthermore, medium-term drought occurrences (6-month SPEI timescale) of at least six consecutive months was negatively related to shrubland encroachment to new NEF in the second period, denoting better conifer species plasticity to growth in lower drought conditions.

Lastly, in the Thermomediterranean BR, precipitation and slope followed a negative tendency, together with a negative trend in long-term drought occurrences (24-month SPEI timescale) over at least three consecutive months. Unexpectedly, these results suggest that lower precipitation rates favored new NEF forests on low-sloped hillsides, which, to a certain extent, could promote drought-tolerant conifers species (*Pinus halepensis*) adapted to arid climatic conditions. This pattern agrees with local studies in the Murcia region, where land abandonment processes and related successional dynamics were negatively associated with precipitation [119]. Therefore, climate factors and water availability, specifically in semiarid regions, determine land productivity (even irrigated plots, depending partly on precipitation) and increase the uncertainty about the rain irregularity [11], affecting cropland and natural vegetation productivity. Moreover, Vidal-Macua et al. [19] found a positive relation between crop abandonment and medium-term droughts occurrences (6-month SPEI timescale) over at least 7–8 months in the central Ebro basin.

4.3. Answers to the Hypotheses

According to our first hypothesis, NFs are mainly associated with successional dynamics, i.e., shrublands and grasslands, and secondarily with crop abandonment processes, i.e., the main sources along the transect. Natural/semi-natural source categories predominate in absolute values along the transect. In relative terms, 17.2% and 7.52% of natural surfaces, in addition to 2.86% and 0.69% of croplands, evolved towards NF in the Eurosiberian and Mediterranean biogeographic regions, respectively. The transect also revealed contrasting driving forces (topoclimatic and socioeconomic) throughout space and time. In the Eurosiberian area, distance to forests was selected in 20.0% of cases, solar radiation in 17.8% and precipitation in 15.6% in the first period, while the distance to provincial capitals was selected in 17.5% of cases and precipitation and slope in 15.0% in the second period. Only on one occasion were socioeconomic drivers selected in the Eurosiberian context. On the contrary, the distance to forests in the Mediterranean area was selected in 19.2% of cases, precipitation in 14.4% and temperature in 11.2% in the first period, while the same drivers showed similar values in the second. Remarkably, socioeconomic drivers were selected in 7.2% and 6.7% of the first and second period cases in the Mediterranean context, respectively.

According to our second hypothesis, the distance to provincial capitals and urban settlements explained NF occurrence in remote territories (the longer the distance, the more likelihood of NF appearance). Moreover, two factors constraining the productivity and mechanization of traditional farming practices triggered rural abandonment and subsequent forest expansion processes, representing an increase in employment outside agriculture (industry and service activities) and small agricultural areas (small and fragmented, less competitive, and economically viable fields), especially in depopulated regions and regions with steeper slopes [17,141]. Spatially, the forestation processes associated with agricultural land abandonment were most intensive in mountain regions (i.e., Montane and Supramediterranean BRs) and in the piedmont transitions to plain areas along large hydrographic basins (i.e., Southern and Northern Mesomediterranean), especially for new BEF and NEF groups. These constraints make mountainous areas (Pyrenees, Iberian, and Baetic mountain systems) less competitive, but more susceptible to a higher rate of agricultural abandonment in the future [151].

Regarding the third hypothesis, NF appearance depicted different temporal patterns (besides changes in drivers' explanatory power, order, and drops). Generally speaking, the appearance of NF in relative terms was more extensive in the Eurosiberian context in the P1, being more extensive in the Mediterranean in the P2. During the P1, NFs were closely related to previously forested areas (consolidation, patch completion process) and further

away in the P2, during which the explanatory power of the driver decreased. Furthermore, soil erosion showed a clear decrease in importance in the P2. Grasslands denoted a higher temporal variability in the Eurosiberian context for BDF/BEF (increasing the explanatory power of the number of holdings in the P2) and especially in the Mediterranean for NEF (the utilized agricultural area drop as a driver, and its appearance in neighboring BRs between periods). Crop categories (rainfed and irrigated) in new BEF were related to the workers in the building/service sectors, the utilized agricultural area in the P1, and the population density in the P2. In the case of rainfed and irrigated crops to new NEF, the number of holdings and the livestock units decreased in importance in the P2.

4.4. Future Research Lines

Several aspects of our results require additional research to elucidate new questions arising from this work. (i) As we have shown, we have covered the sample size used for modeling, representativeness, etc., with full attention; nevertheless, those aspects could be explored in depth, including the design of testbeds expanding different sample structures, LC changes, and autocorrelation levels in the sample tested using BRT models. (ii) The bias reduction in the absence samples should also be analyzed thoroughly in the context of extensive and widely spread sample locations, as well as scarce and localized presence–absence sample locations. (iii) This study provides the basis to investigate new forests in detail over more specific regions in the transect; for instance, in the transition between the Supramediterranean and the Southern Mesomediterranean BRs, topoclimatic and socioeconomics drivers may have conditioned new forests due to their proximity to big cities and capitals. Furthermore, the Iberian range, the Pyrenees, and the Sierra Nevada mountain ranges are contrasting biogeographical regions with high interest as climate laboratories and areas in the future, affected by land abandonment processes and successional dynamics. (iv) The role of drought, together with other climate drivers, require a more detailed analysis in order to elucidate spatio-temporal patterns along the transect.

5. Conclusions

This research aimed to apply a consistent and rigorous methodology to extract and assess NF occurrences over a regional gradient in the Iberian Peninsula, focusing on crop abandonment and successional dynamics. According to our methodological approach, NF extraction benefits from coherent spatio-temporal training areas used for map production (high accuracy maps), the application of uncertainty filtering (higher model performance), the presence–absence selection according to BRs, the absence sampling bias reduction strategy, and a three step modeling approach. LC change analysis was based on 30 potential drivers, both physical and socioeconomic. Our main contributions shed light on three main aspects: thematic, spatial, and temporal.

Regarding thematic aspects, this study uses high-quality remote sensing maps with detailed legends to provide insights on driving forces that explain the LC trajectory, i.e., from the different source categories to the target forest categories. We summarize the main findings below.

- Driving forces involved in new BDF. (i) From crop categories: distance to the hydrographic network, distance to forests, distance to provincial capitals, precipitation, and distance to urban settlements. Unexpectedly, remoteness through the distance to roads little explained crop abandonment. (ii) From grasslands: distance to forests, temperature, solar radiation, precipitation, and distance to provincial capitals. The proximity to forests was the main driver in humid mountainous regions. (iii) From shrublands: precipitation, temperature, distance to forests, solar radiation, and distance to provincial capitals. Topoclimatic (water availability) drivers were the main ones in humid mountainous regions.
- Driving forces involved in new BEF. (i) From crop categories: distance to forests, temperature, soil erosion, precipitation, and slope. Remoteness was hardly relevant, and socioeconomic drivers (population density, workers in building/service sectors)

played a secondary role in the Supramediterranean and Southern Mesomediterranean BRs. (ii) From grasslands: precipitation, distance to forests, distance to provincial capitals, temperature, and solar radiation. Lower humidity conditions at lower altitudes on steep hillsides favored the transition. (iii) From shrublands: distance to forests, precipitation, solar radiation, temperature, and distance to provincial capitals. The proximity to forests showed a significant forest encroachment and expansion process in the mountainous regions.

- Driving forces involved in new NEF. (i) From crop categories: distance to provincial capitals, the number of holdings, distance to forests, distance to main roads, and precipitation. Remoteness and socioeconomic drivers (number of holdings, livestock units and the utilized agricultural area) played a secondary role in the Southern Mesomediterranean region, and an unexpected positive trend was related to livestock units. (ii) From grasslands: distance to forests, precipitation, slope, distance to provincial capitals, and temperature. The proximity to forests showed a densification and expansion in mountainous regions, associated with lower humidity requirements and slope steepness. (iii) From shrublands: distance to forests, precipitation, solar radiation, slope, and distance to provincial capitals. In terms of climatic conditions, forest densification and expansion occurred from the humid northern conditions (*Pinus sylvestris*, *P. nigra*) to the more xeric southern conditions (*P. halepensis*), with the latter being unexpectedly favored by lower precipitation rates.

Concerning spatial patterns, Supramediterranean and Mesomediterranean BRs were the areas of higher NF appearance regarding cropland abandonment and natural succession dynamics. This is not surprising as they are the both regions with more NF occurrences in first and second periods (Table 3). Nevertheless, in relative terms, it was in the Thermomediterranean and Northern Mesomediterranean BRs where the NF increase was more significant regarding the previously forested area in the region. Rural depopulation was a widespread process in most of the Mediterranean fringe, affecting mainly mountainous areas. In our study ambit, most NF occurrences took place in the Supramediterranean BR, which gathers a large proportion of municipalities with a clear population decline; hence, leading to the abandonment of traditional agricultural activities, crops, and pastures activities. Natural/semi-natural succession mainly occurred in the Montane and Supramediterranean BRs due to natural successions derived in part from abandoned land and natural/semi-natural dynamics in the proximity to previously mountainous forested areas. Overall, in the Eurosiberian context, precipitation appeared in 15.3% of cases, solar radiation in 15.2%, distance to forests in 14.1%, slope in 14.0%, and temperature in 11.8%. In the Mediterranean context, precipitation appeared in 16.6% of cases, distance to forests in 14.8%, solar radiation in 11.7%, temperature in 10.7%, and slope in 9.7%.

Regarding temporal resolution, during the second analysis period, the rate of change (area of change) was slightly superior to the first one, and consequently, a higher number of dynamics was evaluated. Nevertheless, differences between regions were observed. During the first period, NFs were related to a fulfilling process (encroachment and densification) in the open spaces within forested areas (combination of forests and grasslands in mosaic landscape), while expanding throughout their limits. Furthermore, abandoned crop fields in the proximity to forests were annexed to pre-established forests in more remote locations. In this period, the distance to forests appeared in 19.4% of cases, precipitation in 14.7%, temperature in 11.8%, solar radiation in 10.6%, and slope in 9.4%. In the second period, the patterns show a significant forest expansion process from the original patches and to a greater distance (throughout the upper and lower forests limits), creating new forest nuclei in areas where shrublands and grasslands dominated, like in lowlands close to human settlements. In the case of new broadleaf deciduous forests, this pattern was notably located in areas close to the hydrographic network. In this period, the distance to forests appeared in 16.1% of cases, precipitation in 14.6%, distance to provincial capitals in 12.2%, temperature in 10.2%, and distance to the hydrographic network in 10.2%.

In summary, considering all forest groups, the main drivers that have conditioned NF occurrence in the last thirty years have also been associated with topoclimatic variables (i.e., temperature, precipitation, solar radiation, and slope), as well as accessibility and distance drivers (distance to forests the hydrography network, capitals, and urban settlements). In addition, other predictors, as socioeconomic drivers and climatic water availability (drought/water oversupply), have played a secondary role at more specific BRs and temporal resolution. The rate of change was slightly higher during the second period of analysis (2002–2017), with a higher number of NF dynamics evaluated. Because of their considerable extension, Supramediterranean, Southern, and Northern Mesomediterranean BRs gathered most of the NF dynamics and changed areas in absolute terms, while the Thermomediterranean and the Northern Mesomediterranean gathered the most dynamics in relative terms. In our opinion, this study will contribute to the understanding of forest dynamics in the Iberian Peninsula since it has been performed in light of a representative transect of the entire area after a rigorous methodological treatment of high-detail data.

References

1. FAO. *Global Forest Resources Assessment 2020: Main Report*; FAO: Rome, Italy, 2020; ISBN 978-92-5-132974-0.
2. Keenan, R.J.; Reams, G.A.; Achard, F.; de Freitas, J.V.; Grainger, A.; Lindquist, E. Dynamics of global forest area: Results from the FAO Global Forest Resources Assessment 2015. *For. Ecol. Manag.* **2015**, *352*, 9–20. [CrossRef]
3. Potapov, P.; Hansen, M.C.; Stehman, S.V.; Pittman, K.; Turubanova, S. Gross forest cover loss in temperate forests: Biome-wide monitoring results using MODIS and Landsat data. *J. Appl. Remote Sens.* **2009**, *3*, 1–23. [CrossRef]
4. Vidal-Macua, J.J.; Ninyerola, M.; Zabala, A.; Domingo-Marimon, C.; Pons, X. Factors affecting forest dynamics in the Iberian Peninsula from 1987 to 2012. The role of topography and drought. *For. Ecol. Manag.* **2017**, *406*, 290–306. [CrossRef]
5. Jones, N.; de Graaff, J.; Rodrigo, I.; Duarte, F. Historical review of land use changes in Portugal (before and after EU integration in 1986) and their implications for land degradation and conservation, with a focus on Centro and Alentejo regions. *Appl. Geogr.* **2011**, *31*, 1036–1048. [CrossRef]
6. Weissteiner, C.J.; Boschetti, M.; Böttcher, K.; Carrara, P.; Bordogna, G.; Brivio, P.A. Spatial explicit assessment of rural land abandonment in the Mediterranean area. *Glob. Planet. Chang.* **2011**, *79*, 20–36. [CrossRef]
7. Kolecka, N.; Kozak, J.; Kaim, D.; Dobosz, M.; Ostafin, K.; Ostapowicz, K.; Wężyk, P.; Price, B. Understanding farmland abandonment in the Polish Carpathians. *Appl. Geogr.* **2017**, *88*, 62–72. [CrossRef]
8. Macdonald, D.; Crabtree, J.R.; Wiesinger, G.; Dax, T.; Stamou, N.; Fleury, P.; Gutierrez Lazpita, J.; Gibon, A. Agricultural abandonment in mountain areas of Europe: Environmental consequences and policy response. *J. Environ. Manag.* **2000**, *59*, 47–69. [CrossRef]
9. Regos, A.; Ninyerola, M.; Moré, G.; Pons, X. Linking land cover dynamics with driving forces in mountain landscape of the Northwestern Iberian Peninsula. *Int. J. Appl. Earth Obs. Geoinf.* **2015**, *38*, 1–14. [CrossRef]
10. Lasanta, T.; Arnáez, J.; Pascual, N.; Ruiz-Flaño, P.; Errea, M.P.; Lana-Renault, N. Space–time process and drivers of land abandonment in Europe. *Catena* **2017**, *149*, 810–823. [CrossRef]
11. Lasanta, T.; Nadal-Romero, E.; Khorchani, M.; Romero-Díaz, A. Una revisión sobre las tierras abandonadas en España: De los paisajes locales a las estrategias globales de gestion. *Cuad. Investig. Geográfica* **2021**, *47*, 477–521. [CrossRef]
12. Serra, P.; Vera, A.; Tulla, A.F.; Salvati, L. Beyond urban–rural dichotomy: Exploring socioeconomic and land-use processes of change in Spain (1991–2011). *Appl. Geogr.* **2014**, *55*, 71–81. [CrossRef]
13. Ninyerola, M.; Pons, X.; Roure, J.M. A methodological approach of climatological modelling of air temperature and precipitation through GIS techniques. *Int. J. Clim.* **2000**, *20*, 1823–1841. [CrossRef]
14. Hill, J.; Stellmes, M.; Udelhoven, T.; Röder, A.; Sommer, S. Mediterranean desertification and land degradation: Mapping related land use change syndromes based on satellite observations. *Glob. Planet. Chang.* **2008**, *64*, 146–157. [CrossRef]
15. Del Barrio, G.; Puigdefábregas, J.; Sanjuán, M.E.; Stellmes, M.; Ruiz, A. Assessment and monitoring of land condition in the Iberian Peninsula, 1989–2000. *Remote Sens. Environ.* **2010**, *114*, 1817–1832. [CrossRef]
16. Vilà-Cabrera, A.; Espelta, J.M.; Vayreda, J.; Pino, J. "New Forests" from the Twentieth Century are a Relevant Contribution for C Storage in the Iberian Peninsula. *Ecosystems* **2017**, *20*, 130–143. [CrossRef]
17. Serra, P.; Pons, X.; Saurí, D. Land-cover and land-use change in a Mediterranean landscape: A spatial analysis of driving forces integrating biophysical and human factors. *Appl. Geogr.* **2008**, *28*, 189–209. [CrossRef]
18. Bielsa, I.; Pons, X.; Bunce, B. Agricultural Abandonment in the North Eastern Iberian Peninsula: The Use of Basic Landscape Metrics to Support Planning. *J. Environ. Plan. Manag.* **2005**, *48*, 85–102. [CrossRef]
19. Vidal-Macua, J.J.; Ninyerola, M.; Zabala, A.; Domingo-Marimon, C.; Gonzalez-Guerrero, O.; Pons, X. Environmental and socioeconomic factors of abandonment of rainfed and irrigated crops in northeast Spain. *Appl. Geogr.* **2018**, *90*, 155–174. [CrossRef]
20. Gelabert, P.J.; Rodrigues, M.; de la Riva, J.; Ameztegui, A.; Sebastià, M.; Vega-Garcia, C. LandTrendr smoothed spectral profiles enhance woody encroachment monitoring. *Remote Sens. Environ.* **2021**, *262*, 112521. [CrossRef]
21. Palmero-Iniesta, M.; Espelta, J.M.; Padial-Iglesias, M.; Gonzàlez-Guerrero, Ò.; Pesquer, L.; Domingo-Marimon, C.; Ninyerola, M.; Pons, X.; Pino, J. The Role of Recent (1985–2014) Patterns of Land Abandonment and Environmental Factors in the Establishment and Growth of Secondary Forests in the Iberian Peninsula. *Land* **2021**, *10*, 817. [CrossRef]
22. Mantovani, A.C.D.M.; Setzer, A.W. Deforestation detection in the Amazon with an AVHRR-based system. *Int. J. Remote Sens.* **1997**, *18*, 273–286. [CrossRef]
23. Gonzalez-Hidalgo, J.C.; Peña-Angulo, D.; Brunetti, M.; Cortesi, N. Recent trend in temperature evolution in Spanish mainland (1951–2010): From warming to hiatus. *Int. J. Clim.* **2016**, *36*, 2405–2416. [CrossRef]
24. Pérez, F.F.; Boscolo, R. (Eds.) *Climate in Spain: Past, Present and Future; Regional Climate Change Assesment Report*; CLIVAR, Ministerio de Medio Ambiente y Medio Rural y Marino, Ministerio de Ciencia e Innovación (MICINN): Madrid, 2010; 83p, ISBN 978-84-614-8115-6.
25. del Río, S.; Herrero, L.; Fraile, R.; Penas, A. Spatial distribution of recent rainfall trends in Spain (1961–2006). *Int. J. Clim.* **2011**, *31*, 656–667. [CrossRef]
26. Acero, F.J.; Gallego, M.C.; Garcia, J.A. Multi-day rainfall trends over the Iberian Peninsula. *Theor. Appl. Climatol.* **2012**, *108*, 411–423. [CrossRef]

27. Vicente-Serrano, S.M.; Rodríguez-Camino, E.; Dominguez-Castro, F.; El Kenawy, A.; Azorín-Molina, C. An updated review on recent trends in observational surface atmospheric variables and their extremes over Spain. *Cuad. Investig. Geográfica* **2017**, *43*, 209–232. [CrossRef]

28. Sanchez-Lorenzo, A.; Calbó, J.; Wild, M. Global and diffuse solar radiation in Spain: Building a homogeneous dataset and assessing their trends. *Glob. Planet. Chang.* **2013**, *100*, 343–352. [CrossRef]

29. Gerard, F.; Petit, S.; Smith, G.; Thomson, A.; Brown, N.; Manchester, S.; Wadsworth, R.; Bugár, G.; Halada, L.; Bezák, P.; et al. Land cover change in Europe between 1950 and 2000 determined employing aerial photography. *Prog. Phys. Geogr. Earth Environ.* **2010**, *34*, 183–205. [CrossRef]

30. Pazúr, R.; Bolliger, J. Land changes in Slovakia: Past processes and future directions. *Appl. Geogr.* **2017**, *85*, 163–175. [CrossRef]

31. Hellwig, N.; Walz, A.; Markovic, D. Climatic and socioeconomic effects on land cover changes across Europe: Does protected area designation matter? *PLoS ONE* **2019**, *14*, e0219374. [CrossRef]

32. Stellmes, M.; Röder, A.; Udelhoven, T.; Hill, J. Mapping syndromes of land change in Spain with remote sensing time series, demographic and climatic data. *Land Use Policy* **2013**, *30*, 685–702. [CrossRef]

33. Müller, D.; Leitão, P.J.; Sikor, T. Comparing the determinants of cropland abandonment in Albania and Romania using boosted regression trees. *Agric. Syst.* **2013**, *117*, 66–77. [CrossRef]

34. de Espindola, G.M.; de Aguiar, A.P.D.; Pebesma, E.; Camara, G.; Fonseca, L. Agricultural land use dynamics in the Brazilian Amazon based on remote sensing and census data. *Appl. Geogr.* **2012**, *32*, 240–252. [CrossRef]

35. Kennedy, R.E.; Yang, Z.; Cohen, W.B. Detecting trends in forest disturbance and recovery using yearly Landsat time series: 1. LandTrendr—Temporal segmentation algorithms. *Remote Sens. Environ.* **2010**, *114*, 2897–2910. [CrossRef]

36. Zhu, Z.; Woodcock, C.E. Continuous change detection and classification of land cover using all available Landsat data. *Remote Sens. Environ.* **2014**, *144*, 152–171. [CrossRef]

37. Zhu, Z.; Woodcock, C.E.; Holden, C.; Yang, Z. Generating synthetic Landsat images based on all available Landsat data: Predicting Landsat surface reflectance at any given time. *Remote Sens. Environ.* **2015**, *162*, 67–83. [CrossRef]

38. Sun, B.; Robinson, D.T. Comparisons of Statistical Approaches for Modelling Land-Use Change. *Land* **2018**, *7*, 144. [CrossRef]

39. Muñoz, J.; Felicísimo, Á.M. Comparison of statistical methods commonly used in predictive modelling. *J. Veg. Sci.* **2004**, *15*, 285–292. [CrossRef]

40. Prishchepov, A.V.; Müller, D.; Dubinin, M.; Baumann, M.; Radeloff, V.C. Determinants of agricultural land abandonment in post-Soviet European Russia. *Land Use Policy* **2013**, *30*, 873–884. [CrossRef]

41. Díaz, G.I.; Nahuelhual, L.; Echeverría, C.; Marín, S. Drivers of land abandonment in Southern Chile and implications for landscape planning. *Landsc. Urban Plan.* **2011**, *99*, 207–217. [CrossRef]

42. Kosmas, C.; Kairis, O.; Karavitis, C.; Acikalin, S.; Alcalá, M.; Alfama, P.; Atlhopheng, J.; Barrera, J.; Belgacem, A.; Solé-Benet, A.; et al. An exploratory analysis of land abandonment drivers in areas prone to desertification. *Catena* **2015**, *128*, 252–261. [CrossRef]

43. Müller, D.; Munroe, D.K. Changing Rural Landscapes in Albania: Cropland Abandonment and Forest Clearing in the Postsocialist Transition. *Ann. Assoc. Am. Geogr.* **2008**, *98*, 855–876. [CrossRef]

44. Yee, T.W.; Mitchell, N.D. Generalized additive models in plant ecology. *J. Veg. Sci.* **1991**, *2*, 587–602. [CrossRef]

45. Pedersen, E.J.; Miller, D.L.; Simpson, G.L.; Ross, N. Hierarchical generalized additive models in ecology: An introduction with mgcv. *PeerJ* **2019**, *7*, e6876. [CrossRef]

46. Abdullah, A.Y.M.; Masrur, A.; Gani Adnan, M.S.; Al Baky, M.A.; Hassan, Q.K.; Dewan, A. Spatio-temporal Patterns of Land Use/Land Cover Change in the Heterogeneous Coastal Region of Bangladesh between 1990 and 2017. *Remote Sens.* **2019**, *11*, 790. [CrossRef]

47. Colin, B.; Clifford, S.; Wu, P.; Rathmanner, S.; Mengersen, K. Using Boosted Regression Trees and Remotely Sensed Data to Drive Decision-Making. *Open J. Stat.* **2017**, *07*, 859–875. [CrossRef]

48. Elith, J.; Leathwick, J.R.; Hastie, T. A working guide to boosted regression trees. *J. Anim. Ecol.* **2008**, *77*, 802–813. [CrossRef]

49. Gu, H.; Wang, J.; Ma, L.; Shang, Z.; Zhang, Q. Insights into the BRT (Boosted Regression Trees) Method in the Study of the Climate-Growth Relationship of Masson Pine in Subtropical China. *Forests* **2019**, *10*, 228. [CrossRef]

50. Fernández-Nogueira, D.; Corbelle-Rico, E. Land Use Changes in Iberian Peninsula 1990–2012. *Land* **2018**, *7*, 99. [CrossRef]

51. Rivas Martínez, S. Pisos bioclimáticos de España. *Lazaroa* **1983**, *5*, 33–43.

52. U.S. Geological Survey. EarthExplorer. Available online: https://earthexplorer.usgs.gov (accessed on 11 May 2018).

53. Pons, X. MiraMon. Geographic Information System and Remote Sensing Software. Centre de Recerca Ecològica i Aplicacions Forestals, CREAF. Bellaterra. 2004. Available online: https://www.miramon.cat/Index_usa.htm (accessed on 12 January 2022).

54. Padial-Iglesias, M.; Serra, P.; Ninyerola, M.; Pons, X. A Framework of Filtering Rules over Ground Truth Samples to Achieve Higher Accuracy in Land Cover Maps. *Remote Sens.* **2021**, *13*, 2662. [CrossRef]

55. Vidal-Macua, J.J.; Zabala, A.; Ninyerola, M.; Pons, X. Developing spatially and thematically detailed backdated maps for land cover studies. *Int. J. Digit. Earth* **2017**, *10*, 175–206. [CrossRef]

56. González-Guerrero, O.; Pons, X. The 2017 Land Use/Land Cover Map of Catalonia based on Sentinel-2 images and auxiliary data. *Revista Teledetección* **2020**, *55*, 81–92. [CrossRef]

57. Álvarez Martínez, J.-M.; Suárez-Seoane, S.; De Luis Calabuig, E. Modelling the risk of land cover change from environmental and socio-economic drivers in heterogeneous and changing landscapes: The role of uncertainty. *Landsc. Urban Plan.* **2011**, *101*, 108–119. [CrossRef]

58. Álvarez-Martínez, J.M.; Stoorvogel, J.J.; Suárez-Seoane, S.; de Luis Calabuig, E. Uncertainty analysis as a tool for refining land dynamics modelling on changing landscapes: A case study in a Spanish Natural Park. *Landsc. Ecol.* **2010**, *25*, 1385–1404. [CrossRef]

59. Ninyerola, M.; Pons, X.; Roure, J.M. Monthly precipitation mapping of the Iberian Peninsula using spatial interpolation tools implemented in a Geographic Information System. *Theor. Appl. Climatol.* **2007**, *89*, 195–209. [CrossRef]

60. Stokland, J.N.; Halvorsen, R.; Støa, B. Species distribution modelling—Effect of design and sample size of pseudo-absence observations. *Ecol. Model.* **2011**, *222*, 1800–1809. [CrossRef]

61. Moudrý, V.; Šímová, P. Influence of positional accuracy, sample size and scale on modelling species distributions: A review. *Int. J. Geogr. Inf. Sci.* **2012**, *26*, 2083–2095. [CrossRef]

62. Wisz, M.S.; Hijmans, R.J.; Li, J.; Peterson, A.T.; Graham, C.H.; Guisan, A.; NCEAS Predicting Species Distributions Working Group. Effects of sample size on the performance of species distribution models. *Divers. Distrib.* **2008**, *14*, 763–773. [CrossRef]

63. Stockwell, D.R.; Peterson, A.T. Effects of sample size on accuracy of species distribution models. *Ecol. Model.* **2002**, *148*, 1–13. [CrossRef]

64. Pazúr, R.; Lieskovský, J.; Bürgi, M.; Müller, D.; Lieskovský, T.; Zhang, Z.; Prischchepov, A.V. Abandonment and Recultivation of Agricultural Lands in Slovakia—Patterns and Determinants from the Past to the Future. *Land* **2020**, *9*, 316. [CrossRef]

65. Curtis, P.G.; Slay, C.M.; Harris, N.L.; Tyukavina, A.; Hansen, M.C. Classifying drivers of global forest loss. *Science* **2018**, *361*, 1108–1111. [CrossRef]

66. Borda-Niño, M.; Meli, P.; Brancalion, P.H.S. Drivers of tropical forest cover increase: A systematic review. *Land Degrad. Dev.* **2019**, *31*, 1366–1379. [CrossRef]

67. Pugh, T.A.M.; Lindeskog, M.; Smith, B.; Poulter, B.; Arneth, A.; Haverd, V.; Calle, L. Role of forest regrowth in global carbon sink dynamics. *Proc. Natl. Acad. Sci. USA* **2019**, *116*, 4382–4387. [CrossRef]

68. Kondo, M.; Ichii, K.; Patra, P.K.; Poulter, B.; Calle, L.; Koven, C.; Pugh, T.A.M.; Kato, E.; Harper, A.; Zaehle, S.; et al. Plant Regrowth as a Driver of Recent Enhancement of Terrestrial CO_2 Uptake. *Geophys. Res. Lett.* **2018**, *45*, 4820–4830. [CrossRef]

69. Rubiano, K.; Clerici, N.; Norden, N.; Etter, A. Secondary Forest and Shrubland Dynamics in a Highly Transformed Landscape in the Northern Andes of Colombia (1985–2015). *Forests* **2017**, *8*, 216. [CrossRef]

70. Borda-Niño, M.; Ceccon, E.; Meli, P.; Hernández-Muciño, D.; Mas, J.-F.; Brancalion, P.H. Integrating farmers' decisions on the assessment of forest regeneration drivers in a rural landscape of Southeastern Brazil. *Perspect. Ecol. Conserv.* **2021**, *19*, 338–344. [CrossRef]

71. Aerial Orthophotography National Plan (PNOA). Available online: https://pnoa.ign.es/el-proyecto-pnoa-lidar (accessed on 1 July 2021).

72. Florinsky, I.; Kuryakova, G. Influence of topography on some vegetation cover properties. *Catena* **1996**, *27*, 123–141. [CrossRef]

73. Pons, X.; Ninyerola, M. Mapping a topographic global solar radiation model implemented in a GIS and refined with ground data. *Int. J. Clim.* **2008**, *28*, 1821–1834. [CrossRef]

74. Ninyerola, M.; Pons, X.; Roure, J.M. *Atlas Climático Digital de la Península Ibérica. Metodología y Aplicaciones en Bioclimatología y Geobotánica*; CREAF, Centre de Recerca Ecológica i Aplicacions Forestals: Bellaterra, Spain, 2005; ISBN 932860-8-7.

75. Domingo-Marimon, C. Contributions to the knowledge of the multitemporal spatial patterns of the Iberian Peninsula droughts from a Geographic Information Science perspective. *Rev. Teledetección* **2016**, *171*. [CrossRef]

76. Vicente-Serrano, S.M.; Beguería, S.; López-Moreno, J.I. A Multiscalar Drought Index Sensitive to Global Warming: The Standardized Precipitation Evapotranspiration Index. *J. Clim.* **2010**, *23*, 1696–1718. [CrossRef]

77. Pasho, E.; Camarero, J.J.; de Luis, M.; Vicente-Serrano, S.M. Impacts of drought at different time scales on forest growth across a wide climatic gradient in north-eastern Spain. *Agric. For. Meteorol.* **2011**, *151*, 1800–1811. [CrossRef]

78. Inventario Nacional de Erosion de Suelos (INES). Available online: https://www.miteco.gob.es/en/biodiversidad/temas/inventarios-nacionales/inventario-nacional-erosion-suelos/default.aspx (accessed on 1 July 2021).

79. Renard, K.G.; Foster, G.R.; Weesies, G.A.; McCool, D.K.; Yoder, D.C. *Predicting Soil Erosion by Water: A Guide to Conservation Planning with the Revised Universal Soil Loss Equation (RUSLE)*; US Department of Agriculture: Washington, DC, USA, 1997; ISBN 0160489385.

80. Lasanta, T.; Sánchez-Navarrete, P.; Medrano-Moreno, L.M.; Khorchani, M.; Nadal-Romero, E. Soil quality and soil organic carbon storage in abandoned agricultural lands: Effects of revegetation processes in a Mediterranean mid-mountain area. *Land Degrad. Dev.* **2020**, *31*, 2830–2845. [CrossRef]

81. Benayas, J.M.R.; Martins, A.; Nicolau, J.M.; Schulz, J.J. Abandonment of agricultural land: An overview of drivers and consequences. *CAB Rev. Perspect. Agric. Vet. Sci. Nutr. Nat. Resour.* **2007**, *2*, 1–14. [CrossRef]

82. Zornoza, R.; Guerrero, C.; Mataix-Solera, J.; Scow, K.M.; Arcenegui, V.; Mataix-Beneyto, J. Changes in soil microbial community structure following the abandonment of agricultural terraces in mountainous areas of Eastern Spain. *Appl. Soil Ecol.* **2009**, *42*, 315–323. [CrossRef] [PubMed]

83. Díaz-Delgado, R.; Lloret, F.; Pons, X. Influence of fire severity on plant regeneration by means of remote sensing imagery. *Int. J. Remote Sens.* **2003**, *24*, 1751–1763. [CrossRef]

84. Friedman, J.H. Greedy function approximation: A gradient boosting machine. *Ann. Stat.* **2001**, *29*, 1189–1232. [CrossRef]

85. Heinrich, V.H.A.; Dalagnol, R.; Cassol, H.L.G.; Rosan, T.M.; de Almeida, C.T.; Silva Junior, C.H.L.; Campanharo, W.A.; House, J.I.; Sitch, S.; Hales, T.C.; et al. Large carbon sink potential of secondary forests in the Brazilian Amazon to mitigate climate change. *Nat. Commun.* **2021**, *12*, 1–11. [CrossRef]

86. Hosseini, F.S.; Malekian, A.; Choubin, B.; Rahmati, O.; Cipullo, S.; Coulon, F.; Pradhan, B. A novel machine learning-based approach for the risk assessment of nitrate groundwater contamination. *Sci. Total Environ.* **2018**, *644*, 954–962. [CrossRef]

87. Maskooni, E.K.; Naghibi, S.A.; Hashemi, H.; Berndtsson, R. Application of Advanced Machine Learning Algorithms to Assess Groundwater Potential Using Remote Sensing-Derived Data. *Remote Sens.* **2020**, *12*, 1–25. [CrossRef]

88. Dedman, S.; Officer, R.; Clarke, M.; Reid, D.G.; Brophy, D. Gbm.auto: A software tool to simplify spatial modelling and Marine Protected Area planning. *PLoS ONE* **2017**, *12*, e0188955. [CrossRef]

89. Hastie, T.; Tibshirani, R.; Friedman, J.H. *The Elements of Statistical Learning: Data Mining, Inference, and Prediction*, 2nd ed.; Springer Series in Statistics; Springer: New York, NY, USA, 2009; ISBN 978-0-387-84857-0.

90. Greenwell, B.; Boehmke, B.; Cunningham, J.; GBM Developers. Generalized Boosted Regression Models. 2020. Available online: https://CRAN.R-project.org/package=gbm (accessed on 15 February 2022).

91. Kuhn, M. Caret: Classification and Regression Training. 2021. Available online: https://CRAN.R-project.org/package=caret (accessed on 15 January 2022).

92. R Core Team. *R: A Language and Environment for Statistical Computing*; R Foundation for Statistical Computing: Vienna, Austria, 2021. Available online: https://www.R-project.org/ (accessed on 15 January 2022).

93. Hanley, J.A.; McNeil, B.J. The meaning and use of the area under a receiver operating characteristic (ROC) curve. *Radiology* **1982**, *143*, 29–36. [CrossRef] [PubMed]

94. Pepe, M.S. Receiver Operating Characteristic Methodology. *J. Am. Stat. Assoc.* **2000**, *95*, 308–311. [CrossRef]

95. Pontius, R.G.; Parmentier, B. Recommendations for using the relative operating characteristic (ROC). *Landsc. Ecol.* **2014**, *29*, 367–382. [CrossRef]

96. Jiménez-Valverde, A. Insights into the area under the receiver operating characteristic curve (AUC) as a discrimination measure in species distribution modelling. *Glob. Ecol. Biogeogr.* **2012**, *21*, 498–507. [CrossRef]

97. Friedman, J.H.; Meulman, J.J. Multiple additive regression trees with application in epidemiology. *Stat. Med.* **2003**, *22*, 1365–1381. [CrossRef] [PubMed]

98. Moua, Y.; Roux, E.; Seyler, F.; Briolant, S. Correcting the effect of sampling bias in species distribution modeling—A new method in the case of a low number of presence data. *Ecol. Inform.* **2020**, *57*, 101086. [CrossRef]

99. Anderson, R.P.; Gonzalez, I., Jr. Species-specific tuning increases robustness to sampling bias in models of species distributions: An implementation with Maxent. *Ecol. Model.* **2011**, *222*, 2796–2811. [CrossRef]

100. Openshaw, S. *The Modifiable Areal Unit Problem*, 38th ed.; Geo Book: Norwich, UK, 1984; ISBN 0306-6142.

101. Tuson, M.; Yap, M.; Kok, M.R.; Murray, K.; Turlach, B.; Whyatt, D. Incorporating geography into a new generalized theoretical and statistical framework addressing the modifiable areal unit problem. *Int. J. Health Geogr.* **2019**, *18*, 1–15. [CrossRef]

102. Jelinski, D.E.; Wu, J. The modifiable areal unit problem and implications for landscape ecology. *Landsc. Ecol.* **1996**, *11*, 129–140. [CrossRef]

103. Hatna, E.; Bakker, M.M. Abandonment and Expansion of Arable Land in Europe. *Ecosystems* **2011**, *14*, 720–731. [CrossRef]

104. Zaragozí, B.; Rabasa, A.; Rodríguez-Sala, J.J.; Navarro, J.T.; Belda, A.; Ramón, A. Modelling farmland abandonment: A study combining GIS and data mining techniques. *Agric. Ecosyst. Environ.* **2012**, *155*, 124–132. [CrossRef]

105. Palmero-Iniesta, M.; Pino, J.; Pesquer, L.; Espelta, J.M. Recent forest area increase in Europe: Expanding and regenerating forests differ in their regional patterns, drivers and productivity trends. *Eur. J. For. Res.* **2021**, *140*, 793–805. [CrossRef]

106. Lasanta, T.; Nadal-Romero, E.; Arnáez, J. Managing abandoned farmland to control the impact of re-vegetation on the environment. The state of the art in Europe. *Environ. Sci. Policy* **2015**, *52*, 99–109. [CrossRef]

107. Van Vliet, J.; de Groot, H.L.F.; Rietveld, P.; Verburg, P.H. Manifestations and underlying drivers of agricultural land use change in Europe. *Landsc. Urban Plan.* **2015**, *133*, 24–36. [CrossRef]

108. Gellrich, M.; Zimmermann, N.E. Investigating the regional-scale pattern of agricultural land abandonment in the Swiss mountains: A spatial statistical modelling approach. *Landsc. Urban Plan.* **2007**, *79*, 65–76. [CrossRef]

109. Tasser, E.; Walde, J.; Tappeiner, U.; Teutsch, A.; Noggler, W. Land-use changes and natural reforestation in the Eastern Central Alps. *Agric. Ecosyst. Environ.* **2007**, *118*, 115–129. [CrossRef]

110. Lasanta, T.; Errea, M.P.; Nadal-Romero, E. Traditional Agrarian Landscape in the Mediterranean Mountains. A Regional and Local Factor Analysis in the Central Spanish Pyrenees. *Land Degrad. Dev.* **2017**, *28*, 1626–1640. [CrossRef]

111. Douglas, T.; Critchley, D.; Park, G. The Deintensification of Terraced Agricultural Land Near Trevelez, Sierra Nevada, Spain. *Glob. Ecol. Biogeogr. Lett.* **1996**, *5*, 258. [CrossRef]

112. Lieskovský, J.; Bezák, P.; Špulerová, J.; Lieskovský, T.; Koleda, P.; Dobrovodská, M.; Bürgi, M.; Gimmi, U. The abandonment of traditional agricultural landscape in Slovakia–Analysis of extent and driving forces. *J. Rural Stud.* **2015**, *37*, 75–84. [CrossRef]

113. Gellrich, M.; Baur, P.; Koch, B.; Zimmermann, N.E. Agricultural land abandonment and natural forest re-growth in the Swiss mountains: A spatially explicit economic analysis. *Agric. Ecosyst. Environ.* **2007**, *118*, 93–108. [CrossRef]

114. Schulz, J.J.; Cayuela, L.; Rey-Benayas, J.M.; Schröder, B. Factors influencing vegetation cover change in Mediterranean Central Chile (1975-2008). *Appl. Veg. Sci.* **2011**, *14*, 571–582. [CrossRef]

115. Abadie, J.; Dupouey, J.-L.; Avon, C.; Rochel, X.; Tatoni, T.; Bergès, L. Forest recovery since 1860 in a Mediterranean region: Drivers and implications for land use and land cover spatial distribution. *Landsc. Ecol.* **2017**, *33*, 289–305. [CrossRef]

116. Propopulus. Available online: https://propopulus.eu/en (accessed on 1 July 2021).

117. De Rezende, C.L.; Uezu, A.; Scarano, F.R.; Araujo, D.S.D. Atlantic Forest spontaneous regeneration at landscape scale. *Biodivers. Conserv.* **2015**, *24*, 2255–2272. [CrossRef]

118. Peña-Angulo, D.; Khorchani, M.; Errea, P.; Lasanta, T.; Martínez-Arnáiz, M.; Nadal-Romero, E. Factors explaining the diversity of land cover in abandoned fields in a Mediterranean mountain area. *Catena* **2019**, *181*, 104064. [CrossRef]

119. Alonso-Sarría, F.; Martínez-Hernández, C.; Romero-Diaz, A.; Cánovas-García, F.; Gomariz-Castillo, F. Main Environmental Features Leading to Recent Land Abandonment in Murcia Region (Southeast Spain). *Land Degrad. Dev.* **2016**, *27*, 654–670. [CrossRef]

120. Pazúr, R.; Lieskovský, J.; Feranec, J.; Oťaheľ, J. Spatial determinants of abandonment of large-scale arable lands and managed grasslands in Slovakia during the periods of post-socialist transition and European Union accession. *Appl. Geogr.* **2014**, *54*, 118–128. [CrossRef]

121. Zgłobicki, W.; Karczmarczuk, K.; Baran-Zgłobicka, B. Intensity and Driving Forces of Land Abandonment in Eastern Poland. *Appl. Sci.* **2020**, *10*, 3500. [CrossRef]

122. Nash, M.; Chaloud, D.; Kepner, W.; Sarri, S. Regional Assessment of Landscape and Land Use Change in the Mediterranean Region: Morocco Case Study (1981–2003). In *Environmental Change and Human Security*; Springer Science + Business Media B.V.: Berlin/Heidelberg, Germany, 2008; pp. 143–165. ISBN 978-1-4020-8549-9.

123. Zgłobicki, W.; Gawrysiak, L.; Baran-Zgłobicka, B.; Telecka, M. Long-term forest cover changes, within an agricultural region, in relation to environmental variables, Lubelskie province, Eastern Poland. *Environ. Earth Sci.* **2016**, *75*, 1–12. [CrossRef]

124. Poyatos, R.; Latron, J.; Llorens, P. Land Use and Land Cover Change After Agricultural Abandonment. *Mt. Res. Dev.* **2003**, *23*, 362–368. [CrossRef]

125. Lieskovský, J.; Kenderessy, P.; Špulerová, J.; Lieskovský, T.; Koleda, P.; Kienast, F.; Gimmi, U. Factors affecting the persistence of traditional agricultural landscapes in Slovakia during the collectivization of agriculture. *Landsc. Ecol.* **2014**, *29*, 867–877. [CrossRef]

126. Kosmas, C.; Danalatos, N.; Cammeraat, L.H.; Chabart, M.; Diamantopoulos, J.; Farand, R.; Gutierrez, L.; Jacob, A.; Marques, H.; Martinez-Fernandez, J.; et al. The effect of land use on runoff and soil erosion rates under Mediterranean conditions. *Catena* **1997**, *29*, 45–59. [CrossRef]

127. Thornes, J.B.; Wainwright, J. *Environmental Issues in the Mediterranean. Processes and Perspectives from the Past and Present*; Routledge: London, UK, 2004; ISBN 9781134729869.

128. García-Ruiz, J.M. The effects of land uses on soil erosion in Spain: A review. *Catena* **2010**, *81*, 1–11. [CrossRef]

129. Lesschen, J.P.; Kok, K.; Verburg, P.H.; Cammeraat, L.H. Identification of vulnerable areas for gully erosion under different scenarios of land abandonment in Southeast Spain. *Catena* **2007**, *71*, 110–121. [CrossRef]

130. Bakker, M.M.; Govers, G.; Kosmas, C.; Vanacker, V.; van Oost, K.; Rounsevell, M. Soil erosion as a driver of land-use change. *Agric. Ecosyst. Environ.* **2005**, *105*, 467–481. [CrossRef]

131. Bakker, M.M.; Govers, G.; van Doorn, A.; Quetier, F.; Chouvardas, D.; Rounsevell, M. The response of soil erosion and sediment export to land-use change in four areas of Europe: The importance of landscape pattern. *Geomorphology* **2008**, *98*, 213–226. [CrossRef]

132. Melendez-Pastor, I.; Hernández, E.I.; Navarro-Pedreño, J.; Gómez, I. Socioeconomic factors influencing land cover changes in rural areas: The case of the Sierra de Albarracín (Spain). *Appl. Geogr.* **2014**, *52*, 34–45. [CrossRef]

133. Plieninger, T.; Draux, H.; Fagerholm, N.; Bieling, C.; Bürgi, M.; Kizos, T.; Kuemmerle, T.; Primdahl, J.; Verburg, P.H. The driving forces of landscape change in Europe: A systematic review of the evidence. *Land Use Policy* **2016**, *57*, 204–214. [CrossRef]

134. Doblas-Miranda, E.; Alonso, R.; Arnan, X.; Bermejo, V.; Brotons, L.; de las Heras, J.; Estiarte, M.; Hódar, J.A.; Llorens, P.; Lloret, F.; et al. A review of the combination among global change factors in forests, shrublands and pastures of the Mediterranean Region: Beyond drought effects. *Glob. Planet. Chang.* **2017**, *148*, 42–54. [CrossRef]

135. Meneses, B.M.; Reis, E.; Pereira, S.; Vale, M.J.; Reis, R. Understanding Driving Forces and Implications Associated with the Land Use and Land Cover Changes in Portugal. *Sustainability* **2017**, *9*, 351. [CrossRef]

136. Mottet, A.; Ladet, S.; Coqué, N.; Gibon, A. Agricultural land-use change and its drivers in mountain landscapes: A case study in the Pyrenees. *Agric. Ecosyst. Environ.* **2006**, *114*, 296–310. [CrossRef]

137. Díaz-Delgado, R.; Lloret, F.; Pons, X.; Terradas, J. Satellite evidence of decreasing resilience in mediterranean plant communities after recurrent wildfires. *Ecology* **2002**, *83*, 2293–2303. [CrossRef]

138. Pérez-Luque, A.J.; Bonet-García, F.J.; Zamora, R. Colonization Pattern of Abandoned Croplands by *Quercus pyrenaica* in a Mediterranean Mountain Region. *Forests* **2021**, *12*, 1584. [CrossRef]

139. Kozak, J. Forest Cover Changes and Their Drivers in the Polish Carpathian Mountains Since 1800. *Landsc. Ser.* **2009**, 253–273. [CrossRef]

140. Clement, F.; Orange, D.; Williams, M.; Mulley, C.; Epprecht, M. Drivers of afforestation in Northern Vietnam: Assessing local variations using geographically weighted regression. *Appl. Geogr.* **2009**, *29*, 561–576. [CrossRef]

141. Vicente-Serrano, S.M.; Lasanta, T.; Romo, A. Analysis of Spatial and Temporal Evolution of Vegetation Cover in the Spanish Central Pyrenees: Role of Human Management. *Environ. Manag.* **2004**, *34*, 802–818. [CrossRef]

142. Sanjuán, Y.; Arnáez, J.; Beguería, S.; Lana-Renault, N.; Lasanta, T.; Gómez-Villar, A.; Álvarez-Martínez, J.; Coba-Pérez, P.; García-Ruiz, J.M. Woody plant encroachment following grazing abandonment in the subalpine belt: A case study in northern Spain. *Reg. Environ. Chang.* **2018**, *18*, 1103–1115. [CrossRef]

143. Dinca, L.; Nita, M.D.; Hofgaard, A.; Alados, C.L.; Broll, G.; Borz, S.A.; Wertz, B.; Monteiro, A.T. Forests dynamics in the montane–alpine boundary: A comparative study using satellite imagery and climate data. *Clim. Res.* **2017**, *73*, 97–110. [CrossRef]

144. Camarero, J.J.; Gutierrez, E. Pace and Pattern of Recent Treeline Dynamics: Response of Ecotones to Climatic Variability in the Spanish Pyrenees. *Clim. Chang.* **2004**, *63*, 181–200. [CrossRef]

145. Sanz-Elorza, M.; Dana, E.D.; González, A.; Sobrino, E. Changes in the High-mountain Vegetation of the Central Iberian Peninsula as a Probable Sign of Global Warming. *Ann. Bot.* **2003**, *92*, 273–280. [CrossRef]

146. Roura-Pascual, N.; Pons, P.; Etienne, M.; Lambert, B. Transformation of a Rural Landscape in the Eastern Pyrenees Between 1953 and 2000. *Mt. Res. Dev.* **2005**, *25*, 252–261. [CrossRef]

147. Améztegui, A.; Brotons, L.; Coll, L. Land-use changes as major drivers of mountain pine (*Pinus uncinata* Ram.) expansion in the Pyrenees. *Glob. Ecol. Biogeogr.* **2010**, *19*, 632–641. [CrossRef]

148. Nadal-Romero, E.; Otal-Laín, I.; Lasanta, T.; Sánchez-Navarrete, P.; Errea, P.; Cammeraat, E. Woody encroachment and soil carbon stocks in subalpine areas in the Central Spanish Pyrenees. *Sci. Total Environ.* **2018**, *636*, 727–736. [CrossRef] [PubMed]

149. Gehrig-Fasel, J.; Guisan, A.; Zimmermann, N.E. Tree line shifts in the Swiss Alps: Climate change or land abandonment? *J. Veg. Sci.* **2007**, *18*, 571–582. [CrossRef]

150. Lasanta, T.; Vicente-Serrano, S.M. Cambios en la cubierta vegetal en el Pirineo aragonés en los últimos 50 años. *Pirineos* **2007**, *162*, 125–154. [CrossRef]

151. Perpiña Castillo, C.; Coll Aliaga, E.; Lavalle, C.; Martínez Llario, J.C. An Assessment and Spatial Modelling of Agricultural Land Abandonment in Spain (2015–2030). *Sustainability* **2020**, *12*, 560. [CrossRef]

4.2. Artículo 3: Supplementary materials

Padial-Iglesias, M.; Ninyerola, M.; Serra, P.; González-Guerrero, Ò.; Espelta, J.M.; Pino, J.; Pons, X. Driving Forces of Forest Expansion Dynamics across the Iberian Peninsula (1987–2017): A Spatio-Temporal Transect. *Forests.* 2022, *13*, 475. https://doi.org/10.3390/f13030475 (Journal Impact Factor (JIF): 2.634, Q1: 13/67 (2020) [Forestry]).

Hipervínculo: https://www.mdpi.com/1999-4907/13/3/475/s1?version=1647594274

Driving forces of forest expansion dynamics across the Iberian Peninsula (1987–2017): A spatio-temporal transect

(A) Complementary information to the main text

2.2. Methodological framework

2.2.2. New forests' occurrence extraction, sampling on each BR, and filtering
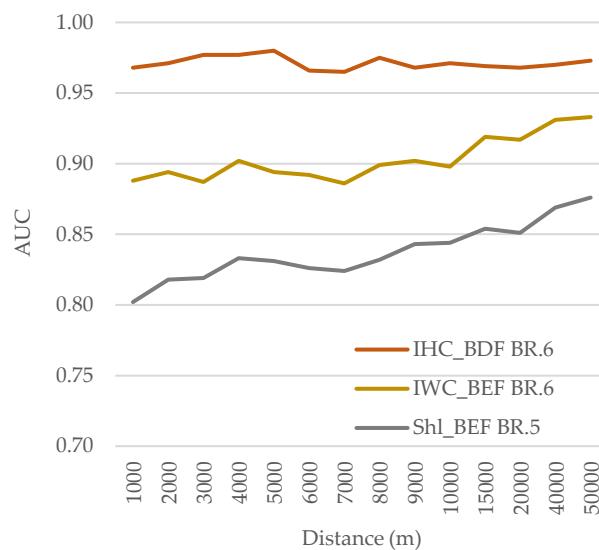
The classified maps were overlaid to derive the land cover (LC) changes and temporal trajectories in the last thirty years. We selected forest locations in 2002 and 2017 (*needleleaf evergreen forests*, *broadleaf evergreen forests*, *broadleaf deciduous forests*) that were classified as crops categories, *grasslands*, or *shrublands* in the previous dates. Then, a set of sampling strategies were used for modeling focusing on (i) reducing the absence bias, (ii) applying uncertainty filtering, (iii) evaluating the presence-absence spatial autocorrelation, (iv) subsampling in bioclimatic regions (BRs), and finally, (v) equalizing the presence-absence locations (by prevalence). LC dynamics were classified in the form of binary presence-absence events. Thus, remaining stable locations in all periods were considered to be absences while changing locations towards new forest (NF) were considered to be presences.

Commonly, presence and absence points are extracted randomly, regardless of the density of presences-absences in a local neighborhood. However, in the context of extensive LC change analyses (as in this research), considering random sampling over all the available absence points implies incorporating into the model locations with biophysical and socioeconomic attributes significantly distanced or without spatial relation to the presences, even within a BR (**absence sample bias**). A set of testbeds was performed to approximate an optimal distance to extract absence samples, which analyzed how the sampling distance to select absences according to presences influences the modeling results. This strategy allows for generating more spatially balanced presence-absence samples, fitting the number of absences according to the frequency of local presences. Three NF dynamics' (IHC to BDF, IWC to BEF, and Shl to BEF) sample locations and a predefined set of predictors were considered to evaluate the BRT models' performance (the area under the receiver operating curve, AUC) at specific sampling distances (Figure S1).

Figure S1. Square buffering distance testbeds for presence-absence balanced sampling. In (a), BRT models' performance results evaluated for each square buffer distance are shown, with their (b) graphical evolution.

Square buffer distance	IHC-BDF BR.6	IWC-BEF BR.6	Shl-BEF BR.5
1000 [1]	0.968 [2]	0.888 [2]	0.802 [2]
2000	0.971	0.894	0.818
3000	0.977	0.887	0.819
4000	0.977	0.902	0.833
5000	0.980	0.894	0.831
6000	0.966	0.892	0.826
7000	0.965	0.886	0.824
8000	0.975	0.899	0.832
9000	0.968	0.902	0.843
10000	0.971	0.898	0.844
15000	0.969	0.919	0.854
20000	0.968	0.917	0.851
40000	0.970	0.931	0.869
50000	0.973	0.933	0.876

[1] distance in meters. [2] Area under the curve (AUC).

(**a**)

(**b**)

Calculating the presence-absence density within a sampling distance required the considered BR area to be divided into equal-sized squares (as tiles), with a diagonal length (as the sampling dimension) ranging from 1,000 to 50,000 m. The numbers of presence and absence locations were estimated, and the minimum of the two values were calculated for each square. Then, absences in each square were

randomly sampled according to the minimum value calculated. This strategy permitted deriving a more spatially balanced presence-absence sample for modeling. The higher performance in the models was achieved by applying sampling distances over 20,000 m. This threshold distance value was used to derive absence samples for modeling.
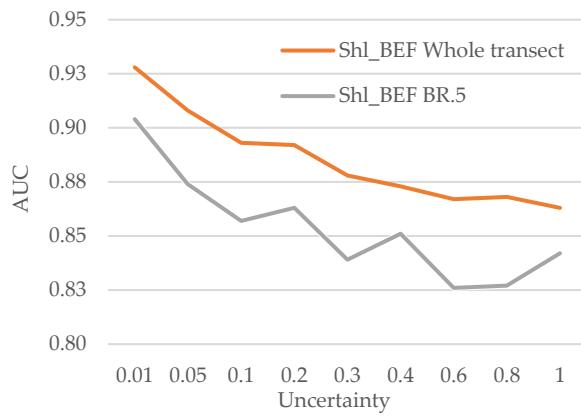
Each classified map had an associated **uncertainty** layer that specified the confidence of the classified pixels according to highly reliable training areas [54]. Using these uncertainty layers, the effect of different uncertainty restrictions on model performance and the number of pixels remaining for modeling were evaluated. As was expected, the global accuracy of the model increased when pixels with higher values of uncertainty were eliminated [57,58]. Therefore, due to the existing trade-off between uncertainty restrictions and an adequate number of pixels for modeling, two uncertainty levels were used: *uncertainty* < 0.1 was applied when there was a large sample size (e.g., NF from shrublands and grasslands that theoretically should provide ultra-high quality models), and *uncertainty* < 0.3 for classes with a limited number of pixels available for modeling (e.g., NF from crop categories). Figure S2 provides further details about the testbeds performed, and Table S6a details the remaining sample size after the uncertainty filtering.

Figure S2. Testbeds modeling using a set of *uncertainty* restrictions. In (a), BRT models' performance results are shown, with their (b) graphical correspondence.

Uncertainty	Shl to BEF Whole transect	Shl to BEF BR.5
0.01	0.928 [1]	0.904 [1]
0.05	0.908	0.874
0.1	0.893	0.857
0.2	0.892	0.863
0.3	0.878	0.839
0.4	0.873	0.851
0.6	0.867	0.826
0.8	0.868	0.827
1	0.863	0.842

[1] area under the curve (AUC).

(**a**)   (**b**)
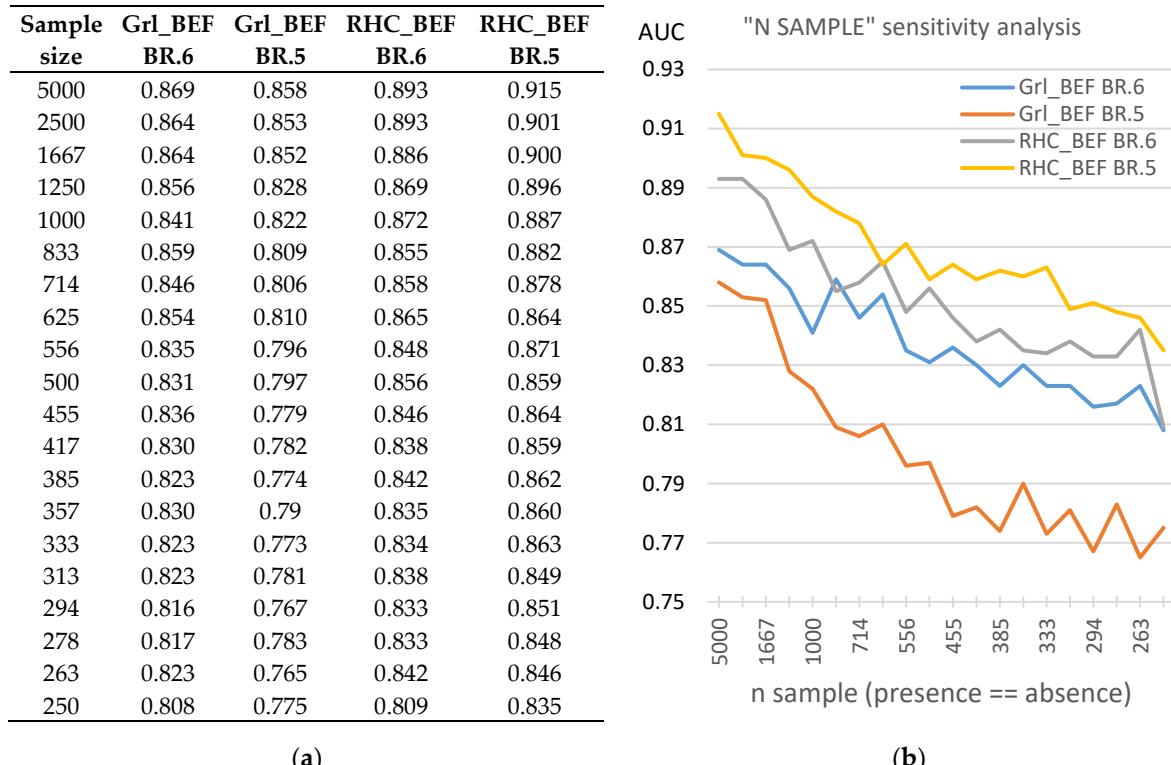
The Moran index was calculated at discrete distances to **identify uncorrelated sampling points** of the dependent (i.e., presences-absences) and independent variables in the geographic space. The Moran index calculates the distance a point can be considered independent of another. Testbeds were performed, which found that at a distance between points of 140 m, the correlation coefficient dropped below 0.7, where the slope (a topoclimatic variable) was considered the independent variable serving to evaluate the autocorrelation test. We applied this minimum distance threshold to derive spatially uncorrelated presence-absence points for modeling.

The transect area was subdivided into **bioclimatic regions** (BRs) to analyze NF transition models in a more meaningful climatic way. The average of the mean temperature surfaces [59] comprising the 1987–2017 period and the BR's formulation [51], were used to subdivide the transect according to its climatic characteristics. A general overview of the BRs is detailed in Figure S4.

A **presence-absence balanced** sample was generated to be used for modeling, which assured the presence-absence sample's prevalence. In addition, when the number of presences-absences in the BRs exceeded 5 000 points, the points were randomly selected and limited to this value to reduce time processing. We admit that this sample restriction value could have compromised the extent to which the sample size might affect NF modeling. Several studies have evaluated the effect of sample size on species distribution model performance [60–63]. However, due to the lack of previous literature references regarding the optimal number of samples used for BRT modeling and the fact that diverse

sample size was assumed in other research [4,33,47,48], we performed a set of testbeds to investigate how a sampling size affected the model's performance and hence, established a minimum sampling size for modeling. The Grl to BEF and RHC to BEF dynamics samples in the Supramediterranean (BR.5) and Southern Mesomediterranean (BR.6) bioclimatic regions were selected because they provided a large initial sample size of around 5 000 presence-absence points (Figure S3). A first BRT model with the whole sample (5 000 points) served to derive the reference accuracy estimate. Then, we consecutively split the original sample from 2 to 20 parts (randomly and without replacement), generating k-subsamples used to evaluate the models' performance in each subsample. For instance, dividing the original sample into five parts would yield 5 BRT models that consider 1 000 presence-absence points each to evaluate each model's performance. As expected, the accuracy and AUC dropped when the sample size was reduced, increasing the models' performance dispersion (standard deviation) evaluated in each k-parts subsample. Therefore, we assumed an accuracy loss limit of 5% (maximum) from the initial model's performance estimated with the whole sample. Averaging the models' accuracy loss series, the accuracy loss limit percentage corresponds with 580 presence-absence points, a threshold used as a criterion to discard models (and therefore NF dynamics) with low sample representativeness in the BRs. Table S6b presents the number of pixels used for modeling, disaggregated by NF dynamics and BR.

Figure S3. Testbeds for the evaluation of the minimum sampling size through BRT modeling. In (a), the BRT models' performance results are shown, with their (b) graphical correspondence.

Sample size	Grl_BEF BR.6	Grl_BEF BR.5	RHC_BEF BR.6	RHC_BEF BR.5
5000	0.869	0.858	0.893	0.915
2500	0.864	0.853	0.893	0.901
1667	0.864	0.852	0.886	0.900
1250	0.856	0.828	0.869	0.896
1000	0.841	0.822	0.872	0.887
833	0.859	0.809	0.855	0.882
714	0.846	0.806	0.858	0.878
625	0.854	0.810	0.865	0.864
556	0.835	0.796	0.848	0.871
500	0.831	0.797	0.856	0.859
455	0.836	0.779	0.846	0.864
417	0.830	0.782	0.838	0.859
385	0.823	0.774	0.842	0.862
357	0.830	0.79	0.835	0.860
333	0.823	0.773	0.834	0.863
313	0.823	0.781	0.838	0.849
294	0.816	0.767	0.833	0.851
278	0.817	0.783	0.833	0.848
263	0.823	0.765	0.842	0.846
250	0.808	0.775	0.809	0.835

(**a**)   (**b**)

Lastly, once the presence-absence sample points were generated, they were intersected with the predictor variables, resulting in point features with data included in their attribute table.

2.2.3. Land Cover Change Modeling: Explanatory variables

The spatial determinants potentially driving the past NF transitions listed in Table 2 in the main text are described in the following paragraphs.

The **topography** defines physical characteristics that may have influenced NF occurrence. A 10 m per cell Digital Elevation Model (DEM) was used, derived from a 1:5 000 lidar dataset from the Spanish National Plan for Aerial Orthophotography 2010 (PNOA, https://pnoa.ign.es/el-proyecto-pnoa-lidar, last accessed on 1 July 2021) [71]. From that, several variables were derived:

- Slope, calculated in degrees.
- General curvature (dimensionless), estimated as the second derivative of the DEM, defines how convex or concave a surface is, which approximates soil moisture and the convergence/divergence of overland accumulated water flow [72]. A positive value denotes a convex surface, a negative value denotes a concave surface, and values close to 0 denote flat terrain landforms.
- Potential solar radiation (10 kJ / (m2 × day × μm)), evaluated on winter solstice dates following [73], indicates the available energy for NF growth in the most restrictive conditions.

Climatic conditions were characterized by the averaged mean temperature (d°C), the accumulated precipitation (dmm), and the Standardized Precipitation-Evapotranspiration Index (SPEI), extracted from the Topoclimatic Drought Atlas of the Spanish Iberian Peninsula [74–76]. The dataset includes monthly aggregates at a 100 m spatial resolution between 1950–2017, which was then aggregated annually. Each LC map produced was characterized by averaging the 15 years of climatic data prior to its reference date, i.e., 1972–1986 for LCM-1987, 1987–2001 for LCM-2002, and 2002–2016 for LCM-2017. The SPEI was considered a possible explanatory variable to evaluate drought impact on vegetation, given its multiscale analysis capacity for characterizing water availability, a driver that constrains primary and secondary forest growth [77]. Furthermore, SPEI indexes were calculated for 3, 6, 12, and 24 months using the 1950-2017 climate time series, providing a wide variety of drought aggregation to characterize the drought tolerance of vegetation (i.e., crops, natural/seminatural). Two temporal ranges were adapted to the analysis periods. For P1, SPEI indexes ranged from 1978–2002 and for P2, from 1993–2017, representing a buffer time of 25 years of drought characterization. Then, the number of drought episodes during which the drought intensity overcame -1 (SPEI < -1 as a measure of water deficit) and +1 (SPEI > +1 for water oversupply conditions) were counted, generating sixteen drought/humid intensity variables for each period.

To assess the influence of land accessibility and the topographic effect in the NF appearance, distance measures were calculated based on Euclidean distances and Cost distances. Euclidean distances were considered precise enough to avoid Geodetic distance computation, which would take into account the limited scopes considered and the characteristics of the cartographic projection used (UTM). The Euclidean distance variables used included the Euclidean distance to hydrography (first, second, and third stream order with perennial/intermittent streamflow regimes), the Euclidean distance to protected areas (national and natural parks), and the Euclidean distance to any forest patch (without discriminating between forest groups) with an area more than 120 × 120 m². Cost distance variables were used in two ways; first, using cost distance to urban areas and cost distance to provincial capitals, in both cases weighting the Euclidean distance with the slope and friction coefficients according to cell values (i.e., primary or secondary road network). Secondly, we estimated the cost distance to the main roads and the cost distance to secondary roads, using the slope as the cost surface. All distance variables were calculated using datasets from the Spanish National Geographic Institute (https://www.ign.es/web/ign/portal/cbg-area-cartografia, accessed on 01/07/2021). In addition, the LCM-1987 was used to derive the Euclidean distance to preexisting forests.

The lithological substrate may influence the nature of soils and, hence, the vegetation tolerance to acidic pH conditions (low pH, as in silicate rocks) or alkaline (high pH, as in carbonate rocks). As there is not a soil map for the whole area, we extracted the lithologic groups from the Geologic map of Spain at a scale of 1:1 000 000 (https://info.igme.es/catalogo/, accessed on 01/07/2021), and we reclassified them according to three categories: acidic, mixed, and alkaline.

Soil degradation is a severe environmental problem. Of several forms of soil erosion (water, wind, or landslide), water is the most influential on the fast degradation of natural ecosystems and land productivity. The European Union proposed a Directive (22/9/2006) that establishes a framework for soil protection. On this basis, the Spanish National Soil Erosion Inventory [78] provided a decennial

map (2002–2012) of the principal soil erosion agents at a 1:50 000 scale. We considered the water erosion agent ("sheet and rill erosion" product), estimated by applying the RUSLE (Revised Universal Soil Loss Equation) model [79]. This model is simple in its application and is widely disseminated and accepted by the scientific community. It predicts soil erosion based on six factors: the aggressiveness of the rain, the susceptibility of the soil to erosion, the length of the slope, the slope, the vegetation cover, and the soil conservation practices. Together, these factors predict the rate of soil loss (Mg/(ha × year)), which were aggregated into seven categorical levels (Table S5). Therefore, "sheet and rill erosion" is considered a driver that determines the local soil quality (carbon content, soil depth, fertility), which may affect forest regrowth, especially when related to cropland abandonment processes in marginal lands [80–82].

The level of protection in natural areas may have influenced forest regrowth associated with natural succession dynamics, in addition to agricultural abandonment in more inaccessible regions with less productive lands. The special status of protected areas with a historic long-term high-grade protection was considered, i.e., national parks and natural parks, according to the Spanish Natural Protected Areas database (https://www.redeuroparc.org/, accessed on 01/07/2021). The protected areas were split according to their initial protection date, adapted to the analysis periods (P1, P2) in the form of a dichotomous variable.

Population and agricultural censuses were collected to consider the potential repercussion of population characteristics in agrarian land-use change decisions and related forest regrowth dynamics. Datasets were collected at the municipality level by the Spanish National Statistics Institute (INE, https://www.ine.es/, accessed on 01/07/2021). We included the Agricultural Census 1989, 1999, and 2009, and the Population Census 1991, 2001, and 2011 datasets due to their temporal proximity to the LC maps' reference dates. The variables from the datasets allowed for evaluating population density and migration, the ageing structure, the economic activity and workforce composition, and the productivity of agricultural holdings.

Finally, fires directly impact forest ecosystems and land cover dynamics analyses, so we collected historical fire perimeter datasets through the Spanish regional forest management administrations (e.g., Andalucía, Aragón, Castilla-La Mancha, Castilla y León, Euskadi, Navarra, Madrid, Murcia) at the maximum temporal resolution. Therefore, burned areas were masked from the analysis, a process necessary to avoid matching artifacts between LCM temporal resolution (15 years), the year of the wildfire, and the time it takes for a forest to recover from fire disturbances, which depends on humidity and fire severity [83].

3.3. New forests' main drivers

The following paragraphs provide a detailed description of the results section, which serves as a basis for the discussion section detailed in the main text.

The NF driving forces were analyzed, focusing on the source categories (rainfed crop categories, irrigated crop categories, grasslands, and shrublands). The maps detailed in Figure 5a/b/c in the main text describe the drivers' temporal and spatial variation characteristics, detailed by period and BR. In this section, drivers are listed by their relative importance, accompanied by a symbol (in brackets) denoting a partial dependence main pattern, which is described in the main text section entitled 3.3 *New forests main drivers*. For instance, the (+grad) means that the transition probability increases with the variable; the (-grad) represents the opposite; and the (≠grad) means that there is not a clear positive or negative tendency. The (A-shape) indicates that the higher suitable conditions occur between two low values, while the (V-shape) denotes two high suitable conditions between a minimum. The (и-shape) depicts relatively high suitable conditions in low values that sharply decrease, then increase to a second peak, and finally decrease at larger values. Lastly, the (±grad) is used in the case of a specific driver depicts different patterns when aggregating BRs.

3.3.1. Drivers of new broadleaf deciduous forests (BDF)

Regarding rainfed (herbaceous and woody crops) source categories, according to Table 4, enough occurrences were detected to perform an analysis in the Supramediterranean BR for the RHC source category in the first period. The most important driver was the distance to forests (-grad), followed by precipitation (*и*-shape), distance to hydrography network (-grad), distance to provincial capitals (+grad), and distance to urban settlements (-grad). Therefore, drivers suggest that the increase of deciduous forest from rainfed crops in the Supramediterranean BR was a process of forest completion in areas near forested areas, streams and torrents, and while far from capitals, relatively close to urban settlements.

In the second period, the number of occurrences increased in the Northern and Southern Mesomediterranean BRs (Figure 5a in the main text) for the RHC and RWC source categories. For RHC, the distance to the hydrographic network (-grad) was the main driver in the Northern Mesomediterranean BR, and in the Southern Mesomediterranean and Supramediterranean BRs (Figure S7a1), the distance to forests (-grad) was the main driver, followed by precipitation (±grad), distance to provincial capitals (V-shape) and urban settlements (-grad). Therefore, compared to the first period, the new BDF areas from rainfed crops appeared closer to rivers or streams, further from forests, further from provincial capitals, relatively close to local urban settlements and secondary roads, and with different precipitation patterns. In the case of RWC in the Southern Mesomediterranean BR, the number of holdings (-grad) was the main driver, followed by the distance to the hydrographic network (-grad), precipitation (-grad), and distance to forests (-grad).

For irrigated crops (herbaceous and woody crops) source categories during the first period, the most important drivers were the distance to the hydrographic network (-grad) followed by the distance to forests (-grad), which was clearly visible in Northern and Southern Mesomediterranean BRs (Table S7). Other primary drivers were the distance to provincial capitals (+grad) in the Southern Mediterranean BR, the slope (+grad), and the distance to main roads (+grad) in Coline and Southern and Northern Mesomediterranean BRs. Secondary drivers were the general curvature, temperature, distance to urban settlements, distance to secondary roads, soil erosion, and precipitation. Therefore, the drivers suggested that new BDF from irrigated crops was a process of forest aggregation or completion on lands closer to rivers, torrents, and streams (associated with riparian vegetation), with a steeper slope, and further from human activities, represented by primary and secondary roads, urban settlements (in less intensity), and provincial capitals.

In the second period, the most crucial drivers remained in the same BRs as in the first period but drivers appeared notably in the Thermomediterranean in this period. Other main drivers affecting the same BRs were temperature (±grad), distance to capitals (+grad), and slope (+grad for herbaceous and -grad for woody crops). Secondary drivers included the general curvature (V-shape), soil erosion (-grad), and with less importance, precipitation (+grad) and distance to urban settlements. Moreover, new drivers were identified in this period: solar radiation (V-shape) and population density (-grad). When comparing the temporal PDPs (Figure S7a2), the patterns observed are consistent with forest consolidation and completion occurring during the first period and forest expansion in the second period, the latter of which appeared within the limits of forested areas or at an even greater distance. Therefore, compared to the first period, the process of forest aggregation and completion was more clearly associated with riparian vegetation near rivers, streams, and torrents, a greater distance from provincial capitals and, in less intensity, with the distance to main roads and urban settlements, and population density. The relative importance of the distance to the hydrography network and the distance to forests decreased when comparing both periods (Table S7).

Concerning the grasslands source category during the first period, the main driver was the distance to forests (-grad) very clearly in the Montane and Supramediterranean BRs, though less important in the Coline and Southern Mesomediterranean BRs. Other main drivers were the temperature (-grad) and precipitation (+grad) in the Southern Mesomediterranean, versus soil erosion (-grad) and distance to provincial capitals (-grad) in the Coline BR. Secondary drivers were solar

radiation, slope, distance to urban settlements (-grad), number of holdings (-grad), and distance to main roads (-grad). Therefore, during the first period, drivers suggest that the new BDF from grasslands tended to be a forest completion and consolidation process in areas close to preexisting forested areas, between a range of temperature values, and with humid conditions, shady conditions, steeper slopes, and a lower number of holdings.

During the second period, the drivers in the Supramediterranean and Southern Mesomediterranean BRs followed a similar order of importance, with a slight increase in the number of holdings in the Southern Mesomediterranean (Figure S7a). Conversely, the importance of distance to forests decreased clearly in the Montane BR. The solar radiation driver disappeared (indicating no solar radiation constraints), and the importance of slope increased, with a higher probability of NF occurrence at lower slope values and lower probability at higher slope values (Figure S7a3). Moreover, the soil erosion driver disappeared in the Coline BR, while the importance of solar radiation increased. Therefore, NF continued expanding in the second period beyond the limits of previously forested areas, mainly on steeper slopes (at higher altitudes), close to provincial capitals with temperature-altitudinal restrictions, and shadier conditions.

For the shrublands source category in the Montane BR during the first period, the most important drivers were precipitation (+grad) and temperature (-grad), and secondarily the distance to forests (-grad), distance to urban settlements (+grad), and solar radiation (-grad). Conversely, the Supramediterranean BR denotes the opposite driver order, with the distance to forests (-grad) and to provincial capitals (V-shape) being the main drivers, followed by temperature (A-shape), precipitation (-grad), and drought episodes (-grad). Consequently, the drivers suggested that the new BDF derived from shrublands was a forest consolidation process principally located in humid, temperature-restricted areas with shady conditions.

In the second period, the main drivers in the Montane BR were similar to those in the first period, with temperature (-grad) and precipitation (+grad) increasing in their importance (Figure S7a4). However, two new drivers of lower importance were found: the distance to the hydrographic network (V-shape) and the distance to provincial capitals (V-shape). Conversely, distance to forests was not found to be a driver. Therefore, new BDF transitions were controlled mainly by water availability (with an increase in the mean value compared to the first period), temperature in locations far from capitals, and the hydrographic network. In the Supramediterranean BR, there was a significant change in the drivers' order, with the main drivers being the temperature (A-shape) (Figure S7a4), precipitation (A-shape) and solar radiation (-grad), and the secondary drivers being the distance to forests (-grad) and the distance to urban settlements (+grad). Thus, precipitation and temperature constraints (as their mean values increased in the second period) determined the new BDF appearance in areas close and far from urban settlements with shady conditions.

3.3.2. Drivers of new broadleaf evergreen forests (BEF)

For the rainfed crops' source categories (herbaceous and woody crops) during the first period when woody crops were the most important source category, the distance to forests (-grad) was the most important driver, followed by precipitation (±grad), slope (+grad), and soil erosion in the Supramediterranean and Southern Mesomediterranean BRs (Table 4 and Figure 5b in the main text). Secondary drivers were temperature, the number of workers in the building (construction) (+grad) and service (+grad) sectors, the distance to the hydrographic network (-grad), the distance to urban settlements (+grad), and the utilized agricultural area (-grad). Thus, the new BEF from rainfed crops was related to areas closer to forests, with higher water availability, steeper slopes, and lower soil erosion. It was also associated with higher rates of the population occupied in building (construction) and service activities. Socioeconomic drivers manifested in land cover change in the Supramediterranean BR, a mountainous area with lower farmland availability. In contrast, the distance and accessibility drivers predominated in the Southern Mesomediterranean BR, with more productive lowland agricultural areas, transitional zones near the border, and high relief nearby.

During the second period, the distance to forests (-grad) (Figure S7b1) and precipitation (±grad) remained as the main factors in the Supramediterranean and Southern Mesomediterranean BRs. Secondary drivers were temperature (-grad), slope (+grad) (Figure S7b1), distance to the hydrographic network (-grad), soil erosion (-grad), solar radiation (A-shape), population density (-grad), workers in the building (construction) sector (+grad), and drought episodes. Therefore, during the second period, new BEF was again associated with areas close to forested areas, with water resources, relatively close to the hydrographic network, and with lower temperature, a moderate slope, lower soil erosion values, and lower population density.

Concerning irrigated crops' source categories, only IWC in the Southern Mesomediterranean BR contained enough locations for modeling during both periods. In the first period, the most important driver was soil erosion (-grad), followed by the distance to forests (-grad), temperature (-grad), distance to secondary roads (+grad), and solar radiation (+grad). Thus, drivers suggest that the new BEF in this BR was a conversion process in areas close to previously forested areas, with lower soil degradation, lower temperature, higher solar radiation, and greater distance from secondary roads.

During the second period, the main driver was the temperature (-grad), which increased in importance compared to the first period, followed by the distance to forests (-grad) (Figure S7b2), slope (-grad), population density (+grad), and soil erosion (-grad), which decreased significantly in importance compared to the first period. Consequently, new BEF from IWC was associated with areas characterized by lower temperatures, proximity to forests, steeper slopes, more densely populated municipalities, and lower soil erosion rates.

Regarding the grasslands source category, during the first period, the distance to forests (-grad) was the main driver in the Supramediterranean and Southern Mesomediterranean BR, the temperature (+grad) in the Montane and the Supramediterranean BRs, and the soil erosion (-grad) and slope (-grad) in the Coline region. Secondary drivers were precipitation and solar radiation in all aforementioned regions, and distance to capitals and livestock units in specific bioclimatic regions. The drivers suggested that new BEF from grasslands occurred close to preexisting forested areas, with relatively low water availability (depending on the BR) and shady conditions (except in Coline), besides being temperature-constrained in higher slope areas farther from capitals.

During the second period, when not enough occurrences appeared in the Coline BR, distance to provincial capitals (-grad) (Figure S7b3) was the main driver in the Southern Mesomediterranean BR, precipitation (-grad) was the main driver in the Montane BR, and temperature (+grad) was the main driver in the Supramediterranean BR (Figure S7b3). In the last two regions, the distance to provincial capitals (±grad) was the second most important driver. Drivers with lower importance included slope (V-shape), distance to the hydrographic network (V-shape), solar radiation (-grad), the number of holdings (-grad), and the number of workers in the industry sector (-grad). Overall, the drivers suggest that the new BEF in the second period was mainly related to distance to provincial capitals, precipitation, temperature, and distance to forests, with different importances and patterns according to the BRs.

Concerning the shrublands source category, in the first period, the distance to forests (-grad) was the main driver in the Supramediterranean and Northern Mesomediterranean BRs, and the second driver after distance to urban settlements in the Montane BR (Figure S7b4). Solar radiation was the main driver in the Southern Mesomediterranean BR and the second in the Northern Mesomediterranean. Moreover, the temperature (±grad), precipitation (±grad), and slope (±grad) were the main secondary drivers in almost all of the BRs. Therefore, the drivers indicated that new BEF from shrublands was a process of forest consolidation in areas near previously forested areas, with shady conditions, within a range of values for temperature and precipitation (varying by BR), far from urban areas, and with lower slopes.

In the second period, temperature (±grad) was the main driver in the Montane and Southern Mesomediterranean BRs, distance to forests (V-shape) was the main driver in the Northern Mesomediterranean, and distance to provincial capitals (-grad) was the main driver in the

Supramediterranean BR. Precipitation (±grad) (Figure S7b4) and solar radiation (-grad) were also significant in all of the BRs. Secondary drivers were the slope (-grad), the distance to the hydrographic network (+grad), and the distance to secondary roads (+grad). Overall, during the second period, the new BEF from shrublands continued expanding in more distant locations from forests, with moderate precipitation, within a limited temperature range, with shady conditions, both close and far from capitals, and with lower slope values.

3.3.3. Drivers of new needleleaf evergreen forests (NEF)

Regarding the rainfed source categories (herbaceous and woody crops), enough occurrences to perform an analysis were located in the Southern Mesomediterranean BR for the RWC category during the first period (Table 4 and Figure 5c in the main text). The main driver was the distance to provincial capitals (+grad), followed by the distance to forests (-grad), the number of holdings (-grad), the distance to main roads (+grad), and soil erosion (-grad). Thus, the drivers suggested that the new NEF derived from rainfed woody crops was a conversion process in areas far from provincial capitals and main roads, close to forests, in areas with a lower number of holdings, and with lower soil erosion rates.

In the second period, new forested locations in the Northern and Southern Mesomediterranean BRs appeared. The main drivers in the Northern Mesomediterranean BR (related to RHC) were the distance to the hydrographic network (-grad) and the distance to provincial capitals (A-shape). In the Southern Mesomediterranean BR (related to RWC), the main drivers were the distance to provincial capitals (V-shape) and the distance to forests (-grad) (Figure S7c1). Secondary drivers were solar radiation (-grad), precipitation (-grad), distance to secondary (-grad), distance to main roads (+grad), and drought episodes (-grad). Consequently, in the second period, new NEF appeared in areas close and far from provincial capitals, near forests and the hydrographic network, and far from secondary roads, with shady conditions, low precipitation, and low drought recurrence events.

For irrigated crops' (herbaceous and woody crops) source categories, enough occurrences for analysis were detected in only the Southern Mesomediterranean BR for woody crops in the first period. In this context, the most relevant driver was soil erosion (-grad), followed by distance to main roads (+grad), the number of holdings (-grad), precipitation (V-shape), and livestock units (+grad). Therefore, the drivers suggest that the new NEF derived from irrigated woody crops was a conversion process in areas with lower soil erosion, greater distance from main roads (Figure S7c2), a lower number of holdings, precipitation constraints, and higher livestock units.

In the second period, new locations in the Northern and Southern Mesomediterranean BRs appeared. Precipitation (V-shape) was the main driver in the Southern Mesomediterranean BR and the secondary driver in the northern region. In the Northern Mesomediterranean BR, the main driver was the distance to provincial capitals (V-shape) in the case of woody crops and the distance to the hydrographic network (A-shape) for herbaceous crops. Secondary drivers were solar radiation, soil erosion, distance to forests, the number of holdings, livestock units, and distance to secondary roads. Consequently, new NEF from irrigated crops was associated with areas characterized by various precipitation patterns, far from provincial capitals, with a hydrographic network and preexisting forests, and with shady and sunny conditions.

Concerning the grasslands source category, in the first period, the distance to forests (-grad) was the main driver in the Montane and Supramediterranean BRs, and the distance to provincial capitals (V-shape) was the main driver in the Southern Mesomediterranean region. Secondary drivers were the distance to urban settlements (+grad), precipitation, solar radiation, slope, temperature, the utilized agriculture area, and protected areas. Therefore, the drivers suggest that new NEF from grasslands occurred close to preexisting forests, far from provincial capitals and urban settlements, and with different precipitation and temperature patterns in BRs, shady conditions, and steeper slopes.

In the second period, the slope (A-shape) (Figure S7c3) was the main driver in the Montane BR, the percentage of workers in the industry sector (A-shape) was the main driver in the Supramediterranean region, and precipitation (A-shape) in the Southern Mesomediterranean.

Furthermore, the distance to forests (±grad) (Figure S7c3) and temperature (±grad) were also significant in all BRs. Secondary drivers included the distance to provincial capitals (±grad), the utilized agriculture area, and solar radiation. Therefore, during the second period, the new NEF from grasslands continued expanding at more distant locations from forests, with moderate temperature and precipitation constraints, with steeper slopes up to a limit (Figure S7c3), relatively close and far from capitals, and with shady conditions.

For the shrublands source category, in the first period, the distance to forests (-grad) was the main driver in the Supramediterranean and Northern Mesomediterranean BRs, and the second driver after the solar radiation (-grad) in the Montane BR. Precipitation was the main driver in the Southern Mesomediterranean BR and the second driver in the Supramediterranean and Northern Mesomediterranean BRs. Secondary drivers included slope, temperature, distances to provincial capitals, urban settlements, the hydrographic network, the main roads, and soil erosion. Therefore, the drivers suggested that the increase of needleleaf evergreen forests from shrublands was a process of forest consolidation in locations close to previously forested areas, with different precipitation and humidity regimes (which varied by BR), with shady conditions (Figure S7c4), with lower slope values, within a range of temperature constraints (differing depending on BR), and far from urban areas.

In the second period, precipitation (±grad) was the main driver in the Southern Mesomediterranean and Thermomediterranean BRs, and the most important driver after distance to forests (-grad) (Figure S7c4) in the Northern Mesomediterranean, Supramediterranean, and Montane BRs. Secondary drivers included slope (-grad), distance to provincial capitals, distance to the hydrographic network, solar radiation (Figure S7c4), temperature, and drought or humid events. Therefore, during the second period, the increase of needleleaf evergreen forests from shrublands occurred in more distant locations from previously forested areas, within a wide variety of precipitation values (depending on the BR), with shady conditions, relatively far from provincial capitals and the hydrographic network, and with low drought recurrence and higher water oversupply events.

(B) Tables section

Table S1. Details of the imagery used for each land cover map (LCM). Dates are in day-month-year format.

LCM	200-030	200-031	200-032	200-033	200-034
1987			15/03/1988	15/03/1988	15/03/1988
	30/4/1987	14/4/1987	14/04/1987	14/04/1987	14/04/1987
	17/6/1987	17/6/1987	14/06/1986	17/06/1987	17/06/1987
	4/8/1987	4/8/1987	21/07/1988	21/07/1987	21/07/1987
	20/8/1987	20/8/1987	14/08/1985	20/08/1987	20/08/1987
	2/9/1986	2/9/1986	23/09/1988	02/09/1986	02/09/1986
2002			08/03/2000	08/03/2000	16/03/2000
	28/4/2001	28/4/2001	12/04/2001	28/04/2001	12/04/2001
	30/5/2001	30/5/2001	30/05/2001	30/05/2001	10/06/2002
	1/7/2001	1/7/2001	28/06/2000	01/07/2001	
	25/7/2001	25/7/2001	17/07/2001	25/07/2001	25/07/2001
			15/08/2000	15/08/2000	21/08/2002
	17/9/2003	11/9/2001	24/09/2000	24/09/2000	01/09/2003
2017	15/3/2017	15/3/2017	15/03/2017	15/03/2017	15/03/2017
	19/4/2018	19/4/2018	19/04/2018	19/04/2018	19/14/2018
	19/6/2017	19/6/2017	30/06/2015	30/06/2015	11/06/2020
	5/7/2017	5/7/2017	18/07/2016	18/07/2016	13/07/2020
	3/8/2016	3/8/2016			
	22/8/2017	22/8/2017	19/08/2016	19/08/2016	14/08/2020
	7/9/2017	7/9/2017	29/09/2019	29/09/2019	1/10/2020

Table S2. LCM-1987 confusion matrix for Landsat scenes 200–030 to 200–034.

Classified map	Ground truth samples													Total	CE (%)	UA (%)
	NEF	BDF	BEF	Shl	Grl	BrS	Urb	WaB	IHC	RHC	IWC	RWC	Grh			
(NEF) Needleleaf evergreen forest	**573 842**	996	5 940	8 600	126	80	1	4	3	6	219	21	0	589 839	2.7	97.3
(BDF) Broadleaf deciduous forest	269	**342 174**	1 866	1 443	449	0	0	0	217	20	31	0	0	346 469	1.2	98.8
(BEF) Broadleaf evergreen forest	14 153	3 367	**724 699**	31 566	4 440	0	5	0	9	25	2 434	332	0	781 031	7.2	92.8
(Shl) Shrublands	2 353	711	8 160	**1 224 637**	78 091	784	53	8	43	488	833	1 731	0	1 317 893	7.1	92.9
(Grl) Grasslands	33	3 884	789	65 427	**1 275 094**	14 347	642	2	176	17 068	207	7 291	0	1 384 959	7.9	92.1
(BrS) Bare soils	1	0	0	1 570	4 608	**187 122**	410	10	17	3 320	22	131	0	197 211	5.1	94.9
(Urb) Urban areas and Infrastructures	0	0	0	0	36	131	**31 614**	0	0	2	0	0	0	31 783	0.5	99.5
(WaB) Water bodies	0	2	0	0	0	10	0	**24 141**	7	1	0	0	0	24 161	0.1	99.9
(IHC) Irrigated herbaceous crops	0	287	0	133	245	0	3	1	**241 215**	877	1 206	252	0	244 219	1.2	98.8
(RHC) Rainfed herbaceous crops	0	4	0	3 146	9 275	10 979	196	89	1 983	**2 380 492**	501	14 319	0	2 420 986	1.7	98.3
(IWC) Irrigated woody crops	54	89	526	1 643	928	50	265	0	973	450	**279 723**	43 491	0	328 192	14.8	85.2
(RWC) Rainfed woody crops	0	2	31	1 105	5 362	9 561	2 847	2	137	27 225	11 007	**1 067 022**	2	1 124 302	5.1	94.9
(Grh) Greenhouses	0	0	0	0	0	20	77	0	0	2	0	1	**11 378**	11 478	0.9	99.1
NoData	6	0	0	199	6	80	0	0	0	0	0	0	0	291		
Total	590 711	351 518	742 010	1 339 469	1 378 659	223 165	36 114	24 257	244 780	2 429 976	296 185	1 134 592	11 380	8 802 814	OA = 95.0%	
OE (%)	2.9	2.7	2.3	8.6	7.5	16.2	12.5	0.5	1.5	2.0	5.6	6.0	0.0	OAw = 97.2%		
PA (%)	97.1	97.3	97.7	91.4	92.5	83.8	87.5	99.5	98.5	98.0	94.4	94.0	100.0	k = 0.9		

OE: omission error, CE: commission error, PA: producer's accuracy, UA: user's accuracy, *k*: kappa index of agreement, OA: overall accuracy, OAw: overall accuracy weighted by the ground truth area considering only classified pixels (unclassified pixels are not considered errors and are solved by spatial proximity). Figures in bold represent locations where the predicted and the true labels match.

Table S3. LCM-2002 confusion matrix for Landsat scenes 200–030 to 200–034.

Classified map	Ground truth samples														Total	CE (%)	UA (%)
	NEF	BDF	BEF	Shl	Grl	BrS	Urb	WaB	IHC	RHC	IWC	RWC	RiC	Grh			
(NEF) Needleleaf evergreen forest	**823 747**	3 903	19 314	24 536	3 720	0	2	0	16	27	742	45	0	0	876 052	6.0	94.0
(BDF) Broadleaf deciduous forest	5 863	**482 145**	24 327	13 142	10 049	0	0	0	833	13	97	0	0	0	536 468	10.1	89.9
(BEF) Broadleaf evergreen forest	76 891	7 260	**1 155 685**	207 405	36 961	0	5	0	170	597	7 014	2 032	0	0	1 494 020	22.6	77.4
(Shl) Shrublands	28 787	1 902	72 707	**1 460 560**	318 082	1 965	85	6	71	1 746	4 437	5 356	0	0	1 895 703	23.0	77.0
(Grl) Grasslands	2 738	2 008	12 320	164 349	**1 518 469**	33 801	1 333	0	352	93 428	432	21 685	0	1	1 850 916	18.0	82.0
(BrS) Bare soils	8	0	0	26 615	20 967	**199 711**	2 048	180	34	19 252	41	843	0	305	270 004	26.0	74.0
(Urb) Urban areas and Infrastructures	0	0	0	12	28	175	**50 776**	0	0	13	0	20	0	1	51 025	0.5	99.5
(WaB) Water bodies	0	2	0	0	28	28	0	**44 105**	28	10	0	0	0	0	44 201	0.2	99.8
(IHC) Irrigated herbaceous crops	2	1 111	44	128	708	6	0	0	**252 189**	1 333	1 449	2	127	0	257 097	1.9	98.1
(RHC) Rainfed herbaceous crops	63	56	87	5 865	44 110	29 305	2 056	55	2 747	**3 594 131**	102	11 939	6	30	3 690 554	2.6	97.4
(IWC) Irrigated woody crops	1 192	391	6 641	19 559	5 698	45	153	0	3 005	1 436	**378 139**	85 307	0	0	501 565	24.6	75.4
(RWC) Rainfed woody crops	1 114	11	796	8 990	45 651	11 544	13 893	0	3 167	91 239	42 435	**1 610 655**	0	20	1 829 515	12.0	88.0
(RiC) Rice crops	0	2	0	0	0	0	0	0	372	2	0	0	**6 685**	0	7 062	5.3	94.7
(Grh) Greenhouses	0	0	0	0	0	56	178	0	0	3	0	0	0	**29 640**	29 878	0.8	99.2
NoData	663	3 481	383	3 897	1 565	38 624	0	0	0	0	0	0	0	0	48 613		
Total	941 067	502 273	1 292 303	1 935 059	2 006 037	315 261	70 527	44 345	262 983	3 803 228	434 887	1 737 886	6 819	29 998	13 382 673	OA = 86.7%	
OE (%)	12.5	4.0	10.6	24.5	24.3	36.7	28.0	0.5	4.1	5.5	13.0	7.3	2.0	1.2		OAw = 92.2%	
PA (%)	87.5	96.0	89.4	75.5	75.7	63.3	72.0	99.5	95.9	94.5	87.0	92.7	98.0	98.8		k = 0.9	

OE: omission error, CE: commission error, PA: producer's accuracy, UA: user's accuracy, *k*: kappa index of agreement, OA: overall accuracy, OAw: overall accuracy weighted by the ground truth area considering only classified pixels (unclassified pixels are not considered errors and are solved by spatial proximity). Figures in bold represent locations where the predicted and the true labels match.

Table S4. LCM-2017 confusion matrix for Landsat scenes 200–030 to 200–034.

Classified map	Ground truth samples														Total	CE (%)	UA (%)
	NEF	BDF	BEF	Shl	Grl	BrS	Urb	WaB	IHC	RHC	IWC	RWC	RiC	Grh			
(NEF) Needleleaf evergreen forest	**715 557**	802	5 953	6 276	33	0	0	1	20	2	171	4	0	0	728 817	1.8	98.2
(BDF) Broadleaf deciduous forest	257	**424 599**	1 739	2 272	2 403	0	0	0	358	39	24	1	0	0	431 692	1.6	98.4
(BEF) Broadleaf evergreen forest	9 000	1 027	**866 533**	64 636	2 841	0	0	1	24	32	2 391	321	0	0	946 805	8.5	91.5
(Shl) Shrublands	4 483	595	28 744	**1 195 923**	76 336	489	8	1	24	193	1 712	954	3	0	1 309 465	8.7	91.3
(Grl) Grasslands	264	820	3 490	67 951	**1 138 744**	13 115	498	11	327	18 274	598	13 289	0	2	1 257 383	9.4	90.6
(BrS) Bare soils	0	15	0	1 050	2 086	**191 240**	835	17	20	5 101	19	415	0	55	200 853	4.8	95.2
(Urb) Urban areas and Infrastructures	0	0	0	41	22	2 955	**67 573**	0	0	52	1	36	0	1	70 680	4.4	95.6
(WaB) Water bodies	0	87	0	0	5	11	2	**30 809**	67	0	2	0	0	0	30 984	0.6	99.4
(IHC) Irrigated herbaceous crops	0	168	0	25	219	0	6	0	**149 625**	951	447	6	50	0	151 496	1.2	98.8
(RHC) Rainfed herbaceous crops	0	18	0	2 519	4 182	8 933	196	11	1 322	**2 382 902**	279	6 830	0	2	2 407 194	1.0	99.0
(IWC) Irrigated woody crops	22	138	656	1 304	657	45	28	0	967	282	**341 843**	19 136	0	0	365 078	6.4	93.6
(RWC) Rainfed woody crops	1	3	11	820	2 047	2 318	2 817	0	163	32 916	24 966	**1 213 489**	0	2	1 279 555	5.2	94.8
(RiC) Rice crops	0	18	0	0	0	0	0	0	130	1	2	0	**3 227**	0	3 377	4.5	95.5
(Grh) Greenhouses	0	0	0	0	0	11	117	0	0	3	0	0	0	**22 809**	22 940	0.6	99.4
NoData	199	45	84	74	44	80	0	0	0	0	0	0	0	0	525		
Total	729 781	428 335	907 212	1 342 891	1 229 620	219 199	72 080	30 852	153 045	2 440 747	372 455	1 254 480	3 279	22 870	9 206 845	OA = 95.0%	
OE (%)	1.9	0.9	4.5	10.9	7.4	12.8	6.3	0.1	2.2	2.4	8.2	3.3	1.6	0.3		OAw = 96.9%	
PA (%)	98.1	99.1	95.5	89.1	92.6	87.2	93.7	99.9	97.8	97.6	91.8	96.7	98.4	99.7		k = 0.9	

OE: omission error, CE: commission error, PA: producer's accuracy, UA: user's accuracy, *k*: kappa index of agreement, OA: overall accuracy, OAw: overall accuracy weighted by the ground truth area considering only classified pixels (unclassified pixels are not considered errors and are solved by spatial proximity). Figures in bold represent locations where the predicted and the true labels match.

Table S5. Soil loss' categorical value ranges and interpretation descriptions. Units of soil loss: Mg/(ha × year)

Soil loss	Interpretation
0	Areas not susceptible to the erosive process, such as urban spaces, roads, reservoirs, etc.
0 – 5	Areas with very low levels of erosion and tolerable soil loss. There is no net erosion.
5 – 10	Areas with low levels of erosion and soil loss that may be tolerable. There is probably no net erosion.
10 – 25	Areas with mild erosive processes. There is erosion, although it is not visible to the naked eye.
25 – 50	Areas with moderate erosive processes. There is erosion, although it may not be visible to the naked eye.
50 – 100	Areas with severe erosive processes. There is erosion, and it is visible to the naked eye.
100 – 200	Areas with very serious erosive processes. There is erosion, and it is evident to the naked eye.
> 200	Areas with extreme erosive processes. There is erosion, and it is obvious to the naked eye.

Table S6a. The number of presences after applying uncertainty restrictions. The bioclimatic regions' (BR) numbers assignation is detailed in Figure S4.

Bio. region	BR.1		BR.2		BR.3		BR.4		BR.5		BR.6		BR.7		BR.8	
NF dynamic	P1	P2	P1	P2	P1	P2	P1	P2	P1	P2	P1	P2	P1	P2	P1	P2
RHC-BDF [1]	0	0	204	2716	1	339	0	0	1977	12646	725	3986	2	51	173	1226
RHC-BEF [1]	0	0	84	308	2	42	0	0	2063	16155	1663	15504	12	5	79	359
RHC-NEF [1]	0	0	97	184	1	389	0	0	52	448	239	776	0	22	141	1365
RWC-BDF [1]	0	0	0	1	0	0	0	0	150	1327	371	2780	16	215	7	261
RWC-BEF [1]	0	0	0	0	0	0	0	0	2620	7439	21615	72939	71	170	10	53
RWC-NEF [1]	0	0	0	0	0	3	0	0	66	94	1049	2368	213	214	59	312
IHC-BDF [1]	0	0	308	122	3360	1486	0	0	3271	3658	5307	8300	85	337	1290	4557
IHC-BEF [1]	0	0	23	33	118	11	0	0	121	307	1364	1589	20	0	75	257
IHC-NEF [1]	0	0	25	8	231	1859	0	0	13	14	328	879	18	5	49	2548
IWC-BDF [1]	0	0	170	114	1109	953	0	0	1185	2273	3967	9632	493	8250	4222	7810
IWC-BEF [1]	0	0	98	115	50	26	0	0	7336	4545	65198	52404	646	321	553	342
IWC-NEF [1]	0	0	6	22	45	223	0	0	167	47	3819	4138	674	532	382	1569
Grl-BDF [2]	29	275	31328	37624	11612	3505	136	77	14310	35806	1067	3323	0	35	326	476
Grl-BEF [2]	3	80	2061	1054	1293	302	389	194	45600	66619	72322	157122	131	37	169	200
Grl-NEF [2]	218	499	6391	2871	4819	8607	316	73	1127	1686	2010	4452	206	296	166	481
Shl-BDF [2]	0	0	2397	3465	275	538	4	1	21458	20335	841	417	1	1	196	418
Shl-BEF [2]	0	2	11311	16234	130	83	57	325	334428	292334	129296	84458	165	164	3204	4905
Shl-NEF [2]	1	0	3974	6028	508	1760	355	599	74017	65752	26391	44419	760	2384	12198	27249

[1] Presences given an *uncertainty* < 0.3 (crop categories). [2] Presences given an *uncertainty* < 0.1 (Shl and Grl).

Table S6b. The number of presence-absence locations used for modeling after applying uncertainty and spatial autocorrelation restrictions. Presence-absences were extracted within BRs, using absence points with a steady thematic temporal pattern. Grey highlights indicate which NF dynamics were analyzed. The figures refer to the number of sites (equal number of presence and absence) available for analysis. The bioclimatic regions' (BR) numbers assignation is detailed in Figure S4.

Bio. region	BR.1		BR.2		BR.3		BR.4		BR.5		BR.6		BR.7		BR.8	
NF dynamic	P1	P2	P1	P2	P1	P2	P1	P2	P1	P2	P1	P2	P1	P2	P1	P2
RHC-BDF [1]	0	0	61	316	1	170	0	0	1059	4807	371	1730	1	26	94	613
RHC-BEF [1]	0	0	42	154	1	21	0	0	1168	5000	853	5000	6	3	40	180
RHC-NEF [1]	0	0	49	92	1	195	0	0	26	224	120	388	0	11	69	600
RWC-BDF [1]	0	0	0	1	0	0	0	0	15	97	198	1315	8	108	4	131
RWC-BEF [1]	0	0	0	0	0	0	0	0	450	921	5000	5000	36	85	5	27
RWC-NEF [1]	0	0	0	0	0	2	0	0	33	47	503	1141	107	107	30	156
IHC-BDF [1]	0	0	154	61	562	706	0	0	159	225	1733	2197	43	169	489	1691
IHC-BEF [1]	0	0	12	17	59	6	0	0	61	154	477	545	10	0	38	129
IHC-NEF [1]	0	0	13	4	51	201	0	0	7	7	164	440	9	3	25	847
IWC-BDF [1]	0	0	85	57	555	477	0	0	86	253	1808	4329	207	1972	1421	3239
IWC-BEF [1]	0	0	49	58	25	13	0	0	342	313	5000	5000	323	161	277	171
IWC-NEF [1]	0	0	3	11	23	112	0	0	84	24	1536	2052	337	266	152	789
Grl-BDF [2]	15	138	4729	5000	950	1119	68	39	5000	5000	1025	3132	0	18	163	238
Grl-BEF [2]	2	40	1867	910	1228	294	195	97	5000	5000	5000	5000	66	19	85	100
Grl-NEF [2]	109	250	2129	2207	411	346	158	37	1113	1644	1928	4179	103	148	83	241
Shl-BDF [2]	0	0	1202	1611	138	269	2	1	5000	5000	421	209	1	1	98	209
Shl-BEF [2]	0	1	5000	5000	65	42	29	163	5000	5000	5000	5000	83	82	3169	4876
Shl-NEF [2]	1	0	3739	5000	51	65	178	300	5000	5000	5000	5000	378	1079	5000	5000

[1] Presences given an *uncertainty* of < 0.3 (crop categories). [2] Presences given an *uncertainty* of < 0.1 (Shl and Grl).

Table S7. Models' results by source category and forest group. The main drivers' relative importances and related PDP patterns are provided. For the sake of simplicity, only BDF modeling results are shown. The bioclimatic regions' (BR) number equivalence is described in Figure S4.

BDF - Period 1	RHC			RWC	IHC			IWC			Grl				Shl	
Variable \ BR.	BR.5	BR.6	BR.8	BR.6	BR.3	BR.6	BR.8	BR.6	BR.7	BR.8	BR.2	BR.3	BR.5	BR.6	BR.2	BR.5
Slope					13.4 +		8.3 +	17.6 V			28.3 A	19.3 +				
General Curvature					28 -					6.2 -						
Pot_Rad_Wint											10.9 -	19.6 -	20.8 -		11.2 -	
Ac_Rain	21.9 и					13.4 A					10 -		17 +	26.7 +	38.5 +	17.7 A
Av_Me_Temp								25.1 -			20.4 A		11.7 A	37.5 -	19.2 -	18.2 A
DE6_S6																12.9 -
DE9_S6																
DE3_S12																
DE3_S24																
HE3_S12																
Eu_Dist_Hyd	20.6 -					17 -	56.8 -	25 -		49.2 -						
Co_Dist_M_Roads						13.8 +	9 =	12.6 +							9.7 -	
Co_Dist_S_Roads							9.9 =			7.3 +						
Co_Dist_Urb	12.7 -				22.1 +								17.5 -		15.3 +	
Co_Dist_Cap	18.7 +					36.3 +				18.5 V		22.2 -				18.9 -
Eu_Dist_Forest	26 -				20.4 -	19.6 -	16 -	19.6 -		18.9 -	30.4 -	15.3 -	33 -	11.3 -	15.8 -	32.3 -
Soil_Erosion					16.1 -							23.6 -				
Protected_Areas																
Pop_Density																
W_Building																
W_Services																
W_Industry																
Num_Hold														14.8 -		
LSU																
UAA																
Model accuracy	0.84				0.83	0.88	0.86	0.85		0.85	0.85	0.81	0.79	0.94	0.87	0.8

BDF - Period 2	RHC			RWC	IHC			IWC			Grl				Shl	
Variable \ BR.	BR.5	BR.6	BR.8	BR.6	BR.3	BR.6	BR.8	BR.6	BR.7	BR.8	BR.2	BR.3	BR.5	BR.6	BR.2	BR.5
Slope					14.4 +		8 +	22.1 -	7.1 -		22.9 A	20.1 V				
General Curvature		8.1 V			32.5 V		6.3 V			6 -						
Pot_Rad_Wint					17.9 V							26.2 -	21.2 -		11.1 -	18.1 -
Ac_Rain	18.9 N	23.3 +		15.4 -		17.6 +			5.7 =		19.9 -		18.8 A		24.7 +	22.7 A
Av_Me_Temp		15.2 V		12.8 -				19.8 -	73.3 +		19.9 A			40.8 -	35 -	26.9 A
DE6_S6																
DE9_S6																
DE3_S12																
DE3_S24																
HE3_S12																
Eu_Dist_Hyd	18.4 -	22.9 -	38.7 -	18.7 -		18.1 -	46.7 -	26.8 V	9.4 -	41.1 -			18.1 -	15.6 -	14.9 V	
Co_Dist_M_Roads						12.9 A										
Co_Dist_S_Roads			12.3 -													
Co_Dist_Urb	14.9 -		20.1 -		21.1 +							18.8 +		12.2 -		15.6 V
Co_Dist_Cap	22.1 V		16 +			34.2 +	20.7 +			19.8 +	21.1 +	20.6 -	19.5 -		14.4 +	
Eu_Dist_Forest	25.6 -	30.6 -	12.9 -	14.4 -		17.2 -	18.4 V	17.2 -	4.5 =	21.6 -	16.2 -		22.4 -	11.8 -		16.7 -
Soil_Erosion					14.3 -			14.2 -				14.3 -				
Protected_Areas																
Pop_Density										11.4 -						
W_Building																
W_Services																
W_Industry																
Num_Hold				38.7 -										19.7 -		
LSU																
UAA																
Model accuracy	0.79	0.83	0.85	0.9	0.77	0.77	0.8	0.78	0.95	0.79	0.75	0.77	0.73	0.9	0.85	0.73

Figure S4. Climatic segmentation of the Iberian Peninsula in bioclimatic regions (BRs) and the spatial context of the transect. Due to the reduced spatial representativeness of the transect, the Alpine and Subalpine regions were aggregated into region 1, and the Criomediterranean and Oromediterranean regions in the Sierra Nevada mountain range were aggregated into region 4. Furthermore, the extensive Mesomediterranean region was subdivided into two parts, separated by the Iberian System mountain range; thus, the Southern part is represented by region 6 while the Northern part is represented by region 8.
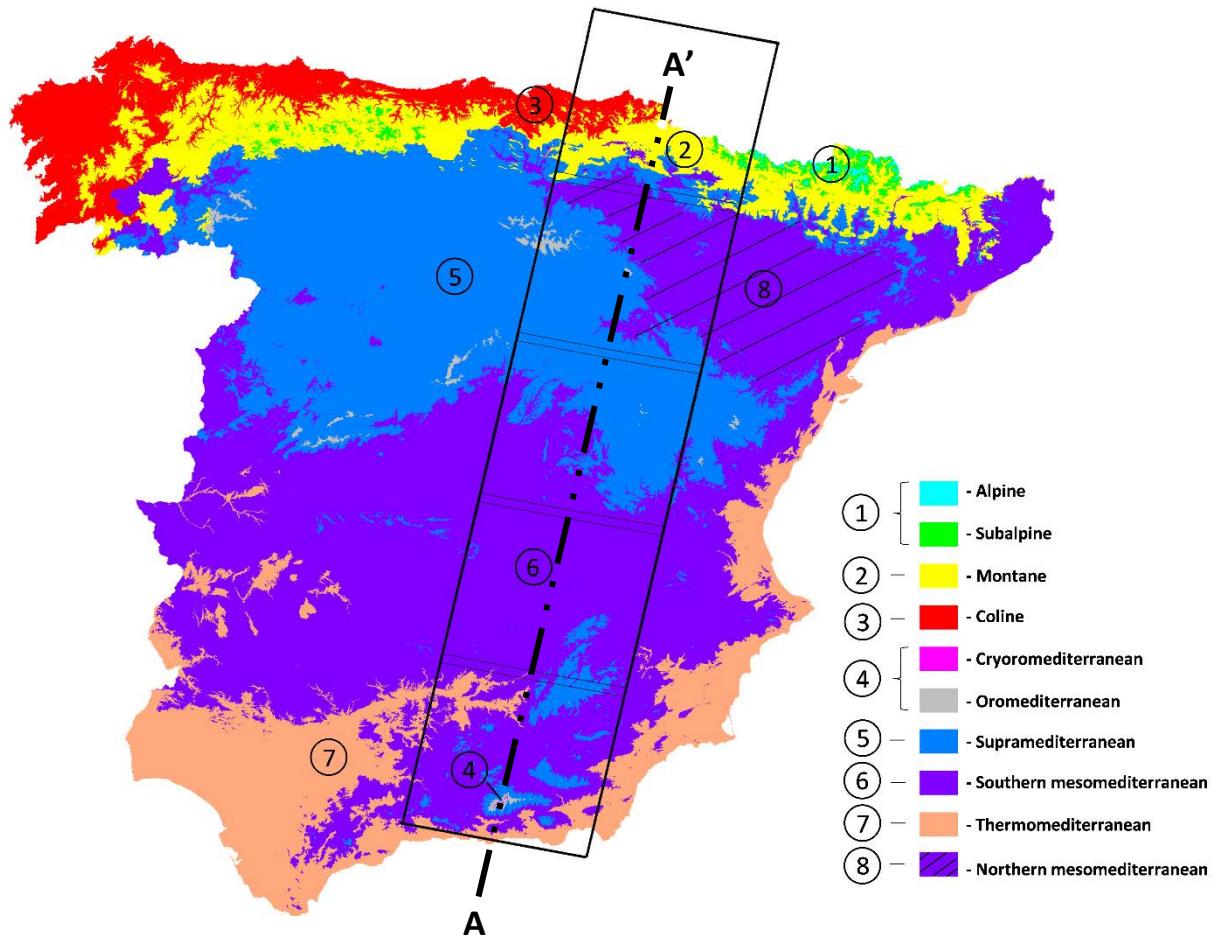
Figure S5. Profiles of altitude, average mean temperature, average accumulated annual precipitation, and potential solar radiation, as measured along the transect line (**A-A'**) depicted in Figure S4. Note the well-known and high correlation between altitude and average mean temperature.
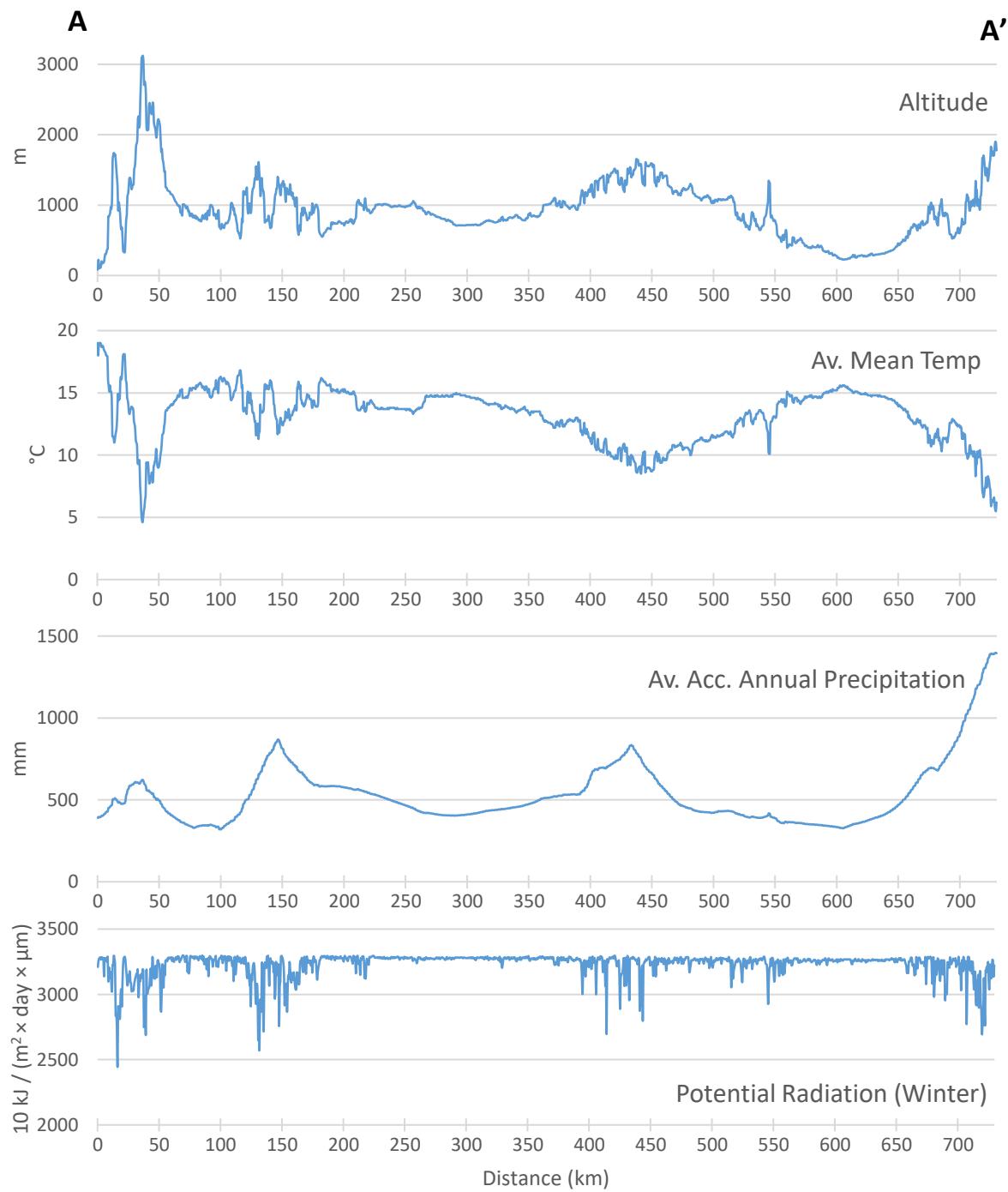
Figure S6. New forest dynamics disaggregated by bioclimatic region (BR). In (a), a histogram of the frequency of the categories evolving to NF in three temporal moments is shown. The chord diagram between 1987–2002 (b) and between 2002–2017 (c) are represented. The numbers on the chord diagrams represent the absolute frequency of each category disaggregated by BR.

(a) (b) (c)

BR. 1
Alpine
Subalpine

BR. 2
Montane

BR. 3
Coline

BR. 4
Cryoro.
Oromed.
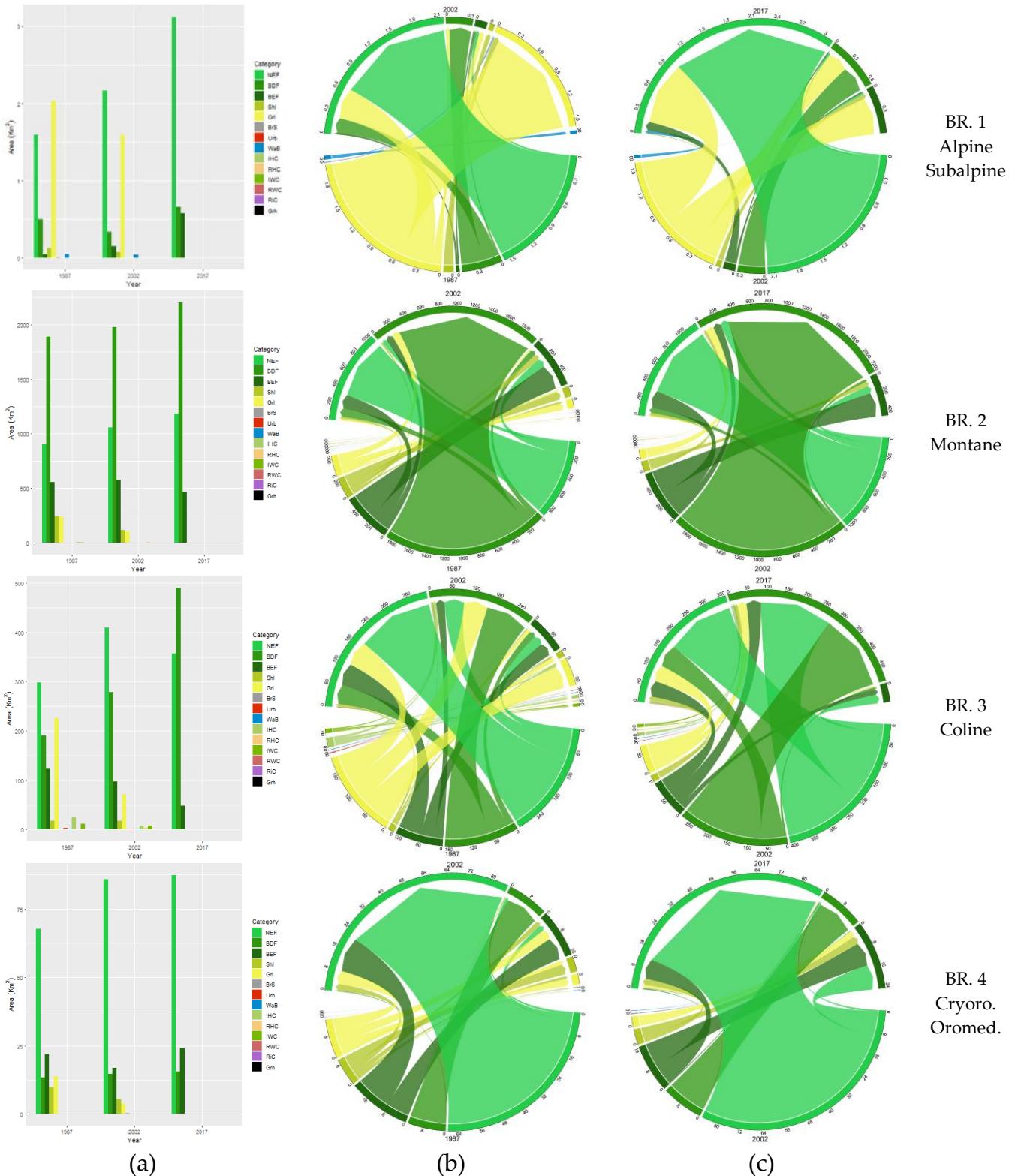
Figure S6. New forest dynamics disaggregated by BR (Figure continued).

BR. 5
Supramed.

BR. 6
Mesomed.
South

BR. 7
Thermomed.

BR. 8
Mesomed
North

(**a**)   (**b**)   (**c**)
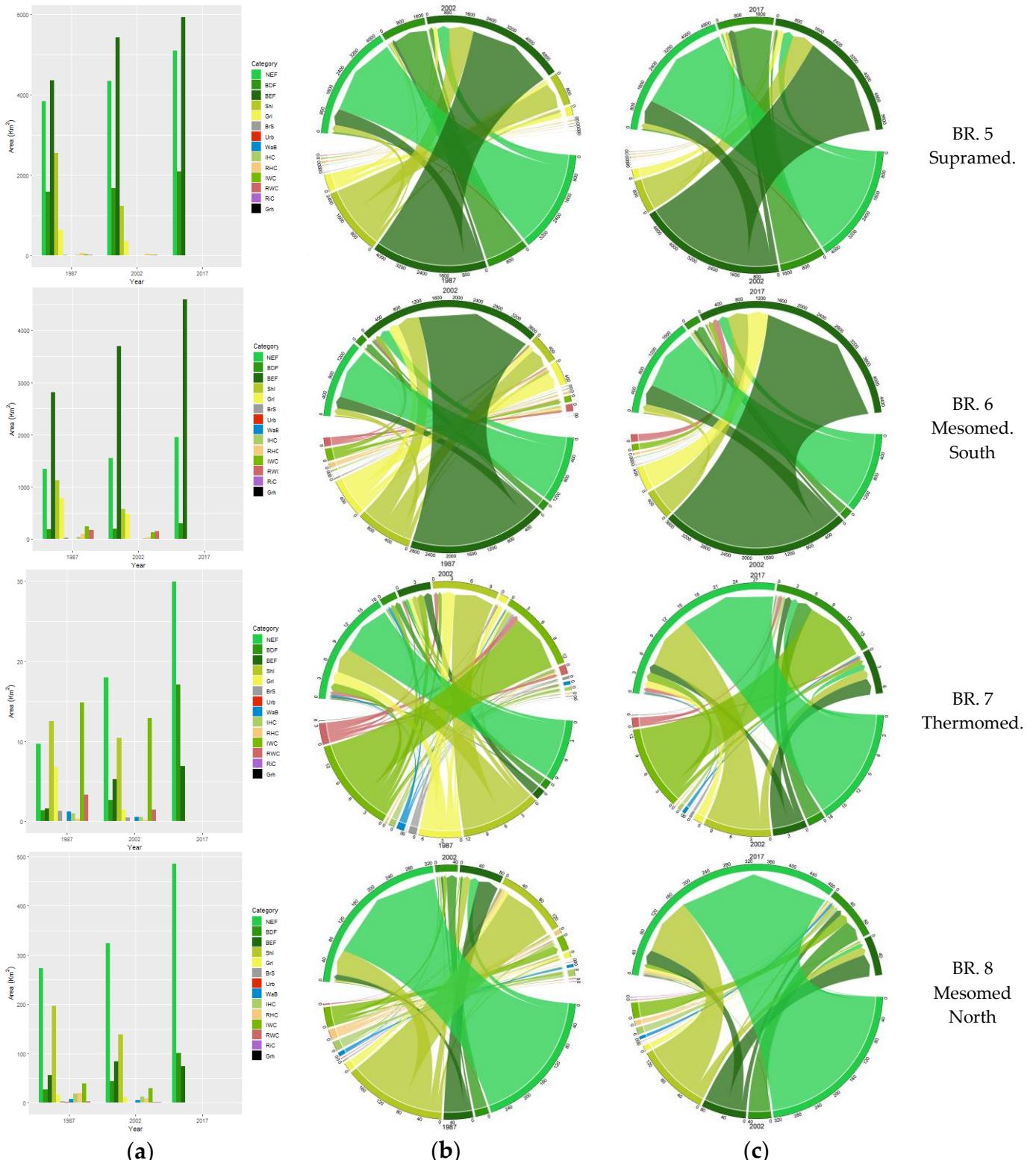
Figure S7a. Examples of representative dependence plots for the new BDF source categories. Blue and red colors correspond to the first (1987–2002) and second (2002–2017) periods. The density of occurrences is represented by vertical lines on the x-axes, with black rug lines denoting the 5%, 50%, and 95% percentiles.

NF dynamic	Dependence plots
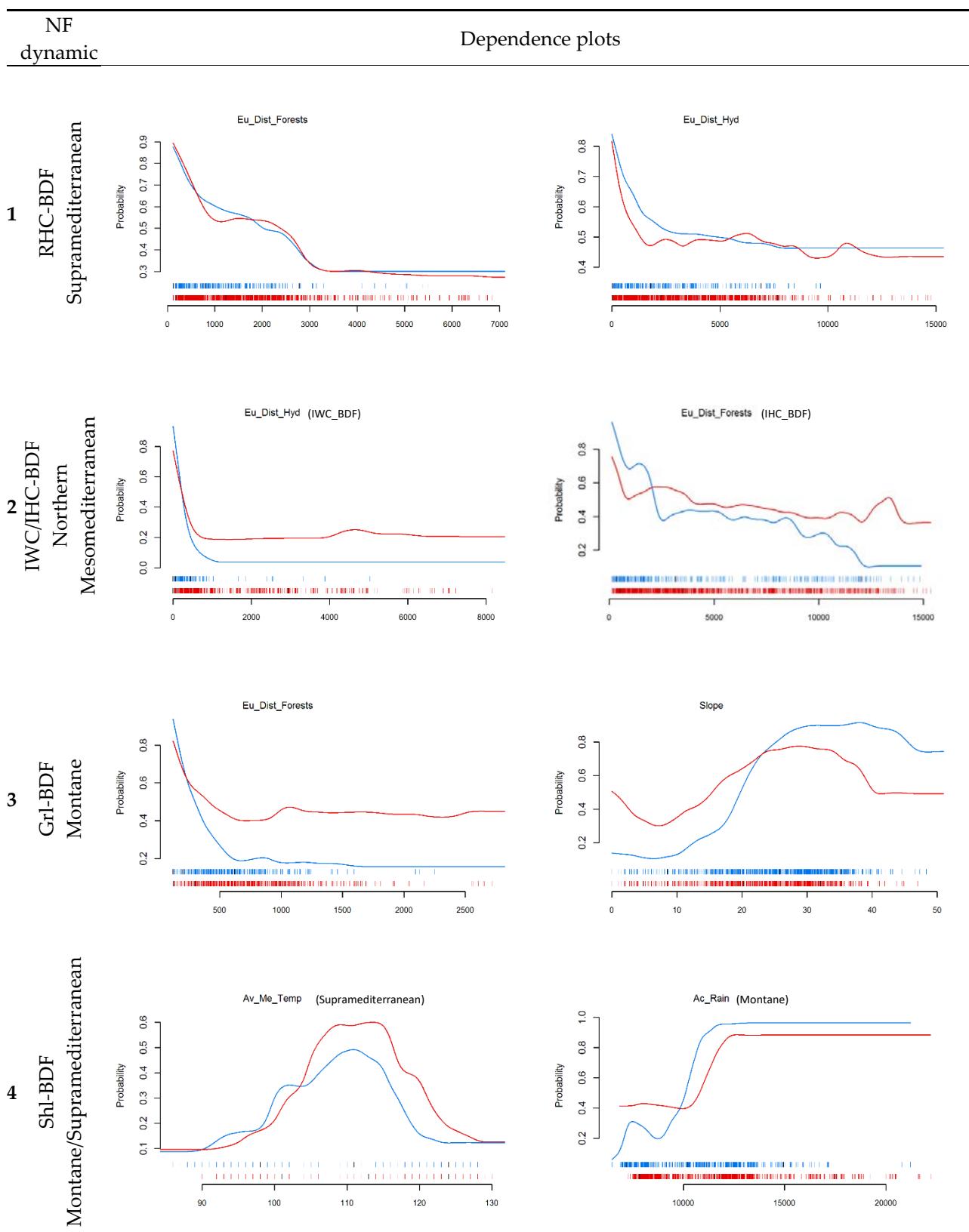
Figure S7b. Examples of representative dependence plots for the new BEF source categories. Blue and red colors correspond to the first (1987–2002) and second (2002–2017) periods. The density of occurrences is represented by vertical lines on the x-axes, with black rug lines denoting the 5%, 50%, and 95% percentiles.

NF dynamic	Dependence plots
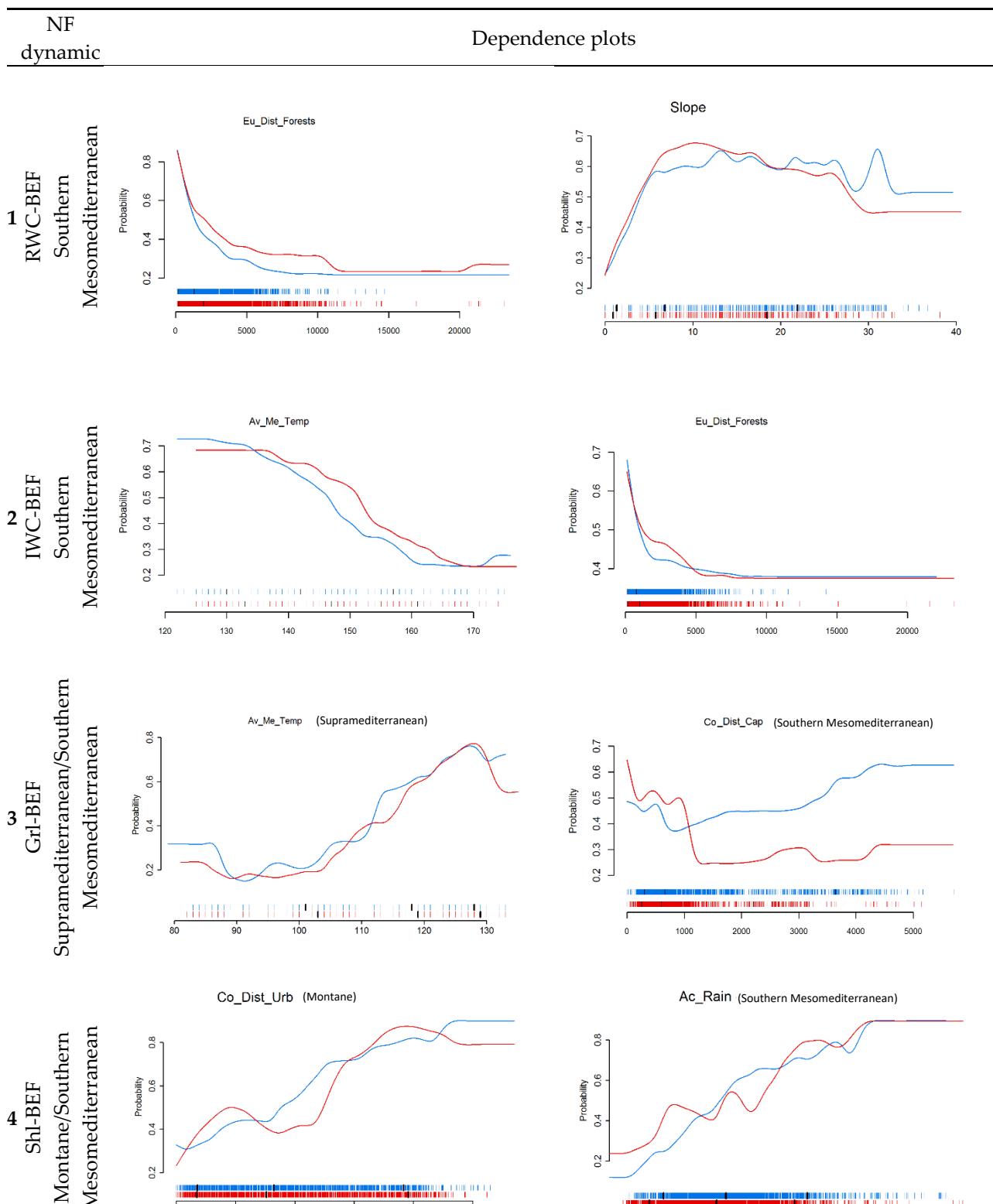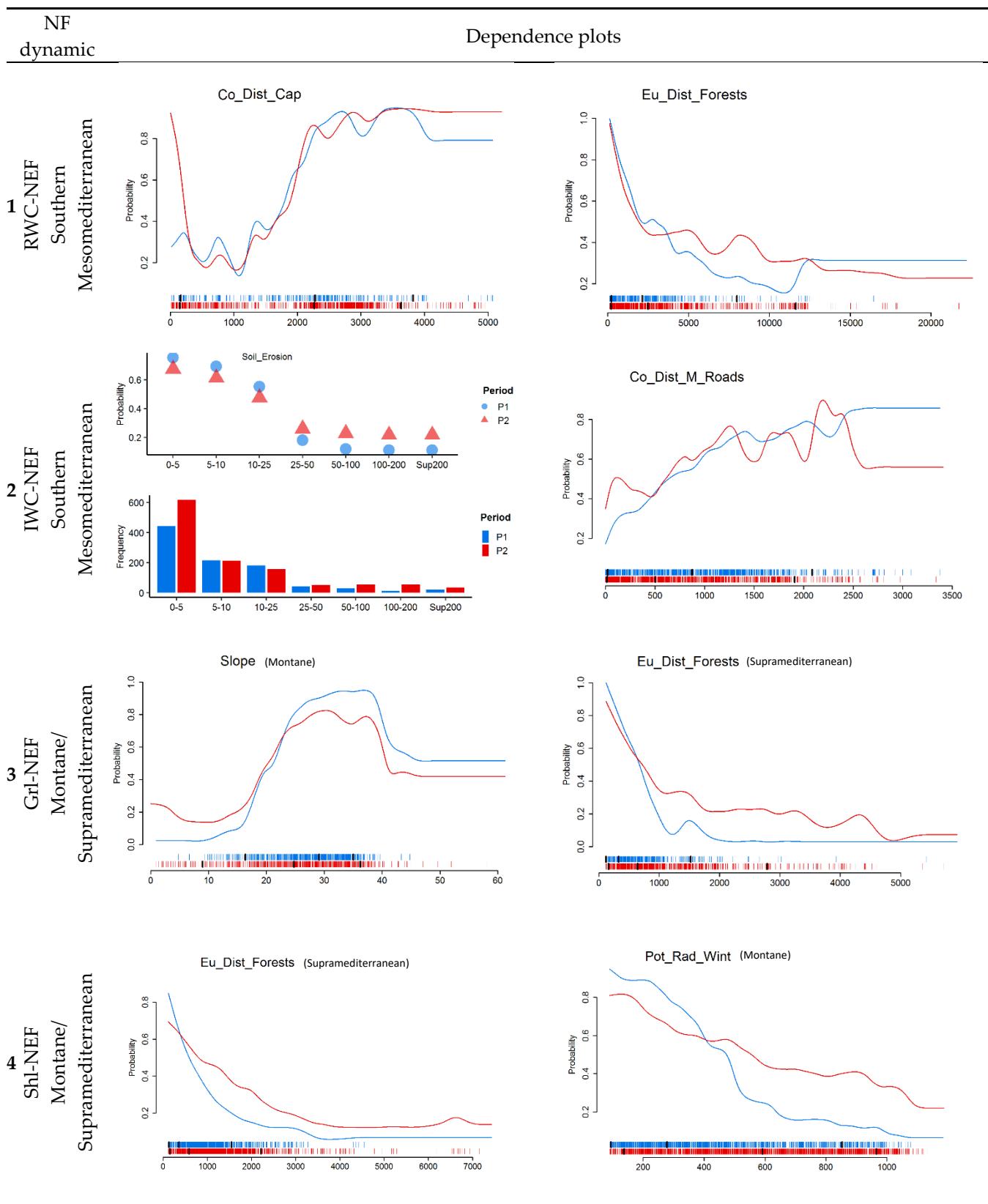
Figure S7c. Examples of representative dependence plots for the new NEF source categories. Blue and red colors correspond to the first (1987–2002) and second (2002–2017) periods. The density of occurrences is represented by vertical lines on the x-axes, with black rug lines denoting the 5%, 50%, and 95% percentiles.

NF dynamic	Dependence plots

RESUMEN DE RESULTADOS Y DISCUSIÓN GENERAL

5. RESUMEN DE RESULTADOS Y DISCUSIÓN GENERAL

Esta Tesis aborda distintos aspectos metodológicos y de análisis desde una perspectiva de trabajo *Big Data*, en la cual se han recopilado, procesado y analizado grandes volúmenes de datos de distinta naturaleza: climáticos, socioeconómicos, imágenes de teledetección y diferentes bases de datos auxiliares (SIOSE, Inventario Forestal Nacional, Censos de Población y Censos Agrarios, entre otros), lo que ha sido posible gracias a la utilización de distintos códigos de programación, como son *Matlab*, ficheros de procesado por lotes (*Batch scripts*) y finalmente código *R*, además del empleo de programas GIS, incluyendo MiraMon, ArcGIS y ENVI. A diferencia de otras aproximaciones o estudios más locales, la presente Tesis aporta unas conclusiones que se derivan de un análisis a gran escala, sin renunciar a un nivel de detalle espacial importante, además de gran robustez metodológica.

En el **artículo 1**, se pone de manifiesto la necesidad de realizar un relleno de series, debido a la elevada proporción de datos faltantes en las estaciones climáticas a nivel peninsular.

Se evaluaron las implicaciones de distintos métodos de relleno sobre las tendencias climáticas de la temperatura media mensual y la precipitación acumulada mensual. Así, se desprende que los métodos que consideran estaciones vecinas próximas, presentaron tendencias similares independientemente del nivel de agregación temporal de los datos. Además, los métodos se diferenciaron claramente del método MONTH, espacialmente autocoherente, lo que derivó en una fuerte reducción en la variabilidad—aspecto ampliamente evidenciado en estudios previos (Serrano-Notivoli *et al.*, 2017; Teegavarapu and Nayak, 2017; Beguería *et al.*, 2019)—debido a la propagación iterativa de valores promediados. Es evidente, por tanto, que su aplicabilidad se enfocaría preferentemente al relleno de datos faltantes aislados, descartándose su aplicabilidad en un contexto de relleno iterativo. La reducción de la variabilidad, además, tendría un efecto en la compresión de los valores extremos de las series, lo que tendría una implicación clara a la hora de realizar análisis de fenómenos climáticos extremos (Acero et al., 2014; Teegavarapu and Nayak, 2017; Bhatti et al., 2020).

El papel que ha jugado la estructura espaciotemporal de la base de datos ha quedado manifiesto cuando se comparan los periodos analizados. Las mayores diferencias espaciales entre métodos se observaron en el primer periodo (1950–1979), caracterizado por un menor número de observaciones disponibles. En el segundo periodo los patrones espaciales de las tendencias mostraron mayor similitud entre métodos, debido a la mayor cantidad de datos disponibles y una distribución espaciotemporal más densa. Ello viene a indicar que la selección del método de relleno importa, sobre todo cuando el número de observaciones disponibles es menor y su distribución espaciotemporal es más dispersa.

Si se atiende a la variable de la temperatura, se observa una mayor variabilidad espacial de las tendencias en los meses de verano entre los distintos métodos en el primer periodo. Este hecho indicaría que existe una mayor complejidad en el análisis e interpretación de los patrones espaciales en los meses estivales, lo que en parte podría estar justificado por el porcentaje ligeramente superior de huecos faltantes existente en estos meses. De otro lado, en el segundo periodo se observa un patrón de calentamiento más marcado en la vertiente mediterránea, mientras que la vertiente norte y atlántica de la PI presenta un mayor número de meses con tendencias de enfriamiento.

En cuanto a los métodos de relleno se refiere y centrándonos en la variable temperatura, el método IDW considera 7 estaciones próximas a la hora de estimar el valor faltante, otorgando mayor peso a las más estaciones más próximas con datos. Durante el periodo 1950–1979 el relleno de las series se realiza en un contexto de menor densidad de información. Así, en los mapas de la Figura 10 del artículo 1, se observaron tendencias locales de calentamiento en el primer periodo, en áreas de la provincia de Cáceres al sur de la cordillera del Sistema Central. En este contexto, existe un conjunto local de estaciones más longevas (3439, 3510, 3519, 3448, 3525O, 3531) que son proveedoras de datos para nuevas estaciones instaladas en la misma zona a partir de 1975. Estas nuevas estaciones no contienen información anterior a 1975, siendo rellenadas a partir de los datos locales que proveen las estaciones anteriormente indicadas. El efecto observado es un patrón de calentamiento geográficamente localizado potenciado por el método empleado. Otros ejemplos similares tienen lugar en la Sierra de Grazalema (Cádiz), en la Sierra de la Cabrera (entre León, Zamora y Ourense), en el Massís del Montseny (entre Barcelona y Girona), en áreas del Pirineo próximo a Pamplona o en el entorno de la ciudad de Lisboa, en las cuales se observan tendencias climáticas locales negativas.

De otro lado, el método REGR considera 45 observaciones próximas a partir de las cuales se resuelve un modelo de regresión múltiple, utilizando la latitud, la longitud, la altitud, la radiación potencial solar y la distancia euclidiana a la costa como regresores a la hora de imputar el valor faltante. El mayor número de observaciones empleado implica incorporar en el modelo una mayor variabilidad de observaciones de estaciones meteorológicas con distintas características climáticas, lo que hace que el valor estimado presente una respuesta promediada de un mayor conjunto de estaciones. Como resultado, el patrón espacial de las tendencias del primer periodo claramente se suaviza en comparación al patrón observado en el método IDW, especialmente en los meses estivales. Así, las tendencias locales de calentamiento evidenciadas por el método IDW desaparecieron, permaneciendo las tendencias negativas del Massís del Montseny y las de la región de Lisboa.

El método SIMILAR localiza dentro de un buffer espacial la estación que presenta mayor similitud al comparar un conjunto de 'n' observaciones comunes entre series. Posteriormente, se resuelve un modelo lineal simple con las observaciones comunes a las estaciones comparadas para aproximar el valor faltante. Las fases iterativas iniciales dan prioridad a estaciones próximas con largas series de datos, lo que en fases iterativas posteriores se extiende a un rango de estaciones mayor (Δ RMSE + ∇ *Buffer* Temporal + Δ *Buffer* Espacial). A la hora de rellenar aquellas estaciones de reciente implantación (posterior a 1975), los valores previos a esta fecha son estimados en base al conjunto de 'n' observaciones disponibles en la estación problema y que tienen correspondencia en estaciones vecinas próximas. El relleno iterativo de estas series extiende por sus extremos de una forma paulatina el conjunto de datos disponibles utilizados en iteraciones sucesivas. Como resultado de este planteamiento iterativo, el patrón espacial observado es diferente al resto de métodos espaciales analizados.

A la hora de imputar el valor del dato faltante en el método SIMILAR, se evaluaron tres opciones: (i) La asignación directa del valor de la estación con mayor similitud en base el RMS calculado. En este primer caso no se realiza ningún tipo de ajuste que minimice el posible sesgo (diferencias entre la variabilidad de las series) existente entre las series comparadas, lo que genera el mayor error global en los valores predichos. (ii) Mediante la asignación directa del valor de la estación con mayor similitud, pero aplicando una

corrección del sesgo existente entre series, calculado a partir de la estimación del promedio de las desviaciones. Esta corrección reportó una mejora del error global respecto al sub-método anterior. (iii) A partir de la estación con mayor R^2, y la resolución de un modelo de regresión lineal simple a partir de las observaciones comunes entre las series comparadas. Este sub-método proporciona los mejores resultados en las pruebas realizadas (menor RMSE global), además de presentar mayor flexibilidad a la hora de imputar datos faltantes a partir de series con una marcada variabilidad en sus datos como, por ejemplo, aquellas estaciones ubicadas próximas a la costa, de menor variabilidad climática, respecto a estaciones situadas en el interior, con una mayor variabilidad en sus datos característica. Por defecto, se consideran series con un R^2 superior a 0.6, aunque en futuras pruebas, se podría considerar un nivel de exigencia mayor. A su vez, un umbral de distancia geográfica en los métodos espaciales (SIMILAR, REGR e IDW) acotaría el ámbito geográfico dentro del cual localizar las estaciones vecinas. No obstante, se habría de aplicar con cautela, ya que aplicar una restricción geográfica podría excluir aquellas estaciones que presenten características climáticas similares ubicadas fuera del *buffer* espacial considerado (*e.g.*, zonas de grandes valles y cuencas hidrográficas), y considerar estaciones más próximas y de menor semejanza climática (*e.g.*, estaciones singulares a media ladera de relieves montañosos). En definitiva, el método SIMILAR presentó el menor error global en las series de precipitación y temperatura, empleando el sub-método R^2. A pesar de mostrar una gran efectividad en el relleno, ha quedado poco manifiesta la repercusión de propagar valores estimados/rellenados dentro de una metodología iterativa, más allá de la compresión de la variabilidad de los datos observada también en el resto de los métodos.

Un aspecto adicional por considerar es el hecho de que las parametrizaciones utilizadas en cada método se estimaron considerando todo el periodo temporal completo (1950–2019). No obstante, en futuros análisis se derivarían de forma particular para cada periodo temporal, siendo más acordes a la estructura espaciotemporal de cada periodo. Sería razonable pensar que el número de estaciones vecinas requeridas a la hora de imputar los valores faltantes podría ser algo mayor para el primer periodo, y menor en el segundo periodo, debido a la mayor densidad de información existente.

Otras aproximaciones de relleno de datos faltantes que resultan de interés se basan en la generación de series de referencia, creadas para una ubicación concreta (típicamente, una estación problema), empleando distintos esquemas de ponderación de las observaciones contenidas en las *kNN* estaciones más próximas (Serrano-Notivoli et al., 2017; Beguería et al., 2019). Los métodos de ponderación que tradicionalmente son utilizados se basan en el criterio de la distancia geográfica, otorgando un peso mayor a las estaciones más próximas, o bien en función de la correlación (de Pearson) existente entre las series de datos. Además en Beguería et al. (2019), se proponen estrategias que permiten adaptar las series vecinas a las características (promedio y desviación estándar) de la serie problema. Para ello, los datos de las *kNN* estaciones vecinas se escalan de acuerdo con la variabilidad de la estación problema, previamente al cálculo de los valores en la serie de referencia. De otro lado, a fin de minimizar la reducción de la variabilidad de los datos en la serie de referencia generada (consecuencia del promedio ponderado de las *kNN* observaciones vecinas), proponen una segunda corrección que minimice el efecto de la compresión de la variabilidad existente entre la serie de referencia y la serie problema. Estas aproximaciones metodológicas presentan interés, ya que generan series de referencia normalizadas respecto a la serie problema, además de minimizar el efecto de la compresión de la variabilidad en los datos.

Sin embargo, estas aproximaciones no han sido aplicadas debido al elevado número de estaciones consideradas en este estudio, lo que derivaría en un elevado tiempo de computación en las implementaciones disponibles, a lo que se sumaría la implementación del diseño experimental requerido.

Los patrones de las tendencias climáticas observadas apuntan a un incremento global de 1.45 °C (0.21 °C/década) en la temperatura media para el periodo 1950–2019, valores algo inferiores a los reportados en otros estudios, aunque empleando un menor número de estaciones y distinto rango temporal (Luna et al., 2011). El mayor incremento se observa en los meses de primavera y verano, lo que tiene una influencia decisiva sobre la tendencia anual observada, aspecto que coincide con estudios previos (Gonzalez-Hidalgo et al., 2016). Además, los meses de la primavera presentaban una tendencia al enfriamiento en el primer periodo que se invierte de forma clara en el segundo periodo (Bilbao et al., 2019). Las tendencias en la precipitación fueron poco marcadas y en elevado número no significativas, lo que viene a estar asociado con una alta variabilidad temporal en las series. Esta situación ha hecho suponer que los métodos de regresión lineal no son especialmente sensibles a la hora de captar las tendencias a largo plazo de la precipitación. Además, se puso de manifiesto la importancia de analizar las tendencias a diferentes niveles de agregación temporal (mensual, estacional, anual), ya que, aunque a nivel general existe un calentamiento generalizado, a nivel de detalle existen tendencias de enfriamiento, que pueden ser especialmente determinantes en los ciclos vitales de ciertos grupos de organismos, como puede ser el caso de algunas poblaciones de insectos (Colom et al., 2022).

En definitiva, los métodos de relleno se han mostrado eficaces a la hora completar grandes bases de datos climáticas, con la novedad de utilizar un método iterativo de relleno. No obstante, cabría analizar más en detalle el efecto de la propagación iterativa de valores rellenados, así como explorar otras aproximaciones que tengan en cuenta la longitud temporal característica del dato faltante, es decir un dato aislado, o bien combinación de dos, tres, cuatro, o más datos faltantes consecutivos. Todo ello derivaría en una mejora en la consistencia espaciotemporal de las superficies climáticas, así como los productos climáticos derivados. En cuanto a las tendencias climáticas, cabría analizarlas considerando distintas ventanas temporales y año de inicio de las series, así como atender a la posible falta de homogeneidad de las series.

En el **artículo 2**, se pone de manifiesto la aplicabilidad de un conjunto de reglas de filtrado empíricas con las que se asegura una mayor calidad temática de las áreas de verdad-terreno extraídas de bases de datos auxiliares (SIOSE), como prerrequisito indispensable para la generación de mapas de usos y cubiertas de calidad a partir de clasificadores supervisados. Además, la estrategia propuesta asegura un número elevado y representativo de muestras, lo que en su ausencia ha sido identificado como una fuente principal de errores (Amani et al., 2019; Elmes et al., 2020).

Se identificaron inconsistencias asociadas a las diferencias existentes entre las imágenes de teledetección y la base de datos SIOSE. Entre ellas, los errores temporales fueron los más determinantes, afectando en mayor medida a las categorías agrícolas, más dinámicas y con mayor multiplicidad de estados fenológicos bajo un mismo polígono SIOSE. Así, procesos de intensificación agrícola (expansión de cultivos irrigados) resultaron no activos en la fecha de las imágenes (previas al SIOSE 2005), así como dinámicas de expansión urbana, o cortas

y aclareos forestales, siendo ejemplos identificados que afectaron áreas extensas dentro de una escena Landsat. Otros errores venían asociados a las diferencias de escala existentes entre la resolución de las imágenes y la escala a la que se elaboró la base de datos SIOSE, lo que generaba que asociaciones de diversas categorías (roquedo, pastizal, bosque) coexistiesen bajo el mismo polígono.

Las cinco reglas propuestas caracterizaron el comportamiento fenológico de las categorías, permitiendo minimizar la afectación de los errores identificados. En el caso de asociaciones de diversas categorías (suelo desnudo, matorral, bosque), la regla 1 (respuesta máxima de NDVI) y la regla 2 (rango NDVI a lo largo de 'n' fechas) corrigieron los errores de escala y los derivados a consecuencia del efecto de las perturbaciones (incendios, cortas o aclareos forestales). Por otro lado, la mejor diferenciación entre los usos de secano/regadío (leñosas) en cultivos agrícolas se consiguió empleando la regla 3 (actividad fotosintética para 'n' fechas). De otro lado, la regla 4 (contraste de los valores $NDVI_{max}$ entre fechas determinadas) resultó especialmente efectiva a la hora de gestionar el gradiente temporal del NDVI de las cubiertas, permitiendo diferenciar entre aquellas con un gradiente positivo (cultivos herbáceos de verano, viñedos, o frondosas caducifolias), de las de presentan un gradiente negativo (cultivos de invierno, pastizales) o neutro (coníferas, frondosas perennifolias, matorrales, cubiertas urbanas, masas de agua). Además, se observó que una elevada variabilidad interanual de fechas de las imágenes puede generar gradientes de NDVI inconsistentes con los esperables para una categoría, de ahí el interés de considerar imágenes de años consecutivos próximos. Finalmente, la regla 5 (estado fenológico), permitió ajustar valores de NDVI en momentos fenológicos específicos.

Con todo ello, las matrices de confusión evidenciaron un claro incremento de la exactitud temática de los mapas elaborados (10.9 puntos porcentuales de incremento promedio), con una disminución clara en los errores de omisión (16.8 puntos porcentuales de decremento promedio) y de comisión (14.0 puntos porcentuales de decremento promedio) prácticamente en todas las categorías. Estas mejoras son especialmente relevantes, ya que se trasladan a las capas de incertidumbre generadas por el clasificador *kNN*, y que acompañan a cada una de las clasificaciones, siendo información decisiva para la extracción de posiciones de cambio de alta calidad en la fase de modelización estadística desarrollada en el artículo 3.

Las cinco reglas de filtrado han demostrado su efectividad y funcionalidad. No obstante, implican un elevado tiempo de dedicación a la exploración y parametrización de los umbrales establecidos. Esta fase exploratoria es de vital importancia, ya que un filtrado excesivo mermaría la variabilidad intraclase de aquellas categorías más heterogéneas (pastizales, matorrales), por lo que se requiere de un criterio experto para la configuración y ajuste sucesivo de los filtros. Además, en un contexto de generación cartográfica para grandes áreas geográficas, cabe plantearse si la definición de los filtros a nivel de una escena completa de Landsat permite un ajuste efectivo de los mismos, cuando existen situaciones de alta variabilidad intraclase en algunas categorías (pastizales). En este punto cabría plantear la posibilidad de realizar una estratificación espacial basada en características climáticas, como apuntan otros autores (Inglada et al., 2017), lo que reduciría la variabilidad intraclase dentro de las regiones climáticas consideradas.

En el **artículo 3**, se desarrolla un robusto esquema metodológico para analizar las principales fuerzas inductoras asociadas a la expansión forestal a lo largo del transecto definido por la órbita 200 de Landsat.

Los aspectos metodológicos incluyen tres fases principales: (1) producción cartográfica, (2) extracción y muestreo de presencias y ausencias, (3) modelización estadística.

1. La fase de producción cartográfica siguió las estrategias desarrolladas en el artículo 2 para generar cartografía temática, así como su incertidumbre asociada, para tres momentos temporales y a lo largo de un transecto compuesto por cinco escenas Landsat. Cabe destacar la exactitud temática obtenida, superior al 92 % empleando millones de píxeles de test ubicuamente distribuidos.

2. La fase de extracción de posiciones de presencia-ausencia de cambio y la aplicación de estrategias de muestreo incluyeron: (i) la reducción del sesgo existente en el muestreo de las ausencias siendo un aspecto escasamente desarrollado en los trabajos consultados. Ello requería determinar una distancia sobre la cual realizar un muestreo local de las ausencias. El banco de pruebas diseñado permitió identificar una distancia (20 km) a partir de la cual el rendimiento de los modelos BRT se incrementaba de forma significativa (consultar Figura S1, del artículo 3). Esta solución mejoraba la prevalencia local de las muestras bajo el umbral de distancia establecido. (ii) La aplicación de filtros de incertidumbre mostró una clara mejora en la calidad temática de las observaciones extraídas, evidenciando un mayor rendimiento predictivo de los modelos. No obstante, se consideraron dos niveles de incertidumbre (0.1 y 0.3) debido a la fuerte reducción de la muestra, especialmente para las dinámicas de abandono agrícola. (iii) El índice de Moran permitió reducir la autocorrelación espacial de las posiciones de presencia y ausencia por debajo de un nivel de correlación ya aceptable (0.7), empleando la pendiente del terreno como variable en el test. No obstante, cabría la posibilidad de haber utilizado una variable socioeconómica en el test, lo que hubiera implicado un nivel más elevado de autocorrelación en los datos, y consecuentemente requerido un espaciado mayor de las muestras para obtener un nivel de autocorrelación inferior al establecido (Vidal-Macua et al., 2018). Este hecho, hubiera de nuevo afectado especialmente a las dinámicas de abandono agrícola, típicamente más agregadas y autocorrelacionadas. (iv) Por otro lado, la segmentación bioclimática del transecto, basada en variables de temperatura, permitió derivar modelos más consistentes y acordes a nivel climático, evitando la mezcla de observaciones pertenecientes a contextos muy dispares. En este sentido, no se han localizado estudios que utilicen una aproximación bioclimática. Además, se exploraron otros enfoques basados en análisis *clúster,* que permitían incluir las variables de radiación solar, precipitación y temperatura de forma conjunta. Esta aproximación mostró soluciones muy aproximadas y equivalentes a las finalmente consideradas. (v) Por último, se analizó la influencia del tamaño de la muestra en el rendimiento de los modelos, determinándose un umbral mínimo de observaciones (580) por encima del cual la dinámica se analizó. Respecto a otros estudios, podría resultar una muestra reducida (Elith et al., 2008; Müller et al., 2013; Colin et al., 2017; Vidal-Macua et al., 2017, 2018). No obstante, las pruebas de consistencia realizadas mostraron resultados sólidos. Finalmente la ecualización de las presencias y ausencias permitió asignarles igual representatividad, aunque los modelos BRT presentan buena tolerancia a muestras no balanceadas (Elith et al., 2008).

3. La fase de modelización estadística con *Boosted Regression Trees* (BRT) incluyó (i) evaluar el grado de multicolinealidad de las variables, para reducir así la dimensionalidad, los tiempos de procesado y el sobreajuste de los modelos. Las variables climáticas, como la sequía, y las socioeconómicas presentaron mayor grado de multicolinealidad. Además, se obtuvo la matriz de correlaciones (Pearson) de las variables remanentes. (ii) La modelización de las dinámicas de expansión forestal se desarrolló en tres fases, lo que permitió evadir la influencia del principal predictor en situaciones en las cuales su importancia relativa es elevada, lo que evita que otras variables secundarias junto con sus relaciones se muestren. Aproximaciones similares han sido utilizadas en estudios previos, como por ejemplo en Müller et al. (2013) y Vidal-Macua et al. (2017). En cada modelo, se realiza un ajuste de los hiperparámetros (*tree complexity, number of trees, shrinkage*), seleccionando la combinación de mayor rendimiento predictivo evaluado a partir de la curva ROC (*receiver operating characteristic curve*), sobre observaciones independientes. Esta gráfica relaciona la proporción de verdaderos positivos (TPR), respecto a la proporción de falsos positivos (FPR), según se varía el umbral de discriminación, permitiendo la comparativa del rendimiento de los modelos. El área bajo la curva ROC, denominado AUC, define la probabilidad de que el modelo identifique correctamente entre las presencias-ausencias seleccionadas aleatoriamente, siendo una métrica ampliamente utilizada para la comparación de los modelos.

Los modelos BRT se han mostrado especialmente robustos a la hora de combinar distintos tipos de predictores: variables dicotómicas, categóricas con distintos niveles, cuantitativas discretas o continuas. Además, las gráficas de dependencia parcial (*partial dependence plots*) permitieron analizar patrones no lineales, así como identificar el rango de valores de la variable respuesta sobre el cual se maximiza la probabilidad de ocurrencia de las dinámicas evaluadas. De otro lado, la contribución del predictor en el modelo final queda determinada a partir de su importancia relativa (Figura S7 del artículo 3). Junto con todo lo anterior, y la espacialización de las ocurrencias, se ha podido configurar un esquema metodológico de gran robustez a la hora de comprender espacial y temporalmente cómo han actuado las principales fuerzas inductoras de cambio sobre el territorio.

En cuanto a las dinámicas de expansión forestal se refiere, éstas superaron en extensión a las dinámicas de pérdida forestal, lo que supone una tasa neta de incremento forestal positiva en el periodo 1987–2017, en línea con lo observado a escala europea y en la PI. Ello ha venido en parte favorecido por la aplicación de políticas de reforestación, como las ayudas a la *forestación de tierras agrícolas* surgidas de la reforma de la Política Agrícola Comunitaria (PAC) del año 1992, y en parte al incremento asociado al establecimiento de dinámicas de sucesión ecológica sobre áreas que han sufrido procesos de abandono agrícola. No obstante, el grado de contribución de las políticas dirigidas a la forestación no ha podido evaluarse debido a la falta de información.

El hecho de considerar la máxima desagregación temática posible de los mapas (6 categorías fuente, 3 categorías forestales), junto con la desagregación espaciotemporal considerada (8 regiones climáticas y 2 periodos temporales), ha incrementado de forma significativa la dimensionalidad y complejidad del análisis, a pesar de reportar información crucial a un elevado nivel de detalle y robustez debido a la información y metodología empleadas.

Las dinámicas de **expansión forestal a partir de cultivos agrícolas** confirmaron patrones claramente diferenciados en función del grupo fisionómico forestal, siendo las frondosas perennifolias (BEF) las que presentaron un mayor crecimiento en términos absolutos.

La expansión de las frondosas caducifolias (BDF) se relacionó con la proximidad a la red hidrográfica y a áreas forestales, lo que vino a asociarse, en términos generales, a una expansión de bosques de ribera, y a la implantación de cultivos forestales (*Populus nigra* L, *Populus Canadensis* L., *Populus Alba* L.) en áreas con una elevada disponibilidad hídrica, generalmente localizadas a mayor distancia de las principales capitales de provincia. Se esperaba una mayor representatividad de las variables socioeconómicas (con la excepción puntual de una disminución en el número de explotaciones agrarias) debido a la relación de las dinámicas poblacionales con el abandono agrícola.

Broadleaf deciduos forests (BDF)

Variable	Rainfed 'n'	Irrigated ; n	Crops Categ. ; n	Grasslands ; n	Shrublands ; n	Natural Categ. ; n	BR.2 ; n	BR.3 ; n	BR.5 ; n	BR.6 ; n	BR.7 ; n	BR.8 ; n	P1 ; n	P2 ; n
Slope		90.9 ; 7	90.9 ; 7	90.6 ; 4		90.6 ; 4	51.2 ; 2	67.2 ; 4		39.7 ; 2	7.1 ; 1	16.3 ; 2	86.9 ; 5	94.6 ; 6
General Curvature	8.1 ; 1	79 ; 5	87.1 ; 6					60.5 ; 2		8.1 ; 1		18.5 ; 3	34.2 ; 2	52.9 ; 4
Pot_Rad_Wint		17.9 ; 1	17.9 ; 1	98.7 ; 5	40.4 ; 3	139.1 ; 8	33.2 ; 3	63.7 ; 3	60.1 ; 3				62.5 ; 4	94.5 ; 5
Ac_Rain	79.5 ; 4	36.7 ; 3	116.2 ; 7	92.4 ; 5	103.6 ; 4	196 ; 9	93.1 ; 4		117 ; 6	96.4 ; 5	5.7 ; 1		145.2 ; 7	167 ; 9
Av_Me_Temp	28 ; 2	118.2 ; 3	146.2 ; 5	130.3 ; 5	99.3 ; 4	229.6 ; 9	94.5 ; 4		56.8 ; 3	151.2 ; 6	73.3 ; 1		132.1 ; 6	243.7 ; 8
DE6_S6					12.9 ; 1	12.9 ; 1			12.9 ; 1				12.9 ; 1	
Co_Dist_M_Roads		48.3 ; 4	48.3 ; 4	9.7 ; 1		9.7 ; 1				49 ; 4		9 ; 1	45.1 ; 4	12.9 ; 1
Co_Dist_S_Roads	12.3 ; 1	17.2 ; 2	29.5 ; 3									29.5 ; 3	17.2 ; 2	12.3 ; 1
Co_Dist_Urb	47.7 ; 3	43.2 ; 2	90.9 ; 5	48.5 ; 3	30.9 ; 2	79.4 ; 5	15.3 ; 1	62 ; 3	60.7 ; 4	12.2 ; 1		20.1 ; 1	67.6 ; 4	102.7 ; 6
Co_Dist_Cap	56.8 ; 3	129.5 ; 5	186.3 ; 8	83.4 ; 4	33.3 ; 2	116.7 ; 6	35.5 ; 2	42.8 ; 2	79.2 ; 4	70.5 ; 2		75 ; 4	114.6 ; 5	188.4 ; 9
Eu_Dist_Forest	109.5 ; 5	173.4 ; 10	282.9 ; 15	140.4 ; 7	64.8 ; 3	205.2 ; 10	62.4 ; 3	35.7 ; 2	156 ; 9	141.7 ; 8		87.8 ; 5	258.6 ; 12	229.5 ; 13
Eu_Dist_Hyd	119.3 ; 5	290.1 ; 9	409.4 ; 14	33.7 ; 2	14.9 ; 1	48.6 ; 3	14.9 ; 1		57.1 ; 3	144.1 ; 7	9.4 ; 1	232.5 ; 5	168.6 ; 5	289.4 ; 12
Soil_Erosion		44.6 ; 3	44.6 ; 3	37.9 ; 2		37.9 ; 2		68.3 ; 4		14.2 ; 1			39.7 ; 2	42.8 ; 3
Pop_density		11.4 ; 1	11.4 ; 1									11.4 ; 1		11.4 ; 1
Num_Holdings	38.7 ; 1		38.7 ; 1	34.5 ; 2		34.5 ; 2				73.2 ; 3			14.8 ; 1	58.4 ; 2

Broadleaf evergreen forests (BEF)

Variable	Rainfed 'n'	Irrigated ; n	Crops Categ. ; n	Grasslands ; n	Shrublands ; n	Natural Categ. ; n	BR.2 ; n	BR.3 ; n	BR.5 ; n	BR.6 ; n	BR.7 ; n	BR.8 ; n	P1 ; n	P2 ; n
Slope	77.9 ; 5	18.1 ; 1	96 ; 6	69.2 ; 3	62.5 ; 4	131.7 ; 7	41.8 ; 2	27.4 ; 1	33.1 ; 2	114.5 ; 7		10.9 ; 1	139.1 ; 8	88.6 ; 5
Pot_Rad_Wint	20.2 ; 1	13.4 ; 1	33.6 ; 2	68.5 ; 5	138.5 ; 8	207 ; 13	37.9 ; 3	11.5 ; 1	68.9 ; 4	92.7 ; 5		29.6 ; 2	143.4 ; 9	97.2 ; 6
Ac_Rain	147.1 ; 7		147.1 ; 7	130.3 ; 7	153.7 ; 7	284 ; 14	94.7 ; 4	16 ; 1	165 ; 8	123.8 ; 7		31.7 ; 1	214 ; 11	217.1 ; 10
Av_Me_Temp	56.2 ; 5	47.7 ; 2	103.9 ; 7	105.8 ; 5	139.4 ; 7	245.2 ; 12	83.1 ; 3		102 ; 6	154 ; 9		9.7 ; 1	163.2 ; 10	185.9 ; 9
DE3_S12	12 ; 1		12 ; 1						12 ; 1					12 ; 1
Co_Dist_S_Roads		16.1 ; 1	16.1 ; 1		9.3 ; 1	9.3 ; 1	9.3 ; 1			16.1 ; 1			16.1 ; 1	9.3 ; 1
Co_Dist_Urb	14.6 ; 1		14.6 ; 1		34.7 ; 2	34.7 ; 2	23.7 ; 1			14.6 ; 1		11 ; 1	49.3 ; 3	
Co_Dist_Cap				99 ; 4	60.6 ; 3	159.6 ; 7	44.4 ; 2		51 ; 2	50.1 ; 2		14.1 ; 1	15.9 ; 1	143.7 ; 6
Eu_Dist_Forest	283 ; 8	41.9 ; 2	324.9 ; 10	132.5 ; 6	191 ; 7	323.5 ; 13	35.5 ; 2	9.8 ; 1	231 ; 8	289.1 ; 10		82.7 ; 2	382.3 ; 13	266.1 ; 10
Eu_Dist_Hyd	45.2 ; 3		45.2 ; 3	18.5 ; 1	10.5 ; 1	29 ; 2	18.5 ; 1		16.4 ; 1	28.8 ; 2		10.5 ; 1	15.9 ; 1	58.3 ; 4
Soil_Erosion	61.1 ; 4	45.6 ; 2	106.7 ; 6	35.4 ; 1		35.4 ; 1		35.4 ; 1	27.6 ; 2	79.1 ; 4			96.4 ; 4	45.7 ; 3
Pop_density	19.5 ; 1	17.1 ; 1	36.6 ; 2							36.6 ; 2				36.6 ; 2
W_Building	32 ; 2		32 ; 2							32 ; 2			18.4 ; 1	13.6 ; 1
W_Services	17.6 ; 1		17.6 ; 1							17.6 ; 1				17.6 ; 1
W_Industry				11.1 ; 1		11.1 ; 1	11.1 ; 1							11.1 ; 1
Num_Holdings				14.3 ; 1		14.3 ; 1			14.3 ; 1					14.3 ; 1
LSU				15.4 ; 1		15.4 ; 1			15.4 ; 1					15.4 ; 1
UAA	13.2 ; 1		13.2 ; 1						13.2 ; 1					13.2 ; 1

Needleleaf evergreen forests (NEF)

Variable	Rainfed 'n'	Irrigated ; n	Crops Categ. ; n	Grasslands ; n	Shrublands ; n	Natural Categ. ; n	BR.2 ; n	BR.3 ; n	BR.5 ; n	BR.6 ; n	BR.7 ; n	BR.8 ; n	P1 ; n	P2 ; n
Slope				89.5 ; 3	95 ; 6	184.5 ; 9			23.5 ; 2	62.4 ; 3	22.2 ; 1		59.7 ; 3	124.8 ; 6
Pot_Rad_Wint	19.5 ; 1	34.4 ; 2	53.9 ; 3	34.7 ; 3	98.8 ; 5	133.5 ; 8	66.1 ; 3		18.3 ; 1	36.9 ; 3		66.1 ; 4	100.9 ; 5	86.5 ; 6
Ac_Rain	17.1 ; 1	85 ; 4	102.1 ; 5	79.8 ; 4	221.3 ; 9	301.1 ; 13	69.7 ; 4		52.8 ; 3	147.1 ; 6	31.2 ; 1	102.4 ; 4	135 ; 7	268.2 ; 11
Av_Me_Temp				61.5 ; 5	45.9 ; 3	107.4 ; 8	36.1 ; 3		46.4 ; 3	24.9 ; 2			38.5 ; 4	68.9 ; 4
DE6_S6					17 ; 1	17 ; 1				17 ; 1				17 ; 1
DE9_S6	8.6 ; 1		8.6 ; 1							8.6 ; 1				8.6 ; 1
DE3_S24					11 ; 1	11 ; 1					11 ; 1			11 ; 1
HE3_S12					11.7 ; 1	11.7 ; 1						11.7 ; 1		11.7 ; 1
Co_Dist_M_Roads	29.6 ; 2	24.2 ; 1	53.8 ; 3		11.5 ; 1	11.5 ; 1			11.5 ; 1	53.8 ; 3			51.8 ; 3	13.5 ; 1
Co_Dist_S_Roads	17.1 ; 1	12.3 ; 1	29.4 ; 2									29.4 ; 2		29.4 ; 2
Co_Dist_Urb				34.2 ; 2	14.8 ; 1	49 ; 3	14.8 ; 1		19.4 ; 1	14.8 ; 1			49 ; 3	
Co_Dist_Cap	92.6 ; 3	62 ; 3	154.6 ; 6	93.5 ; 3	77.3 ; 4	170.8 ; 7	40 ; 2		59.2 ; 3	160 ; 5		66.2 ; 3	95.2 ; 3	230.2 ; 10
Eu_Dist_Forest	61.1 ; 3	21.4 ; 1	82.5 ; 4	137.6 ; 6	226.6 ; 8	364.2 ; 14	96.8 ; 4		124 ; 4	100.4 ; 5	21.3 ; 1	104.6 ; 4	227.9 ; 8	218.8 ; 10
Eu_Dist_Hyd	22.9 ; 1	42.1 ; 2	65 ; 3		47.2 ; 1	47.2 ; 1					14.3 ; 1	97.9 ; 5	15.1 ; 1	97.1 ; 5
Soil_Erosion	12.3 ; 1	46 ; 2	58.3 ; 3		21.7 ; 2	21.7 ; 2				58.3 ; 3		21.7 ; 2	48.3 ; 3	31.7 ; 2
Protected_Areas				4.9 ; 1		4.9 ; 1				4.9 ; 1			4.9 ; 1	
W_Industry				26.6 ; 1		26.6 ; 1			26.6 ; 1					26.6 ; 1
Num_Holdings	19.3 ; 1	43 ; 2	62.3 ; 3							62.3 ; 3			41.2 ; 2	21.1 ; 1
LSU		29.6 ; 2	29.6 ; 2							29.6 ; 2			13.4 ; 1	16.2 ; 1
UAA				37.6		37.6 ; 2			18.5 ; 1	19.1 ; 1			19.1 ; 1	18.5 ; 1

Figura 2. Importancia relativa y frecuencia ('n') acumulada para cada predictor, agregado por categoría fuente (Rainfed: cultivos de secano; Irrigated: regadío; Crops Categ.: cultivos; Grasslands: pastizales; Shrublands: matorrales; Natural Categ.: Pastizales y matorrales), regiones bioclimáticas (BR.2: montana; BR.3: colina; BR.5: supramediterránea; BR.6: mesomediterránea sur; BR.7: termomediterránea; BR.8: mesomediterránea norte) y periodos (P1: 1987–2002; P1: 2002–2017) para cada grupo forestal. Ver Tabla 2 en página 7 del artículo 3 para la definición de los predictores.

Espacialmente, las transiciones han ocurrido en las grandes cuencas hidrográficas (mesomediterránea), y en la transición con áreas de mayor relieve (supramediterránea), siendo zonas caracterizadas por una menor rentabilidad y competitividad de los cultivos, y menor disponibilidad de tierras de cultivo, debido a restricciones de tipo físico (Douglas et al., 1996; Lasanta et al., 2017; Lieskovský et al., 2015), especialmente en cultivos de secanos.

La expansión de las <u>frondosas perennifolias</u> (BEF) desde cultivos se ha relacionado principalmente con la proximidad a áreas forestales en las regiones supramediterránea y mesomediterránea sur, y especialmente en la transición entre ambas. La distancia a la red hidrográfica tuvo una importancia residual debido a los menores requerimientos hídricos de este tipo fisionómico forestal. La escasa representación de las variables de conectividad y distancia no fue la esperada, y contrasta con el patrón observado en los otros dos grupos forestales. Las variables climáticas (temperatura y precipitación, relacionadas con el estudio del artículo 1) revelaron un papel más importante en las regiones más cálidas. El papel de la erosión de suelos se relacionó con los cultivos irrigados, lo que pone en evidencia la capacidad protectora frente a la erosión de la cubierta vegetal del suelo. La pendiente, factor limitante de la actividad agrícola, favoreció el abandonado de tierras de cultivo de secano, efecto ya evidenciado en diversos estudios previos (Poyatos et al., 2003; Lieskovský et al., 2014; Zgłobicki et al., 2016; Abadie et al., 2017). A diferencia de las frondosas caducifolias (BDF), las variables socioeconómicas tuvieron una importancia mayor, relacionando el incremento forestal a áreas con un mayor porcentaje de población ocupada en los sectores de la construcción y servicios, aspecto también identificado en investigaciones previas (Melendez-Pastor et al., 2014; Kolecka et al., 2017; Vidal-Macua et al., 2018), especialmente localizado en el transecto en la transición entre las regiones citadas. De este modo, la diversificación económica hacia empleos en sectores ajenos a la agricultura, en áreas de menor disponibilidad de tierras de cultivo, podría contribuir en mayor medida al abandono de cultivos, especialmente los de secano.

La expansión de los <u>bosques aciculifolios</u> (NEF) se relacionó con variables de distancia a capitales de provincia, a áreas forestales y a las carreteras, siendo las áreas más remotas, inaccesibles y a mayor distancia de áreas urbanas, las más propensas a ser abandonadas como también señalaron Pazúr and Bolliger (2017). Además, entre los factores secundarios destacó la proximidad a la red hidrográfica en la región mesomediterránea norte (Cuenca del Ebro, y sobre cultivos irrigados). Así en la región mesomediterránea sur, la menor tasa de erosión de suelos, el menor número de explotaciones agrícolas y, de forma novedosa, un mayor número de cabezas de ganado favoreció la expansión forestal en esta región. La precipitación fue la principal variable topoclimática, presentando patrones irregulares entre regiones.

En cuanto a las principales fuerzas inductoras de la ***expansión forestal desde pastizales***, mostraron una alta variabilidad tanto a nivel espacial como temporal.

La expansión de las <u>frondosas caducifolias</u> (BDF) desde pastizales estuvo principalmente relacionada con la proximidad a las áreas forestales, la temperatura, la precipitación y la radiación solar, así como la distancia a las capitales de provincia en la mitad norte del transecto. En las regiones montañosas, la proximidad a las áreas forestales fue dominante, lo que indica un proceso de homogeneización y consolidación de las masas forestales y expansión a lo largo de sus límites. La temperatura, la precipitación y la radiación solar fueron los principales factores topoclimáticos, indicando mayores requerimientos hídricos

(mayor precipitación y menor radiación solar) en las regiones sur, patrones identificado por otros autores (Vidal-Macua et al., 2017) y menores requerimientos en las regiones norte, donde la disponibilidad hídrica es más elevada. De otro lado, la proximidad a núcleos urbanos y capitales de provincia favoreció la expansión forestal. Por último, la estructura de las explotaciones agrarias presentó un papel residual, favoreciendo la expansión de las frondosas en áreas con un menor número de explotaciones agrícolas, sobre el límite de la región supramediterránea, un área caracterizada por dinámicas de abandono de cultivos.

Por lo que respecta a la expansión de las frondosas perennifolias (BEF) a partir de pastizales, dominaron los factores topoclimáticos, así como la proximidad a áreas forestales y la distancia a las capitales de provincia. Espacialmente tuvo una mayor intensidad en la región supramediterránea y mesomediterránea sur, regiones en las que especies de frondosas perennifolias (*e.g.*, *Quercus ilex sensu lato*) muestran mayor adaptabilidad a condiciones climáticas más secas. Además, las variables relacionadas con las estructura de las explotaciones agrarias (un menor número de unidades ganaderas y de explotaciones agrarias) aparecieron en la región supramediterránea (*cf.* Vicente-Serrano et al., 2004; Serra et al., 2014; Sanjuán et al., 2018). Durante el segundo periodo, la expansión tuvo lugar en áreas más alejadas de las áreas forestales previas, ocupando zonas de menor altitud y próximas a las capitales de provincia. En cambio, en la región montana, los cambios sucedieron con menor intensidad, y principalmente asociados a condicionantes topoclimáticos como la precipitación, temperatura, y la pendiente.

La expansión de los bosques aciculifolios (NEF) a partir de pastizales se caracterizó por mostrar un fuerte dinamismo entre periodos. Estuvo principalmente relacionada con la proximidad a las áreas forestales, así como la precipitación, la pendiente, la temperatura y la distancia a las capitales de provincia. La mayor intensidad de ocurrencias se localizó en las regiones montana, supramediterránea y mesomediterránea sur, siendo las regiones mediterráneas las más dinámicas entre períodos. Al igual que para BDF y BEF, la proximidad a las áreas forestales fue el factor principal, especialmente en las regiones montañosas. La distancia a núcleos urbanos y capitales de provincia fueron representativos en las regiones mediterráneas. Un patrón destacable es la evolución de los factores de distancia y topoclimáticos hacia determinantes socioeconómicos (trabajadores en el sector de la industria y la superficie agraria útil) en la región supramediterránea. Este patrón evidenciaría un predominio de las ocurrencias en áreas forestales poco accesibles y dotadas de mayor tasa de humedad, que evoluciona en el segundo periodo a localizaciones más próximas a núcleos urbanos, con menor disponibilidad de tierras agrícolas y donde ocupaciones ajenas a la actividad agrícolas desplazan a las primeras. En la región mesomediterránea sur, los factores de distancias y socioeconómicos evolucionan hacia determinantes topoclimáticos, lo que podría evidenciar una primera fase de expansión próxima a áreas urbanas y una segunda fase en localizaciones más forestales.

Las dinámicas ***de expansión forestal a partir de matorrales***:

La expansión de las frondosas caducifolias (BDF) a partir de matorrales estuvo relacionada principalmente con factores topoclimáticos, así como con la proximidad a las áreas forestales y la distancia a las capitales de provincia, localizadas en las regiones más montañosas. Tasas elevadas de precipitación a mayores cotas y una menor radiación determinaron las condiciones preferentes en la región montana, lo que coincide con otros trabajos previos (Vidal-Macua et al., 2017). En la región supramediterránea, la proximidad a

las áreas forestales indicó de nuevo un proceso de homogenización y consolidación, y expansión durante el segundo periodo. La distancia a núcleos urbanos y capitales de provincia mostró patrones claros: mayores distancias dominaron en la región montana, lo que en general indica zonas más aisladas, mientras que menores distancias potenciaron el cambio en la supramediterránea, un patrón también observado para el caso de los pastizales.

La expansión de las frondosas perennifolias (BEF) a partir de matorrales se relacionó principalmente con la proximidad a las áreas forestales y la distancia a capitales de provincia, además de factores topoclimáticos, con distintos patrones según la región climática. En las regiones montañosas, montana y supramediterránea, la proximidad a las áreas forestales fue el factor principal, indicando de nuevo un proceso de densificación y expansión forestal, en línea con el patrón común ya observado y otros estudios previos (Gehrig-Fasel et al., 2007; Améztegui et al., 2010; Nadal-Romero et al., 2018). De otro lado, los factores topoclimáticos predominaron en las regiones más cálidas, generalmente más alejadas de bosques preexistentes, con menor precipitación y mayor temperatura, aunque favorecidas por condiciones de menor radiación solar. Durante el segundo periodo la expansión continua a mayor distancia de áreas forestales sobre localizaciones con una mayor tasa de radiación solar incidente.

Finalmente, la expansión de bosques aciculifolios (NEF) a partir de matorrales estuvo asociada con la proximidad a las áreas forestales, variables topoclimáticas y la distancia a las capitales de provincia. A excepción de la región colina, la expansión de este grupo ocurrió en todas las regiones, lo que viene a manifestar la mayor plasticidad y adaptabilidad de las especies aciculifolias al gradiente climático del transecto (desde *Pinus sylvestris, P. nigra, P. pinaster,* hasta *P. halepensis*). Se identifica de nuevo un proceso de densificación y expansión forestal (Gehrig-Fasel et al., 2007; Améztegui et al., 2010; Nadal-Romero et al., 2018) en ubicaciones más aisladas. En la región montana, las transiciones se produjeron a mayor altitud y menor radiación solar (Vidal-Macua et al., 2017), mientras que en la región supramediterránea fueron favorecidas por una mayor tasa de precipitación (Melendez-Pastor et al., 2014; Sanjuán et al., 2018). En los contextos más secos (mesomediterránea y termomediterránea), incluso menores tasas de precipitación favorecieron la expansión de las coníferas (Alonso-Sarría et al., 2016), y en condiciones de menor radiación solar. Por último, una mayor recurrencia de eventos de sequía influiría de forma negativa sobre la expansión de las coníferas en las regiones más secas, lo que indicaría un límite al desarrollo de especies de coníferas (*P. halepensis*) en condiciones de sequías intensas y prolongadas en el tiempo.

CONCLUSIONES GENERALES

6. CONCLUSIONES GENERALES

La Tesis plantea una serie de contribuciones metodológicas en el contexto del análisis de las dinámicas de las cubiertas del suelo para una mejor comprensión del cambio global en la PI. Estas contribuciones se han mostrado de utilidad tanto en la fase de generación de variables, como durante el análisis de los principales factores implicados en la expansión forestal. Las principales conclusiones se detallan a continuación.

A partir de la utilización de diferentes métodos de relleno de datos faltantes y de su influencia sobre las tendencias a largo plazo (1950–2019) del clima, se puede concluir que:

- Los diferentes métodos de relleno muestran resultados similares en cuanto a las tendencias, pero diferencias a nivel espacial entre métodos.
- Las tendencias climáticas van en línea con las reportadas en estudios previos, indicando un claro incremento de temperaturas, sobre todo en los meses de primavera y verano, además de patrones de mayor irregularidad, más complejos, en cuanto a la precipitación.
- La efectividad de los métodos a la hora de completar grandes bases de datos climáticas ha quedado manifiesta, lo que disminuye la afectación de la presencia de datos faltantes en la generación de superficies continuas derivadas.
- La distribución espaciotemporal de las observaciones repercute en la respuesta de los métodos de relleno a nivel espacial. En condiciones de menor densidad de observaciones, la elección del método de relleno de datos faltantes es importante y condiciona los patrones espaciales en las tendencias resultantes.
- El método MONTH considera las 'n' observaciones próximas al dato faltante de la propia serie, mientras que SIMILAR localiza la estación con mayor similitud a partir de la comparación de 'n' observaciones comunes entre pares de estaciones más próximas. Por otro lado, IDW pondera las observaciones más próximas por el inverso de la distancia y REGR emplea observaciones vecinas para resolver un modelo multivariante considerando un conjunto de regresores. Este abanico de métodos implementados ha demostrado que la elección de uno u otro método no es neutra.
- Los análisis climáticos pueden verse afectados por una fuerte reducción de la variabilidad de los datos debido al proceso de rellenado, indicando tendencias más suavizadas.

A partir de las reglas de filtrado desarrolladas, se puede concluir que:

- La aplicación de un filtrado sobre las áreas verdad-terreno es tanto o más importante que el método de clasificación usado, decisivo en la fase de entrenamiento, como en la propia validación del modelo.
- Definir estrategias de post-procesado de las clasificaciones es esencial para la coherencia temática de las clasificaciones.

Respecto al análisis de las dinámicas de expansión forestal, se puede concluir que:

- La aplicación de una metodología rigurosa para la generación de áreas verdad-terreno de calidad, la aplicación de filtros de incertidumbre y las estrategias de muestreo (reducción del sesgo entre presencias-ausencias, la prevalencia local de

las muestras o los modelos basados en tres pasos) benefician el análisis de dinámicas de cambio global a escala regional.

- No es posible realizar análisis de cambio global de calidad previos a 1980, debido a la falta de información asociada a imágenes de teledetección y a datos socioeconómicos, aunque se disponga de una cierta presencia de datos climáticos desde 1950.
- La falta de estacionariedad en los *drivers* de aparición de bosques sugiere que operan fuerzas distintas tanto a nivel espacial como temporal.
- El primer periodo (1987–2002) se caracteriza por un proceso de densificación y consolidación forestal, seguido de una expansión en el segundo periodo (2002–2019).
- A nivel espacial, el abandono agrícola ha operado en la región mediterránea, especialmente en la transición con áreas de montaña, mientras que las dinámicas naturales/seminaturales se distribuyen de forma ubicua a lo largo de las distintas áreas de montañosas contenidas en el transecto.
- La distribución espacial de los distintos grupos forestales ha estado condicionada, por lo general, a la disponibilidad hídrica de acuerdo con los requerimientos específicos de cada tipo fisionómico, y especialmente relacionada a la red hidrográfica en el caso de las frondosas caducifolias.
- En las dinámicas de abandono agrícola, el papel de los factores de accesibilidad y distancias junto con los socioeconómicos ha mostrado menor repercusión de la esperada para el caso de las frondosas caducifolias, incrementando su representatividad para el caso de las frondosas perennifolias y de los bosques aciculifolios.

Los resultados que se muestran de forma sintética resultan sin duda de gran interés y utilidad para el diseño de estrategias para la gestión de masas forestales en la región mediterránea, así como en el desarrollo de políticas territoriales para paliar la incidencia de la despoblación en el interior peninsular, principalmente atendiendo a regiones donde se pronostica una mayor incidencia de abandono de las actividades tradicionales agrarias en escenarios futuros (Perpiñá et al., 2020).

Para concluir, se desea volver a hacer hincapié en la robustez de las aproximaciones presentadas en este trabajo, que modestamente se consideran una contribución al estudio de las dinámicas del territorio. La combinación de análisis de series climáticas, la teledetección, los sistemas de información geográfica y modelos robustos de análisis de cambios, ha permitido derivar con solidez las principales fuerzas inductoras de la expansión forestal a partir de abandono agrícola y de vegetación natural, contribuciones que creemos que servirán de base para el desarrollo de estudios a un mayor nivel de detalle.

LÍNEAS FUTURAS DE INVESTIGACIÓN

7. LÍNEAS FUTURAS DE INVESTIGACIÓN

En relación con el análisis de las series climáticas y dinámicas del clima, se requiere:
- Evaluar el proceso de relleno de series atendiendo a la estructura temporal de los datos faltantes, en especial los cambios ocurridos en 1975 a nivel administrativo, analizando qué repercusión tiene en función del método de relleno empleado.
- Explorar otras metodologías de relleno, tales como *Normal Ratio*, métodos basados en la generación de series de referencia en base a *kNN* estaciones cercanas u otras estrategias basadas en aproximaciones de aprendizaje computacional.
- Explorar nuevas parametrizaciones para los métodos de *Emmental*, como incrementar el R^2 en el método SIMILAR, en el contexto peninsular y expandir estos análisis a través de bases de datos globales.

Respecto al desarrollo de estrategias de filtrado y la mejora de la calidad temática de las clasificaciones, los siguientes aspectos son sugerencias de futuras mejoras:
- Evaluar en qué medida técnicas de clasificación basadas en algoritmos de aprendizaje computacional se verían influenciadas por áreas de verdad-terreno no filtradas y filtradas.
- Explorar la respuesta de otros índices de vegetación (SAVI y EVI, entre otros) de aplicación en las reglas de filtrado. Diseñar nuevas estrategias de filtrado.
- Explorar en qué medida las reglas de filtrado tienen una repercusión negativa, disminuyendo la variabilidad intraclase de categorías compuestas (*e.g.*, cultivos de regadío, pastizales, matorrales).

Nuevas investigaciones relacionadas con la expansión forestal serían evaluadas a través de:
- Analizar en profundidad la repercusión del tamaño de la muestra en los modelos BRT, así como el nivel de incertidumbre de las observaciones. Para ello, se requeriría el diseño de un banco de pruebas que considere varios aspectos como las distintas dinámicas de cambio, los diversos niveles de incertidumbre, y la autocorrelación espacial de las observaciones.
- Investigar dinámicas de expansión forestal en regiones específicas del transecto, como son las cadenas montañosas que lo atraviesan (Pirineos, Sistema Ibérico y Sierra Nevada), siendo zonas de alto interés como laboratorios climáticos, y más susceptibles a una mayor tasa de abandono agrícola futura (Perpiñá et al., 2020). Por otro lado, constatar la velocidad de recuperación tras perturbaciones en los distintos regímenes climáticos, así como la interacción de factores climáticos con la sequía para dilucidar patrones espaciotemporales a lo largo del transecto.
- Este estudio tiene un carácter exploratorio para todas las transiciones evaluadas, lo que sin duda servirá de base para elaborar diseños experimentales orientados a analizar dinámicas específicas.
- La repercusión que las ayudas destinadas a la *forestación de las tierras agrarias* han tenido sobre la expansión forestal permitiría conocer y entender su distribución espaciotemporal a lo largo del periodo en que se implantaron.
- La incorporación de nuevas bases de datos socioeconómicas (Censo de población y viviendas 2021 y Censo Agrario 2020) permitiría evaluar la importancia de otros factores antrópicos sobre la expansión forestal. Estos nuevos datos permitirían realizar análisis de detalle que incorporasen la tasa de cambio absoluto o relativo (variables dinámicas) entre los periodos evaluados.

REFERENCIAS GENERALES

8. REFERENCIAS GENERALES

Abadie, J., Dupouey, J.-L., Avon, C., Rochel, X., Tatoni, T., Bergès, L., 2017. Forest recovery since 1860 in a Mediterranean region: drivers and implications for land use and land cover spatial distribution. Landsc. Ecol. 33, 289–305. https://doi.org/10.1007/s10980-017-0601-0

Acero, F.J., García, J.A., Gallego, M.C., Parey, S., Dacunha-Castelle, D., 2014. Trends in summer extreme temperatures over the Iberian Peninsula using nonurban station data. J. Geophys. Res. 119, 39–53. https://doi.org/10.1002/2013JD020590

Aerial Orthophotography National Plan (PNOA). Plan Nacional de Ortofotografía Aérea (PNOA), https://pnoa.ign.es/el-proyecto-pnoa-lidar (accessed 7.1.21).

Agencia Estatal de Meteorología (AEMET), http://www.aemet.es/en/portada (accessed 5.1.21).

Alcaraz-Segura, D., Bella, C.M. Di, Straschnoy, J.V. (Eds.), 2013. Earth Observation of Ecosystem Services. CRC Press. https://doi.org/10.1201/b15628

Alonso-Sarría, F., Martínez-Hernández, C., Romero-Díaz, A., Cánovas-García, F., Gomariz-Castillo, F., 2016. Main Environmental Features Leading to Recent Land Abandonment in Murcia Region (Southeast Spain). L. Degrad. Dev. 27, 654–670. https://doi.org/10.1002/ldr.2447

Amani, M., Brisco, B., Afshar, M., Mirmazloumi, S.M., Mahdavi, S., Mirzadeh, S.M.J., Huang, W., Granger, J., 2019. A generalized supervised classification scheme to produce provincial wetland inventory maps: an application of Google Earth Engine for big geo data processing. Big Earth Data 3, 378–394. https://doi.org/10.1080/20964471.2019.1690404

Améztegui, A., Brotons, L., Coll, L., 2010. Land-use changes as major drivers of mountain pine (Pinus uncinata Ram.) expansion in the Pyrenees. Glob. Ecol. Biogeogr. 19, no-no. https://doi.org/10.1111/j.1466-8238.2010.00550.x

Arino, O., Bicheron, P., Achard, F., Latham, J., Witt, R., Weber, J.L., 2008. GlobCover: The most detailed portrait of Earth. Eur. Sp. Agency Bull. 2008, 24–31.

Beguería, S., Tomas-Burguera, M., Serrano-Notivoli, R., Peña-Angulo, D., Vicente-Serrano, S.M., González-Hidalgo, J.C., 2019. Gap filling of monthly temperature data and its effect on climatic variability and trends. J. Clim. 32, 7797–7821. https://doi.org/10.1175/JCLI-D-19-0244.1

Bhatti, A.S., Wang, G., Ullah, W., Ullah, S., Fiifi Tawia Hagan, D., Kwesi Nooni, I., Lou, D., Ullah, I., 2020. Trend in Extreme Precipitation Indices Based on Long Term In Situ Precipitation Records over Pakistan. Water 12, 797. https://doi.org/10.3390/w12030797

Bielsa, I., Pons, X., Bunce, B., 2005. Agricultural Abandonment in the North Eastern Iberian Peninsula: The Use of Basic Landscape Metrics to Support Planning. J. Environ. Plan. Manag. 48, 85–102. https://doi.org/10.1080/0964056042000308166

Bilbao, J., Román, R., De Miguel, A., 2019. Temporal and Spatial Variability in Surface Air Temperature and Diurnal Temperature Range in Spain over the Period 1950–2011. Climate 7, 16. https://doi.org/10.3390/cli7010016

Briassoulis, H., 2020. Analysis of Land Use Change: Theoretical and Modeling Approaches. 2nd edn. Edited by Scott Loveridge and Randall Jackson. WVU Research Repository.

Brito-Morales, I., García Molinos, J., Schoeman, D.S., Burrows, M.T., Poloczanska, E.S., Brown, C.J., Ferrier, S., Harwood, T.D., Klein, C.J., McDonald-Madden, E., Moore, P.J., Pandolfi, J.M., Watson, J.E.M., Wenger, A.S., Richardson, A.J., 2018. Climate Velocity Can Inform Conservation in a Warming World. Trends Ecol. Evol. https://doi.org/10.1016/j.tree.2018.03.009

Calderón-Loor, M., Hadjikakou, M., Bryan, B.A., 2021. High-resolution wall-to-wall land-cover mapping and land change assessment for Australia from 1985 to 2015. Remote Sens. Environ. 252, 112148. https://doi.org/https://doi.org/10.1016/j.rse.2020.112148

Colin, B., Clifford, S., Wu, P., Rathmanner, S., Mengersen, K., 2017. Using Boosted Regression Trees and Remotely Sensed Data to Drive Decision-Making. Open J. Stat. 07, 859–875. https://doi.org/10.4236/ojs.2017.75061

Colom, P., Ninyerola, M., Pons, X., Traveset, A., Stefanescu, C., 2022. Phenological sensitivity and seasonal variability explain climate-driven trends in Mediterranean butterflies. Proc. R. Soc. B Biol. Sci. 289. https://doi.org/10.1098/rspb.2022.0251

del Barrio, G., Puigdefabregas, J., Sanjuan, M.E., Stellmes, M., Ruiz, A., 2010. Assessment and monitoring of land condition in the Iberian Peninsula, 1989–2000. Remote Sens. Environ. 114, 1817–1832. https://doi.org/10.1016/j.rse.2010.03.009

Doblas-Miranda, E., Alonso, R., Arnan, X., Bermejo, V., Brotons, L., de las Heras, J., Estiarte, M., Hódar, J.A., Llorens, P., Lloret, F., López-Serrano, F.R., Martínez-Vilalta, J., Moya, D., Peñuelas, J., Pino, J., Rodrigo, A., Roura-Pascual, N., Valladares, F., Vilà, M., Zamora, R., Retana, J., 2017. A review of the combination among global change factors in forests, shrublands and pastures of the Mediterranean Region: Beyond drought effects. Glob. Planet. Change 148, 42–54. https://doi.org/10.1016/j.gloplacha.2016.11.012

Doblas-Miranda, E., Martínez-Vilalta, J., Lloret, F., Álvarez, A., Ávila, A., Bonet, F.J., Brotons, L., Castro, J., Curiel Yuste, J., Díaz, M., Ferrandis, P., García-Hurtado, E., Iriondo, J.M., Keenan, T.F., Latron, J., Llusià, J., Loepfe, L., Mayol, M., Moré, G., Moya, D., Peñuelas, J., Pons, X., Poyatos, R., Sardans, J., Sus, O., Vallejo, V.R., Vayreda, J., Retana, J., 2015. Reassessing global change research priorities in mediterranean terrestrial ecosystems: how far have we come and where do we go from here? Glob. Ecol. Biogeogr. 24, 25–43. https://doi.org/10.1111/geb.12224

Dobrowski, S.Z., Abatzoglou, J., Swanson, A.K., Greenberg, J.A., Mynsberge, A.R., Holden, Z.A., Schwartz, M.K., 2013. The climate velocity of the contiguous United States during the 20th century. Glob. Chang. Biol. 19, 241–251. https://doi.org/10.1111/gcb.12026

Douglas, T., Critchley, D., Park, G., 1996. The Deintensification of Terraced Agricultural Land Near Trevelez, Sierra Nevada, Spain. Glob. Ecol. Biogeogr. Lett. 5, 258. https://doi.org/10.2307/2997794

Efthymiou–Egleton, T.-W., Sidiropoulos, S., Spanos, E., Stougiannou, E., 2020. Big Data and Democracy. HAPSc Policy Briefs Ser. 1, 18. https://doi.org/10.12681/hapscpbs.26473

Elith, J., Leathwick, J.R., Hastie, T., 2008. A working guide to boosted regression trees. J. Anim. Ecol. 77, 802–813. https://doi.org/10.1111/j.1365-2656.2008.01390.x

Elmes, A., Alemohammad, H., Avery, R., Caylor, K., Eastman, J.R., Fishgold, L., Friedl, M.A., Jain, M., Kohli, D., Bayas, J.C.L., Lunga, D., McCarty, J.L., Pontius, R.G., Reinmann, A.B., Rogan, J., Song, L., Stoynova, H., Ye, S., Yi, Z.F., Estes, L., 2020. Accounting for training data error in machine learning applied to earth observations. Remote Sens. 12, 1–39. https://doi.org/https://doi.org/10.3390/rs12061034

Friedman, J.H., 2002. Stochastic gradient boosting. Comput. Stat. Data Anal. 38, 367–378. https://doi.org/10.1016/S0167-9473(01)00065-2

Friedman, J.H., 2001. Greedy function approximation: A gradient boosting machine. Ann. Stat. 29, 1189–1232. https://doi.org/10.1214/aos/1013203451

Fuller, R.M., Smith, G.M., Devereux, B.J., 2003. The characterisation and measurement of land cover change through remote sensing: Problems in operational applications? Int. J. Appl. Earth Obs. Geoinf. 4, 243–253. https://doi.org/https://doi.org/10.1016/S0303-2434(03)00004-7

Gehrig-Fasel, J., Guisan, A., Zimmermann, N.E., 2007. Tree line shifts in the Swiss Alps: Climate change or land abandonment? J. Veg. Sci. 18, 571–582. https://doi.org/10.1111/j.1654-1103.2007.tb02571.x

Gonzalez-Hidalgo, J.C., Peña-Angulo, D., Brunetti, M., Cortesi, N., 2016. Recent trend in temperature evolution in Spanish mainland (1951–2010): from warming to hiatus. Int. J. Climatol. 36, 2405–2416. https://doi.org/10.1002/joc.4519

Grêt-Regamey, A., Weibel, B., 2020. Global assessment of mountain ecosystem services using earth observation data. Ecosyst. Serv. 46, 101213. https://doi.org/10.1016/j.ecoser.2020.101213

Gutman, G., Janetos, A.C., Justice, C.O., Moran, E.F., Mustard, J.F., Rindfuss, R.R., Skole, D., Turner II, B.L., Cochrane, M.A., 2004. Land change science: observing, monitoring and understanding trajectories of change on the earth's surface. Kluwer Academic Publishers, Dordrecht, The Netherlands.

Hastie, T., Tibshirani, R., Friedman, J., 2009. The Elements of Statistical Learning, 2nd ed, Springer Series in Statistics. Springer New York, New York, NY. https://doi.org/10.1007/978-0-387-84858-7

Hastie, T.J., Tibshirani, R.J., 1990. Generalized Additive Models. Routledge, New York. https://doi.org/10.1201/9780203753781

Helbing, D., Frey, B.S., Gigerenzer, G., Hafen, E., Hagner, M., Hofstetter, Y., van den Hoven, J., Zicari, R. V., Zwitter, A., 2019. Will Democracy Survive Big Data and Artificial Intelligence?, in: Towards Digital Enlightenment. Springer International Publishing, Cham, pp. 73–98. https://doi.org/10.1007/978-3-319-90869-4_7

Hill, J., Stellmes, M., Udelhoven, T., Röder, A., Sommer, S., 2008. Mediterranean desertification and land degradation. Mapping related land use change syndromes based on satellite observations. Glob. Planet. Change 64, 146–157. https://doi.org/10.1016/j.gloplacha.2008.10.005

Inglada, J., Vincent, A., Arias, M., Tardy, B., Morin, D., Rodes, I., 2017. Operational High Resolution Land Cover Map Production at the Country Scale Using Satellite Image Time Series. Remote Sens. 9, 95. https://doi.org/10.3390/rs9010095

Instituto Nacional de Estadística (INE), https://www.ine.es/en/index.htm

Inventario Nacional de Erosion de Suelos (INES), https://www.miteco.gob.es/en/biodiversidad/temas/inventarios-nacionales/inventario-nacional-erosion-suelos/default.aspx (accessed 7.1.21).

Jaffrés, J.B.D., 2019. GHCN-Daily: a treasure trove of climate data awaiting discovery. Comput. Geosci. 122, 35–44. https://doi.org/10.1016/j.cageo.2018.07.003

Justice, C., Gutman, G., Vadrevu, K.P., 2015. NASA Land Cover and Land Use Change (LCLUC): An interdisciplinary research program. J. Environ. Manage. 148, 4–9. https://doi.org/10.1016/j.jenvman.2014.12.004

Kendall, M.G., 1975. Rank correlation measures, 4th editio. ed. Charles Griffin, London, U.K.

Kolecka, N., Kozak, J., Kaim, D., Dobosz, M., Ostafin, K., Ostapowicz, K., Wężyk, P., Price, B., 2017. Understanding farmland abandonment in the Polish Carpathians. Appl. Geogr. 88, 62–72. https://doi.org/10.1016/j.apgeog.2017.09.002

Land Occupation Information System of Spain (SIOSE). Sistema de Información sobre Ocupación del Suelo de España (SIOSE), https://www.siose.es/

Lasanta, T., Arnáez, J., Pascual, N., Ruiz-Flaño, P., Errea, M.P., Lana-Renault, N., 2017. Space–time process and drivers of land abandonment in Europe. Catena 149, 810–823. https://doi.org/10.1016/j.catena.2016.02.024

Lasanta, Teodoro, Errea, M.P., Nadal-Romero, E., 2017. Traditional Agrarian Landscape in the Mediterranean Mountains. A Regional and Local Factor Analysis in the Central Spanish Pyrenees. L. Degrad. Dev. 28, 1626–1640. https://doi.org/10.1002/ldr.2695

Lieskovský, J., Bezák, P., Špulerová, J., Lieskovský, T., Koleda, P., Dobrovodská, M., Bürgi, M., Gimmi, U., 2015. The abandonment of traditional agricultural landscape in Slovakia – Analysis of extent and driving forces. J. Rural Stud. 37, 75–84. https://doi.org/10.1016/j.jrurstud.2014.12.007

Lieskovský, J., Kenderessy, P., Špulerová, J., Lieskovský, T., Koleda, P., Kienast, F., Gimmi, U., 2014. Factors affecting the persistence of traditional agricultural landscapes in Slovakia during the collectivization of agriculture. Landsc. Ecol. 29, 867–877. https://doi.org/10.1007/s10980-014-0023-1

Loarie, S.R., Duffy, P.B., Hamilton, H., Asner, G.P., Field, C.B., Ackerly, D.D., 2009. The velocity of climate change. Nature 462, 1052–1055. https://doi.org/10.1038/nature08649

Loidi, J., 2017. The Vegetation of the Iberian Peninsula, Plant and Vegetation. Springer International Publishing, Cham. https://doi.org/10.1007/978-3-319-54784-8

Luna, M.Y., López, J.A., Guijarro, J.A., 2011. Tendencias observadas en España en precipitacion y temperatura. Rev. Española Fis. 26, 1–13.

MacDonald, D., Crabtree, J.., Wiesinger, G., Dax, T., Stamou, N., Fleury, P., Gutierrez Lazpita, J., Gibon, A., 2000. Agricultural abandonment in mountain areas of Europe: Environmental consequences and policy response. J. Environ. Manage. 59, 47–69. https://doi.org/10.1006/jema.1999.0335

Magliocca, N.R., Rudel, T.K., Verburg, P.H., McConnell, W.J., Mertz, O., Gerstner, K., Heinimann, A., Ellis, E.C., 2015. Synthesis in land change science: methodological patterns, challenges, and guidelines. Reg. Environ. Chang. 15, 211–226. https://doi.org/10.1007/s10113-014-0626-8

Malcolm, J.R., Liu, C., Neilson, R.P., Hansen, L., Hannah, L., 2006. Global Warming and Extinctions of Endemic Species from Biodiversity Hotspots. Conserv. Biol. 20, 538–548. https://doi.org/10.1111/j.1523-1739.2006.00364.x

Mann, H.B., 1945. Nonparametric Tests Against Trend. Econometrica 13, 245. https://doi.org/10.2307/1907187

Mantovani, A.C.D.M., Setzer, A.W., 1997. Deforestation detection in the Amazon with an AVHRR-based system. Int. J. Remote Sens. 18, 273–286. https://doi.org/10.1080/014311697219060

Melendez-Pastor, I., Hernández, E.I., Navarro-Pedreño, J., Gómez, I., 2014. Socioeconomic factors influencing land cover changes in rural areas: The case of the Sierra de Albarracín (Spain). Appl. Geogr. 52, 34–45. https://doi.org/10.1016/j.apgeog.2014.04.013

Müller, D., Leitão, P.J., Sikor, T., 2013. Comparing the determinants of cropland abandonment in Albania and Romania using boosted regression trees. Agric. Syst. 117, 66–77. https://doi.org/10.1016/j.agsy.2012.12.010

Nadal-Romero, E., Otal-Laín, I., Lasanta, T., Sánchez-Navarrete, P., Errea, P., Cammeraat, E., 2018. Woody encroachment and soil carbon stocks in subalpine areas in the Central Spanish Pyrenees. Sci. Total Environ. 636, 727–736. https://doi.org/10.1016/j.scitotenv.2018.04.324

National Forest Inventory (NFI). Inventario Forestal Nacional (IFN), https://www.miteco.gob.es/es/biodiversidad/servicios/banco-datos-naturaleza/informacion-disponible/ifn2.aspx

Ninyerola, M., Pons, X., Roure, J.M., 2007. Monthly precipitation mapping of the Iberian Peninsula using spatial interpolation tools implemented in a Geographic Information System. Theor. Appl. Climatol. 89, 195–209. https://doi.org/10.1007/s00704-006-0264-2

Ninyerola, M., Pons, X., Roure, J.M., 2000. A methodological approach of climatological modelling of air temperature and precipitation through GIS techniques. Int. J. Climatol. 20, 1823–1841. https://doi.org/10.1002/1097-0088(20001130)20:14<1823::AID-JOC566>3.0.CO;2-B

Northrop, A., Galli, L., Ferrara, R., Mica, S., Lavender, S., Biasutti, R., Goryl, P., Gascon, F., Saunier, S., Meloni, M., 2017. Bulk processing of the Landsat MSS/TM/ETM+ archive of the European Space Agency: an insight into the level 1 MSS processing, in: Bruzzone, L., Bovolo, F., Benediktsson, J.A. (Eds.), Image and Signal Processing for Remote Sensing XXIII. SPIE, p. 1. https://doi.org/10.1117/12.2278633

Palmero-Iniesta, M., Espelta, J.M., Padial-Iglesias, M., Gonzàlez-Guerrero, Ò., Pesquer, L., Domingo-Marimon, C., Ninyerola, M., Pons, X., Pino, J., 2021. The role of recent (1985–2014) patterns of land abandonment and environmental factors in the establishment and growth of secondary forests in the iberian peninsula. Land 10, 1–20. https://doi.org/10.3390/land10080817

Pazúr, R., Bolliger, J., 2017. Land changes in Slovakia: Past processes and future directions. Appl. Geogr. 85, 163–175. https://doi.org/10.1016/j.apgeog.2017.05.009

Perpiñá Castillo, C., Coll Aliaga, E., Lavalle, C., Martínez Llario, J.C., 2020. An Assessment and Spatial Modelling of Agricultural Land Abandonment in Spain (2015–2030). Sustainability 12, 560. https://doi.org/10.3390/su12020560

Pijanowski, B.C., Brown, D.G., Shellito, B.A., Manik, G.A., 2002. Using neural networks and GIS to forecast land use changes: a Land Transformation Model. Comput. Environ. Urban Syst. 26, 553–575. https://doi.org/10.1016/S0198-9715(01)00015-1

Pons, X., 2004. MiraMon. Sistema d'Informació Geogràfica i software de Teledetecció. Centre de Recerca Ecològica i Aplicacions Forestals, CREAF. Bellaterra. ISBN:84-931323-4-9. https://www.miramon.cat.

Poyatos, R., Latron, J., Llorens, P., 2003. Land Use and Land Cover Change After Agricultural Abandonment. Mt. Res. Dev. 23, 362–368. https://doi.org/10.1659/0276-4741(2003)023[0362:lualcc]2.0.co;2

Rindfuss, R.R., Entwisle, B., Walsh, S.J., An, L., Badenoch, N., Brown, D.G., Deadman, P., Evans, T.P., Fox, J., Geoghegan, J., Gutmann, M., Kelly, M., Linderman, M., Liu, J., Malanson, G.P., Mena, C.F., Messina, J.P., Moran, E.F., Parker, D.C., Parton, W., Prasartkul, P., Robinson, D.T., Sawangdee, Y., Vanwey, L.K., Verburg, P.H., 2008. Land use change: complexity and comparisons. J. Land Use Sci. 3, 1–10. https://doi.org/10.1080/17474230802047955

Rindfuss, R.R., Walsh, S.J., Turner, B.L., Fox, J., Mishra, V., 2004. Developing a science of land change: Challenges and methodological issues. Proc. Natl. Acad. Sci. 101, 13976–13981. https://doi.org/10.1073/pnas.0401545101

Rounsevell, M.D.A., Pedroli, B., Erb, K.-H., Gramberger, M., Busck, A.G., Haberl, H., Kristensen, S., Kuemmerle, T., Lavorel, S., Lindner, M., Lotze-Campen, H., Metzger, M.J., Murray-Rust, D., Popp, A., Pérez-Soba, M., Reenberg, A., Vadineanu, A., Verburg, P.H., Wolfslehner, B., 2012. Challenges for land system science. Land use policy 29, 899–910. https://doi.org/10.1016/j.landusepol.2012.01.007

Sala, O.E., Stuart Chapin, F., III, Armesto, J.J., Berlow, E., Bloomfield, J., Dirzo, R., Huber-Sanwald, E., Huenneke, L.F., Jackson, R.B., Kinzig, A., Leemans, R., Lodge, D.M., Mooney, H.A., Oesterheld, M., Poff, N.L., Sykes, M.T., Walker, B.H., Walker, M., Wall, D.H., 2000. Global Biodiversity Scenarios for the Year 2100. Science (80-.). 287, 1770–1774. https://doi.org/10.1126/science.287.5459.1770

Sanjuán, Y., Arnáez, J., Beguería, S., Lana-Renault, N., Lasanta, T., Gómez-Villar, A., Álvarez-Martínez, J., Coba-Pérez, P., García-Ruiz, J.M., 2018. Woody plant encroachment following grazing abandonment in the subalpine belt: a case study in northern Spain. Reg. Environ. Chang. 18, 1103–1115. https://doi.org/10.1007/s10113-017-1245-y

Sen, P.K., 1968. Estimates of the Regression Coefficient Based on Kendall's Tau. J. Am. Stat. Assoc. 63, 1379–1389. https://doi.org/10.1080/01621459.1968.10480934

Serra, P., Pons, X., Saurí, D., 2008. Land-cover and land-use change in a Mediterranean landscape: A spatial analysis of driving forces integrating biophysical and human factors. Appl. Geogr. 28, 189–209. https://doi.org/https://doi.org/10.1016/j.apgeog.2008.02.001

Serra, P., Vera, A., Tulla, A.F., Salvati, L., 2014. Beyond urban-rural dichotomy: Exploring socioeconomic and land-use processes of change in Spain (1991-2011). Appl. Geogr. 55, 71–81. https://doi.org/10.1016/j.apgeog.2014.09.005

Serrano-Notivoli, R., de Luis, M., Saz, M., Beguería, S., 2017. Spatially based reconstruction of daily precipitation instrumental data series. Clim. Res. 73, 167–186. https://doi.org/10.3354/cr01476

Servei Meteorològic Nacional, https://www.meteo.ad/en (accessed 5.1.21).

Sishodia, R.P., Ray, R.L., Singh, S.K., 2020. Applications of Remote Sensing in Precision Agriculture: A Review. Remote Sens. 12. https://doi.org/https://doi.org/10.3390/rs12193136

Sistema Nacional de Informação de Recursos Hídricos (SNIRH), https://snirh.apambiente.pt/ (accessed 5.1.21).

Teegavarapu, R.S.V., Nayak, A., 2017. Evaluation of long-term trends in extreme precipitation: Implications of in-filled historical data use for analysis. J. Hydrol. 550, 616–634. https://doi.org/10.1016/j.jhydrol.2017.05.030

Theil, H., 1992. A Rank-Invariant Method of Linear and Polynomial Regression Analysis. pp. 345–381. https://doi.org/10.1007/978-94-011-2546-8_20

Turner, B.L., Lambin, E.F., Reenberg, A., 2007. The emergence of land change science for global environmental change and sustainability. Proc. Natl. Acad. Sci. 104, 20666–20671. https://doi.org/10.1073/pnas.0704119104

Verburg, P.H., Crossman, N., Ellis, E.C., Heinimann, A., Hostert, P., Mertz, O., Nagendra, H., Sikor, T., Erb, K.-H., Golubiewski, N., Grau, R., Grove, M., Konaté, S., Meyfroidt, P., Parker, D.C., Chowdhury, R.R., Shibata, H., Thomson, A., Zhen, L., 2015. Land system science and sustainable development of the earth system: A global land project perspective. Anthropocene 12, 29–41. https://doi.org/10.1016/j.ancene.2015.09.004

Vicente-Serrano, S.M., Lasanta, T., Romo, A., 2004. Analysis of spatial and temporal evolution of vegetation cover in the Spanish central pyrenees: Role of human management. Environ. Manage. 34, 802–818. https://doi.org/10.1007/s00267-003-0022-5

Vidal-Macua, J.J., Ninyerola, M., Zabala, A., Domingo-Marimon, C., Gonzalez-Guerrero, O., Pons, X., 2018. Environmental and socioeconomic factors of abandonment of rainfed and irrigated crops in northeast Spain. Appl. Geogr. 90, 155–174. https://doi.org/10.1016/j.apgeog.2017.12.005

Vidal-Macua, J.J., Ninyerola, M., Zabala, A., Domingo-Marimon, C., Pons, X., 2017. Factors affecting forest dynamics in the Iberian Peninsula from 1987 to 2012. The role of topography and drought. For. Ecol. Manage. 406, 290–306. https://doi.org/10.1016/j.foreco.2017.10.011

Vilà-Cabrera, A., Espelta, J.M., Vayreda, J., Pino, J., 2017. "New Forests" from the Twentieth Century are a Relevant Contribution for C Storage in the Iberian Peninsula. Ecosystems 20, 130–143. https://doi.org/10.1007/s10021-016-0019-6

Wang, J., Bretz, M., Dewan, M.A.A., Delavar, M.A., 2022. Machine learning in modelling land-use and land cover-change (LULCC): Current status, challenges and prospects. Sci. Total Environ. 822, 153559. https://doi.org/10.1016/j.scitotenv.2022.153559

Woodcock, C., Allen, R., Anderson, M., Belward, A., Bindschadler, R., Cohen, W., Gao, F., Goward, S., Helder, D., Helmer, E., Nemani, R., Oreopoulos, L., Schott, J., Thenkabail, P., Vermote, E., Vogelmann, J., Wulder, M., Wynne, R., 2008. Free Access to Landsat Imagery. Science 320, 1011. https://doi.org/https://www.doi.org/10.1126/science.320.5879.1011a

Zgłobicki, W., Gawrysiak, L., Baran-Zgłobicka, B., Telecka, M., 2016. Long-term forest cover changes, within an agricultural region, in relation to environmental variables, Lubelskie province, Eastern Poland. Environ. Earth Sci. 75, 1–12. https://doi.org/10.1007/s12665-016-6195-z

Zhu, Z., Woodcock, C.E., 2014. Continuous change detection and classification of land cover using all available Landsat data. Remote Sens. Environ. 144, 152–171. https://doi.org/10.1016/j.rse.2014.01.011